Structures and Thermal Analyses of Werner Clathrates and Coordination Polymers

by

Mairi Kilkenny

B. Sc. (Hons.) University of Cape Town

A thesis presented to the

University of Cape Town

for the degree of

Master of Science

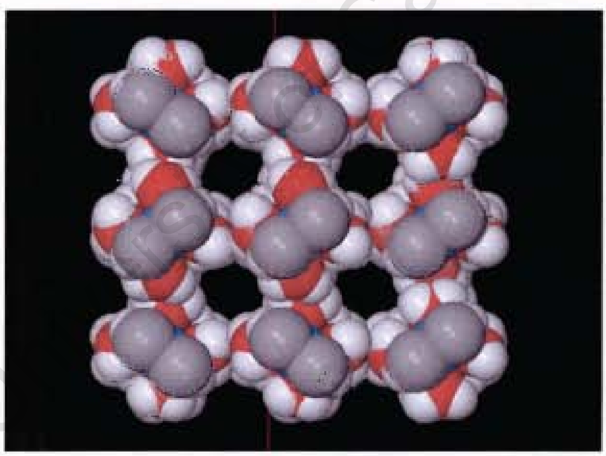

Department of Chemistry

University of Cape Town

Rondebosch

7701

South Africa

May 2001

ACKNOWLEDGEMENTS

I would like to thank

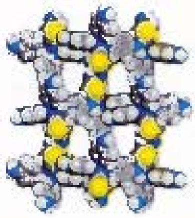

Professor L. R. Nassimbeni, Professor M. R. Caira and Dr. S. A. Bourne, for their excellent supervision and guidance

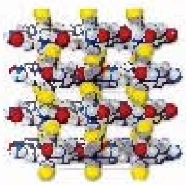

Everyone in the Crystallography Research Group for being so helpful and friendly

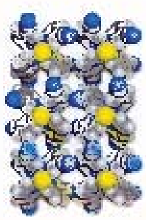

My family for their love and support

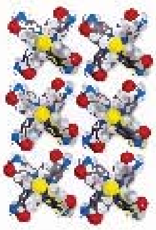

Dr. John Bacsa for the data collections, and Mr Klaus Achleitner for his help with the apparatus

PUBLICATIONS AND CONFERENCES

Parts of this thesis have been published:

1) One- and two-dimensional coordination polymers of zinc(II) with pyrazine. Solid state reactions and decomposition kinetics of the interconversion reactions, S. A. Bourne, M. L. Kilkenny, L. R. Nassimbeni, *J. Chem. Soc., Dalton Transactions,* 2001, 1176.
2) Werner Clathrates. Part 14. Tetrakis(4-NH_2pyridine)diisothiocyanato nickel(II) and its clathrates with EtOH, Me_2CO and DMSO: structures, thermal stabilities and guest exchange, L. R. Nassimbeni, M. L. Kilkenny, *J. Chem. Soc., Dalton Transactions,* 2001, 1172.

Parts of this thesis have been presented at the following conferences:

A poster entitled "Ni(II) Werner Clathrates" was presented at:

Indaba III, Symmetry and Structure: Symmetry Breaking, Chirality and Disorder in Molecules and Crystals, 6-11 August 2000, Skukuza, Kruger National Park, South Africa.

and

ECM19, The 19th European Crystallographic Meeting, 25-31 August, Université Henri Poincaré, Nancy, France.

ABSTRACT

The crystal structures of several organometallic host complexes and their inclusion compounds with small, polar, organic guests have been elucidated. These compounds form a diverse range of structure types, from hydrogen bonded networks of Werner-type inclusion compounds to one- and two-dimensional coordination polymers. Depending on the packing arrangement of the host molecules in the clathrate, the guest molecules (G) may become trapped in cages, stacked in one-dimensional channels or sandwiched between layers of host molecules. Examples of all three clathrate types can be found in the different inclusion compounds presented here.

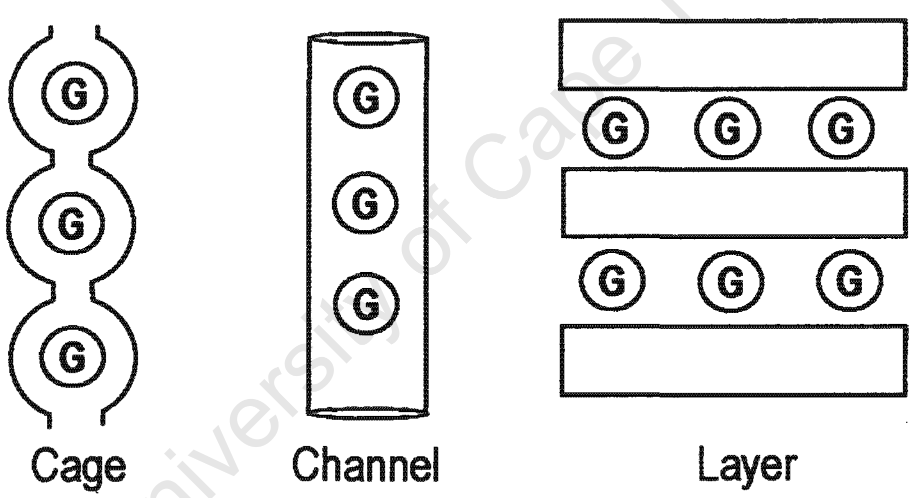

The crystal structures of twelve Werner clathrates and four coordination polymers were solved using single crystal x-ray diffraction techniques. In addition, all compounds were characterised by thermal analysis techniques, including differential scanning calorimetry, thermogravimetry and hot-stage microscopy.

ABBREVIATIONS AND SYMBOLS

Compounds

NiHost1	$Ni(NCS)_2(4\text{-}NH_2\text{-pyridine})_4$
NiEtAc	$Ni(NCS)_2(4\text{-}NH_2\text{-pyridine})_4$.EtOH.Acetone
NiDMSO	$Ni(NCS)_2(4\text{-}NH_2\text{-pyridine})_4$.2DMSO
NiHost2	$Ni(NCS)_2(3\text{-CN-pyridine})_4$
NidiEt	$Ni(NCS)_2(3\text{-CN-pyridine})_4$.2EtOH
NidiDCM	$Ni(NCS)_2(3\text{-CN-pyridine})_4.2CH_2Cl_2$
Nitriaq	$Ni(NCS)_2(\text{isonicotinamide})_3(H_2O).3H_2O$
Nipcres	$Ni(NCS)_2(\text{isonicotinamide})_4$.2*p*-cresol.4EtOH
Nimcres	$Ni(NCS)_2(\text{isonicotinamide})_4$.4*m*-cresol
NiEt	$Ni(NCS)_2(3\text{-}NH_2\text{-pyridine})_3$.EtOH
NiMe	$Ni(NCS)_2(3\text{-}NH_2\text{-pyridine})_3$.MeOH
Niaq	$Ni(NCS)_2(3\text{-}NH_2\text{-pyridine})_2(H_2O).H_2O$
$ZnBr_2pyz_2$	$ZnBr_2(\text{pyrazine})_2$
$ZnBr_2pyz$	$ZnBr_2(\text{pyrazine})_1$
ZnpyzSulf	$Zn(H_2O)_4(\text{pyrazine}).SO_4.2H_2O$
Cudiaq	$Cu(H_2O)(\text{isonicotinamide})_2(SO_4).2H_2O$
pyz	pyrazine

Techniques

DSC	Differential Scanning Calorimetry
GC	Gas chromatography
HSM	Hot stage Microscopy
TG or TGA	Thermogravimetry or Thermogravimetric Analysis
XRD	X-Ray Powder Diffraction

CONTENTS

Acknowledgements *i*
Publications and Conferences *ii*
Abstract *iii*
Abbreviations and Symbols *iv*
Contents *vi*

Chapter 1: Introduction

1.1 What is a Werner Clathrate? 1
1.2 Applications 2
1.3 Structure Types 3
1.4 Kinetic Studies 8
1.5 Interpretation of Enthalpy data 11
1.6 Intermolecular Interactions 13
1.7 New Directions 14
1.8 Related Fields 15
1.9 About this study 18

Chapter 2: Experimental Techniques

2.1 General Synthetic Procedure 24
2.2 Synthesis

2.2.1 **NiHost1** 25
2.2.2 **NiEtAc** 25
2.2.3 **NiDMSO** 26
2.2.4 **NiHost2** 26
2.2.5 **NidiEt** 27
2.2.6 **NidiDCM** 27
2.2.7 **Nitriaq** 28
2.2.8 **Nipcres** 28

2.2.9 **Nimcres** 29
2.2.10 **NiEt** 29
2.2.11 **NiMe** 30
2.2.12 **Niaq** 30
2.2.13 **$ZnBr_2pyz_2$** and **$ZnBr_2pyz$** 30
2.2.14 **ZnpyzSulf** 31
2.2.15 **Cudiaq** 32

2.3 Thermal Analysis

2.3.1 Differential Scanning Calorimetry 33
2.3.2 Thermogravimetry 34
2.3.3 Hot-stage Microscopy 34

2.4 X-Ray Photography

2.4.1 Oscillation Photography 35
2.4.2 Weissenberg Photography 35

2.5 Single Crystal X-Ray Diffractometry 36
2.6 X-Ray Powder Diffraction 37
2.7 Microanalysis 37

Chapter 3: Results: Crystal Structures and Thermal Analyses

3.1 **Werner Clathrates**: Host = $Ni(NCS)_2$(4-aminopyridine)$_4$ 39
3.2 **Werner Clathrates**: Host = $Ni(NCS)_2$(3-cyanopyridine)$_4$ 61
3.3 **Werner Clathrates**:
Host = $Ni(NCS)_2$(isonicotinamide)$_x$$(H_2O)_{4-x}$ 81
3.4 **Polymeric Werner Clathrates**:
Host = $Ni(NCS)_2$(3-aminopyridine)$_x$$(H_2O)_{3-x}$ 102
3.5 **Coordination Polymers** 123

Chapter 4: Conclusions 162

Appendices: 170

Tables of atomic coordinates, bond lengths and angles, thermal parameters, torsion angles and structure factors, as well as .RES files.

Appendix 1: NiHost1, NiEtAc, NiDMSO

Appendix 2: NiHost2, NidiEt, NidiDCM

Appendix 3: Nitriaq, Nipcres, Nimcres

Appendix 4: NiEt, NiMe, Niaq

Appendix 5: $ZnBr_2pyz_2$, $ZnBr_2pyz$, ZnpyzSulf, Cudiaq

INTRODUCTION

1.1 What is a Werner Clathrate?

The term *clathrate*, introduced by H.M.Powell in 1948[1], is derived from the Latin word *clathratus*, meaning enclosed or protected by the cross-bars of a trellis or grating. At the time it was used to describe the imprisonment of one type of molecule (the guest) by another (the host). The history surrounding the introduction of this term is described in a recent review by J.E.D.Davies[2].

Werner clathrates are formed by host molecules of general formula MX_2A_4, where M is a divalent metal ion (typically Ni^{2+}, Co^{2+}, Fe^{2+}, Cu^{2+} or Mn^{2+}), X is an anionic ligand (NCS^-, NO_3^-, Br^-, Cl^-, I^-, and others) and A is a neutral pyridine derivative or arylalkylamine (Fig. 1.1). The host complexes pack to generate a structure containing voids or cavities that are occupied by small organic guest molecules.

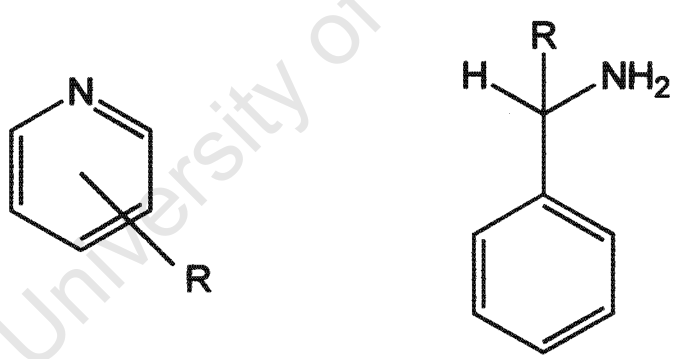

Fig 1.1: Substituted pyridine ligand, left, and α-arylalkylamine, right (R = H, phenyl or alkyl group).

The most widely used host complex to date is $Ni(NCS)_2(4\text{-methylpyridine})_4$, although complexes incorporating ethyl-[3a-e], vinyl-[4a-e], phenyl[5a-e]- and butyl[6]-substituted pyridine ligands have also been reported. de Radzitzky *et. al.* synthesised a series of 28 Werner clathrates with racemic α-substituted benzylamine ligands[7], while Nassimbeni *et. al.* have investigated complexes formed by the chiral ligands (R)- and (S)-1-phenyl-1-ethylamine[8].

1.2 Applications of Werner Clathrates

1.2.1 Separations

An interesting feature of Werner complexes is their ability to selectively enclathrate a variety of aromatic compounds and, more importantly, the selectivity they display towards certain isomers. This property was first exploited by Schaeffer *et. al.* in 1957, in the separation of xylenes, cymenes, methylnaphthalenes and other isomers from mixtures[9].

de Radzitzky *et. al.* investigated the selectivity of a series of Werner complexes, of general formula $Ni(NCS)_2(\alpha\text{-substituted benzylamine})_4$, for xylene isomers[7], while Davies *et. al.* investigated the effects of using different metal centres and pyridine ligands on the separation of isomeric disubstituted benzenes[10]. The host complex $Ni(NCS)_2(4\text{-methylpyridine})_4$ has even been shown to distinguish between isotopically substituted pairs of *p*-xylenes, preferring the more deuterated form in each case[11,12].

1.2.2 The Use of Werner Clathrates in Column Chromatography

The ability of Werner complexes to separate isomers has led to numerous studies in which clathrate formation is utilised in the resolution of isomeric mixtures on a chromatographic column (Fig. 1.2). Some of the compounds separated in this way include isomeric mixtures of nitroaliphatics[13], mononitroethylbenzenes[14], dinitrobenzenes and nitronaphthalenes[15], nitrobenzoic, nitrocinnamic and naphthoic acids[16] as well as bromonitrobenzenes[17].

The success of these complexes in column chromatography lies in the ability of certain clathrate phases to exchange their guest component without disrupting the host structure. This process of guest exchange in Werner clathrates, first alluded to by Belitskus et. al. in 1963[18], allows for the preparation of clathrates of desired chemical composition, and will be discussed further in the next section.

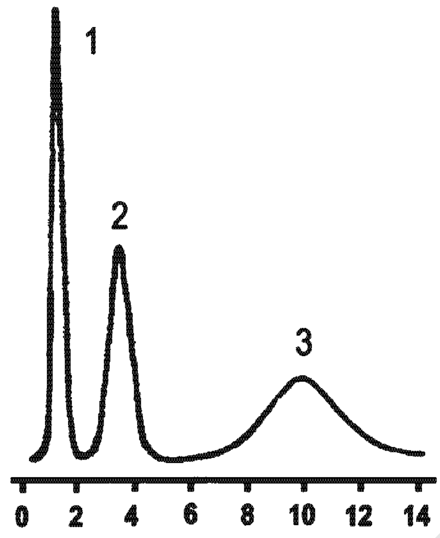

Fig 1.2: The elution curve for dinitrobenzenes using a $Ni(NCS)_2(4\text{-methylpyridine})_4$ sorbent at a molar volume of 505cm^3. **1** = *o*-DNB, **2** = *m*-DNB, **3** = *p*-DNB[17].

1.3 Structure Types

An important discovery was made in 1962, when Hart and Smith carried out structural studies of various clathrates formed by the host complex $Ni(NCS)_2(4\text{-methylpyridine})_4$[19]. XRD, phase and density studies of the initial (empty) host structure and the resulting clathrates revealed a definite change in the structure of the host upon clathration. The two structural forms were designated α and β respectively, according to the equation:

non-porous α-phase + G (guest) $\rightarrow$ **β-clathrate** (complex.nG)

1.3.1 Important Werner Clathrate Phases

1.3.1.1 β-phase

A significant number of the clathrates containing 4-substituted pyridine ligands are found to crystallise in the tetragonal space group $I4_1/a$, with a host:guest ratio close to 1:1[20-24]. This structure type, designated the β-phase, is characterised by a zigzag system of channels in which the guest molecules, usually pyridine or benzene derivatives, are accommodated (Fig. 1.3).

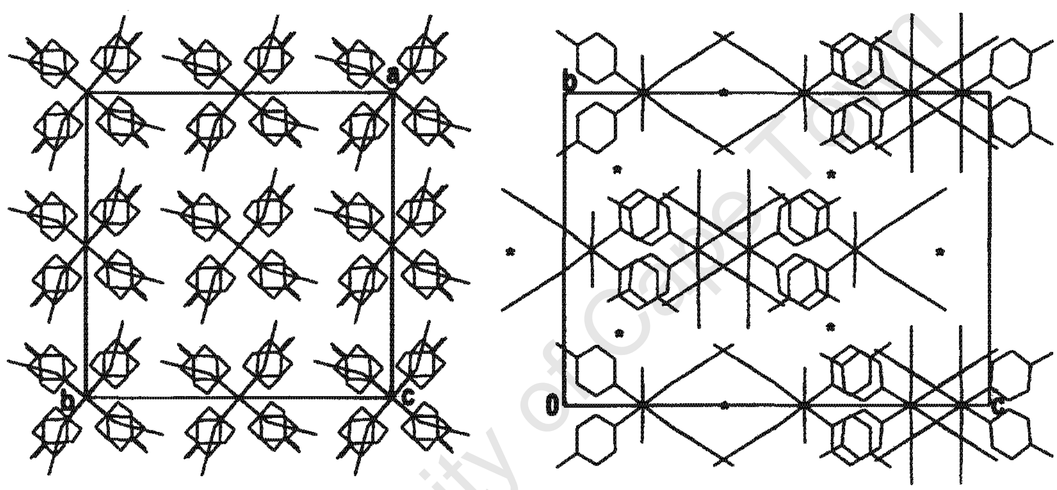

Fig 1.3: The β-phase viewed down [001], left, and [100], right (hydrogen and guest atoms omitted for clarity). Centres of symmetry are represented by * in the [100] projection.

There are two distinct sorption sites in the β-phase: small centrosymmetric cavities and larger cavities with four-fold symmetry. In most of the crystal structures studied to date, the guest molecules occupy the centrosymmetric cavities. While centrosymmetric guest molecules are located on the centres of symmetry, a lack of symmetry in the guest is compensated for by disordering of the guest molecule over two positions[4a,24].

Allison and Barrer[25] found that the behaviour of the β-phase was analogous to that of inorganic zeolites, in that they could withstand the reversible sorption and desorption of guest molecules from the channels without disruption of the host structure. These clathrates were therefore called organic zeolites, with the host lattice able to expand and contract according to the amount of guest present in the crystal[26]. The minimum volume of the organic zeolite is attained by complete desorption of the guest component, to yield the empty host structure. This empty β-clathrate, which is metastable, is called the β_o-phase. The molar volumes for the α, β_o and several β-clathrate forms are given in Table 1.1 below[27].

Table 1.1: Molar volumes of α-, β_o- and β-$Ni(NCS)_2$(4-methylpyridine)$_4$

	Guest component				
	α	β_o	benzene	*p*-xylene	*m*-xylene
Molar volume (cm^3)	431.0	471.6	499.9	512.7	535.7

Schaeffer *et. al.* were the first to recognise that the β-phase, when exposed to an isomeric mixture of guest molecules, displays a marked preference for the *para* isomer, although at the time the structural basis for this apparent selectivity was not known[9]. *para*-Selectivity was also noted in the various experiments utilising $Ni(NCS)_2$(4-methylpyridine)$_4$ as a sorbent in column chromatography. Disubstituted benzenes were almost always eluted in the order *ortho→meta→para*, indicating that the *para* isomer interacts most strongly with the host lattice. This selectivity is due to steric repulsion between the branches of the *o*- and *m*-substituted guests and the cages of the host structure. These cages are much better suited to the shape of the *p*-isomer, which more approximates a linear shape than do the other two isomers[28].

1.3.1.2 γ-phase

Another commonly occurring structure type is the γ-phase[21,29-33]. The host molecules are arranged into layers, with the guest molecules being accommodated in the interlayer spaces. A host:guest ratio of 1:2 is often observed in the γ-phase clathrates. Unlike the β-phase, these clathrates tend to display *ortho*-selectivity[32].

1.3.2 Packing Modes

From the many Werner-type inclusion compounds studied, four general structure types emerge[27].

I. The true clathrate

In the true clathrate the host molecules pack to generate a structure with well-separated cages (Fig. 1.4). The guest molecules are trapped in the cavities and are therefore unable to migrate through the crystal, resulting in a high kinetic stability for the clathrate. The guest molecules are released from the crystal only on decomposition of the host structure. Studies indicate that a host:guest ratio of 1:0.67 is common to this structure type[27,34].

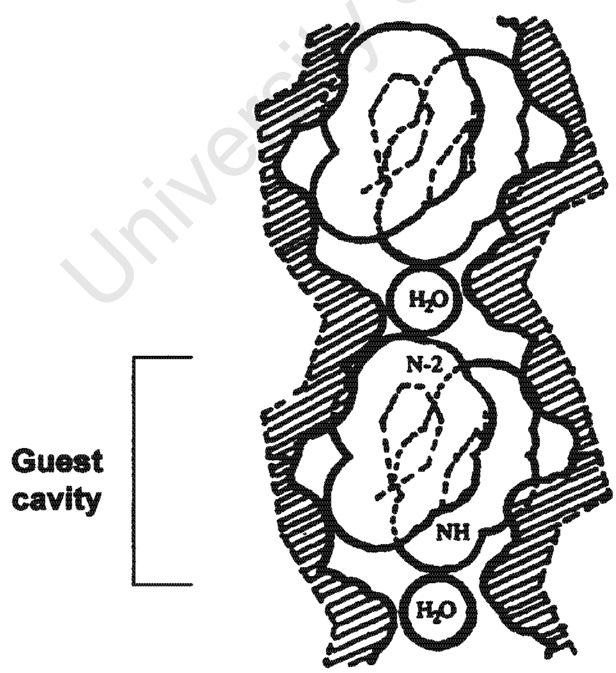

Fig 1.4: The cage structure[27] of $Cd(NCS)_2$(4-methylpyridine)$_4$. 0.67(4-methylpyridine).0.33H_2O

II. The channel structure

The packing of the host molecules in the channel structure is such that the cavities become interconnected in one dimension, resulting in the formation of channels through which the guest molecules can easily diffuse (Fig. 1.5)[35,5e].

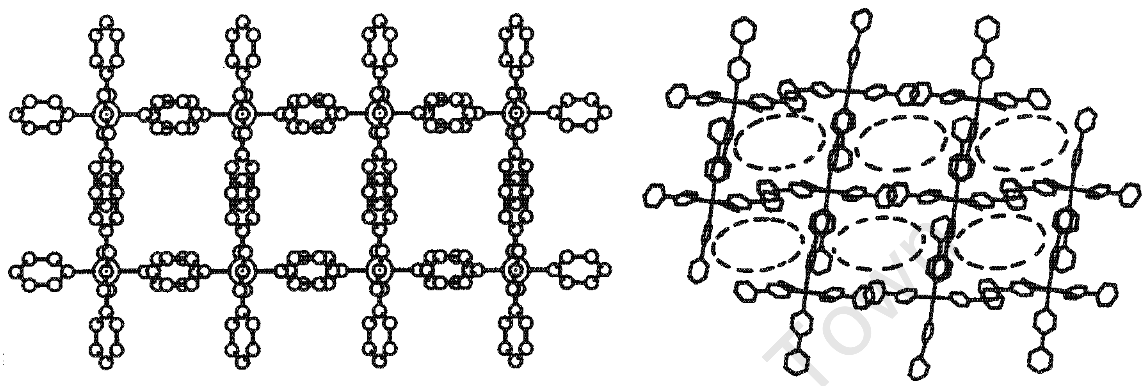

Fig 1.5: Channel structure of $Zn(NO_3)_2(pyridine)_4.2pyridine$[35], left, and $Ni(NCS)_2(4\text{-phenylpyridine})_4$.*p*-xylene.2DMSO[5c], right (hydrogen atoms and guest molecules omitted for clarity).

III. The organic zeolite structure

The formation of zeolite-type structures results from the interconnection of cavities to generate a three-dimensional network of cages[4a,23,24]. Depending on the diameter of the pores, the guest molecules may or may not be able to diffuse through the host structure. The organic zeolites, to which the β-phase clathrates belong, display a remarkable ability to contract and expand according to the quantity of guest absorbed. While in most cases complete guest desorption leads to the collapse of the host structure and regeneration of the non-porous α-phase, in some cases the host may retain its structure, generating the empty, porous β_0-phase[36].

IV. The layer clathrate

In the layer clathrates, the guest molecules occupy the spaces between layers of host molecules[30-33]. In most cases, the isothiocyanate groups project into the spaces between the layers, thus partitioning the interlayer spaces into inclusion cavities (Fig. 1.6)[31]. As indicated above for the γ-clathrates, the typical host:guest ratio is 1:2. In contrast to the true clathrates, the layer clathrates are kinetically unstable, with the guest molecules being released on exposure to air.

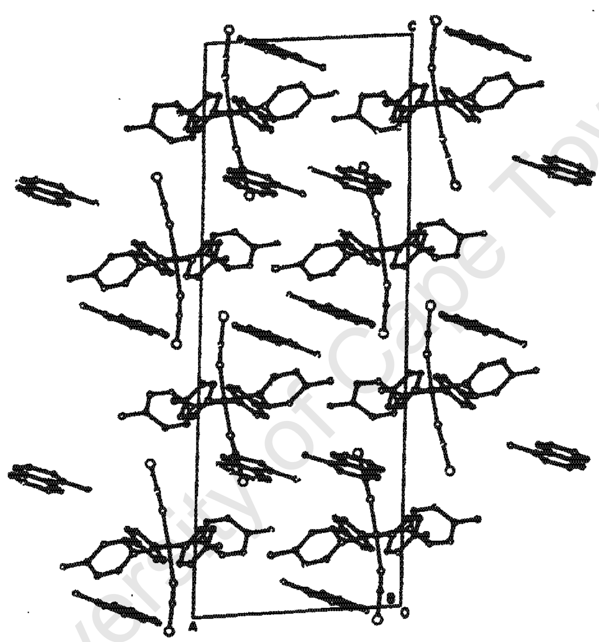

Fig 1.6: Layer structure of $Ni(NCS)_2(4\text{-methylpyridine})_4.2(1\text{-methylnaphthalene})$[31].

1.4 Kinetic Studies

1.4.1 Guest Sorption

The literature contains numerous kinetic studies of both guest sorption and desorption processes. Structural studies of the α and β forms reveal that the α-host structure, which crystallises in the space group $P2_1/c$, cannot directly absorb guest molecules[37]. Therefore, in the course of the guest absorption process, either lattice reconstruction in the solid phase, or host dissolution followed by clathrate crystallisation, must occur.

An investigation into the thermokinetic course of clathration of various aromatic guests by $Ni(NCS)_2$(4-methylpyridine)$_4$, revealed the $\alpha \rightarrow \beta$ transformation to be a two step process[28] (Fig. 1.7):

I. Fast lattice reconstruction occurs, with simultaneous absorption of guest molecules (XRD studies show this step to be complete after 3 minutes for the uptake of *p*-xylene).
II. The guest is absorbed until the cavities reach full occupancy. Requiring diffusion of the guest molecules through the clathrate, this step is found to be rate-determining for the aromatic guests studied (Complete reaction times for the clathration process are given in Table 1.2 below).

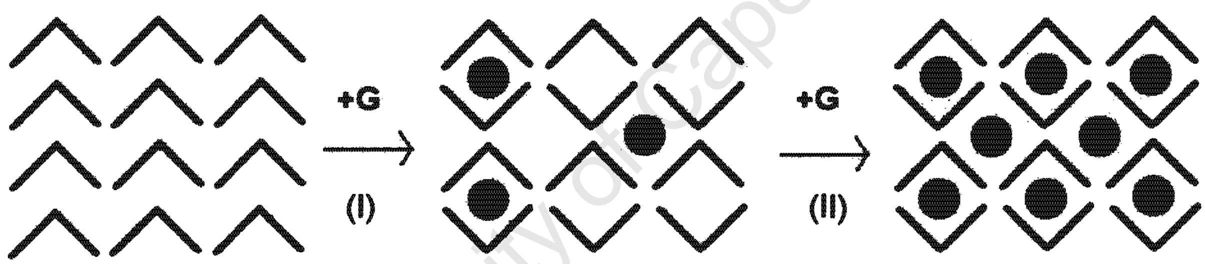

Fig 1.7: Two-step $\alpha \rightarrow \beta$ transformation for $Ni(NCS)_2$(4-methylpyridine)$_4$

Table 1.2: Reaction times for absorption of aromatic guests by $Ni(NCS)_2$(4-methylpyridine)$_4$[28]

	Guest component			
	Benzene	Toluene	*p*-xylene	*m*-xylene
Reaction Time (min.)	2	7	27	50

The thermokinetic plots for the clathration of xylene isomers by $Ni(NCS)_2$(4-methylpyridine)$_4$ clearly show the two separate stages in the sorption process (Fig. 1.8)

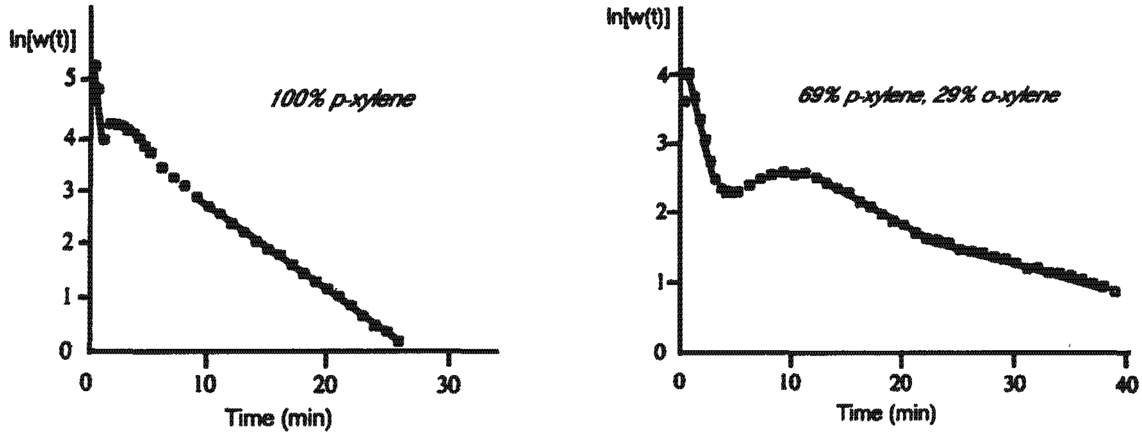

Fig 1.8: Thermokinetic course of clathration for *p*-xylene, left, and a mixture of *p*- and *o*-xylene, right[27].

In a similar study the sorption of xylene isomers by the host $Ni(NCS)_2$(4-vinylpyridine)$_4$ was investigated[4b]. While the uptake of *p*-xylene followed the same two-step process outlined above, sorption of the *o*- and *m*-isomers occurred in a single step. No intermediate product displaying partial occupation of the host cavities was formed, indicating that the α-host undergoes slow recrystallisation to form the host:guest complex.

1.4.2 Guest Desorption

In the reverse process, guest desorption, three stages can be distinguished[38]:

I. *Release of guest from cavity.* The guest molecule is reorientated in the cavity in preparation for diffusion (Rate constant, *k*, is independent of crystal radius, *R*)
II. *Diffusion of guest to crystal surface* ($k \sim R^{-2}$)
III. *Desorption of guest from crystal surface* ($k \sim R^{-1}$)

In the desorption of *p*-xylene from β-$Ni(NCS)_2$(4-methylpyridine)$_4$.*p*-xylene, the rate determining step was found to be (I), due to the energy barrier that must be overcome in reorientating the *p*-xylene molecule in the cavity (Fig. 1.9).

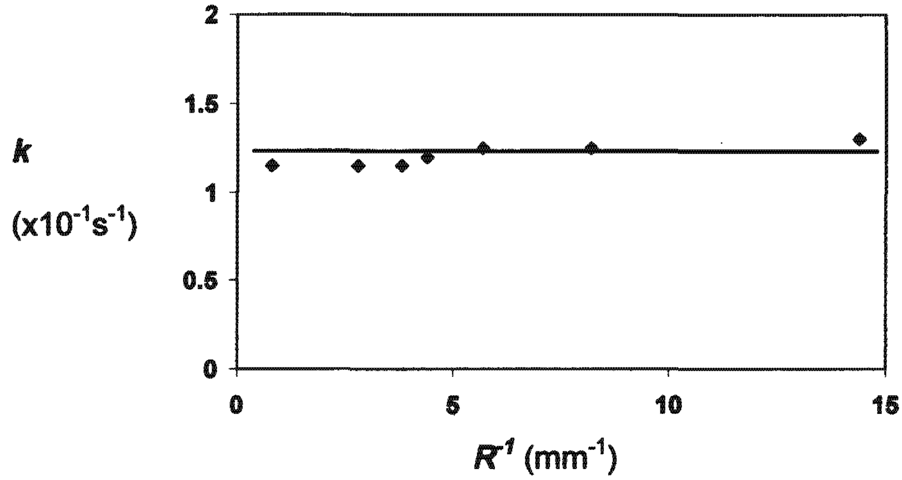

Fig 1.9: Rate constant, *k*, vs. reciprocal linear size of crystals for the desorption of *p*-xylene from β-$Ni(NCS)_2$(4-methylpyridine)$_4$.*p*-xylene at room temperature[38].

Isothermal decomposition kinetics of the desorption of benzene from β-$Ni(NCS)_2$(4-methylpyridine)$_4$.C_6H_6, however, revealed the rate determining step to be the diffusion of the benzene molecules through the clathrate[39].

1.5 Interpretation of Enthalpy Data

There is a general rule in the field of zeolite chemistry that if the sorption process is non-specific (i.e. there are no host···guest interactions), then a plot of the enthalpy of sorption (ΔH_{sorp}) of various guest components *vs.* their respective enthalpies of vapourisation (ΔH_{evap}), defines a straight line with a slope of 2. Analogous studies have revealed the same linear correlation between ΔH_{sorp} and ΔH_{evap} for the clathration of many aromatic[28] and non-aromatic[25] guest species by $Ni(NCS)_2$(4-methylpyridine)$_4$.

In certain cases, however, there is a significant negative deviation from this line. This is due to unfavourable steric (poor fit between cavity and guest) or chemical (hydrophilic guest in hydrophobic cavity) interactions between the host and guest components. This is shown in Fig. 1.10, where steric interactions exist between the β-$Ni(NCS)_2$(4-methylpyridine)$_4$ host and the branches of the *o*- or *m*-xylene guests.

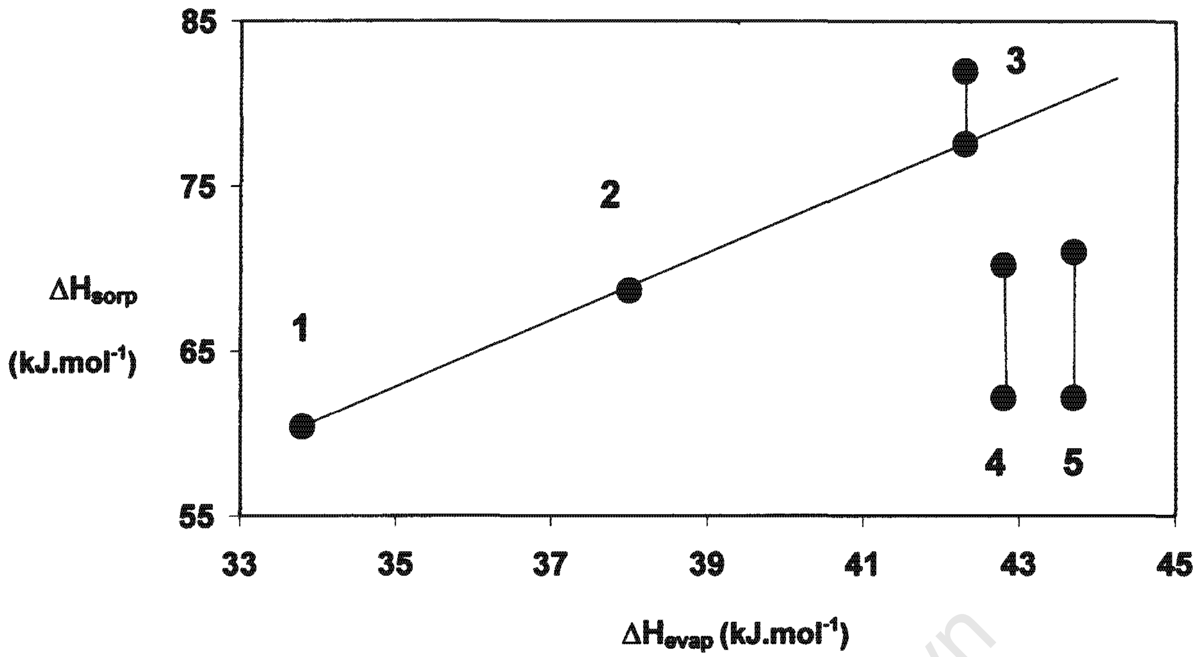

Fig 1.10: Linear correlation between ΔH_{sorp} and ΔH_{evap} for benzene (**1**), toluene (**2**) and *p*-xylene (**3**). *m*- (**4**) and *o*-xylene (**5**) deviate significantly from this line[28]. Vertical lines represent the ranges of partial molar enthalpies of clathration for the respective isomers.

A thermogravimetric and calorimetric study of the mixed guest clathrates formed by $Ni(NCS)_2$(4-methylpyridine)$_4$ with methanol/4-methylpyridine and acetone/4-methylpyridine yielded values of the partial molar enthalpies of enclathration of the individual guests[40]. The enthalpy data, as well as the stoichiometries of the clathrates, indicate that two different mechanisms of clathration are at work in the two systems. In the methanol/4-methylpyridine clathrate, the two types of guest molecules compete for the same sorption sites, with one 4-methylpyridine guest equivalent to two methanol guests, while in the acetone/4-methylpyridine clathrate there is competition for two different sorption sites.

1.5.1 The Induced-Fit Mechanism

Studies show that the partial molar enthalpy of enclathration of a particular isomer, H_{clath}, depends on the quantity of that isomer present in the clathrate, *y*. For ternary mixtures of *o*-, *m*- and *p*-xylene in β-$Ni(NCS)_2$(4-methylpyridine)$_4$, an increase in the concentration of any isomer in the clathrate results in an increase in the enthalpy of clathration for that isomer, according to[26]:

$$(H_{clath})_o = 10.07 + 9.07y_o$$
$$(H_{clath})_m = 13.38 + 5.64y_m$$
$$(H_{clath})_p = 25.12 + 6.27y_p$$

This effect is explained by the adaptation of the host structure to the incoming guest species, such that the occupation of one sorption site by a guest molecule makes it more favourable for another molecule of the same type to bind to an adjacent site.

1.6 Intermolecular Interactions

While the β-host is able to expand and contract to accommodate guest molecules of varying size and shape, in some cases the shape of the guest molecule can influence the conformation of the host, and hence the type of structure formed[41,42]. This is exemplified by the ability of the host complex $Ni(NCS)_2$(4-methylpyridine)$_4$, to crystallise in different phases depending on the composition of the mixture of xylene isomers present in the crystal. When *o*-xylene is present at a mole fraction of greater than 0.65 in the clathrate, it is the γ-phase rather than the β-phase that crystallises[28].

Studies investigating the host··guest interactions within Werner clathrates have been carried out[3a,43]. An excellent review by Lipkowski[27] emphasises the importance of Werner clathrates as subjects for investigating the process of hostΛguest molecular recognition during clathrate formation, and postulates the following stepwise mechanism:

I. *Contact stabilisation of the host structure*. The guest selects a particular host species from those present in solution (tetrahedral, octahedral, *cis* or *trans* etc.) with which to co-crystallise.

II. The host-guest combination may select the most appropriate, thermodynamically-favoured structure type for solvate formation (cage, layer, channel or zeolite).

III. Once the clathrate has formed, the host complexes may adapt their shape and form to best accommodate the guest molecules.

As a result, Werner clathrates become ideal compounds for studying the effects of external non-bonded interactions on the molecular structure of the host complex. Recently the host···host interactions as a function of guest size and shape have been studied, and the change in the geometry of the host complex on inclusion of various guest molecules was analysed[3a,44]. In addition, the influence of guest polarity on the process of clathrate formation was studied[45].

1.7 New Directions in Werner Clathrates

With most of the work in the area of Werner clathrates having been done on complexes containing 4-substituted pyridine or arylalkylamine ligands, the trend recently has been towards exploring other ligand types. The use of larger, bulkier ligands has been shown to generate large pores or cavities. This is exemplified by the synthesis and characterisation of a new series of Werner clathrates of general formula $MX_2A_3.\frac{1}{2}A$, where $X = NO_3^-$, A = *trans*-4-styrylpridine and $M = Co^{2+}$, Cd^{2+} or Zn^{2+} (Fig. 1.11a). The styrylpyridine guest molecules are accommodated in large cavities, resulting in the formation of kinetically stable clathrates[46].

The clathrate $Ni(pyridine)_2(dibenzoylmethanato)_2$ and its clathratogenic properties with guests such as CCl_4, $CHCl_3$, THF, C_6H_6, C_6H_5Cl and C_5H_5N have been investigated (Fig. 1.11b). Initial results indicate that this is a most versatile host complex, forming four different structure types with the above-mentioned guests[47]. The possibilities for guest absorption become even greater if one considers placing substituents on the pyridine ligands.

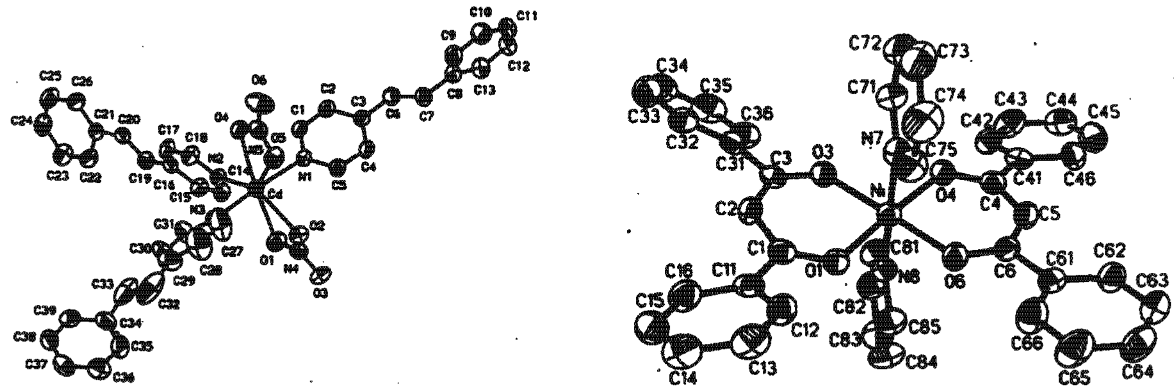

(a) **(b)**

Fig 1.11: The structure of the host complexes in (a) $Cd(NO_3)_2$(trans-4-styrylpyridine)$_3$.½(trans-4-styrylpyridine)[46], and (b) Ni(pyridine)$_2$(dibenzoylmethanato)$_2$.$2CCl_4$[47].

While most Werner clathrates incorporate transition metal centres, clathrates with main group metals have also been synthesised. Two such examples are the Mg-based clathrates, $Mg(NCS)_2$(4-methylpyridine)$_4$. ⅔ (4-methylpyridine). ⅓ H_2O and $Mg(NCS)_2$(4-methylpyridine)$_4$.4-methylpyridine[34].

1.8 Related Fields

The majority of Werner complexes synthesised to date have incorporated hydrocarbon-substituted pyridine ligands, with the result that only weak van der Waals interactions exist between the components of the crystal. If the pyridine ligand were to carry a hydrogen bonding substituent, however, numerous host···host and host···guest hydrogen bonding interactions would become available. Some such substituents include amino ($-NH_2$), hydroxy (-OH), cyano (-CN), amide ($-CONH_2$), oxime (-C(R)=NOH)[48] and carboxylic acid (–COOH). Introducing these hydrophilic substituents into the Werner complex could be seen to have important consequences, including:

I. The numerous hydrogen bonding opportunities that would arise in the crystal may lead to the formation of new structure types with novel physico-chemical properties.

II. The presence of polar substituents would generate hydrophilic instead of hydrophobic cavities, thereby making the sorption of hydrophilic guest molecules more favourable. As a result, these complexes would display entirely different selectivities from the classical Werner complexes.

III. The substituent itself, if it contains an atom with a lone pair, may form a chemical bond to the metal centre of an adjacent complex, resulting in the formation of polymeric Werner clathrates.

1.8.1 Polymeric Werner Clathrates

Polymerisation of Werner complexes may occur in two ways. In the first case the thiocyanate group can act as a bridging ligand, forming a link between two metal centres, as observed in $Ni(NCS)_2$(2-aminopyridine)$_2$.$C_4H_{10}O$[49], [$Ni(NCS)_2$(4-methylpyridine)$_3$]$_2$[50] and others[51]. Alternatively, an appropriately substituted pyridine ligand can act as a bridging ligand, as in $Ni(NCS)_2$(3-aminopyridine)(H_2O).H_2O, where the amino group of one 3-aminopyridine ligand coordinates to a neighbouring Ni atom[49].

1.8.2 Coordination Polymers

Coordination polymers consist of a host framework, built of metal centres linked by organic ligands, which contains pores or channels that may include guest molecules. The metal centres are directly linked by bridging ligands, as shown in Fig. 1.12a, below.

1.8.2.1 The Use of Bridging Ligands

Much of the initial work in this field utilised the rod-like, bridging ligands, pyrazine (**1**)[52a-c] and 4,4'-bipyridine (**2**)[53a-h] (Fig 1.12b), as they readily form stable 1-, 2- and 3-D host frameworks that are able to reversibly include guest molecules. This series has recently been extended to include 2-(4-pyridyl)-4,4,5,5-tetramethyl-1,3-dioxaboralone (**3**), which has been shown to form porous structures with large cavities, that remain intact even after the guest molecules have been removed[54].

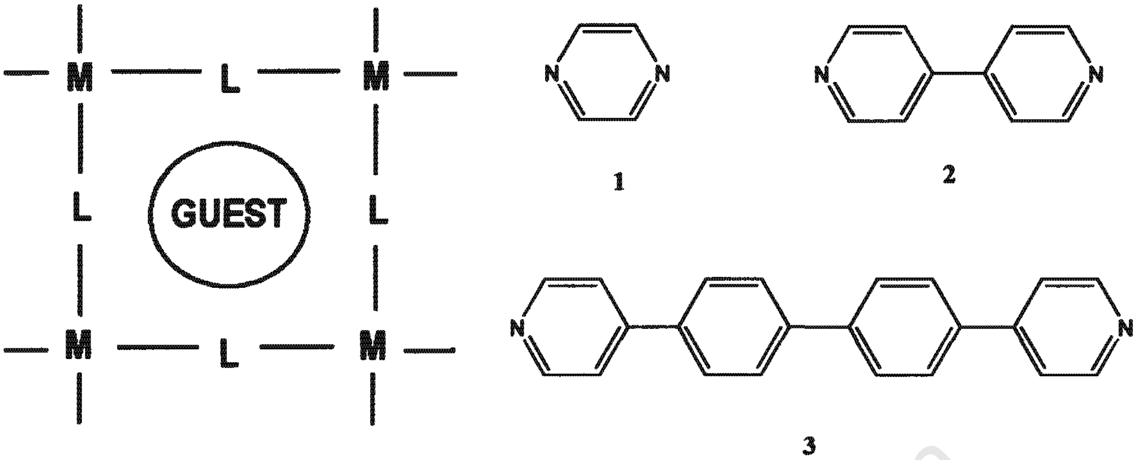

(a) (b)

Fig 1.12: (a) 2-D square grid framework formed by linear, bridging ligands, (b) Ligands **1** (pyrazine), **2** (4,4'-bipyridine), and **3** (2-(4-pyridyl)-4,4,5,5-tetramethyl-1,3-dioxaboralone).

1.8.3 Hydrogen Bonded Networks

Aakeröy et. al. were the first to explore the characteristics of flexible 3-D organometallic host frameworks assembled by head-to-head hydrogen bonds between ligand substituents (Fig. 1.13). They synthesised a series of porous solids containing Ni^{2+} and Pt^{2+} metal centres, linked by 4-pyridinealdoxime, isonicotinamide or isonicotinic acid ligands, in which the included guest molecules were either H_2O or the ligand molecules themselves[55].

As in Werner clathrates, the metal atom is coordinated to four equatorial substituted-pyridine ligands. The counterions, however, are often displaced by water, leaving a cationic host framework containing channels in which the counterions are accommodated. The preparation of Werner clathrates in which hydrogen bonding substituents are present on the pyridine ligands provides the link between the classical Werner clathrates and coordination polymers. These hydrogen bonded Werner clathrate compounds would be closely related to the hydrogen bonded networks described by Aakeröy.

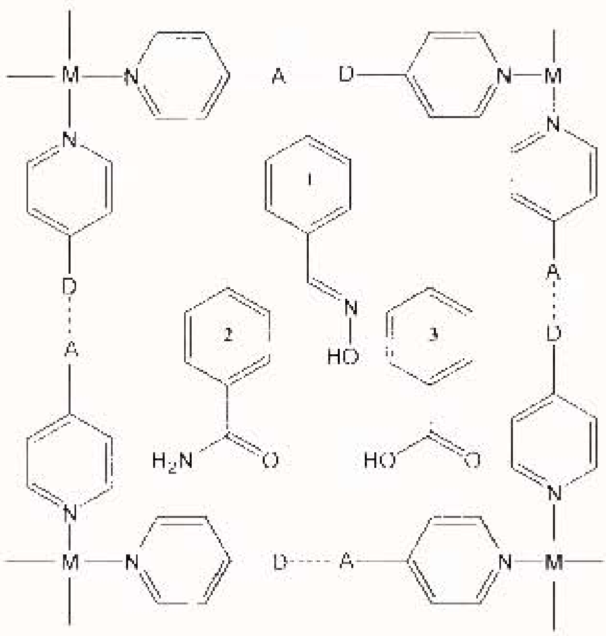

1 = 4-pyridinealdoxime

2 = isonicotinamide

3 = isonicotinic acid

Fig 1.13: The type of host framework generated by head-to-head hydrogen bonds between ligand substituents (A,D = hydrogen bond acceptor and donor, respectively)[55].

1.9 About this Study

One could imagine the various complexes described above as defining a type of spectrum. At one end are the classical Werner clathrates, of general formula MX_2A_4, where A is a pyridine ligand with a hydrocarbon substituent. The guest molecules are located in hydrophobic environments, and only weak van der Waals interactions exist within the crystal structure. At the other end of the spectrum are the **1**-, **2**- and **3**-D coordination networks, in which the metal centres are directly linked by linear, bridging ligands, such as pyrazine and 4,4'-bipyridine.

In the 'grey area' between these two extremes, we find the hydrogen-bonded networks and the polymeric Werner clathrates. In polymeric Werner clathrates, the substituent on the pyridine ring results in one or more ligands in the coordination sphere of the metal atom acting as bridging ligands. The hydrogen bonded networks are generated by ligands in which the substituent on the pyridine ring is not bridging, but rather supports a network of hydrogen bonding interactions. In both of these cases it is highly likely that any guest component with hydrogen bonding capabilities would also contribute to the hydrogen bonded network.

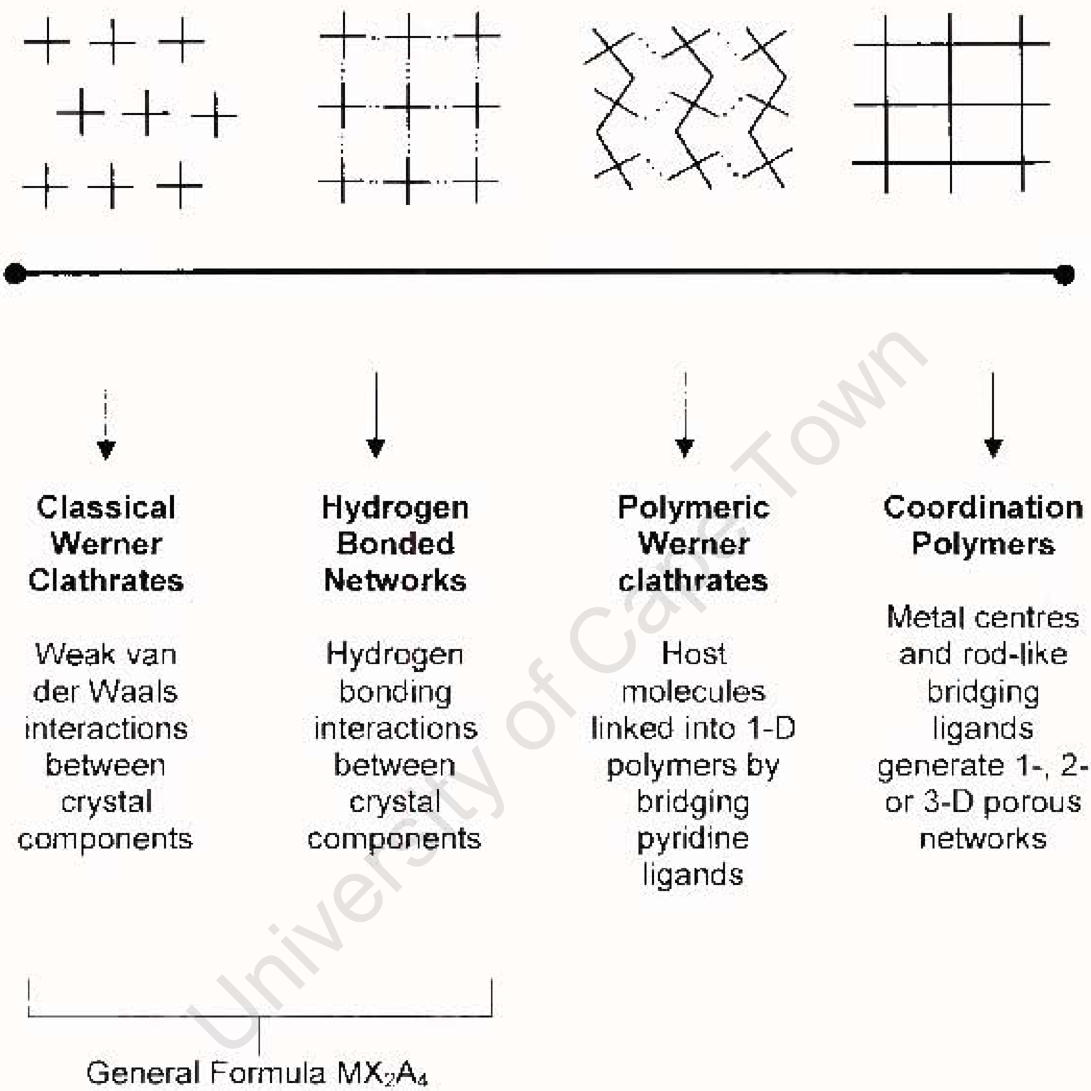

Relatively little work has been done in the area of hydrogen bonded networks, and even less on polymeric Werner clathrates. The aim of this study is to investigate the host-guest compounds formed by a variety of pyridine ligands with hydrogen bonding substituents, and to compare the properties of the compounds formed with those of the classical Werner clathrates and the porous solid structures.

REFERENCES

1) H. M. Powell, *J. Chem. Soc.*, (1948) 61.
2) J. E. D. Davies, *J. Incl. Phenom. Mol. Recog. Chem.*, 32 (1998) 499.
3) (a) E. Jóna, M. Koman, A. Sirota, *J. Incl. Phenom. Mol. Recog. Chem.*, 30 (1998) 1; (b) M. H. Moore, L. R. Nassimbeni, *Acta Cryst. A*, 40 (1984) C111; (c) M. H. Moore, L.R. Nassimbeni, M. L. Niven, *J. Chem. Soc. Dalton Trans.*, (1987) 2125; (d) M. H. Moore, L.R. Nassimbeni, M. L. Niven, *J. Chem. Soc. Dalton Trans.*, (1990) 369; (e) L. Pang, M. A. Whitehead, G. Bernardinelli, E. A. C. Lucken, *J. Chem. Cryst.*, 24, 3 (1994) 203.
4) (a) M. H. Moore, L. R. Nassimbeni, M. L. Niven, M. W. Taylor, *Inorg. Chim. Acta*, 115 (1986) 211; (b) J. Lipkowski, K. Suwinska, J. Hatt, A. Zielenkiewicz, W. Zielenkiewicz, *J. Incl. Phenom.*, 2 (1984) 317; (c) M. H. Moore, L. R. Nassimbeni, M. L. Niven, *Inorg. Chim. Acta*, 131 (1987) 45; (d) L. Lavelle, L. R. Nassimbeni, *J. Incl. Phenom. Molec. Recog. Chem.*, 16 (1993) 25; (e) L. R. Nassimbeni, M. L. Niven, A. P. Suckling, *Inorg. Chim. Acta*, 159 (1989) 209.
5) (a) M. W. Taylor, L. R. Nassimbeni, *Am. Cryst. Assoc. Abstr. Papers*, 14 (1986) 26; (b) L. R. Nassimbeni, S. Papanicolaou, M. H. Moore, *J. Incl. Phenom.*, 4 (1986) 31; (c) L. R. Nassimbeni, M. L. Niven, M. W. Taylor, *Inorg. Chim. Acta*, 132 (1987) 67; (d) L. R. Nassimbeni, M. L. Niven, M. W. Taylor, *J. Chem. Soc. Dalton Trans.*, (1989) 119; (e) L. Lavelle, L. R. Nassimbeni, M. L. Niven, M. W. Taylor, *Acta Cryst. C*, 45 (1989) 591.
6) L. R. Nassimbeni, M. L. Niven, M. W. Taylor, *Acta Cryst. B*, 46 (1990) 354.
7) P. de Radzitzky, J. Hanotier, *I & EC Process Design and Development*, 1 (1962) 10.
8) L. R. Nassimbeni, M. L. Niven, K. J. Zemke, *Acta Cryst. B*, 42 (1986) 453.
9) W. D. Schaeffer, W. S. Dorsey, D. A. Skinner, C. G. Christian, *J. Am. Chem. Soc*, 79 (1957) 5870.
10) J. E. D. Davies, K. T. Holmes, J. Waterhouse, *Polish J. Chem.*, 56 (1982) 335.
11) S. E. Ofodile, N. O. Smith, *J. Phys. Chem.*, 87 (1983) 473.

12)S. E. Ofodile, R. M. Kellet, N. O. Smith, *J. Am. Chem. Soc.*, 101 (1979) 7725.

13)W. Kemula, D. Sybilska, *Nature*, 185 (1960) 237.

14) W. Kemula, D. Sybilska, *Anal. Chim. Acta*, 38 (1967) 97.

15)W. Kemula, D. Sybilska, J. Lipkowski, K. Duszczyk, *J. Chromatography*, 204 (1981) 23.

16)W. Kemula, D. Sybilska, J. Lipkowski. *J. Chromatography*, 218 (1981) 465.

17)J. Lipkowski, M. Pawlowska, D. Sybilska, *J. Chromatography*, 176 (1979) 43.

18)D. Belitskus, G. A. Jeffrey, R. K. McMullan, N. C. Stephenson, *Inorg. Chem.*, 2, 4 (1963) 873.

19)M. I. Hart, N. O. Smith, *J. Am. Chem. Soc.*, 84 (1962) 1816.

20)E. R. de Gil, I. S. Kerr, *J. Appl. Cryst.*, 10 (1977) 315.

21)J. Lipkowski, *Accademia Polacca delle Scienze, Biblioteca e Centro di Studi a Roma*, Conferenze 81 (1980) 3.

22)J. Lipkowski, K. Suwinska, G. D. Andreetti, K. Stadnicka, *J. Mol. Struct.*, 75 (1981) 101.

23)D. R. Bond, G. E. Jackson, L. R. Nassimbeni, *S. Afr. J. Chem.*, 36 (1983) 19.

24)A. Y. Manakov, J. Lipkowski, K. Suwinska, M. Kitamura, *J. Incl. Phenom. Mol. Recog. Chem.*, 26 (1996) 1.

25)S. A. Allison, R. M. Barrer, *J. Chem. Soc. (A)*, (1969) 1717.

26)J. Lipkowski, in Inclusion Compounds, Vol. 1, ed. J. L. Atwood, J. E. D. Davies, D. D. MacNicol, (1984), ch. 3, pp59-103, and references therein.

27)J. Lipkowski, in Comprehensive Supramolecular Chemistry, Vol. 6, ed. D. D. MacNicol, F. Toda, R. Bishop, (1996), Pergamon, ch 20, pp691-714, and references therein.

28)J. Lipkowski, P. Starzewski, W. Zielenkiewicz, *Thermochim. Acta*, 49 (1981) 269.

29)W. Kemula. J. Lipkowski, D. Sybilska, *Roczniki Chemii*, 48 (1974) 3.

30)J. Lipkowski, P. Sgarabotto, G. D. Andreetti, *Acta Cryst. B*, 36 (1980) 51.

31)J. Lipkowski, P. Sgarabotto, G. D. Andreetti, *Acta Cryst. B*, 38 (1982) 416.

32)J. Lipkowski, G. D. Andreetti, *Acta Cryst. B*, 38 (1982) 607.

33)J. Lipkowski, *Acta Cryst. B*, 38 (1982) 1745.

34)J. Lipkowski. D. V. Soldatov, *J. Incl. Phenom. Mol. Recog. Chem.*, 18 (1994) 317.

35)P. Losier, M. J. Zaworotko, *J. Chem. Cryst.*, 26, 4 (1996) 277.

36)G. D. Andreetti, G. Bocelli, P. Sgarabotto, *Cryst. Struct. Comm.*, 1 (1972) 51.

37)I. S. Kerr, D. J. Williams, *Acta Cryst. B*, 33 (1977) 3589.

38)M. Sitarski, J. Lipkowski, *Roczniki Chemii*, 50 (1976) 1129.

39)A. Y. Manakov, J. Lipkowski, *Thermochim. Acta*, 277 (1996) 199.

40)J. Lipkowski, A Zielenkiewicz, J. Hatt, W. Zielenkiewicz, *J. Incl. Phenom. Mol. Recog. Chem.*, 7 (1989) 519.

41)J Lipkowski, *J. Mol. Struct.*, 75 (1981)13.

42)J. Lipkowski, A. Bylina, K. Duszczyk, K. Lesniak, D. Sybilska, *Chemia Analityczna*, 19 (1974)1051.

43)A. Guarino, G. Occhiucci, E Possagno, R. Bassanelli, *Spectrochim. Acta*, 33A (1977) 199.

44)A. Y. Manakov, J. Lipkowski, J. Pielaszek, *J. Incl. Phenom. Macrocyclic Chem.*, 35 (1999) 531.

45)A. Y. Manakov, J. Lipkowski, *J. Incl. Phenom. Macrocyclic Chem.*, 33 (1999) 121.

46)C. Karunakaran, K. R. J. Thomas, A. Shunnugasundaram, R. Murugesan, J. Incl. Phenom. *Macrocyclic Chem.*, 38 (2000) 233.

47)D. V. Soldatov, G. D. Enright, J. A. Ripmeester, *Supramol. Chem.*, 11 (1999) 35.

48)C. B. Aakeröy, A. M. Beatty, D. S. Leinen, *Cryst. Eng. Comm.*, (2000) 27 (http://www.rsc.org/ej/ce/2000/b006043g/index.htm).

49)M. H. Moore, L. R. Nassimbeni, M. L. Niven, *Inorg. Chim. Acta*, 132 (1987) 61.

50)J. Lipkowski, G. D. Andreetti, *Transition Metal Chem.*, 3 (1978) 117.

51)R. M. Semeniuc, E. Ihla, G. D. Roman, L. Ghergari, *Revue Roumaine de Chimie*, 28, 5 (1983) 471.

52)(a) L. Carlucci, G. Ciani, D. M. Proserpio, A. Sironi, *J. Am. Chem. Soc.*, 117 (1995) 4562; (b) L. Carlucci, G. Ciani, D. M. Proserpio, A. Sironi, *Angew. Chem. Int. Ed. Engl.*, 34 (1995) 1895; (c) S. Kitagawa, M. Munakata, T. Tanimura, *Inorg. Chem.*, 31 (1992) 1714.

53)(a) M. Fujita, Y. J. Kwon, S. Washizu, K. Ogurak, *J. Am. Chem. Soc.*, 116 (1994) 1151; (b) S. Subramanian, M. J. Zaworotko, *Angew. Chem. Int. Ed. Engl.*, 34 (1995) 2127; (c) J. Lu, T. Paliwala, S. C. Lim, C. Yu, T. Niu, A. J. Jacobson. *Inorg. Chem.*, 36 (1997) 923; (d) R. W. Gable, B. F. Hoskins, R. Robson, *J. Chem. Soc. Chem. Comm.*, (1990) 1677; (e) K. Biradha, K. V. Domasevitch, C. Hogg, B. Moulton, K. N. Ower, M. J. Zaworotko, *Crystal Engineering*, 2, 1 (1999) 37; (f) J. T. Sampanther, J. J. Vittal, *Crystal Engineering*, 2, 4 (1999) 251; (g) S. Noro, S. Kitagawa, M. Kondo, K. Seki, *Angew. Chem. Int. Ed. Engl.*, 39 (2000) 2081; (h) M. Tong, X. Chen, *Cryst. Eng. Comm.*, (2000) 1 (http://www.rsc.org/ej/ce/2000/a909748a/index.htm)

54)K. Biradha, Y. Hongo, M. Fujita, *Angew. Chem. Int. Ed.*, 39 (2000) 3843.

55)C. B. Aakeröy, A. M. Beatty, D. S. Leinen, *Angew. Chem. Int. Ed.*, 38 (1999) 1815.

CHAPTER 2

EXPERIMENTAL TECHNIQUES

EXPERIMENTAL

2.1 General Synthetic Procedure

All syntheses involved the addition of a solution of the organic ligand to a solution of the metal salt, in metal:ligand ratios of 1:2 and 1:4. All solvents and reagents were used as received, without further purification.

Table 2.1: Metal salts and organic ligands used in syntheses

Metal Salts	Organic ligands
$Ni(NCS)_2$	pyrazine (1)
$ZnSO_4.7H_2O$	isonicotinamide (2)
$ZnBr_2$	3-cyanopyridine (3)
$CuSO_4$	3-aminopyridine (4)
	3-hydroxypyridine (5)
	4-aminopyridine (6)
	4-cyanopyridine (7)

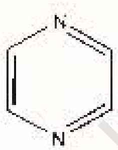

1

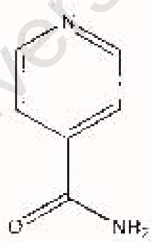

2

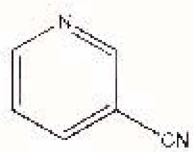

3

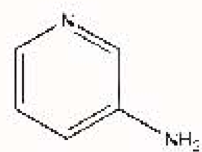

4

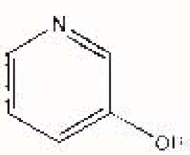

5

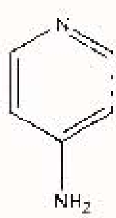

6

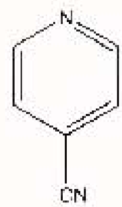

7

2.2 Syntheses

2.2.1 NiHost1: $Ni(NCS)_2$(4-aminopyridine)$_4$

2.2.1.1 Single crystals:

4ml of a 0.1M methanolic solution of 4-aminopyridine (0.4mmol, 0.038g) was added to 1ml of a 0.1M ethanolic solution of $Ni(NCS)_2$ (0.1mmol, 0.017g). The solution was allowed to stand at room temperature and purple, needle-like crystals of $Ni(NCS)_2$(4-aminopyridine)$_4$ formed within one week. The same result was obtained when the ligand was dissolved in either ethanol or water.

2.2.1.2 Powder:

80ml of a 0.1M methanolic solution of 4-aminopyridine (8mmol, 0.753g) was added to 20ml of a 0.1M ethanolic solution of $Ni(NCS)_2$ (2mmol, 0.350g). The solution was stirred at room temperature until most of the solvent had evaporated, and the resulting purple powder of $Ni(NCS)_2$(4-aminopyridine)$_4$ was filtered and dried in air at room temperature.

2.2.2 NiEtAc: $Ni(NCS)_2$(4-aminopyridine)$_4$.EtOH.Acetone

2.2.2.1 Single crystals:

4ml of a 0.1M solution of 4-aminopyridine in acetone (0.4mmol, 0.038g) was added to 1ml of a 0.1M ethanolic solution of $Ni(NCS)_2$ (0.1mmol, 0.017g). The solvent was allowed to evaporate slowly at room temperature and purple, block-like crystals of $Ni(NCS)_2$(4-aminopyridine)$_4$.EtOH.Acetone formed overnight.

2.2.3 NiDMSO: $Ni(NCS)_2(4\text{-aminopyridine})_4.2DMSO$

2.2.3.1 Single crystals:

4ml of a 0.1M methanolic solution of 4-aminopyridine (0.4mmol, 0.038g) was added to 1ml of a 0.1M solution of $Ni(NCS)_2$ in dimethylsulphoxide (DMSO) (0.1mmol, 0.017g). The solution was allowed to stand at room temperature and purple, needle-like crystals of $Ni(NCS)_2(4\text{-aminopyridine})_4.2DMSO$ formed after several weeks.

2.2.4 NiHost2: $Ni(NCS)_2(3\text{-cyanopyridine})_4$

2.2.4.1 Single crystals:

4ml of a 0.1M aqueous solution of 3-cyanopyridine (0.4mmol, 0.042g) was added to 1ml of a 0.1M ethanolic solution of $Ni(NCS)_2$ (0.1mmol, 0.017g). The solution was allowed to stand at room temperature and blue needle-like crystals of $Ni(NCS)_2(3\text{-cyanopyridine})_4$ formed within one week.

2.2.4.2 Powder:

80ml of a 0.1M aqueous solution of 3-cyanopyridine (8mmol, 0.833g) was added to 20ml of a 0.1M ethanolic solution of $Ni(NCS)_2$ (2mmol, 0.350g). The solution was stirred at room temperature until most of the solvent had evaporated, and the resulting blue powder of $Ni(NCS)_2(3\text{-cyanopyridine})_4$ was filtered and dried in air at room temperature.

2.2.5 NidiEt: $Ni(NCS)_2$(3-cyanopyridine)$_4$.2EtOH

2.2.5.1 Single crystals:

4ml of a 0.1M ethanolic solution of 3-cyanopyridine (0.4mmol, 0.042g) was added to 1ml of a 0.1M ethanolic solution of $Ni(NCS)_2$ (0.1mmol, 0.017g). The solvent was allowed to evaporate slowly at room temperature and purple crystals of $Ni(NCS)_2$(3-cyanopyridine)$_4$.2EtOH formed overnight.

2.2.5.2 Powder:

80ml of a 0.1M ethanolic solution of 3-cyanopyridine (8mmol, 0.833g) was added to 20ml of a 0.1M ethanolic solution of $Ni(NCS)_2$ (2mmol, 0.350g). The solution was stirred at room temperature until most of the solvent had evaporated, and the resulting purple powder of $Ni(NCS)_2$(3-cyanopyridine)$_4$.2EtOH was stored under mother liquor until use.

2.2.6 NidiDCM: $Ni(NCS)_2$(3-cyanopyridine)$_4$.2CH_2Cl_2

2.2.6.1 Single crystals:

4ml of a 0.1M solution of 3-cyanopyridine in dichloromethane (0.4mmol, 0.042g) was added to 1ml of a 0.1M ethanolic solution of $Ni(NCS)_2$ (0.1mmol, 0.017g). The solvent was allowed to evaporate slowly at room temperature and purple crystals of $Ni(NCS)_2$(3-cyanopyridine)$_4$.2CH_2Cl_2 formed over several days.

2.2.6.2 Powder:

80ml of a 0.1M solution of 3-cyanopyridine in dichloromethane (8mmol, 0.833g) was added to 20ml of a 0.1M ethanolic solution of $Ni(NCS)_2$ (2mmol, 0.350g). The solution was stirred at room temperature until precipitation of the purple powder of $Ni(NCS)_2$(3-cyanopyridine)$_4$.2CH_2Cl_2 had occurred. The powder was stored under mother liquor until use.

2.2.7 Nitriaq: $Ni(NCS)_2$(isonicotinamide)$_3$(H_2O).3H_2O

2.2.7.1 Single crystals:

4ml of a 0.1M aqueous solution of isonicotinamide (0.4mmol, 0.049g) was added to 1ml of a 0.1M ethanolic solution of $Ni(NCS)_2$ (0.1mmol, 0.017g). The solution was allowed to stand at room temperature and blue aggregates of $Ni(NCS)_2$(isonicotinamide)$_3$(H_2O).3H_2O formed within one week.

2.2.7.2 Powder:

80ml of a 0.1M aqueous solution of isonicotinamide (8mmol, 0.977g) was added to 20ml of a 0.1M ethanolic solution of $Ni(NCS)_2$ (2mmol, 0.350g). The solution was stirred at room temperature until most of the solvent had evaporated, and the resulting blue powder of $Ni(NCS)_2$(isonicotinamide)$_3$(H_2O).3H_2O was stored under mother liquor until use.

2.2.8 Nipcres: $Ni(NCS)_2$(isonicotinamide)$_4$.4EtOH.2*p*-cresol

2.2.8.1 Single crystals:

0.098g (0.8mmol) isonicotinamide was dissolved in a minimum volume of *p*-cresol, and the resulting solution was added to 2ml of a 0.1M ethanolic solution of $Ni(NCS)_2$ (0.2mmol, 0.035g). The solution was allowed to stand at 4°C, and irregular purple crystals of $Ni(NCS)_2$(isonicotinamide)$_4$.2*p*-cresol.4EtOH formed after several months. When the same solution was allowed to stand at room temperature green crystals, unsuitable for structure analysis, were formed. All further attempts to synthesise crystals of **Nipcres** yielded only the green crystals, possibly due to a seeding problem.

2.2.9 Nimcres: $Ni(NCS)_2$(isonicotinamide)$_4$.4*m*-cresol

2.2.9.1 Single crystals:

0.098g (0.8mmol) isonicotinamide was dissolved in a minimum volume of *m*-cresol, and the solution added to 2ml of a 0.1M ethanolic solution of $Ni(NCS)_2$ (0.2mmol, 0.035g). The solution was allowed to stand at 4°C, and purple crystals of $Ni(NCS)_2$(isonicotinamide)$_4$.4*m*-cresol formed after several months. As above, leaving the same solution to stand at room temperature resulted in the formation of green crystals. All further attempts to synthesise pure **Nimcres** resulted in the crystallisation of a mixture of purple and green crystals.

2.2.10 NiEt: $Ni(NCS)_2$(3-aminopyridine)$_3$.EtOH

2.2.10.1 Single crystals:

2ml of a 0.1M aqueous solution of 3-aminopyridine (0.2mmol, 0.019g) was added to 1ml of a 0.1M ethanolic solution of $Ni(NCS)_2$ (0.1mmol, 0.017g). The solvent was allowed to evaporate slowly at room temperature and dark green crystals of $Ni(NCS)_2$(3-aminopyridine)$_3$.EtOH formed within a week.

2.2.10.2 Powder:

40ml of a 0.1M aqueous solution of 3-aminopyridine (4mmol, 0.377g) was added to 20ml of a 0.1M ethanolic solution of $Ni(NCS)_2$ (2mmol, 0.350g). The solution was stirred at room temperature until most of the solvent had evaporated, and the resulting green powder of $Ni(NCS)_2$(3-aminopyridine)$_3$.EtOH was stored under mother liquor until use.

2.2.11 NiMe: $Ni(NCS)_2(3\text{-aminopyridine})_3.MeOH$

2.2.11.1 Single crystals:

2ml of a 0.1M methanolic solution of 3-aminopyridine (0.2mmol, 0.019g) was added to 1ml of a 0.1M methanolic solution of $Ni(NCS)_2$ (0.1mmol, 0.017g). The solvent was allowed to evaporate slowly at room temperature and dark green crystals of $Ni(NCS)_2(3\text{-aminopyridine})_3.MeOH$ formed within a few days. XRD was performed on crushed crystals of **NiMe** rather than the powder form, which did not precipitate readily from solution.

2.2.12 Niaq: $Ni(NCS)_2(3\text{-aminopyridine})_2(H_2O).H_2O$

2.2.12.1 Single crystals:

80ml of a 0.1M aqueous solution of 3-aminopyridine (8mmol, 0.753g) was added to 20ml of a 0.2M ethanolic solution of $Ni(NCS)_2$ (4mmol, 0.699g). The resulting murky solution was filtered and allowed to stand at room temperature. Crystals started forming immediately. Examining the crystals under a microscope revealed two different types of crystals to be present in the system, pale blue single crystals of $Ni(NCS)_2(3\text{-aminopyridine})_2(H_2O).H_2O$, and turquoise clusters. The turquoise clusters did not yield crystals suitable for diffractometry, but thermal analysis indicated a formula of $Ni(NCS)_2(3\text{-aminopyridine})_3$.

2.2.13 $ZnBr_2pyz_2$ and $ZnBr_2pyz$: $ZnBr_2(pyrazine)_2$ and $ZnBr_2(pyrazine)_1$

2.2.13.1 Single crystals:

2ml of a 0.14M ethanolic solution of pyrazine (0.28mmol, 0.022g) was added to 4ml of a 0.018M ethanolic solution of $ZnBr_2$ (0.072mmol, 0.016g). The solution was allowed to stand at room temperature and pale yellow crystals of

$ZnBr_2(pyrazine)_2$ formed over several weeks. When the same procedure was followed, but the solution allowed to stand at 4°C, plate-like colourless crystals of $ZnBr_2(pyrazine)$ formed overnight.

2.2.13.2 Powder:

25ml of a 0.2M ethanolic solution of pyrazine (5mmol, 0.400g) was added to 6.2ml of a 0.2M ethanolic solution of $ZnBr_2$ (1.24mmol, 0.280g). The solution was stirred at room temperature until most of the solvent had evaporated, and the resulting white powder was filtered. The powder was analysed and found to be $ZnBr_2(pyrazine)$.

2.2.13.3 Solid State Synthesis of $ZnBr_2(pyrazine)_2$ from $ZnBr_2(pyrazine)$:

0.039g (0.49mmol) pyrazine was added to 0.150g (0.49mmol) of the $ZnBr_2(pyrazine)$ powder synthesised in 2.2.13.2. The mixture was placed in a glass vial and shaken (without grinding) in a WIG-L-BUG for 30 min at room temperature.

2.2.1 4 ZnpyzSulf: $Zn(H_2O)_4(pyrazine).SO_4.2H_2O$

2.2.14.1 Single crystals:

4ml of a 0.2M ethanolic solution of pyrazine (0.8mmol, 0.064g) was layered on 1ml of a 0.2M aqueous solution of $ZnSO_4.7H_2O$ (0.2mmol, 0.057g). The solution was allowed to stand at room temperature, and colourless crystals of $Zn(H_2O)_4(pyrazine).SO_4.2H_2O$ formed at the H_2O:ethanol boundary after a few days.

2.2.14.2 Powder:

20ml of a 0.2M ethanolic solution of pyrazine (4mmol, 0.32g) was added to 5ml of a 0.2M aqueous solution of $ZnSO_4.7H_2O$ (1mmol, 0.29g). The resulting cloudy solution was stirred overnight at a slightly elevated temperature. A fine white powder of $Zn(H_2O)_4$(pyrazine)$.SO_4.2H_2O$ formed, which was stored under mother liquor until use.

2.2.15 Cudiaq: Cu(isonicotinamide)$_2$(H_2O)(SO_4).$2H_2O$

2.2.15.1 Single crystals:

4ml of a 0.1M aqueous solution of isonicotinamide (0.4mmol, 0.049g) was added to 1ml of a 0.1M aqueous solution of $CuSO_4$ (0.1mmol, 0.016g). The solution was allowed to stand at room temperature and blue, needle-like crystals of Cu(H_2O)(isonicotinamide)$_2$(SO_4).$2H_2O$ formed within one week.

2.2.15.2 Powder:

80ml of a 0.1M aqueous solution of isonicotinamide (8mmol, 0.977g) was added to 20ml of a 0.1M aqueous solution of $CuSO_4$ (2mmol, 0.319g). The solution was stirred at room temperature until most of the water had evaporated, and the resulting blue powder of Cu(H_2O)(isonicotinamide)$_2$(SO_4).$2H_2O$ was filtered and dried in air at room temperature.

2.3 Thermal Analysis

Thermal analysis involves measuring the changes in the physical properties of a sample as a function of temperature or time, as the sample is subjected to a controlled temperature program[1]. Several thermal analysis techniques, namely Differential Scanning Calorimetry (DSC), Thermogravimetry (TG) and Hot-stage

Microscopy (HSM), were employed in the characterisation of the above-mentioned compounds.

2.3.1 Differential Scanning Calorimetry

Power-compensated Differential Scanning Calorimetry measures the difference in energy input (heat flow) into a sample and reference compound as a function of temperature, while the sample and reference are subjected to a controlled temperature program. DSC can detect any reaction occurring in the sample that consumes or releases heat (endothermic and exothermic respectively), and has the advantage that the enthalpy of reaction, ΔH, can be determined from the area under the DSC peak. DSC is commonly applied to the detection of melts, phase transitions, polymorphic transitions, recrystallisations and decomposition reactions.

The instrument used was a Perkin Elmer DSC7. Vented aluminium pans were used for both sample and reference materials. All DSC scans were run with an empty pan as the reference, at a heating rate of $20^{\circ}C.min^{-1}$. The sample sizes varied from 1 to 5mg, and were weighed on an electronic balance sensitive to $1\mu g$. Nitrogen was used as the purge gas, at a flow rate of $30ml.min^{-1}$. The enthalpy of a reaction was calculated in kJ per mole of host:guest compound for the release of the guest component from the host:guest complex, and in kJ per mole of host compound alone for the decomposition of the host complex. At the suggestion of Professor M. E. Brown (Professor of Chemistry at Rhodes University, South Africa, and author of Reference 1), the enthalpy of a guest release reaction was also calculated in kJ per mole of guest alone. This value was then compared with the enthalpy of vaporisation of the liquid guest. For reactions where the DSC peak corresponded to the release of more than one host or guest component, the enthalpy value quoted corresponds to that of the processes combined.

2.3.2 Thermogravimetry

Thermogravimetry measures the mass of a sample as a function of temperature, as the sample is subjected to a controlled temperature program. This technique is extensively employed in the study of host:guest compounds, where the change in mass of the sample during guest release is used to determine the host:guest ratio of the complex. The kinetics of desolvation of a host:guest compound can also be studied by Isothermal Thermogravimetric Analysis.

The instrument used was a Perkin Elmer TGA7. The samples, which varied in size from 2 to 5mg, were placed in an open platinum pan and weighed on the in-built electronic balance. Nitrogen was used as the purge gas, at a flow rate of $40ml.min^{-1}$ through the furnace and $60ml.min^{-1}$ through the balance mechanism. A heating rate of $20°C.min^{-1}$ was used for all samples, unless stated otherwise.

2.3.3 Hot stage Microscopy

Hot stage microscopy involves observing the outward appearance of a sample during heating. The observations can be recorded using high-resolution colour photographic equipment or, more recently, video cameras. HSM is primarily used to verify certain events (including melting, crystallisation, solidification, desolvation and polymorphic transitions) that have been observed using other thermal techniques such as DSC and TG.

All observations were made on a Nikon microscope fitted with a Linkam THMS600 hot stage and Linkam TP92 temperature controller. Images were captured using a real-time Sony Digital Hyper HAD colour video camera, and analysed using the Soft Imaging System program, analySIS[7]. One or several crystals were placed in a drop of silicone oil between two glass coverslips. The crystals were placed on the hot stage, and the heating program initiated. The release of a guest component from a host:guest compound is observed as the evolution of bubbles from the sample into the surrounding oil. A heating rate of 20°C.min^{-1} was used for all samples, so that the observations would be compatible with the data obtained by DSC and TGA.

2.4 X-Ray Photography

X-ray photographs were taken on a Stoe camera using Ni-filtered Cu-K_{α} radiation (λ = 1.5418Å). The camera was used in conjunction with a Philips PW1120/00 generator, operated at 20mA and 40kV. Photography was performed on all new compounds unless the crystals were too unstable or very small.

2.4.1 Oscillation Photography

A single crystal was glued to the tip of a glass fibre and mounted on a goniometer head. The crystal was centred in the x-ray beam, such that it was not precessing. An oscillation photograph was taken, with an exposure time of approximately one hour. The distance between corresponding layer lines (±1 and ±2) was measured in mm and divided by 2 or 4. The results were averaged over the two sets of layer lines and converted to a value in Å. The photograph was inspected for elements of symmetry relating the intensities of the diffracted spots, with mirroring indicating a monoclinic or higher crystal system.

2.4.2 Weissenberg Photography

Weissenberg photography allows a one-dimensional layer line in the oscillation photograph to be expanded into two dimensions[3]. This is achieved by simultaneously rotating the crystal and moving the x-ray film. A screen is used to ensure that only those diffraction spots corresponding to the selected layer line reach the film. A single Weissenberg photograph of the zero layer line was taken for each of the single crystals. The diffraction spots on the photograph were plotted on graph paper, using a transparent Weissenberg coordinate chart, to obtain a representation of the reciprocal lattice. From this plot the lengths of the other two cell axes, as well as one of the angles, could be determined. Mirroring in the Weissenberg photograph alone indicates a monoclinic crystal system, whereas mirroring in both photographs indicates an orthorhombic, or higher, crystal system.

2.5 Single Crystal X-Ray Diffractometry

A single crystal of suitable size and quality was selected and fixed to the tip of a glass fibre with Paratone oil. The intensity data for each crystal were collected on a Nonius Kappa CCD Single Crystal X-ray Diffractometer, using graphite-monochromated Mo-K_{α} radiation (λ = 0.7107Å) generated by an Enraf Nonius FR590 generator operated at 50kV and 30mA. The crystal-detector distance varied between 35mm and 47mm. For those data collections that were performed at low temperature, the crystals were cooled on the diffractometer using an Oxford Cryostream low temperature attachment. The intensity data were processed using the DENZO-SMN software package[4]. The space group was determined by examining the systematic absences and matching the observed conditions to a known space group[5]. Assignment of the correct space group was confirmed using the Xprep program[6].

The structures were solved using the direct methods option in SHELXS-97[7], operated through the X-Seed interface[8]. In cases where direct methods failed, the Patterson method was used. The structures were developed using least-squares refinement and Fourier difference synthesis in SHELXL-97[7]. All non-hydrogen atoms were located on the electron density map and refined anisotropically. Hydrogen atoms that were located on the electron density map were refined isotropically, while those that were not were placed in geometrically calculated positions. Those hydrogen atoms that had to be placed were assigned isotropic thermal parameters 1.2 times that of the parent atom for aromatic, hydroxyl and amino hydrogens, and 1.5 times that of the parent atom for methyl hydrogens.

The Ortep diagrams showing thermal ellipsoids were generated by Ortep-3 for Windows[9], while all packing diagrams were created through POV-Ray for Windows[10]. The calculated XRD traces for the crystal structure solutions were generated by the Lazy-Pulverix software package[11]. Slices through the unit cell were viewed using the Section program in X-Seed.

2.6 X-Ray Powder Diffraction

The powder was ground to obtain a uniform particle size and loaded into an aluminium tray. The sample surface was cut to avoid preferred orientation. The powdered samples were run on a Philips PW1752/00 diffractometer using CuK_{α} radiation (λ = 1.5418Å). The experimental XRD curves obtained in this way were compared with the XRD patterns generated from the single crystal structure solutions. Significant deviations between the calculated and experimental XRD curves indicate a difference in structure and/or chemical composition between the single crystal and powder forms.

2.7 Microanalysis

All microanalyses were performed in duplicate on a Fisons Elemental Analyser 1108. Vacuum techniques were not used in the case of inclusion compounds to prevent desolvation of the host. The samples were analysed for C, H, N and S.

REFERENCES

1) M. E. Brown, Introduction to Thermal Analysis: Techniques and Applications, Chapman and Hall, London, New York, (1988), pp1-39.
2) Soft Imaging System GmbH: Digital Solutions for Imaging and Microscopy, v3.1 for Windows, © 1987-2000.
3) G. H. Stout, L. H. Jensen, X-Ray Structure Determination: a Practical Guide, Macmillan Company, New York, (1968), pp83-109.
4) Z. Otwinowski, W. Minor, In Methods in Enzymology, ed. C. W. Carter, R. M. Sweet, Academic Press. London, (1996).
5) International Tables for Crystallography, Vol. C: Mathematical, Physical and Chemical Tables, ed. A. J. C. Wilson, Kluwer Academic Publishers, Dordrecht, (1992) ch9, pp691-778.
6) Data Preparation and Reciprocal Space Exploration, v. 5.1, © Bruker Analytical X-ray Systems, 1997.
7) G. M. Sheldrick, SHELX-97, University of Göttingen, 1997.
8) L. J. Barbour, X-Seed, A graphical interface to shelx, University of Missouri, Columbia, MO 65211, U.S.A., 1999 (http://www.lbarbour.com/xseed/).
9) C. K. Johnson, M. N. Burnett, Ortep-III Version 1.02, ORNL Report 6895, 1996.
10) Pov-Ray for Windows, v. 3.1e.watcom.win32, The Persistence of Vision Development Team, © 1991 – 1999, (www.povray.org).
11) K. Yvon, W. Jeitschko, E. Parthe, *J. Appl. Cryst.*, 10 (1977) 73.

CHAPTER 3

RESULTS:

CRYSTAL STRUCTURES AND THERMAL ANALYSES

CHAPTER 3.1

WERNER CLATHRATES

H = $Ni(NCS)_2(4\text{-aminopyridine})_4$

Table 3.1.1: Crystal data and refinement parameters for NiHost1

	NiHost1
Molecular Formula	$C_{22}H_{24}N_{10}S_2Ni$
M_r (g/mol)	551.32
Crystal System	Orthorhombic
Space group	Pccn
Z	4
a (Å)	17.046(3)
b (Å)	9.627(2)
c (Å)	16.129(3)
$\alpha = \beta = \gamma$ (°)	90
V (Å^3)	2646.8(9)
D_{calc} (g/cm^3)	1.384
Crystal dimension (mm)	0.40 x 0.33 x 0.24
Temp of data collection (K)	173
Range scanned (θ)	2.39 – 30.24
Index Range	$14 \geq h \geq -23$, $13 \geq k \geq -12$, $20 \geq l \geq -19$
F (000)	1144
μ (mm^{-1})	0.92
No. reflections collected	12674
No. unique reflections	3517(R_{int} = 0.0356)
Completeness	89.0%
Refinement method	Full-matrix L.S. on F^2
Data/restraints/parameters	3517/0/207
Goodness of fit on F^2	1.011
Final R indices ($I>2\sigma(I)$)	R_1=0.0319, wR_2=0.0691
R indices (all data)	R_1=0.0584, wR_2=0.0773
Largest diff. peak and hole	0.335, -0.365 eÅ^{-3}

Table 3.1.2: Crystal data and refinement parameters for NiEtAc and NiDMSO

	NiEtAc	**NiDMSO**
Molecular Formula	$C_{27}H_{36}N_{10}O_2S_2Ni$	$C_{26}H_{36}N_{10}O_2S_4Ni$
M_r (g/mol)	655.47	707.60
Crystal System	Orthorhombic	Orthorhombic
Space group	$P2_12_12_1$	$P2_12_12_1$
Z	4	4
a (Å)	10.5289(2)	10.2639(2)
b (Å)	15.8155(3)	15.7895(3)
c (Å)	21.7001(5)	21.8834(5)
$\alpha = \beta = \gamma$ (°)	90	90
V ($Å^3$)	3613.5(2)	3546.5(2)
D_{calc} (g/cm^3)	1.205	1.325
Crystal dimension (mm)	0.22 x 0.37 X 0.33	0.23 x 0.70 X 0.15
Temp of data collection (K)	173	100
Range scanned (θ)	1.59 – 27.14	1.59 – 27.10
Index Range	$10 \geq h \geq -10$, $17 \geq k \geq -20$, $26 \geq l \geq -27$	$12 \geq h \geq -13$, $17 \geq k \geq -20$, $26 \geq l \geq -28$
F (000)	1376	1480
μ (mm^{-1})	0.69	0.82
No. reflections collected	17030	15491
No. unique reflections	7031 (R_{int} =0.0463)	7790 (R_{int} = 0.0251)
Completeness	90.8%	99.7%
Refinement method	Full-matrix L.S. on F^2	Full-matrix L.S. on F^2
Data/restraints/parameters	7031/0/350	7790/0/403
Goodness of fit on F^2	1.011	1.126
Final R indices ($I>2\sigma(I)$)	R_1=0.0635, wR_2=0.1709	R_1=0.0551, wR_2=0.1234
R indices (all data)	R_1=0.1147, wR_2=0.2001	R_1=0.0629, wR_2=0.1270
Flack x parameter (e.s.d)	-0.0064 (0.0246)	0.0000 (0.0193)
Largest diff. peak and hole	0.745, -0.638 $eÅ^{-3}$	0.780, -0.433 $eÅ^{-3}$

NiHost1 : $Ni(NCS)_2(4\text{-aminopyridine})_4$

MICROANALYSIS:

	%C	%H	%N	%S
Calc for $Ni(NCS)_2(C_5H_6N_2)_4$	47.95	4.39	25.42	11.64
Experimental	47.99	4.39	25.60	11.34

X-RAY PHOTOGRAPHY:

Oscillation photography gave a unit cell length of 15.9Å, while Weissenberg photography revealed the remaining two cell lengths to be 17.0Å and 9.8Å, with an angle between them of 90°. Together the photographs displayed *mmm* Laue symmetry, indicating an orthorhombic unit cell.

SINGLE CRYSTAL X-RAY DIFFRACTOMETRY:

The unit cell obtained by diffractometry was identical to that obtained by photography.

STRUCTURE SOLUTION AND REFINEMENT:

The diffraction data revealed systematic absences indicative of the orthorhombic space group Pccn. The Ni atom was located on a diad at (¾, ¼, z), at Wyckoff position *d*. As a result, only half the complex was located on the electron density map, the other half being generated by the symmetry operation (½-x, ½-y, z).

All non-hydrogen atoms were located on the electron density map and refined anisotropically, while all hydrogen atoms were located on the electron density map and refined isotropically (crystal structure and refinement details are given in Table 3.1.1).

STRUCTURE ANALYSIS:

Solving the structure in Pccn revealed a central Ni atom coordinated to two axial NCS^- counterions and four equatorial 4-aminopyridine ligands, resulting in an irregular octahedral coordination geometry. The pyridine ligands adopt the energetically-favoured propeller conformation (Fig. 3.1.1).

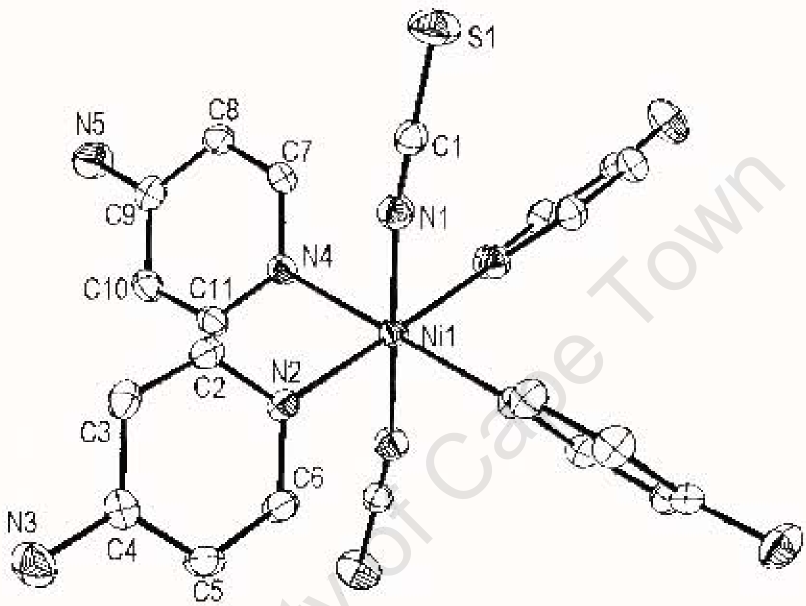

Fig 3.1.1: Ortep diagram for NiHost1, showing thermal ellipsoids (H atoms omitted for clarity).

All bond lengths and angles are within the expected range for compounds of this type. The Ni–N_{CS} bond length is 2.074(2)Å, while both Ni–N_{pyr} bond lengths are 2.118(2)Å. These correspond well with the literature values of 2.04(8)Å and 2.11(6)Å respectively[1]. Full bond lengths and angles are given in Appendix 1.

WEAK HYDROGEN BONDING INTERACTIONS AND CRYSTAL PACKING:

The host molecules are located in columns stacked in the [001] direction, and are related by centres of inversion. The molecules are stabilised by weak intermolecular N–H···N and N–H···S hydrogen bonds, represented in

Fig. 3.1.2a as blue and red dashed lines respectively. Of the two amino groups present in the asymmetric unit, one is planar and acts as a hydrogen bond donor only (N5–H12···S1 and N5–H11···N3). The other is pyramidal, and acts as a hydrogen bond donor (N3–H6···S1) and, via the lone pair on N3, acceptor (N3···H11–N5). Hydrogen bonding data are given in Table 3.1.3.

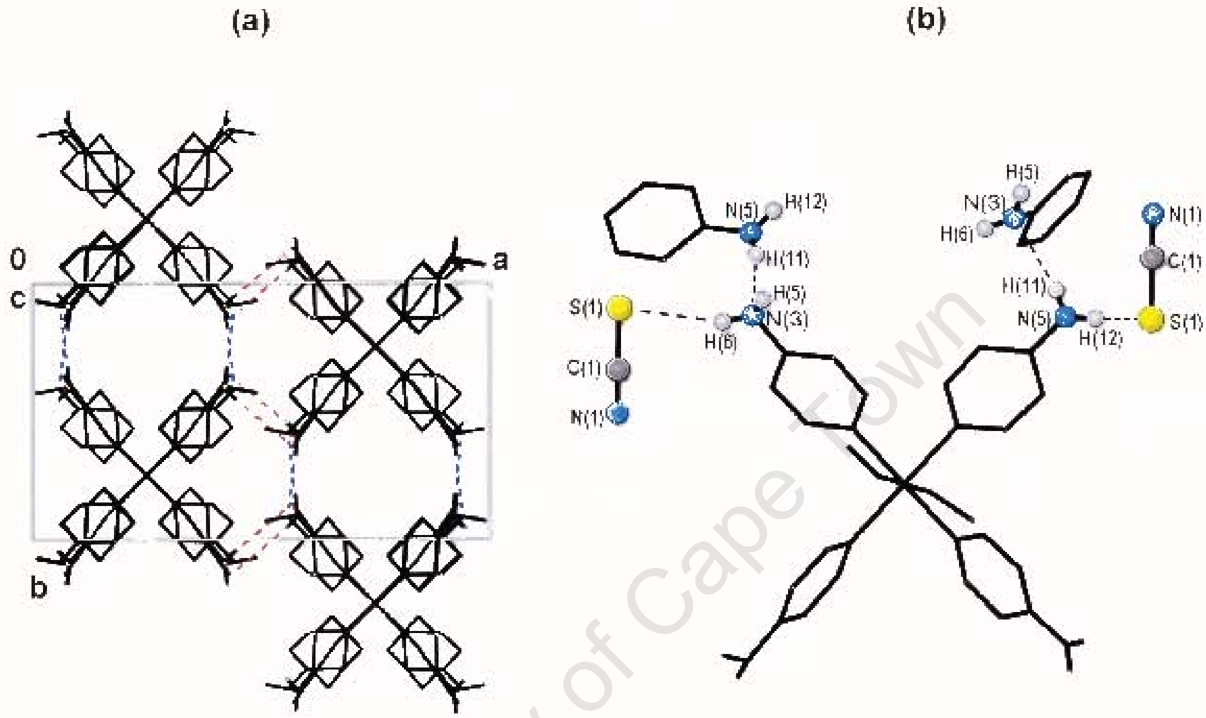

Fig 3.1.2: (a) NiHost1, viewed along [001], showing columns of host molecules linked by intermolecular hydrogen bonding interactions, (b) The three unique hydrogen bonding interactions in NiHost1 (ring H atoms omitted for clarity).

Table 3.1.3: Weak hydrogen bonding interactions in NiHost1

N – H ··· A	N–H (Å)	H···A (Å)	N···A (Å)	Angle (°)
N5 – H11 ··· N3#1	0.843(25)	2.414(25)	3.244(3)	163.4(2.3)
N5 – H12 ··· S1#2	0.854(22)	2.830(21)	3.558(2)	144.1(1.8)
N3 – H6#3 ··· S1	0.820(22)	2.862(23)	3.609(2)	152.4(2.0)

Symmetry codes: #1 = x, ½-y, ½+z, #2 = 1-x, ½+y, ½-z, and #3 = x, ½-y, ½+z.

NiEtAc : $Ni(NCS)_2(4\text{-aminopyridine})_4.EtOH.Acetone$

PRELIMINARY X-RAY PHOTOGRAPHY:

Oscillation photography gave a unit cell length of 10.3Å, while Weissenberg photography revealed the remaining two cell lengths to be 15.6Å and 21.1Å, with an angle between them of 90°. Together the photographs displayed *mmm* Laue symmetry, indicating an orthorhombic unit cell.

SINGLE CRYSTAL X-RAY DIFFRACTOMETRY:

The unit cell obtained by diffractometry was identical to that obtained by photography.

STRUCTURE SOLUTION AND REFINEMENT:

The diffraction data revealed systematic absences indicative of the chiral, orthorhombic space group $P2_12_12_1$. The Ni atom was located in a general position in the unit cell. The ethanol guest was found to be disordered over two positions, with a shared α-C atom. The two fragments were assigned site occupancies which refined to 56.5% and 43.5%.

All non-hydrogen atoms were located on the electron density map and refined anisotropically, with the exception of the acetone and ethanol guest atoms which were refined isotropically. The aromatic and amino hydrogens were placed in geometrically calculated positions, while the hydrogen atoms of the two guest molecules were omitted from the final model (crystal structure and refinement details are given in Table 3.1.2)

STRUCTURE ANALYSIS:

Solving the structure in $P2_12_12_1$ revealed a central Ni atom coordinated to two axial NCS^- counterions and four equatorial 4-aminopyridine ligands. The coordination geometry around the Ni centre is that of an irregular octahedron, and the substituted pyridine ligands adopt the propeller conformation (Fig. 3.1.3).

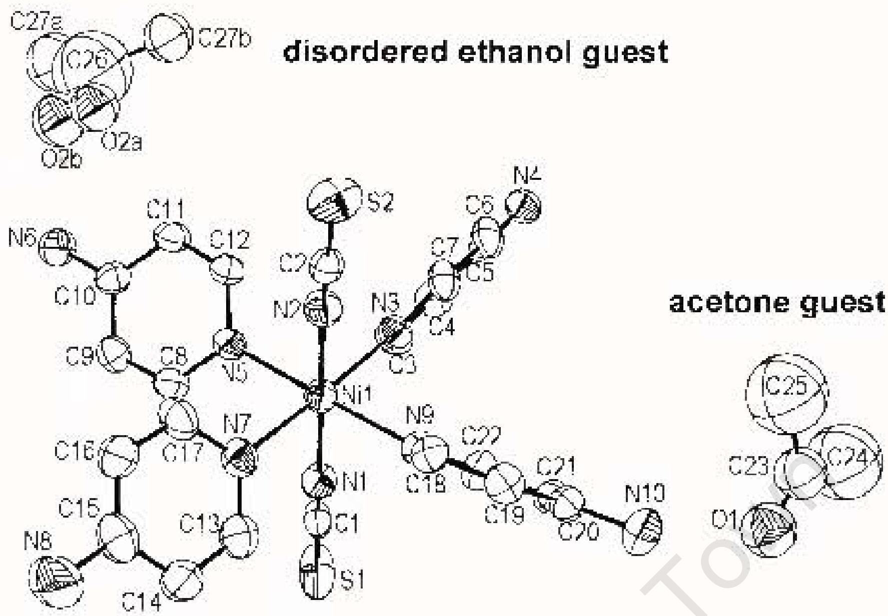

Fig 3.1.3: Ortep plot of NiEtAc showing thermal ellipsoids (H atoms omitted for clarity; a,b notation refers to atoms of a disordered system).

The Ni–N_{CS} bond lengths are 2.068(5)Å and 2.080(5)Å, while the Ni–N_{pyr} bond lengths lie in the range 2.104(5) to 2.128(4)Å. These values correspond well with the literature values of 2.04(8)Å and 2.11(6)Å respectively[1]. Full bond lengths and angles are given in Appendix 1.

The thermal parameters of the ethanol and acetone guest molecules are high compared with those of the host complex. This may be due to the volatile nature of these two liquids, coupled with the potential for excessive thermal motion of the guest molecules in this relatively open channel clathrate.

HYDROGEN BONDING INTERACTIONS:

The hydrogen bonding interactions in **NiEtAc** can be divided into two main groups: (1) those between two host molecules, and (2) those between a host and guest molecule. The host···host interactions are of the type N–H···S. Since each interaction exceeds the sum of the van der Waals radii for the two heavy atoms (3.35Å for N···S), they are classified as weak hydrogen bonds

(Table 3.1.4). Each host molecule is hydrogen bonded to eight neighbouring host complexes, leading to an intricate 3-D hydrogen bonded host network. The ethanol and acetone guests form O···H–N hydrogen bonds to the amino groups of two *trans*-coordinated 4-aminopyridine ligands (Fig. 3.1.4). The host···guest interactions are all shorter than the sum of the van der Waals radii for the two heavy atoms (3.07Å for N···O), falling in the range generally associated with moderately strong hydrogen bonds.

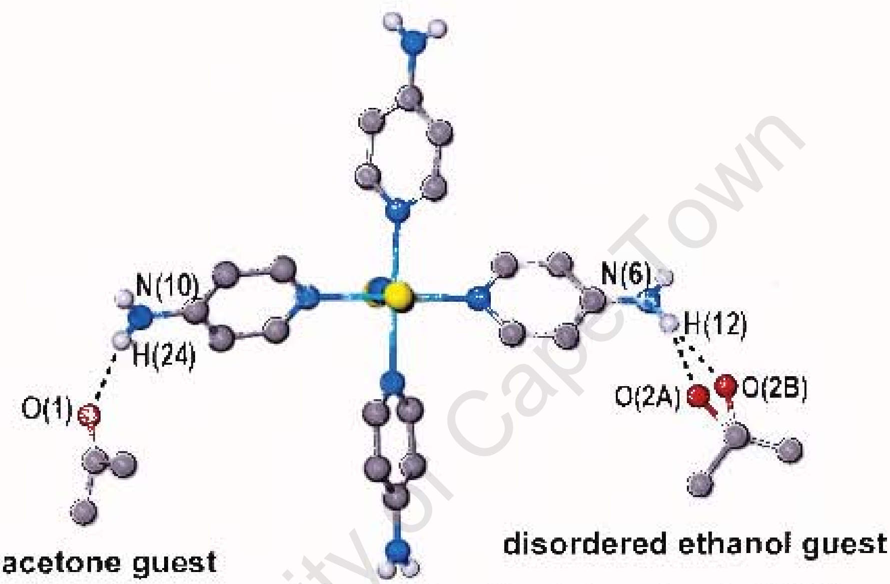

Fig 3.1.4: Host···guest hydrogen bonding interactions in NiEtAc

Table 3.1.4: Hydrogen Bonding data for NiEtAc

N – H ··· O	N–H (Å)	H···O (Å)	N···O (Å)	Angle (°)
HOST···GUEST INTERACTIONS				
N10 – H24 ··· O1	0.880(5)	2.164(6)	3.010(8)	161.0(4)
N6 – H12 ··· O2A	0.880(6)	2.037(14)	2.875(15)	158.7(5)
N6 – H12 ··· O2B	0.880(6)	2.073(13)	2.877(14)	151.4(5)

N – H ··· S	N–H (Å)	H···S (Å)	N···S (Å)	Angle (°)
HOST···HOST INTERACTIONS				
N8 – H18 ··· $S2^{\#1}$	0.880(7)	2.588(2)	3.398(8)	153.4(5)
N6 – H11 ··· $S2^{\#2}$	0.880(5)	2.742(2)	3.502(5)	145.4(3)
N10 – H23 ··· $S1^{\#3}$	0.880(5)	2.783(2)	3.479(5)	137.0(3)
N4 – H5 ··· $S2^{\#4}$	0.880(4)	2.793(2)	3.645(5)	163.2(3)
N4 – H6 ··· $S1^{\#5}$	0.880(5)	2.797(2)	3.640(5)	161.0(3)

Symmetry codes: #1 = x-½, $\frac{3}{2}$-y, 2-z, #2 = $\frac{3}{2}$-x, 2-y, z-½, #3 = ½-x, 2-y, ½+z, #4 = x-½, $\frac{3}{2}$-y, 2-z, and #5 = ½+x, $\frac{3}{2}$-y, 2-z.

NiDMSO : $Ni(NCS)_2(4\text{-aminopyridine})_4.2DMSO$

PRELIMINARY X-RAY PHOTOGRAPHY:

Oscillation photography gave a unit cell length of 10.5Å, while Weissenberg photography revealed the remaining two cell lengths to be 15.7Å and 22.1Å, with an angle between them of 90°. Together the photographs displayed *mmm* Laue symmetry, indicating an orthorhombic unit cell.

SINGLE CRYSTAL X-RAY DIFFRACTOMETRY:

The unit cell obtained by diffractometry was identical to that obtained by photography.

STRUCTURE SOLUTION:

The diffraction data revealed systematic absences indicative of the chiral, orthorhombic space group $P2_12_12_1$. The Ni atom was located in a general position in the unit cell.

In **NiDMSO** and **NiEtAc**, the arrangement of the 4-aminopyridine ligands in a propeller conformation confers chirality on the host molecules. In any one molecule the propeller can define either a clockwise or an anticlockwise rotation. The fact that both **NiEtAc** and **NiDMSO** crystallise in a chiral space group implies that in any one crystal the host molecules all have the same handedness, or chirality. The optical rotation of the mother liquor is zero, indicating that an equal number of 'clockwise' and 'anticlockwise' crystals are formed from solution. As a result, it was found that the host molecules in the crystal of **NiEtAc** chosen for diffractometry were enantiomers of those present in the crystal of **NiDMSO** (Fig. 3.1.5a, the Flack parameter for both structures is given in Table 3.1.2).

(a)

(b)

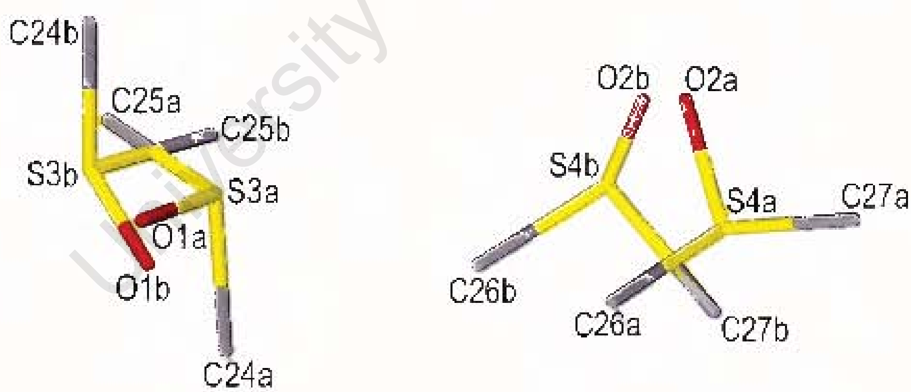

Fig 3.1.5: (a) The enantiomeric host molecules of NiEtAc, left, and NiDMSO, right (H atoms omitted for clarity), (b) disorder in the two DMSO guests.

Both DMSO guest molecules were found to be disordered over two positions, with no shared atoms. The DMSO fragments refined with site occupancies of 63.6% and 36.4% for the first molecule and 68.0% and 32.0% for the second molecule (Fig 3.1.5b).

While all non-hydrogen guest atoms were located on the electron density map and refined, only the four S atoms were refined anisotropically. The hydrogen atoms of the DMSO guests were omitted as a result of the disorder. All non-hydrogen host atoms were located on the electron density map and refined anisotropically. The aromatic and amino hydrogens were placed in geometrically calculated positions.

STRUCTURE ANALYSIS AND REFINEMENT:

As in **NiEtAc**, the Ni atom is coordinated to two axial NCS^- counterions and four equatorial 4-aminopyridine ligands, resulting in an irregular octahedral coordination environment for the Ni centre. The 4-aminopyridine ligands adopt the propeller conformation (Fig. 3.1.5). **NiEtAc** and **NiDMSO** may be regarded as isostructural with respect to the host molecules, differing only in the positions of the guests.

The Ni–N_{CS} bond lengths are 2.068(3)Å and 2.081(3)Å, while the Ni–N_{pyr} bond lengths lie in the range 2.100(3) to 2.121(3)Å. These values are close to the literature values of 2.04(8)Å and 2.11(6)Å respectively[1]. The S=O and S–C bond lengths of the four DMSO guest fragments are all acceptable when compared with the literature values of 1.44(1)Å and 1.78(2)Å respectively (Table 3.1.5)[2]. An investigation of 23 DMSO guest molecules from the CSD gave mean C–S–C and O=S–C angles of 100.6±7.1° and 107.4±4.7° respectively. The angles obtained for the four DMSO fragments in this structure may, therefore, also be considered reasonable. Full bond lengths and angles for **NiDMSO** are given in Appendix 1.

Table 3.1.5: Guest bond lengths and angles for the DMSO fragments

DMSO fragment	S=O (Å)	S–C (Å)	C–S–C Angle (°)	O=S–C Angle (°)
1A	1.460(11)	1.868(19) 1.827(17)	97.6(8)	102.7(8) 107.6(7)
1B	1.512(9)	1.781(8) 1.770(11)	98.7(5)	105.6(5) 105.5(4)
2A	1.474(6)	1.806(16) 1.775(13)	101.3(7)	108.5(5) 103.6(6)
2B	1.462(13)	1.750(20) 1.830(30)	97.6(11)	109.6(10) 107.7(9)

HYDROGEN BONDING INTERACTIONS:

The hydrogen bonding interactions in **NiDMSO** are similar to those in **NiEtAc**. Host···guest N–H···O=S hydrogen bonds are formed between the DMSO fragments and the amino groups of two *trans*-coordinated 4-aminopyridine ligands (Fig. 3.1.6). All four interactions are shorter than sum of the van der Waals radii for the two heavy atoms (3.07Å for N···O), and fall in the range generally associated with moderately strong hydrogen bonds. In addition, several weak N–H···S hydrogen bonding interactions were identified between host molecules (Table 3.1.6).

Table 3.1.6: Hydrogen Bonding data for NiDMSO

N – H ··· O	N–H (Å)	H···O (Å)	N···O (Å)	Angle (°)
HOST···GUEST INTERACTIONS				
N6 – H12 ··· O2A	0.880(5)	2.068(6)	2.899(8)	156.9(3)
N6 – H12 ··· O2B	0.880(5)	1.913(10)	2.769(12)	163.7(4)
N10 – H24$^{\#1}$ ··· O1A	0.880(4)	2.077(10)	2.945(11)	168.6(4)
N10 – H24$^{\#1}$ ··· O1B	0.880(4)	1.985(9)	2.791(10)	151.7(4)

N – H ··· S	N–H (Å)	H···S (Å)	N···S (Å)	Angle (°)
HOST···HOST INTERACTIONS				
N6 – H11 ··· S1#7	0.880(4)	2.729(1)	3.500(4)	147.0(3)
N4 – H5 ··· S1#3	0.880(3)	2.823(1)	3.660(4)	159.5(2)
N4 – H6 ··· S2#4	0.880(3)	2.713(1)	3.554(4)	160.3(2)
N10 – H23 ··· S2#5	0.880(4)	2.690(1)	3.444(4)	144.4(2)
N8 – H18 ··· S1#6	0.880(4)	2.610(1)	3.384(5)	147.2(3)

Symmetry codes: #1 = $\frac{3}{2}$-x, 1-y, z-½, #2 = $\frac{3}{2}$-x, 1-y, z-½, #3 = ½+x, ½-y, 2-**z**, #4 = x-½, ½-y, 2-z, #5 = $\frac{3}{2}$-x, 1-y, ½+z, and #6 = ½+x, $\frac{3}{2}$-y, 2-z

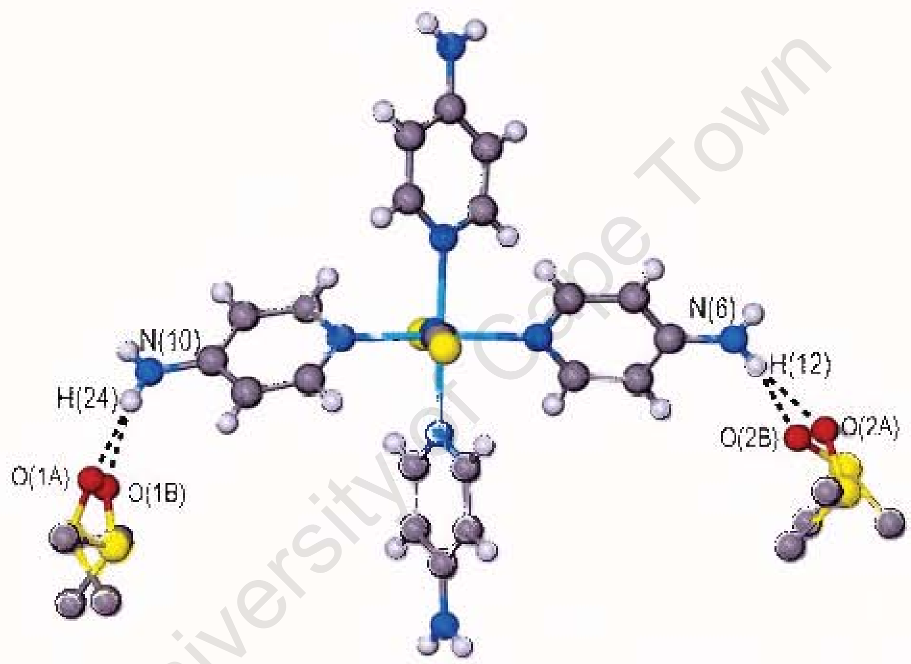

Fig 3.1.6: Host:guest hydrogen bonding interactions in NiDMSO

CRYSTAL PACKING FEATURES OF NiEtAc AND NiDMSO

Assuming that one is considering **NiEtAc** and **NiDMSO** structures of the same polarity, the packing of **NiEtAc** and **NiDMSO** is similar, and the two structures may be regarded as isostructural with respect to the host molecules. The packing of **NiEtAc**, as shown in Fig. 3.1.7a, reveals the guest molecules to be located in channels running parallel to the [100] direction. The minimum channel cross-section is 4.9ÅX5.3Å. Although the aromatic rings of the host molecules appear to be stacked along the [100] direction, adjacent rings are tilted at an angle of approximately 45° relative to each other. A space-filling projection of the channels in **NiEtAc**, with the guest molecules omitted, is shown in Fig. 3.1.7b.

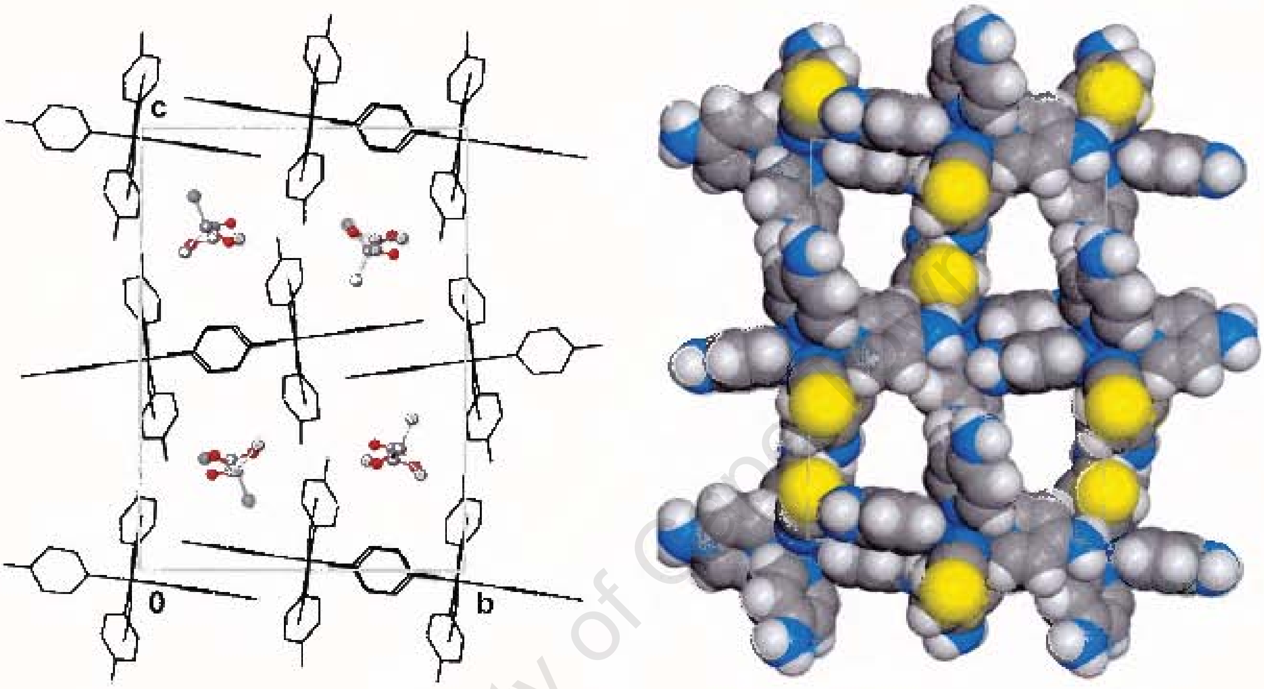

(a) **(b)**

Fig. 3.1.7: The channel structure of NiEtAc, viewed down [100]. (a) Stick representation with hydrogen atoms omitted, (b) space-filling representation with guest atoms omitted.

THERMAL ANALYSIS

The thermal analyses of all three compounds are shown in Figs 3.1.8 and 3.1.10. The host compound, **NiHost1**, decomposes in three distinct steps (Fig. 3.1.8). The first step, **b**, corresponds to the loss of two 4-aminopyridine ligands, followed by steps **c** and **d**, each corresponding to the loss of one 4-aminopyridine ligand. The DSC shows two endotherms corresponding to steps **b** and **c**, but the trace for step **d** is complex due to ligand decomposition. This multi-step decomposition was followed by hot-stage microscopy (Fig. 3.1.9a). The first change observed in the crystals occurs in the temperature range associated with step **b**, when the translucent purple crystals bubble and turn opaque blue-green. The bubbling continues during step **c**, and the crystals turn light green. In the early stages of step **d** the crystals melt to a dark black-brown liquid, confirming the ligand decomposition reaction observed in the DSC.

The inclusion compounds **NiEtAc** and **NiDMSO** undergo an additional, single-step weight loss reaction, shown as step **a** in Figs 3.1.10a and b. This step corresponds to the release of the guest molecules from the channels. The observed weight loss justifies the assignment of a host:guest ratio of 1:2 for both compounds (in the case of **NiEtAc** the presence of two different guests in a 1:1 ratio was also confirmed by GC. The sample was run on a Varian 3400 gas chromatograph with a polar carbowax column 25m in length and 0.25mm in diameter, using He as the carrier gas). Following guest release, the host decomposition reactions, **b-d**, follow the same pattern observed for **NiHost1**. A comparison of the thermal analysis data for **NiEtAc** and **NiDMSO** reveals that the more volatile EtOH/Me_2CO guests are released *ca.* 90° before the DMSO guests. During step **a**, in both **NiEtAc** and **NiDMSO**, the translucent purple crystals turn opaque blue. Thereafter, the crystals turn blue-green, followed by light green, before melting to a brown-black liquid, as observed in the HSM of **NiHost1** (Fig. 3.1.9b). Full TG and DSC data for all three compounds are given in Tables 3.1.7-3.1.9 below.

Table 3.1.7: TG and DSC data for NiHost1

Reaction	TG			DSC	
	Calc %	Exp %	T_{onset} (°C)	T_{onset} (°C)	ΔH ($kJ.mol^{-1}$)
$Ni(NCS)_2(L)_4 \rightarrow Ni(NCS)_2(L)_2 + 2L$	34.2	33.0	215.2	242.1	116.1
$Ni(NCS)_2(L)_2 \rightarrow Ni(NCS)_2(L) + L$	17.1	17.8	289.9	301.0	52.8
$Ni(NCS)_2(L) \rightarrow Ni(NCS)_2 + L$	17.1	16.7	332.6	-	-

Table 3.1.8: TG data for NiEtAc and NiDMSO

Reaction	NiEtAc			NiDMSO		
	Calc %	Exp %	T_{onset} (°C)	Calc %	Exp %	T_{onset} (°C)
$Ni(NCS)_2(L)_4.2G \rightarrow Ni(NCS)_2(L)_4 + 2G$	15.9	17.0	58.7	22.1	22.7	131.4
$Ni(NCS)_2(L)_4 \rightarrow Ni(NCS)_2(L)_2 + 2L$	28.7	28.0	211.5	26.6	25.2	215.8
$Ni(NCS)_2(L)_2 \rightarrow Ni(NCS)_2(L)_1 + L$	14.4	14.3	288.6	13.3	12.6	288.6
$Ni(NCS)_2(L)_1 \rightarrow Ni(NCS)_2 + L$	14.4	13.9	327.6	13.3	13.3	333.3

Table 3.1.9: DSC data for NiEtAc and NiDMSO

Reaction	NiEtAc		NiDMSO	
	T_{onset} (°C)	ΔH ($kJ.mol^{-1}$)	T_{onset} (°C)	ΔH ($kJ.mol^{-1}$)
$Ni(NCS)_2(L)_4.2G \rightarrow Ni(NCS)_2(L)_4 + 2G$	88.7	53.9 (EtOH=3.4)* (Ace=5.4)*	148.5	79.0 (8.8)*
$Ni(NCS)_2(L)_4 \rightarrow Ni(NCS)_2(L)_2 + 2L$	250.9	107.4	266.4	66.9
$Ni(NCS)_2(L)_2 \rightarrow Ni(NCS)_2(L)_1 + L$	301.9	57.4	304.5	53.2
$Ni(NCS)_2(L)_1 \rightarrow Ni(NCS)_2 + L$	-	-	-	-

* values in brackets indicate enthalpies calculated in terms of kJ per mole of guest alone, for the release of one mole of guest per mole of host compound. For NiEtAc the values were weighted according to the ratio of the molar mass of EtOH to acetone

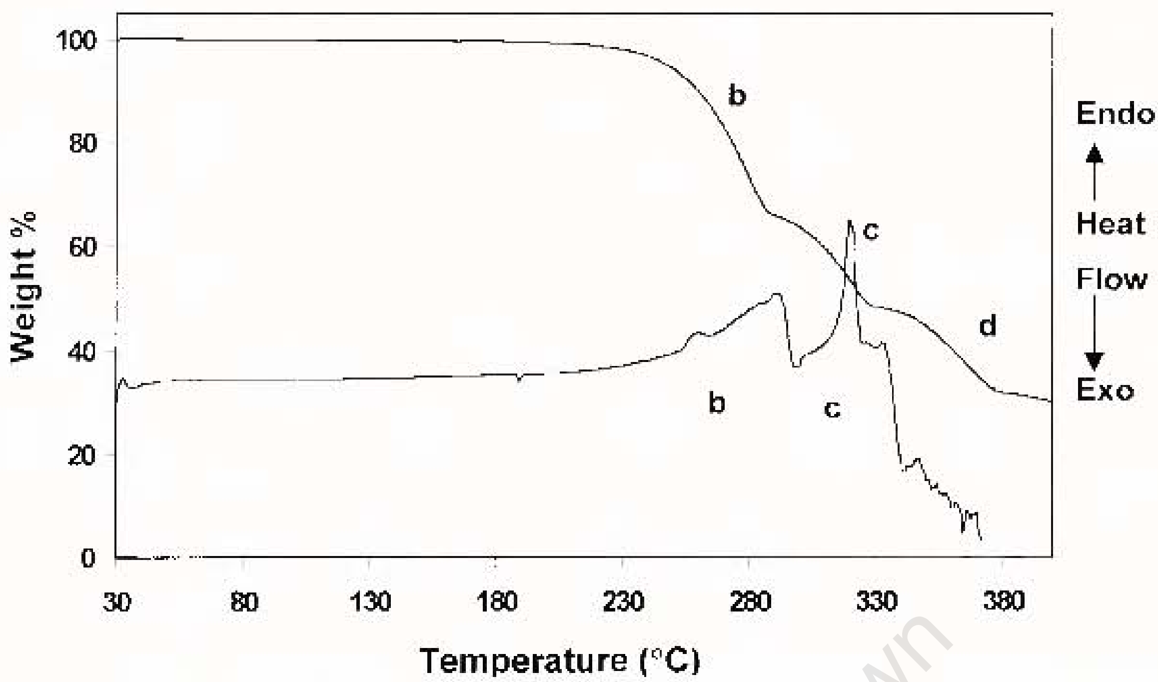

Fig 3.1.8: Thermal analysis of NiHost1

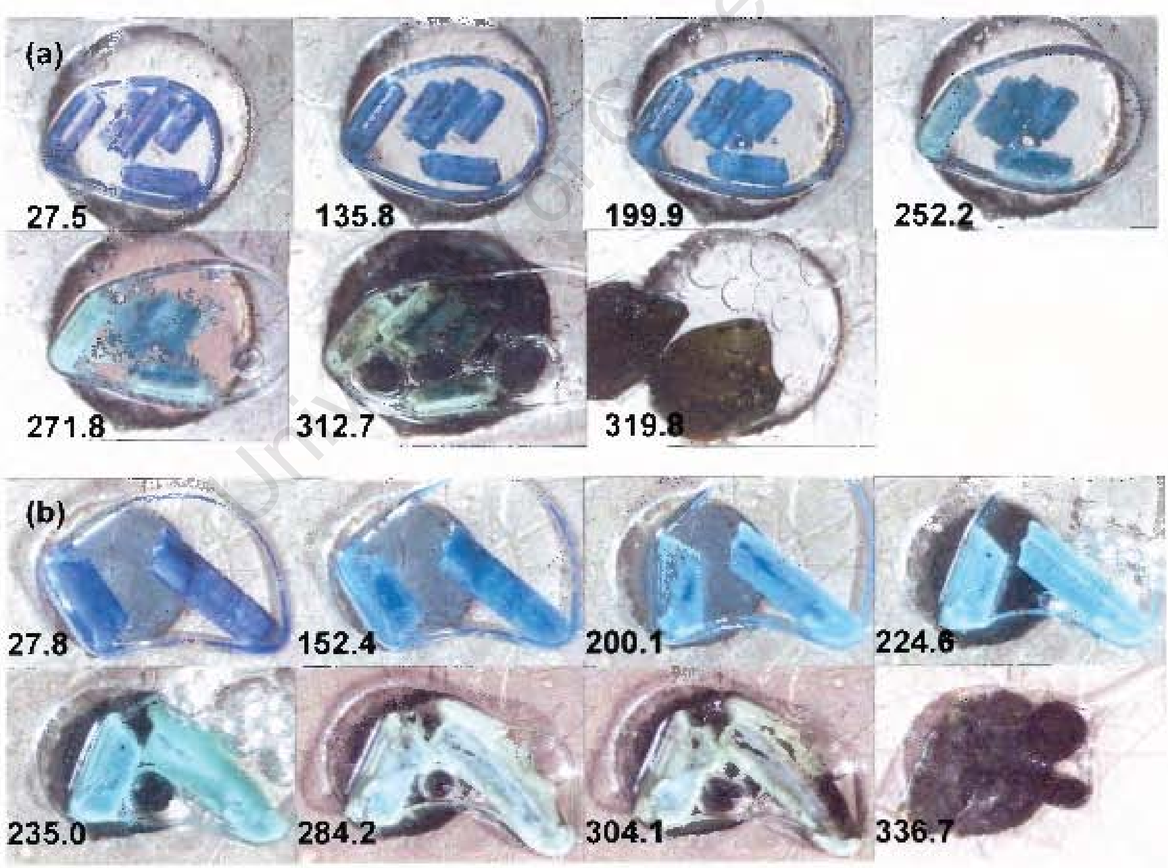

Fig 3.1.9: HSM of (a) NiHost1 and (b) NiDMSO (Temperatures, in °C, are given in bottom left hand corner).

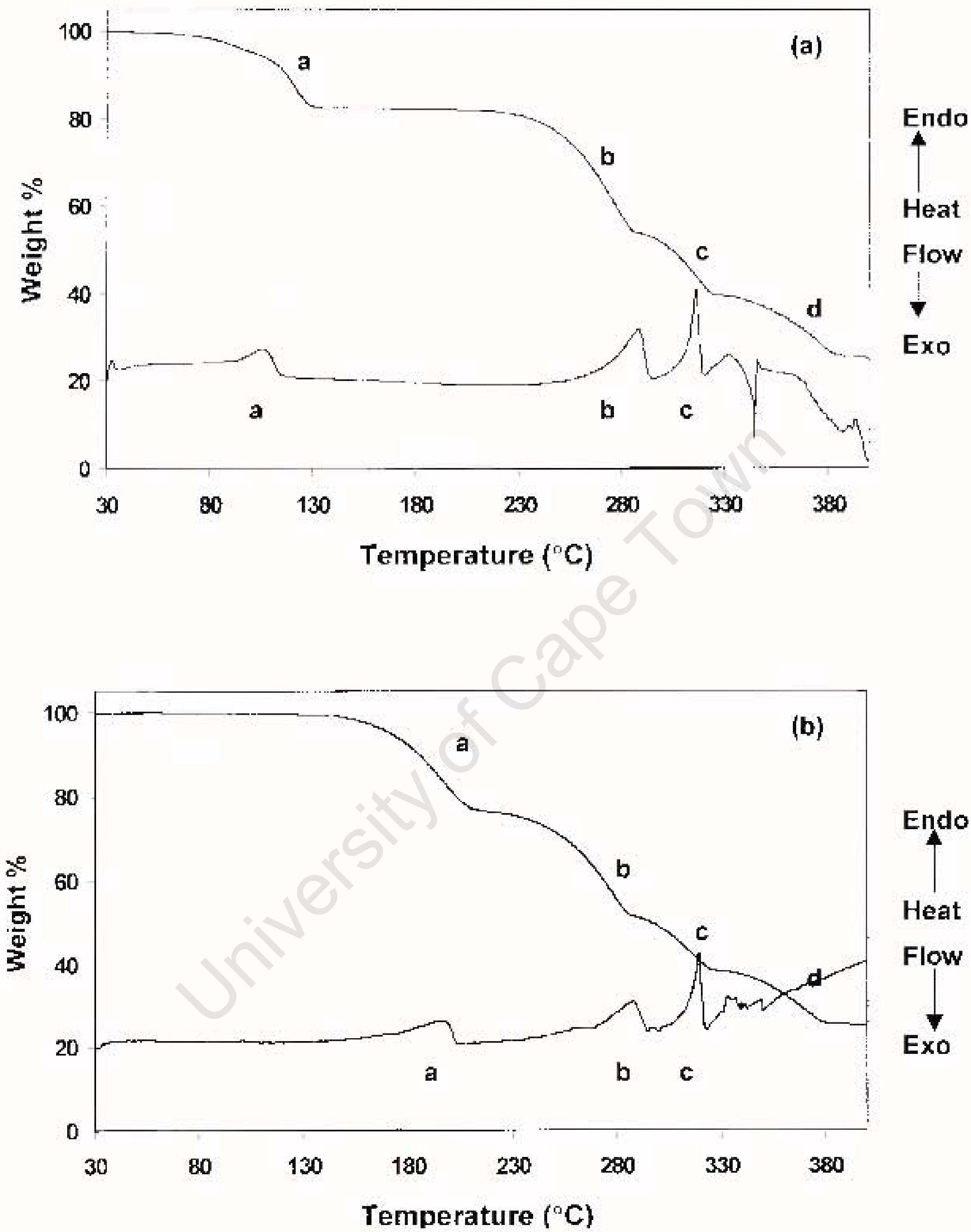

Figs 3.1.10: Thermal analysis of (a) NiEtAc, and (b) NiDMSO.

GUEST EXCHANGE BY DSC

The fact that **NiEtAc** and **NiDMSO** have the same open channel structure makes it possible to exchange one guest for another. The release of the EtOH and Me_2CO guests from **NiEtAc** is observed as an endothermic peak in the DSC at T_{peak}=107°C, whereas the release of the DMSO guests from **NiDMSO** occurs at T_{peak}=198°C. By observing the shift in position of the guest release peak during the guest exchange process, it is possible to monitor the extent to which the original guest has been replaced.

A quantity of **NiEtAc** crystals were removed from the mother liquor and dried with filter paper. The crystals were placed in a small glass beaker, which was placed inside a larger, sealed glass jar containing a small volume of DMSO. In this way the crystals were exposed to DMSO vapour. The system was maintained at 33°C for the duration of the exchange experiment. Small quantities of crystals were removed at regular intervals over a 5 day period and analysed by DSC.

The initial endotherm at T_{peak}=107°C, corresponding to the release of the EtOH/Me_2CO guests, migrates to the right until it reaches 198°C, corresponding to the release of pure DMSO (Fig. 3.1.11). A single, moving endotherm indicates that a continuous solid solution of the mixed guests is formed in the channels of the host.

It was found that **NiDMSO** or **NiEtAc** could also be generated by exposing the single crystal or powder forms of **NiHost1** to the vapour of the appropriate guest in a sealed vessel at 35°C. The inclusion processes were confirmed by TG and XRD, and the XRD trace of the product of the **NiHost1 + 2DMSO →** **NiDMSO** inclusion reaction is shown in Fig. 3.1.12a (This experimental curve is slightly left-shifted when compared to the calculated pattern for **NiDMSO**. This may be due to a slight deformation in the channel structure of the **NiDMSO** inclusion product when it loses a small amount of guest on exposure to air).

In addition, the product obtained on heating **NiEtAc** or **NiDMSO** at *ca.* 70°C for 30 minutes was found to be the pure host, **NiHost1**, indicating that the inclusion process is fully reversible. These desolvation reactions (**NiDMSO/NiEtAc** → **NiHost1**) were also confirmed by TG and XRD. The XRD trace of **NiHost1**, as well as that of the product obtained on heating **NiEtAc**, are shown in Fig. 3.1.12b.

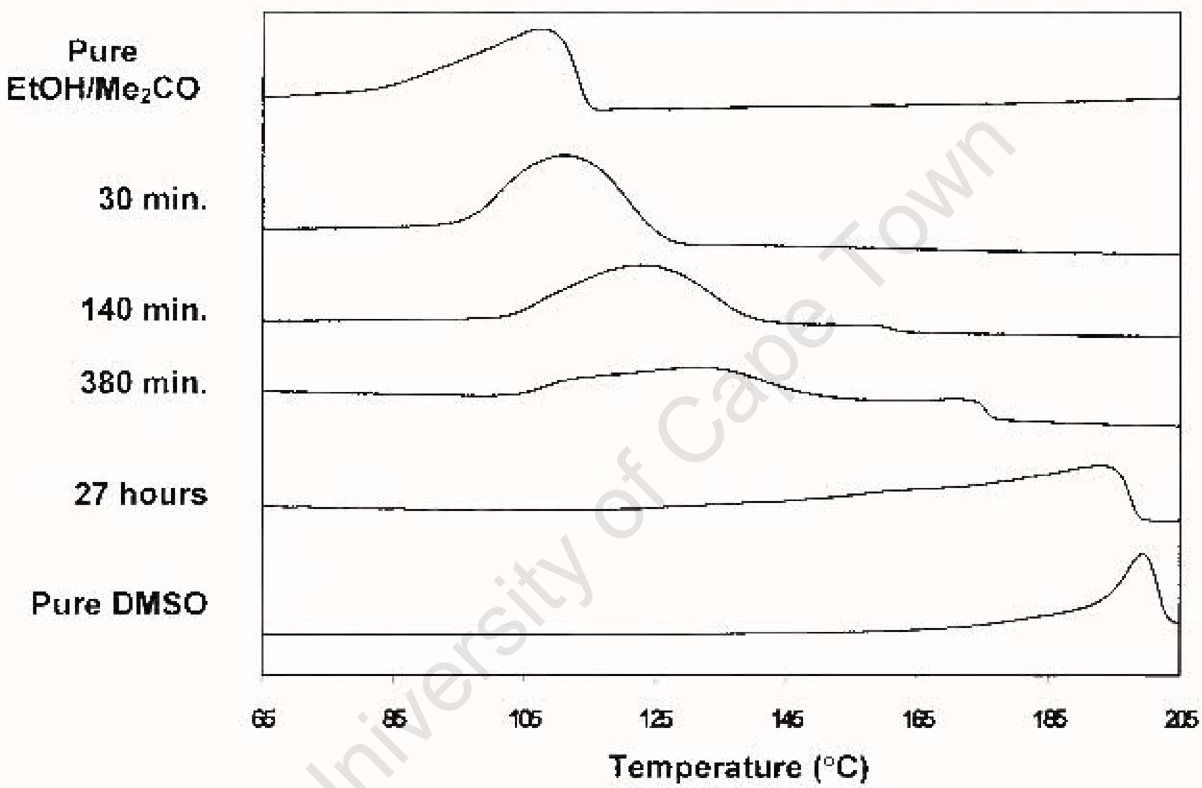

Fig 3.1.11: The shifting endotherm observed as a result of the guest exchange process: **NiEtAc + 2DMSO → NiDMSO + EtOH + Acetone**.

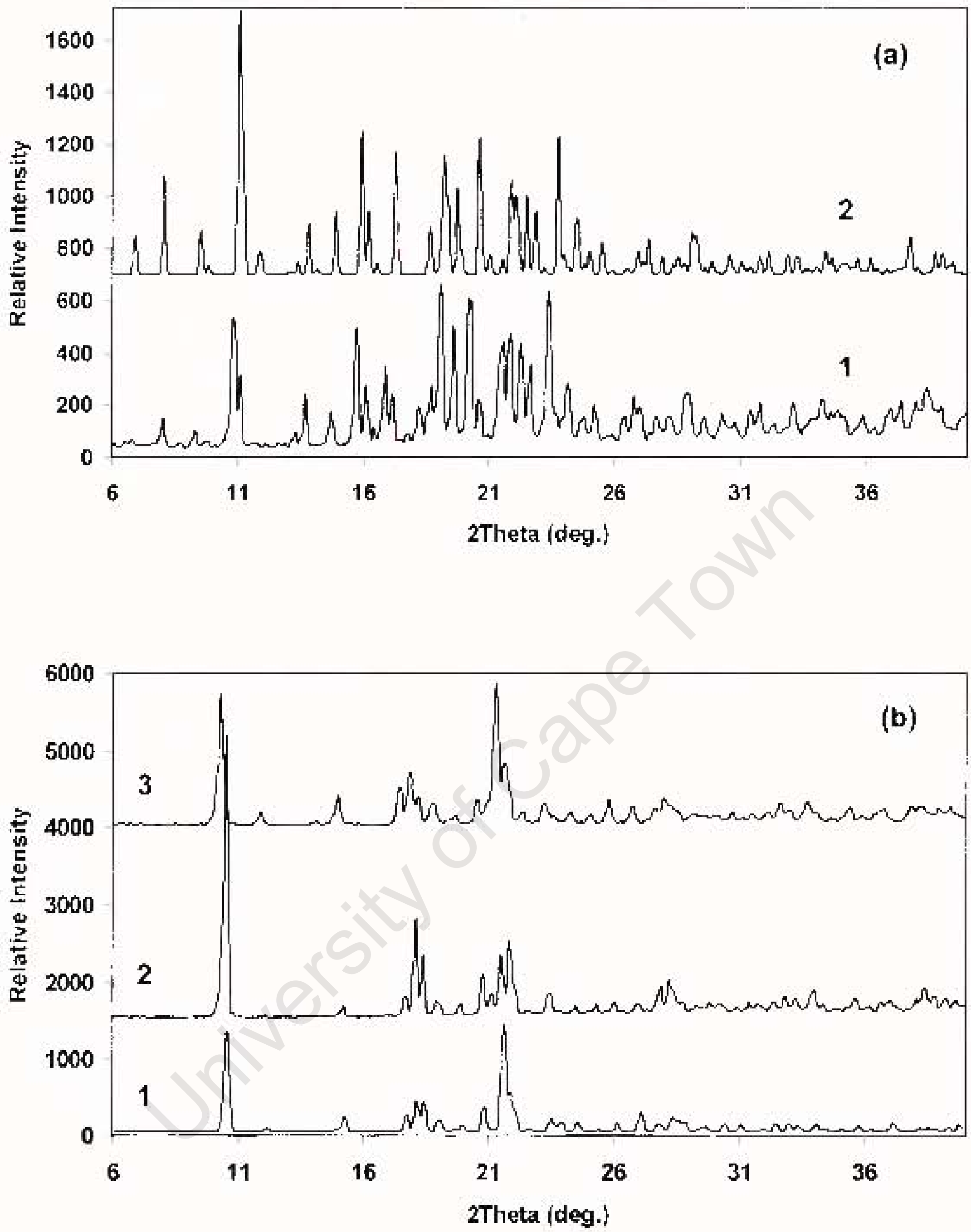

Fig 3.1.12: XRD traces for (a) DMSO inclusion product (**1**, experimental), and NiDMSO (**2**, calculated). (b) NiHost1 (**1**, calculated and **2**, experimental) and the product obtained upon desolvation of NiEtAc (**3**, experimental).

DISCUSSION

NiEtAc and **NiDMSO** are isostructural, and conform to the classical Werner clathrate formula, MX_2A_4. These structures belong to the channel clathrates, and the guest molecules are located in channels with a dome-shaped cross-section running parallel to the [100] direction. The structure is stabilised by host∧host and host∧guest hydrogen bonding interactions. These clathrates can be classified as kinetically unstable, as the guest molecules are released before the onset of host decomposition. The DMSO guests are released at a much higher temperature than the EtOH and acetone guests, due to the higher boiling point of this solvent.

The difference in temperature between the two guest release processes allowed us to follow the **NiEtAc + 2DMSO → NiDMSO + EtOH + Acetone** exchange process by monitoring the shift in the DSC peak for the guest release step. In addition, it was found that the α-host complex could be converted into **NiDMSO** or **NiEtAc** by exposing the powder form of **NiHost1** to the vapour of the appropriate guest at a suitable temperature. This reaction was found to be fully reversible, as **NiEtAc** and **NiDMSO** both revert to the **NiHost1** structure upon loss of the guest molecules from the channels. These transformations can be represented by:

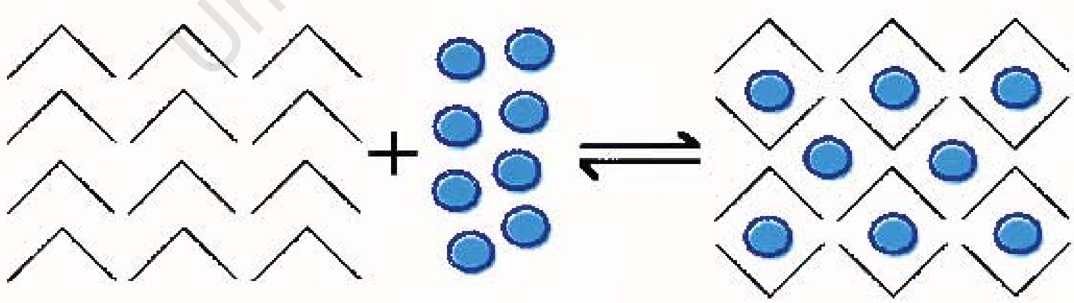

α-**HOST** $\qquad\qquad$ β-**CLATHRATE**

(NiHost1) $\qquad\qquad$ **(NiEtAc;NiDMSO)**

CHAPTER 3.2

WERNER CLATHRATES

H = $Ni(NCS)_2$(3-cyanopyridine)$_4$

Table 3.2.1: Crystal data and refinement parameters for NiHost2

	NiHost2
Molecular Formula	$C_{26}H_{16}N_{10}S_2Ni$
M_r (g/mol)	591.32
Crystal System	Orthorhombic
Space group	$Pna2_1$
Z	4
a (Å)	20.439(4)
b (Å)	10.413(2)
c (Å)	12.946(3)
$\alpha = \beta = \gamma$ (°)	90
V ($Å^3$)	2755.3(10)
D_{calc} (g/cm^3)	1.425
Crystal dimension (mm)	0.47 x 0.35 X 0.33
Temp of data collection (K)	173
Range scanned (θ)	1.99 – 27.48
Index Range	$26 \geq h \geq -7$, $5 \geq k \geq -13$, $16 \geq l \geq -16$
F (000)	1208
μ (mm^{-1})	0.89
No. reflections collected	7207
No. unique reflections	6333 (R_{int} = 0.0202)
Completeness	100.0%
Refinement method	Full-matrix L.S. on F^2
Data/restraints/parameters	6333/1/353
Goodness of fit on F^2	1.008
Final R indices ($I > 2\sigma(I)$)	R_1=0.0340, wR_2=0.0789
R indices (all data)	R_1=0.0748, wR_2=0.0890
Flack x parameter (e.s.d.)	-0.0044(0.0106)
Largest diff. Peak and hole	0.349, -0.339 e.$Å^{-3}$

Table 3.2.2: Crystal data and refinement parameters for NidiEt and NidiDCM

	NidiEt	**NidiDCM**
Molecular Formula	$C_{30}H_{28}N_{10}O_2S_2Ni$	$C_{28}H_{20}N_{10}Cl_4S_2Ni$
M_r (g/mol)	683.4	761.2
Crystal System	Monoclinic	Monoclinic
Space group	C2/c	C2/c
Z	4	4
a (Å)	17.737(4)	17.813(1)
b (Å)	11.527(2)	11.553(1)
c (Å)	17.120(3)	17.112(1)
β (deg.)	96.648(2)	97.668(2)
V ($Å^3$)	3476.7(2)	3490.1(2)
D_{calc} (g/cm^3)	1.306	1.449
Crystal dimension (mm)	0.30 x 0.25 X 0.19	0.20 x 0.27 x 0.23
Temp of data collection (K)	150	150
Range scanned (θ)	2.36 – 27.45	2.11 – 27.00
Index Range	$15 \geq h \geq -22$, $13 \geq k \geq -14$, $22 \geq l \geq -20$	$22 \geq h \geq -13$, $12 \geq k \geq -13$, $18 \geq l \geq -21$
F (000)	1416	1544
μ (mm^{-1})	0.72	1.02
No. reflections collected	8683	6867
No. unique reflections	3923 (R_{int} = 0.0392)	3598 (R_{int} = 0.0356)
Completeness	98.7	94.3
Refinement method	Full-matrix L.S. on F^2	Full-matrix L.S. on F^2
Data/restraints/parameters	3923/3/194	3598/4/233
Goodness of fit on F^2	1.055	1.031
Final R indices ($I>2\sigma(I)$)	R_1=0.0562, wR_2=0.1386	R_1=0.0550, wR_2=0.1453
R indices (all data)	R_1=0.1050, wR_2=0.1584	R_1=0.0737, wR_2=0.1594
Largest diff. peak and hole	1.127*, -0.646 e.$Å^{-3}$	1.220*, -0.864 e.$Å^{-3}$

* in vicinity of guest molecules

NiHost2 : $Ni(NCS)_2(3\text{-cyanopyridine})_4$

MICROANALYSIS:

	%C	%H	%N	%S
Calc for $Ni(NCS)_2(C_6H_4N_2)_4$	52.81	2.73	23.69	10.85
Experimental	52.36	2.23	23.54	10.45

PRELIMINARY X-RAY PHOTOGRAPHY:

Oscillation photography gave a unit cell length of 12.4Å, while Weissenberg photography revealed the remaining two unit cell lengths to be 10.3Å and 20.6Å, with an angle between them of 90°. Together the photographs displayed *mmm* Laue symmetry, indicating an orthorhombic unit cell.

SINGLE CRYSTAL X-RAY DIFFRACTOMETRY:

Th unit cell obtained by diffractometry was identical to that obtained by photography.

STRUCTURE SOLUTION AND REFINEMENT:

The diffraction data revealed systematic absences indicative of the orthorhombic space groups $Pna2_1$ or Pnma. Xprep gave an $|E^2\text{-}1|$ value of 0.856, indicating neither the centrosymmetric nor the non-centrosymmetric arrangement. An attempt was made to solve the structure in Pnma, and the metal atom was located on a mirror plane at (x, ¾, z). The rest of the molecule, however, could not be located on the electron density map. The correct space group was therefore taken to be $Pna2_1$, a choice that was vindicated by the eventual successful refinement of the structure in this space group. This is a classic example of the metal atoms, which dominate the scattering of x-rays, forcing the structure towards a centrosymmetric arrangement when the rest of the metal complex is non-centrosymmetric.

All non-hydrogen atoms were located on the electron density map and refined anisotropically. The aromatic hydrogen atoms were placed in geometrically calculated positions. The Ni atom was located in a general position in the unit cell (crystal structure and refinement details are given in Table 3.2.1).

STRUCTURE ANALYSIS:

Solving the structure in $Pna2_1$ revealed a central Ni atom coordinated to two axial NCS^- counterions and four equatorial 3-cyanopyridine ligands. The coordination geometry around the Ni centre is that of an irregular octahedron, with the four substituted-pyridine ligands adopting the propeller conformation (Fig. 3.2.1). If the plane bisecting the central Ni atom and four equatorial N atoms is viewed edge on (i.e. parallel to the [010] direction), three of the cyano substituents project above this plane, and one projects below it.

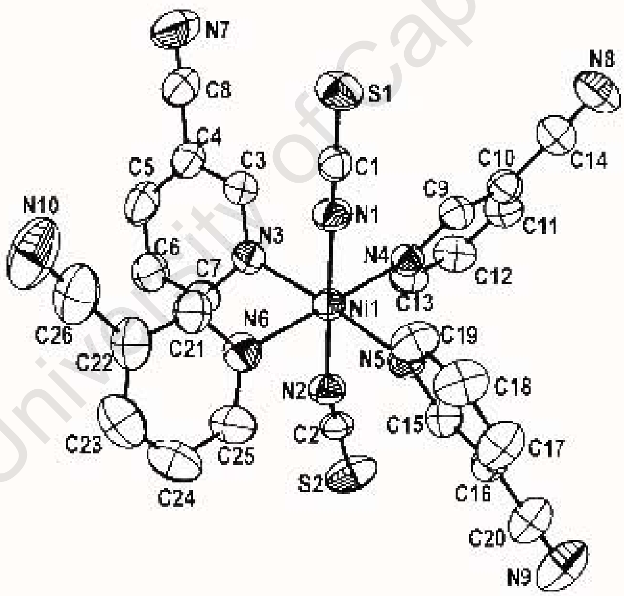

Fig 3.2.1: Ortep diagram of NiHost2 showing thermal ellipsoids (H atoms omitted for clarity).

All bond lengths and angles are within the expected range for compounds of this type. The two $Ni–N_{CS}$ bonds are 2.011(2)Å and 2.030(3)Å in length, while the four $Ni–N_{pyr}$ bonds lie in the range 2.145(2)Å to 2.191(2)Å. The literature values are given as 2.04(8)Å and 2.11(6)Å respectively[1]. Full bond lengths and angles are given in Appendix 2.

WEAK HYDROGEN BONDING INTERACTIONS AND CRYSTAL PACKING:

The host molecules pack to generate layers which run perpendicular to the [001] direction. The layers, which cut the *c* axis at 0.09 and 0.59, are related by rotation through 180°, followed by translation of half a unit cell length along *c* (Fig. 3.2.2).

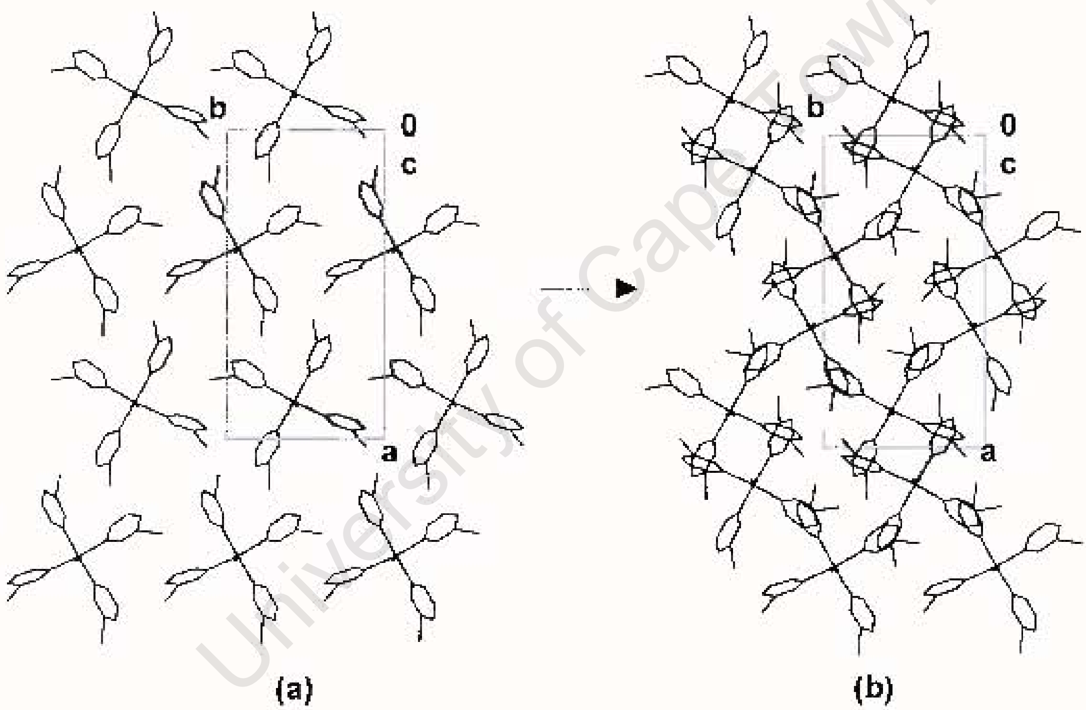

Fig 3.2.2: NiHost2 viewed along the [001] direction. (a) single layer, (b) multiple layers (ring H atoms omitted for clarity).

Intermolecular C–H···N≡C hydrogen bonds connect adjacent layers (Fig. 3.2.3). All interactions exceed the sum of the van der Waals radii of the two heavy atoms (3.25Å for C···N), and lie in the range generally associated with weak hydrogen bonds (Table 3.2.3).

Table 3.2.3: Weak Hydrogen Bonding Data for NiHost2

C – H ··· N	C – H (Å)	H ··· N (Å)	C ··· N (Å)	Angle (°)
C7 – H4$^{\#1}$ ··· N7	0.930(4)	2.824(4)	3.618(5)	144.0(2)
C25 – H16$^{\#2}$ ··· N8	0.930(3)	2.696(3)	3.547(5)	152.6(2)
C3 – H1$^{\#3}$ ··· N9	0.930(4)	2.629(4)	3.487(5)	153.9(2)
C13 – H8$^{\#4}$ ··· N10	0.930(4)	2.769(4)	3.531(5)	139.9(2)

Symmetry codes: #1 = $\frac{3}{2}$-x, ½+y, ½+z, #2 = 2-x,1-y, ½+z #3 = 2-x, 1-y, z-½ and #4 = $\frac{3}{2}$-x, y-½, ½+z.

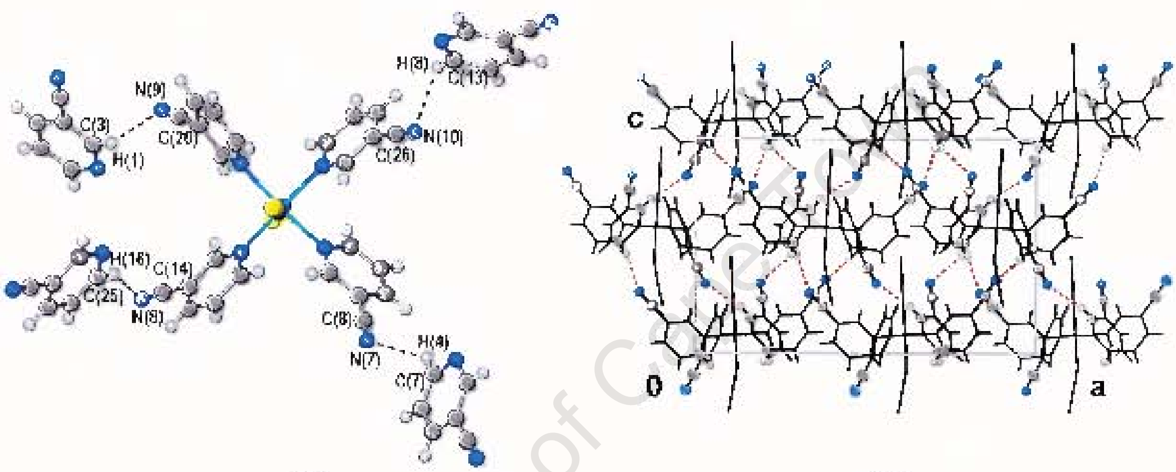

(a) (b)

Fig 3.2.3: (a) Hydrogen bonding environment of a single host molecule, (b) Layers of host molecules are stacked along the [001] direction, and are linked by intermolecular C–H···N≡C hydrogen bonds, shown as broken red lines (hydrogen bond donor and acceptor groups are shown in ball-and-stick form).

NidiEt : Ni(NCS)$_2$(3-cyanopyridine)$_4$.2EtOH

PRELIMINARY X-RAY PHOTOGRAPHY:

The single crystals of **NidiEt** were unsuitable for photography due to the small crystal size and unstable nature of the clathrate.

SINGLE CRYSTAL X-RAY DIFFRACTOMETRY

STRUCTURE SOLUTION AND REFINEMENT:

The diffraction data revealed *2/m* Laue symmetry, indicating a monoclinic unit cell. Systematic absences were indicative of the monoclinic space groups C2/c or Cc. The structure could be solved and refined to R_1<6% in both of these space groups. Xprep, however, calculated a mean $|E^2\text{-}1|$ value of 1.030, indicating that the centrosymmetric space group, C2/c, is correct.

In C2/c, the Ni atom is located on a diad at (½, y, ¼), and the asymmetric unit comprises one half of the $Ni(NCS)_2$(3-cyanopyridine)$_4$.2EtOH complex. The other half of the molecule and the second ethanol guest are generated by the symmetry operation (1-x, y, ½-z). The oxygen atom of the ethanol guest molecule is disordered over two positions, which refined with site occupancies of 36.3% and 63.7%. Owing to excessive thermal motion within the ethanol guest, the C–O and C–C bond lengths were fixed at 1.43Å and 1.53Å respectively.

All non-hydrogen host atoms were located on the electron density map and refined anisotropically, while the non-hydrogen atoms of the ethanol guest were refined isotropically. The aromatic hydrogen atoms were placed in geometrically calculated positions, while the guest hydrogen atoms were omitted from the final model (crystal structure and refinement details are given in Table 3.2.2).

STRUCTURE ANALYSIS:

Solving the structure in C2/c revealed the Ni atom, in an irregular octahedral coordination environment, to be coordinated to two axial NCS^- counterions and four equatorial 3-cyanopyridine ligands (Fig. 3.2.4). The four cyano-substituted pyridine ligands adopt the propeller conformation.

The Ni–N_{CS} bond is 2.034(3)Å in length, while the two Ni–N_{pyr} bonds are 2.119(3)Å and 2.135(3)Å. These correspond well with the literature values of 2.04(8)Å and 2.11(6)Å respectively[1]. All bond lengths and angles within the pyridine ring systems also correspond well with their respective literature values (Appendix 2). The thermal parameters of the guest atoms are large compared with those of the host complex, due to the volatile nature of this liquid.

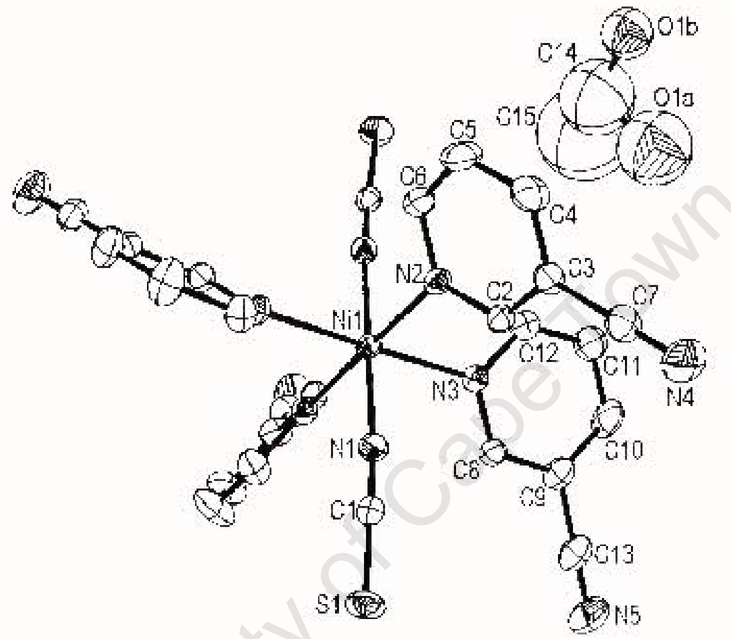

Fig 3.2.4: Ortep diagram of NidiEt, showing thermal ellipsoids for host atoms and spheres for guest atoms (H atoms omitted for clarity). The complete host molecule, with the Ni atom located on a diad, is shown. The asymmetric unit (half the host complex and one ethanol guest) is labelled.

HYDROGEN BONDING INTERACTIONS:

Weak intermolecular C–H···N≡C hydrogen bonds exist between the cyano moieties and ring hydrogen atoms of the 3-cyanopyridine ligands. In addition, two host···guest hydrogen bonding interactions were found between one of the oxygen atoms (O1B) of the disordered ethanol guest and the isothiocyanato S and ring H atoms of a single nearby host complex (Table 3.2.4). All interactions lie in the range generally associated with weak hydrogen bonds.

Table 3.2.4: Weak Hydrogen Bonding Data for NidiEt

D – H···A	D – H (Å)	H ··· A (Å)	D ··· A (Å)	Angle (°)
		HOST···HOST INTERACTIONS		
C6–H8$^{\#1}$ ··· N4	0.930(4)	2.513(4)	3.412(5)	162.8(2)
C2–H3$^{\#2}$ ··· N5	0.930(3)	2.472(4)	3.358(5)	159.4(2)
		HOST···GUEST INTERACTIONS		
C8–H6$^{\#3}$ ··· O1B	0.930(4)	2.396(9)	3.288(10)	160.7(3)
O1B ··· S1$^{\#3}$	-	-	3.331(8)	-

Symmetry codes: #1 = x, 1-y, z-½, #2 = 1-x, -y, -z and #3 = x-½, ½+y, z.

NidiDCM : $Ni(NCS)_2(3\text{-cyanopyridine})_4.2CH_2Cl_2$

PRELIMINARY X-RAY PHOTOGRAPHY:

The single crystals of **NidiEt** were unsuitable for photography due to the small crystal size and unstable nature of the clathrate.

SINGLE CRYSTAL X-RAY DIFFRACTOMETRY

STRUCTURE SOLUTION AND REFINEMENT:

The diffraction data revealed *2/m* Laue symmetry, indicating a monoclinic unit cell. Systematic absences were indicative of the monoclinic space groups C2/c or Cc. Again the attempt was made to solve the structure in both space groups. In this case, however, the structure only refined to $R_1 \approx 15\%$ in Cc, whereas a refinement to $R_1 < 6\%$ was obtained in C2/c. In addition, Xprep calculated a mean $|E^2\text{-}1|$ value of 1.022, indicating that the centrosymmetric space group, C2/c, is correct.

As in **NidiEt**, the Ni atom lies on a 2-fold axis of rotation at (½, y, ¼), with the result that only half the metal complex and one dichloromethane guest molecule were located on the electron density map. This dichloromethane guest was found to be disordered over two sites, with site occupancies which refined to 57.9% and 42.1% for the two fragments. The four C–Cl bond lengths were fixed at 1.79Å, while the Cl–C–Cl angles were allowed to refine.

All non-hydrogen host and guest atoms were located on the electron density map and refined anisotropically. The aromatic and guest hydrogen atoms were placed in geometrically calculated positions (crystal structure and refinement details are given in Table 3.2.2).

STRUCTURE ANALYSIS:

NidiDCM and **NidiEt** are isostructural with respect to the host molecules, and differ only in the positions of the guest molecules. The asymmetric unit is labelled in Fig. 3.2.5.

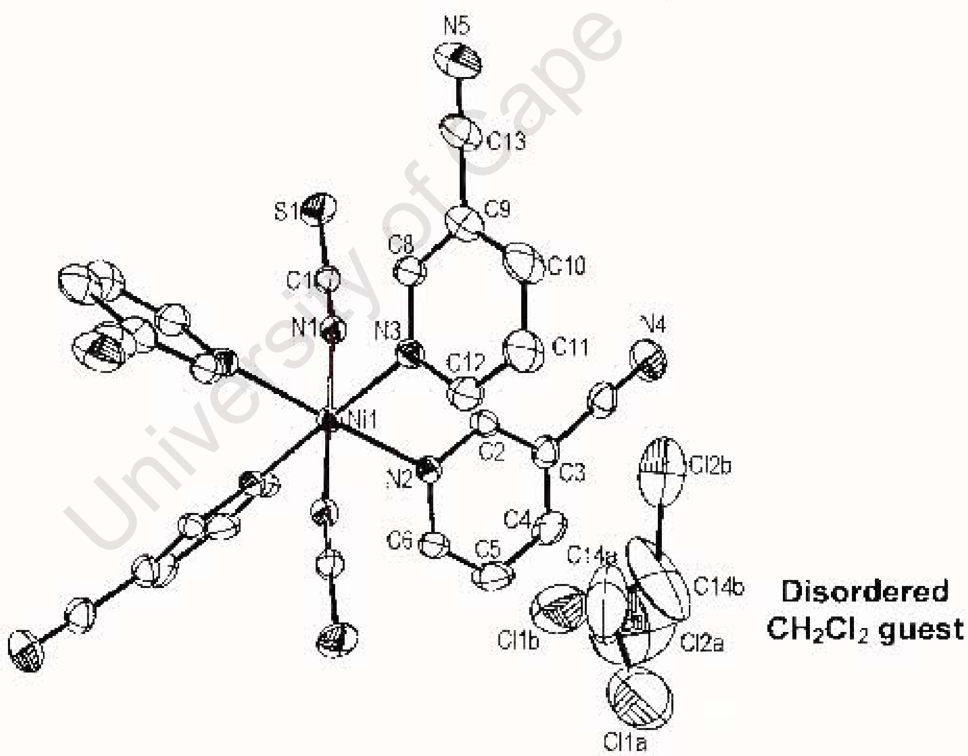

Fig 3.2.5: Ortep diagram of NidiDCM, showing thermal ellipsoids (H atoms omitted for clarity). The complete host molecule, with the **Ni** atom located on a diad, is shown. The asymmetric unit (half the host complex and one disordered dichloromethane guest) is labelled.

The Ni–N_{CS} bond is 2.039(3)Å in length, while the two Ni–N_{pyr} bonds are 2.116(3)Å and 2.146(3)Å. These correspond well with the literature values of 2.04(8)Å and 2.11(6)Å respectively[1]. The Cl–C–Cl angles refined to 104.4(5)° and 112.1(3)°. A study of 15 dichloromethane guests on the CSD gave a mean angle of 111.5±1.9°. Full bond lengths and angles are given in Appendix 2.

The thermal parameters for the two dichloromethane fragments are large compared with those of the metal complex (Fig. 3.2.5). However, dichloromethane is a highly volatile liquid (b.p. = 40°C), and one would expect to observe a significant increase in the thermal motion of these atoms compared with those of the metal complex.

HYDROGEN BONDING INTERACTIONS:

As in **NidiEt**, weak C–H···N≡C hydrogen bonds were identified between the cyano moieties and ring hydrogens of the 3-cyanopyridine ligands. Weak intermolecular C–H···N≡C hydrogen bonds were also identified between the cyano moieties of 3-cyanopyridine ligands and the C–H groups of both dichloromethane guest fragments (Fig. 3.2.6, Table 3.2.5).

Table 3.2.5: Weak Hydrogen Bonding Data for NidiDCM

C–H···N	C–H (Å)	H···N (Å)	C···N (Å)	Angle (°)
HOST···HOST INTERACTIONS				
C6–H4$^{\#1}$···N4	0.930(3)	2.515(3)	3.408(5)	161.0(2)
C2–H1$^{\#2}$···N5	0.930(3)	2.471(4)	3.363(5)	160.8(2)
HOST···GUEST INTERACTIONS				
C14A–H9A$^{\#3}$···N4	0.970(14)	2.488(4)	3.350(13)	147.9(7)
C14B–H9B$^{\#4}$···N5	0.970(10)	2.364(4)	3.285(10)	158.4(5)

Symmetry codes: #1 = x, 1-y, z-½, #2 = 1-x, -y, -z, #3 = ½-x, ½-y, -z and #4 = ½+x, y-½, z.

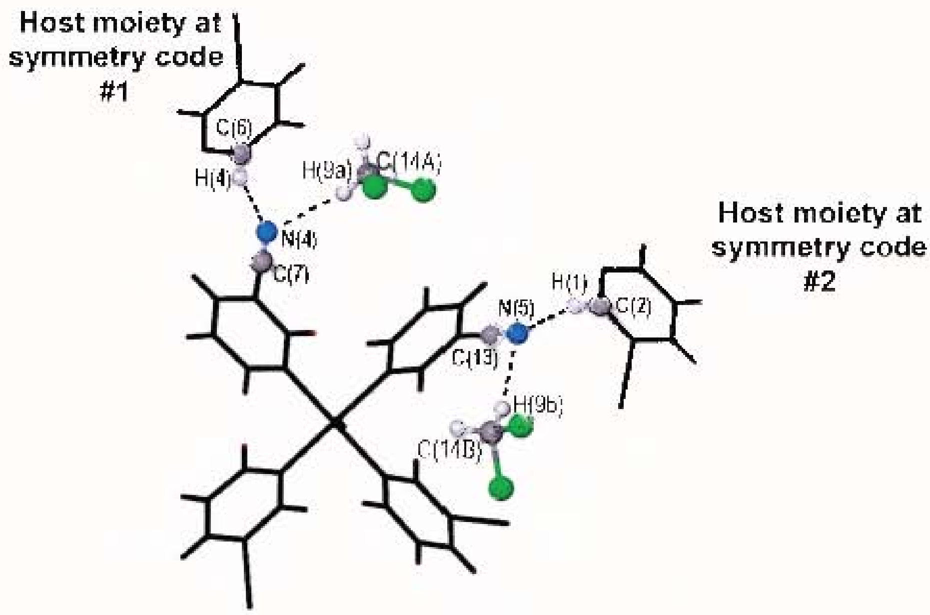

Fig 3.2.6: Hydrogen bonding interactions in NidiDCM

CRYSTAL PACKING FEATURES OF NidiEt AND NidiDCM

The packing of **NidiEt** and **NidiDCM** is similar, and the two compounds may be regarded as isostructural with respect to the host molecules. The host molecules pack to form layers, which run perpendicular to the $[10\bar{1}]$ direction, and are related by centres of inversion (Fig. 3.2.7). The isothiocyanato and cyano moieties project into the spaces between the layers. The layers are staggered, such that the isothiocyanate groups of one layer project into cavities generated by the two adjacent layers.

A single layer of host molecules is shown in Fig. 3.2.8a, where site **y** represents the positions of the isothiocyanato counterions of the two adjacent layers and site **x** represents the positions of the guest molecules (Fig. 3.2.8b). The layers of host molecules pack to generate channels, sinusoidal in shape, which run parallel to the $[10\bar{1}]$ direction. The guest molecules are located in these channels (Fig. 3.2.9).

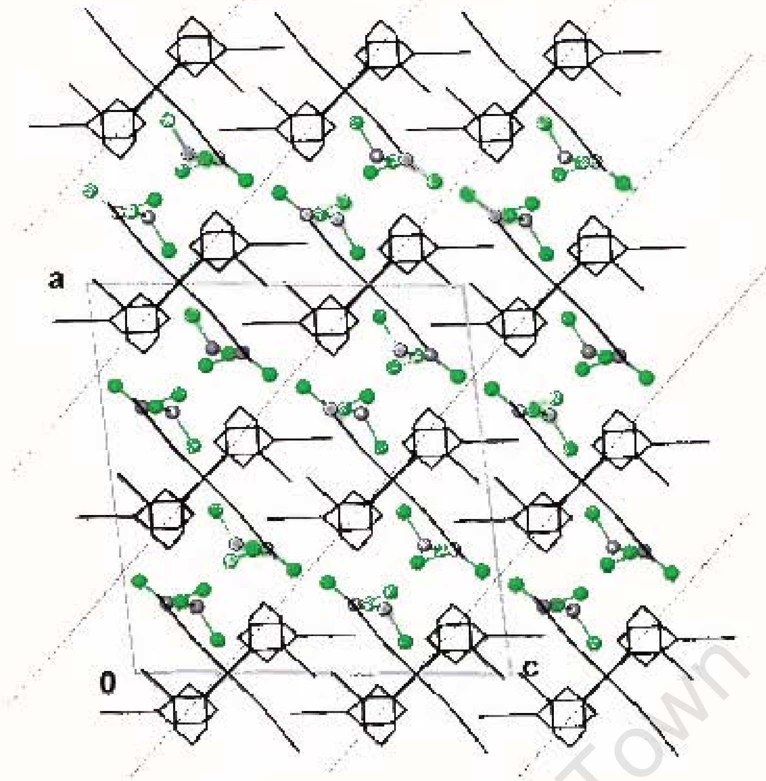

Fig 3.2.7: The packing of NidiDCM, viewed along the [010] direction. Host molecules are shown in stick form and guest molecules in ball-and-stick form (broken lines represent layers of host molecules, H atoms omitted for clarity).

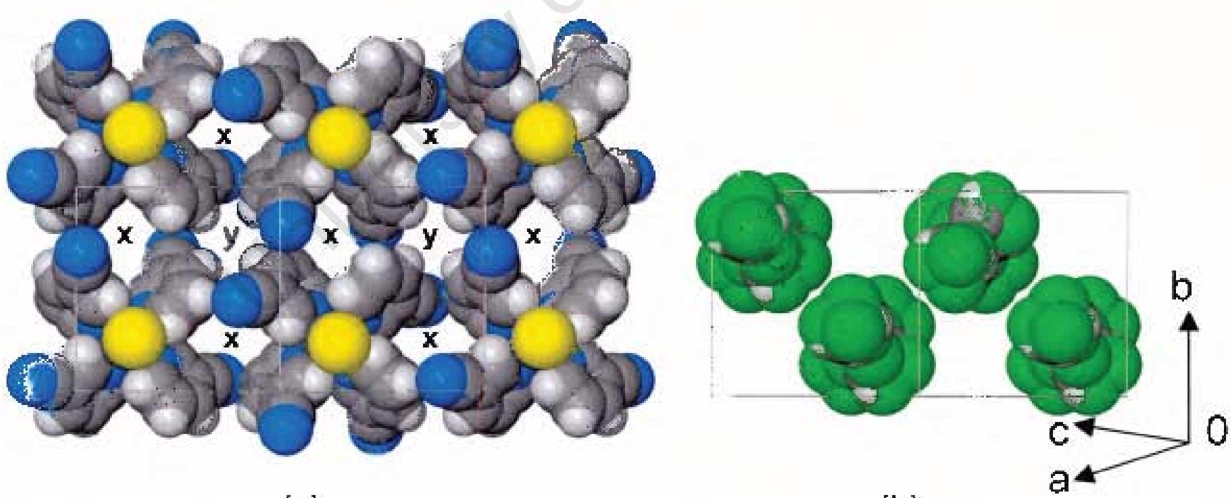

(a) (b)

Fig 3.2.8: Space-filling representation of NidiDCM (a) a single layer of host molecules (**y** = position of NCS$^-$ groups of adjacent layers, **x** = position of guest molecules in channels), viewed along the [$10\bar{1}$] direction, and (b) the packing arrangement of the dichloromethane guests.

(a)

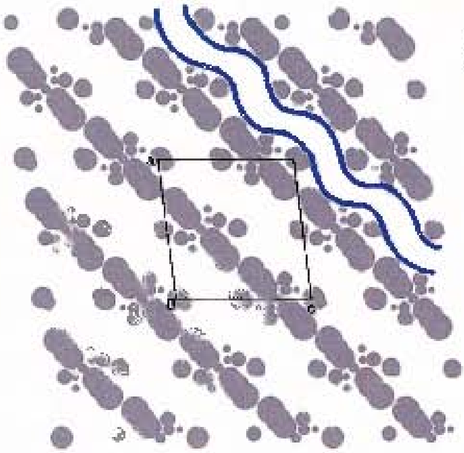

(b)

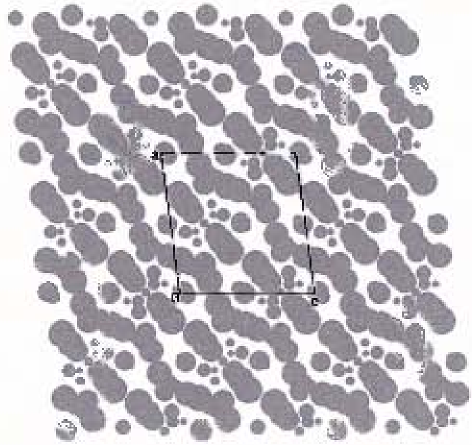

Fig. 3.2.9: Space filling representation of NidiDCM at *b*=0.25, viewed along the [010] direction. (a) host molecules only, showing sinusoidal channels, (b) host and guest molecules, showing positions of CH_2Cl_2 guests in channels.

THERMAL ANALYSIS

The thermal analyses of all three compounds are shown in Figs. 3.2.10a–c. The host compound, **NiHost2**, decomposes in two steps, shown as **b** and **c** in Fig. 3.2.10a. Each step corresponds to the loss of two 3-cyanopyridine ligands. The DSC shows two distinct endotherms corresponding to steps **b** and **c**. In the TG, however, the two weight-loss processes overlap. During step **b** the translucent blue crystals bubble and turn opaque green. Bubbling continues during step **c**, and the crystals turn orange-brown (Fig. 3.2.11a).

NidiEt and **NidiDCM** undergo an additional single-step weight loss process, shown as step **a** in Figs 3.2.10b and c, corresponding to the release of the guest molecules from the host channels. The observed weight loss justifies the assignment of a host:guest ratio of 1:2 for both compounds. The DSC scans show a broad endotherm corresponding to step **a,** which occurs in the same position for **NidiEt** and **NidiDCM.** Following the guest release process, the host decomposition reactions, **b** and **c**, follow the same pattern observed for **NiHost2**. The decomposition of **NidiEt** was followed by HSM (similar results were obtained for **NidiDCM**). During step **a** the translucent purple crystals bubble and turn opaque blue. The bubbling is resumed in steps **b** and **c**, and the crystals turn light yellow-green and orange-brown in turn, in accordance with the colour changes observed for **NiHost2** (Fig. 3.2.11b). The relevant TG and DSC data are given below in Tables 3.2.6-3.2.8.

Table 3.2.6: TG and DSC data for NiHost2

Reaction	TG			DSC	
	Calc %	Exp %	T_{onset} (°C)	T_{onset} (°C)	ΔH ($kJ.mol^{-1}$)
$Ni(NCS)_2(L)_4 \rightarrow Ni(NCS)_2(L)_2 + 2L$	35.0	34.4	179.4	174.5	130.2
$Ni(NCS)_2(L)_2 \rightarrow Ni(NCS)_2 + 2L$	35.0	34.4	217.8	216.5	127.9

Table 3.2.7: TG data for NidiEt and NidiDCM

Reaction	NidiEt			NidiDCM		
	Calc %	Exp %	T_{onset} (°C)	Calc %	Exp %	T_{onset} (°C)
$Ni(NCS)_2(L)_4.2G \rightarrow Ni(NCS)_2(L)_4 + 2G$	13.5	12.7	57.4	22.3	22.0	46.8
$Ni(NCS)_2(L)_4 \rightarrow Ni(NCS)_2(L)_2 + 2L$	30.5	30.2	179.2	27.4	27.7	179.5
$Ni(NCS)_2(L)_2 \rightarrow Ni(NCS)_2 + 2L$	30.5	29.9	230.5	27.4	27.7	230.2

Table 3.2.8: DSC data for NidiEt and NidiDCM

Reaction	NidiEt		NidiDCM	
	T_{onset} (°C)	ΔH ($kJ.mol^{-1}$)	T_{onset} (°C)	ΔH ($kJ.mol^{-1}$)
$Ni(NCS)_2(L)_4.2G \rightarrow Ni(NCS)_2(L)_4 + 2G$	82.6	50.6 (3.4)*	96.6	21.2 (2.4)*
$Ni(NCS)_2(L)_4 \rightarrow Ni(NCS)_2(L)_2 + 2L$	158.9	117.3	169.2	98.1
$Ni(NCS)_2(L)_2 \rightarrow Ni(NCS)_2 + 2L$	224.7	113.5	220.8	105.9

* values in brackets indicate enthalpies calculated in terms of kJ per mole of guest alone, for the release of one mole of guest per mole of host compound.

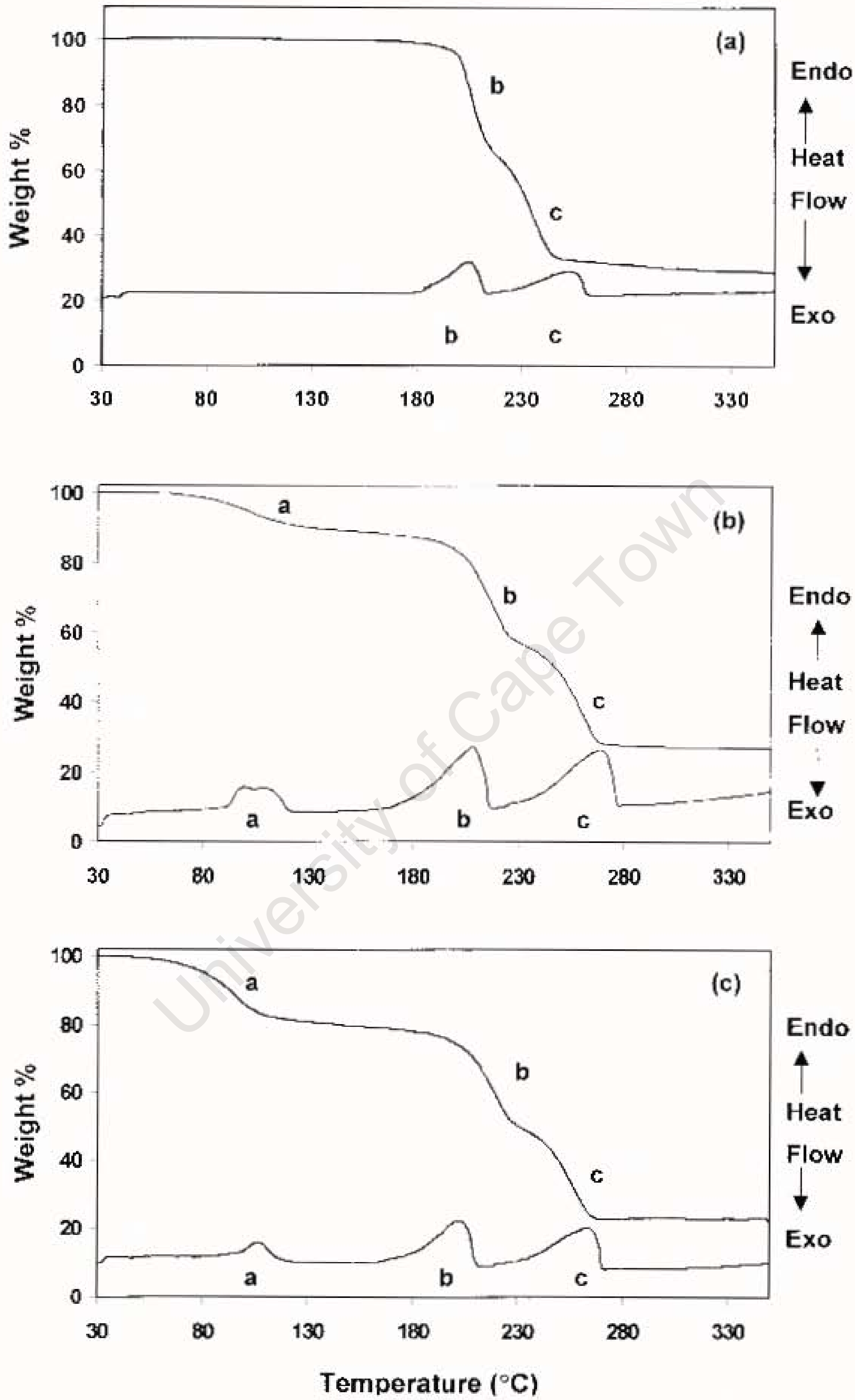

Fig 3.2.10: Thermal analyses of (a) NiHost2, (b) NidiEt and (c) NidiDCM

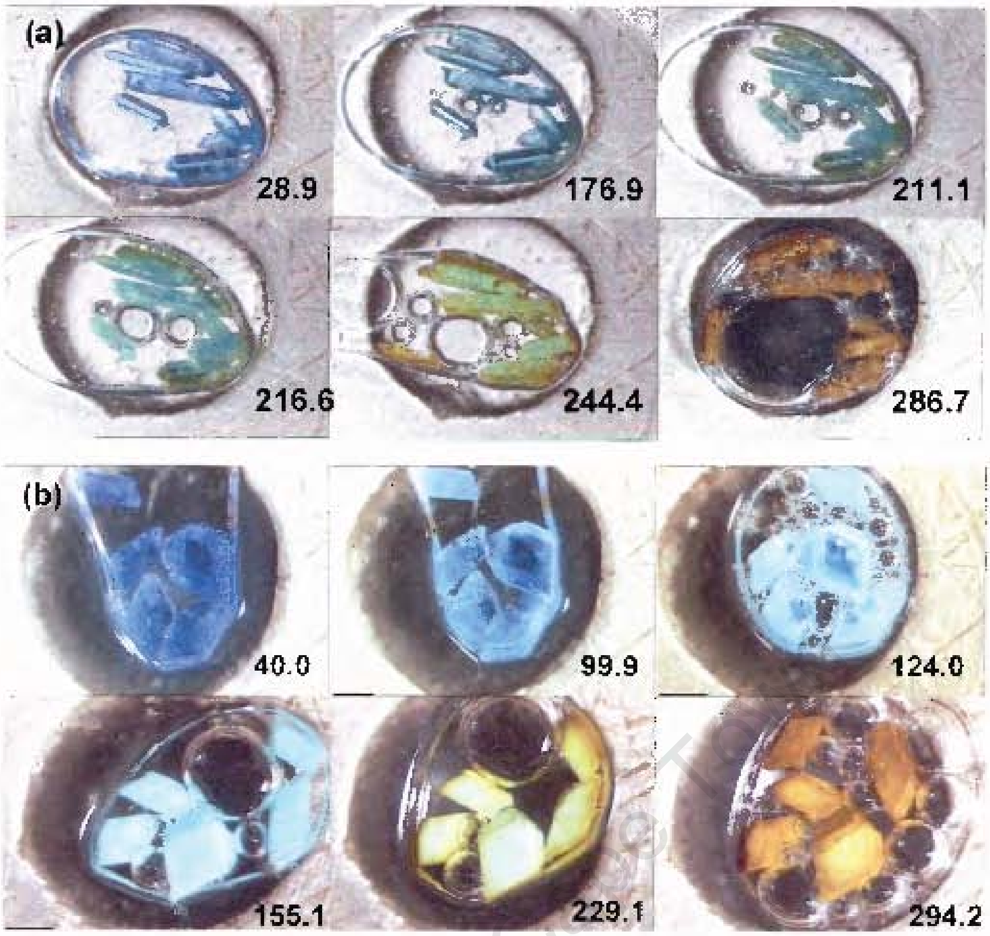

Fig 3.2.11: HSM of (a) NiHost2 and (b) NidiEt

INTERCONVERSION REACTIONS

It was found that the pure host, **NiHost2**, could be converted into the inclusion compound **NidiDCM**, by exposing the single crystal or powder form of **NiHost2** to CH_2Cl_2 vapour in a sealed vessel at room temperature. Single crystals of **NiHost2** were placed in a small beaker, which was then placed in a sealed jar containing a small volume of CH_2Cl_2 vapour. The system was maintained at room temperature. A few single crystals were removed at regular time intervals over a 24 hour period and analysed by TG. XRD and microscopy techniques were also used to monitor this reaction. The corresponding sorption process **NiHost2** + **2EtOH** $\rightarrow$ **NidiEt** was unsuccessful.

Reaction Progress by TG and Microscopy:

Microscopy shows crystals of **NiHost2** to change from a clear blue to an opaque light purple colour, as the dichloromethane guest is included in the crystal structure (Fig. 3.2.12). The crystals were totally opaque after 24 hours. Similarly, TG of the single crystals, taken at t = 40, 160, 240, 330, 390, 420 and 1380 minutes, show an increase in the % mass loss over the temperature range associated with the release of the dichloromethane guests. The % mass loss increases from 0% (pure **NiHost2**) to 21.9% (pure **NidiDCM**) over the 23 hour period.

t = 0 **t = 10 hours** **t = 24 hours**

Fig. 3.2.12: Microscope pictures of the crystals during the inclusion process:

NiHost2 +2CH_2Cl_2 → NidiDCM

XRD:

The XRD traces of **NidiEt** and **NidiDCM** show them to be isostructural, the subtle differences between the two scans being attributable to the effect of the guest molecules (Fig. 3.2.13). The XRD trace of the crystals of **NiHost2** that had been exposed to CH_2Cl_2 vapour (**7**) is superimposable on the XRD trace for **NidiDCM** (**6**), proving that the inclusion process **NiHost2 +2CH_2Cl_2 → NidiDCM** had been successful. Some of the XRD traces for the clathrate compounds are slightly shifted compared with their calculated traces. This can be attributed to a small amount of desolvation, resulting in a slight deformation in the channel structure, when the clathrate is exposed to air. In addition, both **NidiEt** and **NidiDCM** revert to the empty α-host structure, **NiHost2**, when allowed to desolvate at room temperature in air.

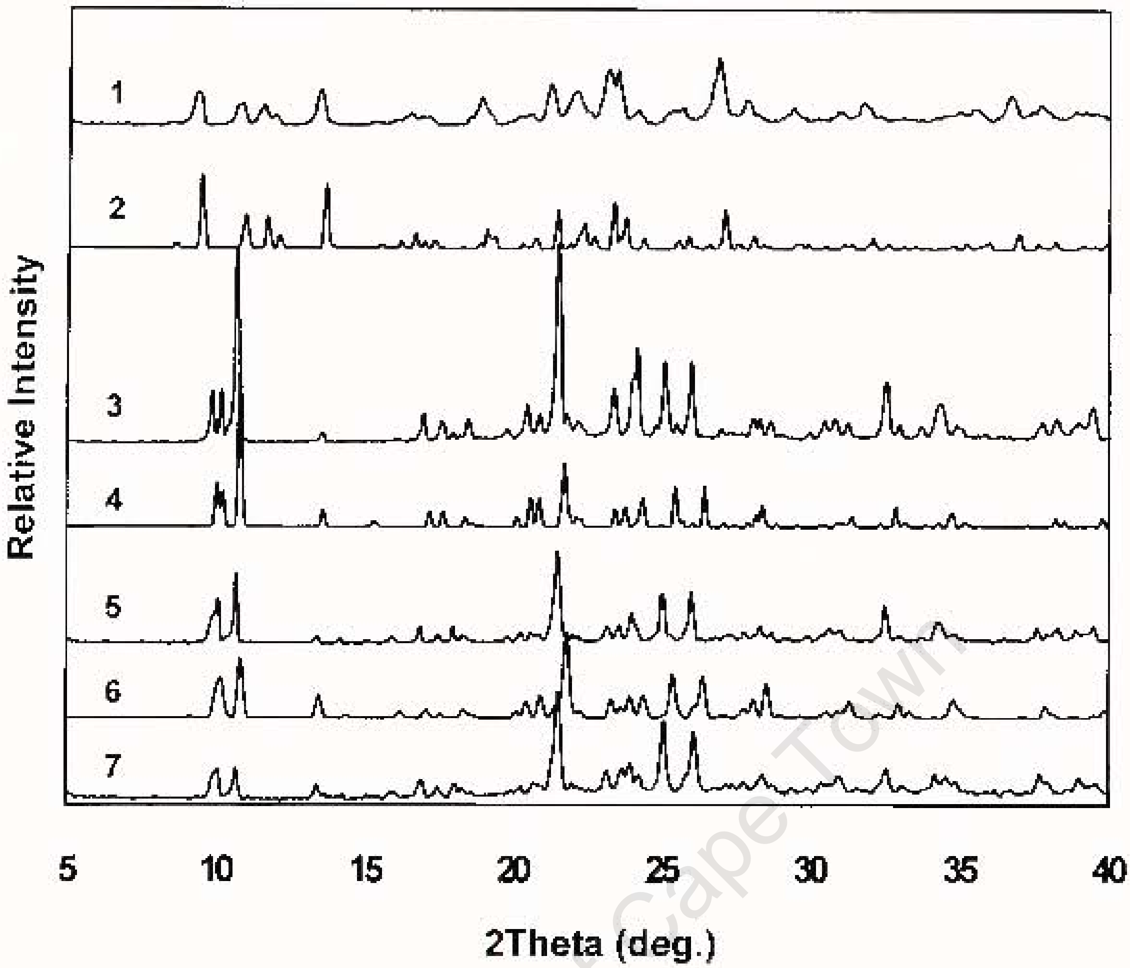

Fig 3.2.13: NiHost2 (1, experimental and **2**, calculated), NidiEt (**3**, experimental and **4**, calculated), NidiDCM (**5**, experimental and **6**, calculated), and (**7**) the product obtained on exposure of NiHost2 to CH_2Cl_2 vapour for 23 hours.

Attempts were also made to exchange one guest for another in the channel structure. TG was again used to confirm the success of the exchange process. The exchange reaction **NidiEt + 2CH$_2$Cl$_2$ → NidiDCM + 2EtOH** was found to be complete after only 30 minutes at 4°C. The reverse reaction, **NidiDCM + 2EtOH → NidiEt + 2CH$_2$Cl$_2$**, however, took several days at 35°C to reach completion.

DISCUSSION

NidiEt and **NidiDCM** are isostructural, and both display the classical Werner clathrate formula, $MX_2A_4.nG$. Host···host and host···guest hydrogen bonding interactions, however, result in the generation of a 3-D hydrogen bonded network. The guest molecules are located in sinusoidal channels, which run parallel to the $[10\bar{1}]$ direction. The relatively open channel structure results in a clathrate with low kinetic stability, as the guest molecules can easily diffuse through the channels to the crystal surface. This is confirmed by TG, which reveals the guest molecules to be released at least 50°C before the onset of host decomposition.

XRD and thermal analysis results show that **NidiEt** and **NidiDCM** both revert to the **NiHost2** structure upon loss of the guest molecules from the channel structure. In addition, the guest molecules in **NidiEt** and **NidiDCM** are interchangeable. The guest exchange process occurs when crystals of one clathrate are exposed to the vapour of the second guest. TGA shows the exchange process **NidiEt + 2CH_2Cl_2 → NidiDCM + 2EtOH** to be much more rapid than the reverse reaction. In addition, powdered **NiHost2** is converted into **NidiDCM** upon exposure to CH_2Cl_2 vapour, whereas the corresponding guest sorption process with EtOH is unsuccessful. We can summarise:

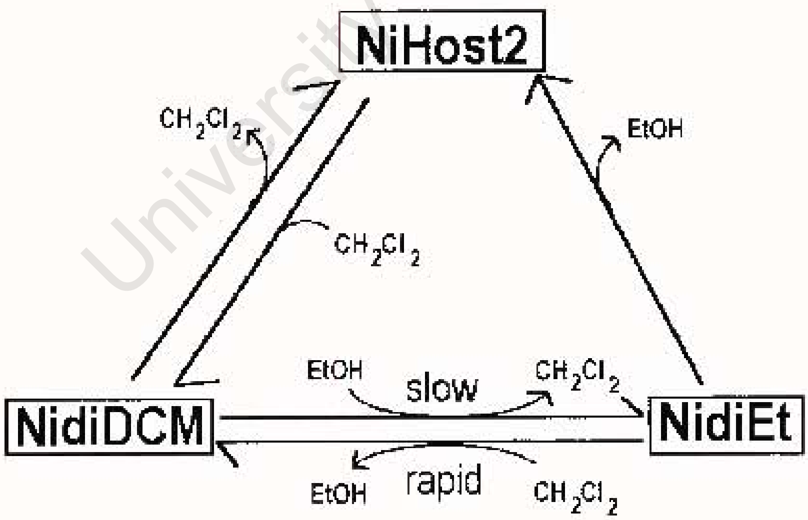

The evidence suggests that CH_2Cl_2 as a guest is better able to support the channel structure than EtOH. As the shape of these two guests is similar, it may be a host···guest hydrogen bonding effect that appears to give the clathrate structure an increased affinity for CH_2Cl_2.

CHAPTER 3.3

WERNER CLATHRATES

$H = Ni(NCS)_2(isonicotinamide)_x(H_2O)_{4-x}$

Table 3.3.1: Crystal data and refinement parameters for Nitriaq

	Nitriaq
Molecular Formula	$C_{20}H_{26}N_8O_7S_2Ni$
M_r (g/mol)	613.29
Crystal System	Monoclinic
Space group	C2/c
Z	8
a (Å)	19.216(2)
b (Å)	13.052(1)
c (Å)	20.639(2)
β (deg.)	97.029(3)
V (Å^3)	5137.5(7)
D_{calc} (g/cm^3)	1.586
Crystal dimension (mm)	0.20 x 0.25 x 0.16
Temp of data collection (K)	173
Range scanned (θ)	1.89 – 25.31
Index Range	$20 \geq h \geq -23$, $184 \geq k \geq -13$, $13 \geq l \geq -23$
F (000)	2544
μ (mm^{-1})	0.98
No. reflections collected	7668
No. unique reflections	3782 (R_{int} = 0.0314)
Completeness	80.8%
Refinement method	Full-matrix L.S. on F^2
Data/restraints/parameters	3782/0/419
Goodness of fit on F^2	1.044
Final R indices (I>2σ(I))	R_1=0.0470, wR_2=0.1039
R indices (all data)	R_1=0.0697, wR_2=0.1135
Largest diff. Peak and hole	0.741, -0.344 eÅ^{-3}

Table 3.3.2: Crystal data and refinement parameters for Nipcres and Nimcres

	Nipcres	**Nimcres**
Molecular Formula	$C_{48}H_{64}N_{10}O_{10}S_2Ni$	$C_{54}H_{56}N_{10}O_8S_2Ni$
M_r (g/mol)	1063.9	1096.6
Crystal System	Triclinic	Monoclinic
Space group	$P\overline{1}$	$P2_1$
Z	2	2
a (Å)	14.3563(3)	12.9232(2)
b (Å)	14.8709(3)	16.2155(3)
c (Å)	15.0563(3)	13.1266(2)
α (deg.)	74.463(1)	90
β (deg.)	73.784(1)	98.762(1)
γ (deg.)	61.488(1)	90
V ($Å^3$)	2677.46(9)	2718.66(8)
D_{calc} (g/cm^3)	1.320	1.339
Crystal dimension (mm)	0.55 x 0.47 x 0.39	0.39 x 0.33 X 0.34
Temp of data collection (K)	173	173
Range scanned (θ)	1.64 – 27.48	2.01 – 27.48
Index Range	$14\geq h\geq -17$, $18\geq k\geq -18$, $19\geq l\geq -19$	$16\geq h\geq -16$, $21\geq k\geq -21$, $16\geq l\geq -17$
F (000)	1124	1148
μ (mm^{-1})	0.50	0.50
No. reflections collected	15476	28537
No. unique reflections	10960 (R_{int} = 0.0176)	11880 (R_{int} = 0.0232)
Completeness	89.1%	99.6%
Refinement method	Full-matrix L.S. on F^2	Full-matrix L.S. on F^2
Data/restraints/parameters	10960/0/874	11880/1/789
Goodness of fit on F^2	1.019	1.022
Final R indices ($I>2\sigma(I)$)	R_1=0.0365, wR_2=0.0817	R_1=0.0384, wR_2=0.0934
R indices (all data)	R_1=0.0523, wR_2=0.0895	R_1=0.0481, wR_2=0.0980
Flack x parameter (e.s.d.)	-	0.0000(0.0290)
Largest diff. peak and hole	0.436, -0.321 $eÅ^{-3}$	0.948, -0.350 $EÅ^{-3}$

Nitriaq : $Ni(NCS)_2(isonicotinamide)_3(H_2O).3H_2O$

PRELIMINARY X-RAY PHOTOGRAPHY:

Single crystals of **Nitriaq** were unsuitable for photography due to their small size.

SINGLE CRYSTAL X-RAY DIFFRACTOMETRY:

STRUCTURE SOLUTION AND REFINEMENT:

The diffraction data revealed *2/m* Laue symmetry, indicating a monoclinic unit cell. Systematic absences were indicative of the monoclinic space groups C2/c or Cc. Xprep calculated a mean $|E^2-1|$ value of 0.959, indicating that the centrosymmetric space group, C2/c, is correct. The structure was solved and fully refined in this space group, with the Ni atom occupying a general position in the unit cell.

All non-hydrogen atoms were located on the electron density map and refined anisotropically. All host hydrogen atoms were also located on the electron density map, but refined isotropically. The hydrogen atoms of the three water guest molecules could not be located, and were consequently omitted from the final model (crystal structure and refinement details are given in Table 3.3.1).

STRUCTURE ANALYSIS:

Solving the structure in C2/c revealed a central Ni atom coordinated to two axial NCS^- counterions, three isonicotinamide ligands and one water molecule (Fig.3.3.1). The coordination geometry around the Ni centre is that of an irregular octahedron.

The Ni–N_{CS} and Ni–N_{pyr} bond lengths correspond well with the literature values of 2.04(8)Å and 2.11(6)Å respectively (Table 3.3.3)[1]. The Ni–OH_2 bond is slightly longer than the literature value of 2.08(4)Å[1], possibly due to the hydrogen bonding interactions of this water ligand. Full bond lengths and angles are given in Appendix 3.

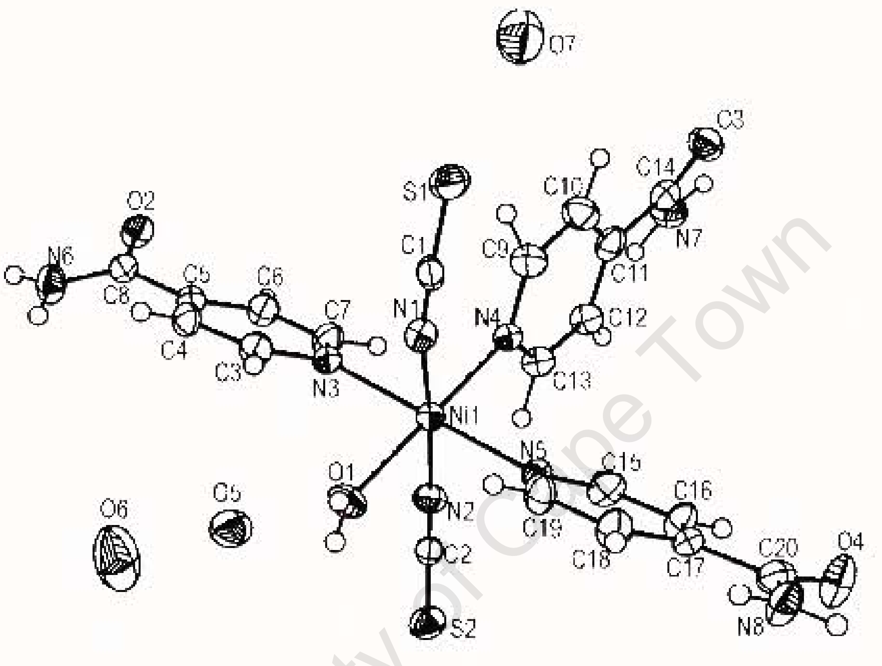

Fig 3.3.1: Ortep diagram of Nitriaq showing thermal ellipsoids

Table 3.3.3: Selected bond lengths and angles around the Ni centre

Bond	Length (Å)	Angle	Angle (°)
Ni1 – N1	2.045(4)	N1 – Ni1 – O1	88.2(2)
Ni1 – N2	2.034(4)	N1 – Ni1 – N3	89.1(1)
Ni1 – N3	2.118(3)	N3 – Ni1 – N5	177.9(1)
Ni1 – N4	2.152(4)	N2 – Ni1 – N4	91.7(1)
Ni1 – N5	2.120(3)	N3 – Ni1 – O1	88.4(1)
Ni1 – O1	2.130(3)	O1 – Ni1 – N4	177.0(2)

HYDROGEN BONDING INTERACTIONS AND CRYSTAL PACKING:

The water ligand, water guests and amide moieties form an intricate web of host···host, host···guest and guest···guest hydrogen bonding interactions. The eight contacts where the distance between the two heavy atoms was less than the sum of their van der Waals radii (3.04Å for O···O and 3.07Å for O···N) were examined (Table 3.3.4).

Table 3.3.4: Hydrogen Bonding Data for Nitriaq

D–H ··· A	D – H (Å)	H ··· A (Å)	D ··· A (Å)	Angle (°)
		HOST···HOST INTERACTIONS		
N8–H17 ··· O2$^{\#1}$	0.859(55)	2.079(55)	2.916(6)	164.7(5.3)
O1–H19$^{\#3}$ ··· O3	0.821(53)	2.007(51)	2.795(5)	160.5(5.2)
O1–H20$^{\#4}$ ··· O3	0.735(66)	2.128(65)	2.819(5)	157.0(6.5)
		HOST···GUEST INTERACTIONS		
N7–H12 ··· O5$^{\#2}$	1.095(68)	1.817(68)	2.872(6)	160.2(5.4)
O4$^{\#5}$ ··· O7	-	-	2.658(5)	-
O2 ··· O6$^{\#6}$	-	-	2.964(6)	-
		GUEST···GUEST INTERACTIONS		
O5 ··· O6	-	-	2.681(6)	-
O6 ··· O7$^{\#7}$	-	-	2.891(5)	-

Symmetry codes: #1 = x-½, ½-y, z-½, #2 = ½–x, ½-y, 1-z, #3 = ½-x, ½+y, ½-z, #4 = ½+x, ½+y, z, #5 = ½+x, y-½, z, #6 = ½-x, y-½, 1-z, and #7 = x-½, y-½, z.

The host molecules are arranged into layers, which run perpendicular to the [10$\bar{1}$] direction. Host···host N–H···O hydrogen bonds link the host molecules into layers, while host···host O–H···O hydrogen bonds link the layers into bilayers, as well as connecting adjacent bilayers (Fig. 3.3.2a). The water guest molecules also contribute to the linking of adjacent bilayers, as shown in Fig. 3.3.2b. The isothiocyanato moieties project into the spaces between the layers and bilayers.

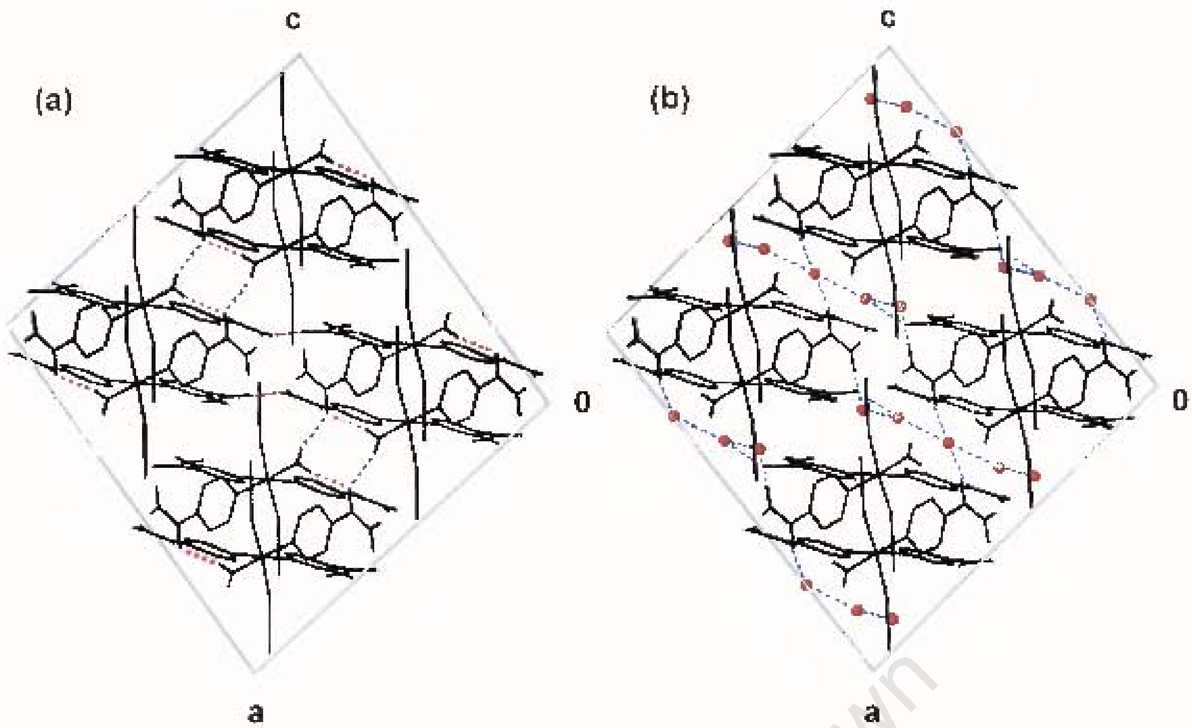

Fig 3.3.2: Nitriaq viewed along [010] (a) Stick representation of host molecules showing intermolecular hydrogen bonding interactions within and between bilayers (shown as red and blue broken lines respectively; ring H atoms omitted for clarity), (b) Stick representation of host molecules, with guest oxygen atoms shown as red circles (Host···guest and guest···guest hydrogen bonds shown as blue broken lines; ring H atoms omitted for clarity).

The water guest molecules are located in V-shaped cavities, each cavity enclosing five water guests (Fig. 3.3.3). The five water guests are hydrogen bonded to each other, and the walls of the cavities, as shown in Fig. 3.3.2b above.

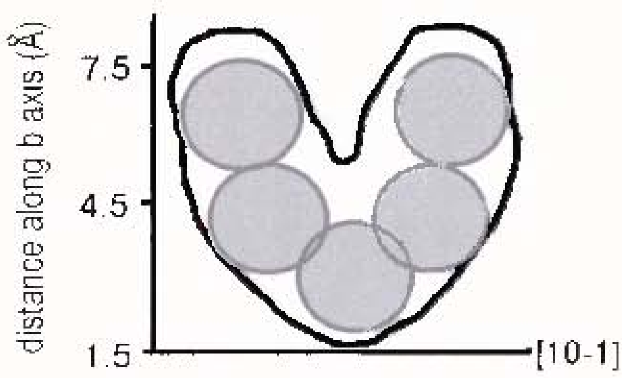

Fig 3.3.3: Diagrammatic representation of the V-shaped cavities in Nitriaq (guest water molecules are shown as solid grey spheres).

Nipcres: $Ni(NCS)_2(isonicotinamide)_4.2p$-cresol.4EtOH

PRELIMINARY X-RAY PHOTOGRAPHY:

Single crystals of **Nipcres** were unsuitable for photography, as they decompose at room temperature, as well as being highly unstable in air.

SINGLE CRYSTAL X-RAY DIFFRACTOMETRY:

STRUCTURE SOLUTION AND REFINEMENT:

The diffraction data revealed $\bar{1}$ Laue symmetry, indicating the triclinic unit cells P1 or $P\bar{1}$. Xprep calculated a mean $|E^2-1|$ value of 0.977, indicating that the centrosymmetric space group, $P\bar{1}$, is correct. The structure was solved and fully refined in this space group.

All non-hydrogen atoms were located on the electron density map and refined anisotropically. All hydrogen atoms were located on the electron density map and refined isotropically, with the exception of the methyl hydrogens of *p*-cresol, which were placed in geometrically calculated positions (crystal structure and refinement details are given in Table 3.3.2).

STRUCTURE ANALYSIS:

Solving the structure in $P\bar{1}$ revealed a central Ni atom coordinated to two axial NCS^- counterions and four equatorial isonicotinamide ligands. The coordination geometry around the Ni centre is that of an irregular octahedron, with the isonicotinamide ligands adopting the propeller conformation (Fig. 3.3.4).

The $Ni–N_{CS}$ bonds are 2.040(2)Å and 2.058(2)Å in length, while the $Ni–N_{pyr}$ bonds lie in the range 2.128(2) to 2.135(2)Å. These values correspond well with the literature values of 2.04(8)Å and 2.11(6)Å respectively[1]. Full bond lengths and angles are given in Appendix 3.

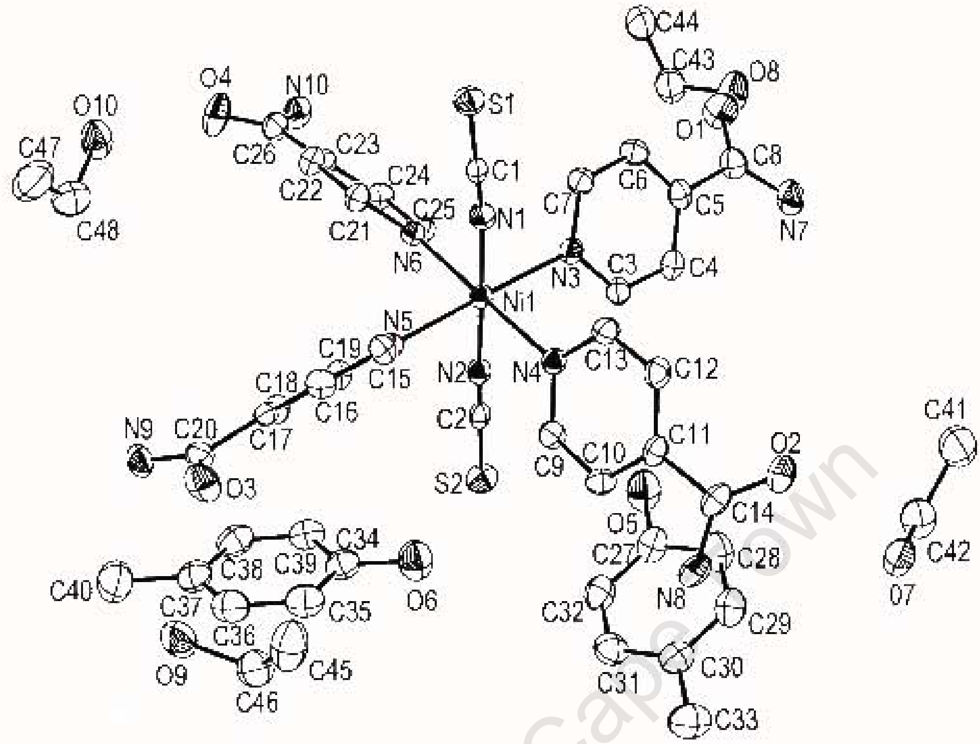

Fig 3.3.4: Ortep diagram of Nipcres, showing thermal ellipsoids (H atoms omitted for clarity).

HYDROGEN BONDING INTERACTIONS AND CRYSTAL PACKING:

Ten unique hydrogen bonds, where the distance between the two heavy atoms was less than the sum of their van der Waals radii, could be identified within the crystal structure. All are host···guest interactions. Each ethanol guest forms an O–H···O=C and an O···H–N hydrogen bond to the amide groups of two adjacent isonicotinamide ligands (Fig. 3.3.5). In addition, the S atom of one isothiocyanato counterion is weakly hydrogen bonded to the hydroxyl group of both *p*-cresol guests (Table 3.3.5).

Table 3.3.5: Hydrogen bonding Data for Nipcres

D–H···A	D–H (Å)	H···A (Å)	D···A (Å)	Angle (°)
HOST ··· ETHANOL INTERACTIONS				
N7–H5···O10[#1]	0.899(26)	1.910(23)	2.783(2)	163.3(2.7)
N8–H11···O8[#2]	0.885(24)	1.973(25)	2.839(3)	166.1(2.4)
N9–H18···O7[#3]	0.872(21)	1.978(21)	2.837(2)	168.2(2.3)
N10–H23···O9[#4]	0.847(31)	2.002(28)	2.835(3)	167.2(2.5)
O7–H46···O2	0.803(41)	1.976(39)	2.772(3)	171.1(3.2)
O8–H52···O1	0.875(34)	1.876(35)	2.751(2)	177.5(3.4)
O9–H58···O3	0.827(30)	1.930(27)	2.749(2)	170.3(3.3)
O10–H64···O4	0.841(30)	1.893(30)	2.731(2)	174.4(3.0)
HOST ··· *p*-CRESOL INTERACTIONS				
O5–H29···S2	0.811(30)	2.532(31)	3.340(2)	174.0(2.8)
O6–H37···S2	0.851(28)	2.535(28)	3.383(2)	175.7(2.8)

Symmetry codes: #1 = x, y, 1+z, #2 = 1+x, y-1, z, #3 = x, y, z-1, and #4 = x-1, 1+y, z.

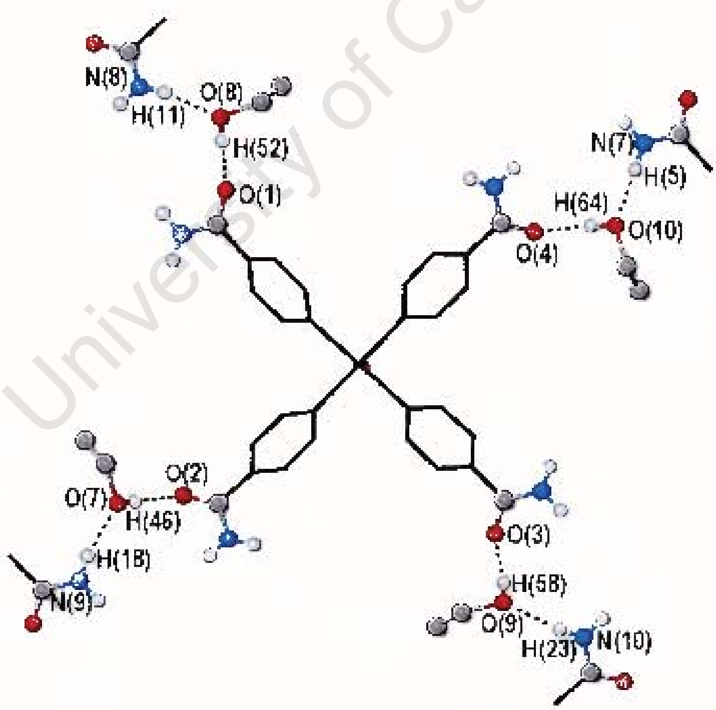

Fig 3.3.5: Hydrogen bonding interactions of the four unique ethanol guest molecules (aromatic and methyl hydrogen atoms omitted for clarity).

The host complexes and ethanol guests form layers, which run perpendicular to the [110] direction. The layers are stabilised by host···ethanol hydrogen bonds, as shown in Fig. 3.3.6a. The layers stack to form bilayers, in which the isothiocyanato moieties of one layer project into the cavities generated by the adjacent layer (Fig. 3.3.6b).

The bilayers are stacked along the [110] direction. Layers of p-cresol guest molecules (Fig. 3.3.7) occupy the spaces between the bilayers. If sections of the unit cell are viewed along the [001] direction, it is found that in the range $0.27<c<0.73$, isothiocyanate moieties project into the spaces between the bilayers, partitioning them into inclusion channels (Fig. 3.3.8a). In the range $0<c<0.27$ and $0.73<c<1$, however, no groups project into the interlayer spaces, and the channels widen out into layers (Fig. 3.3.8b).

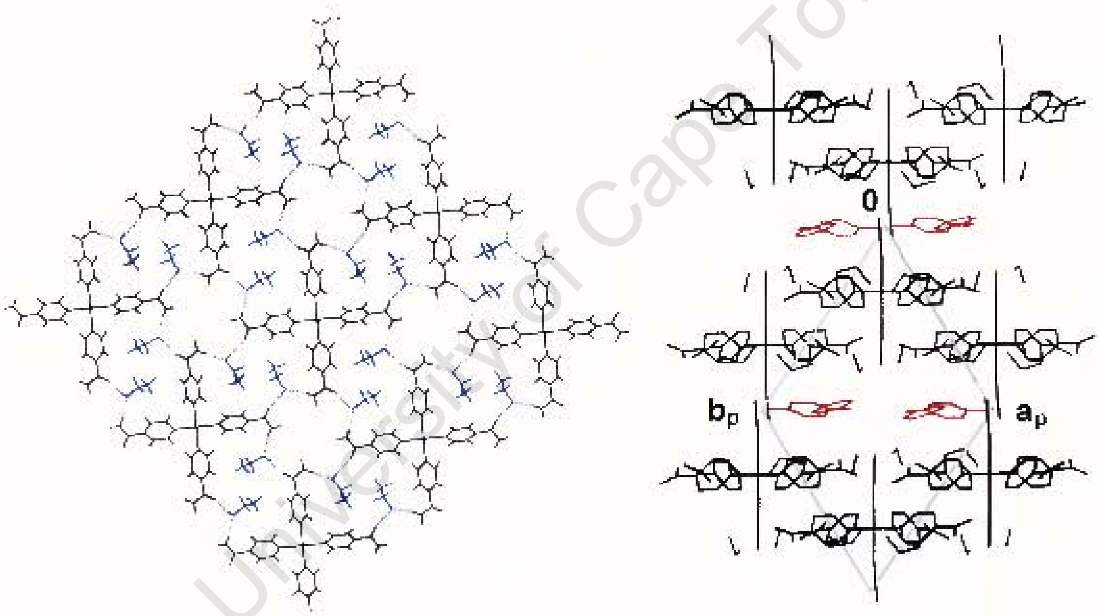

(a) (b)

Fig 3.3.6: Stick representation of (a) a single layer of host (black) and ethanol (blue) molecules viewed along [110] (hydrogen bonds shown as broken lines), and (b) the stacking of bilayers to accommodate *p*-cresol guest molecules (red).

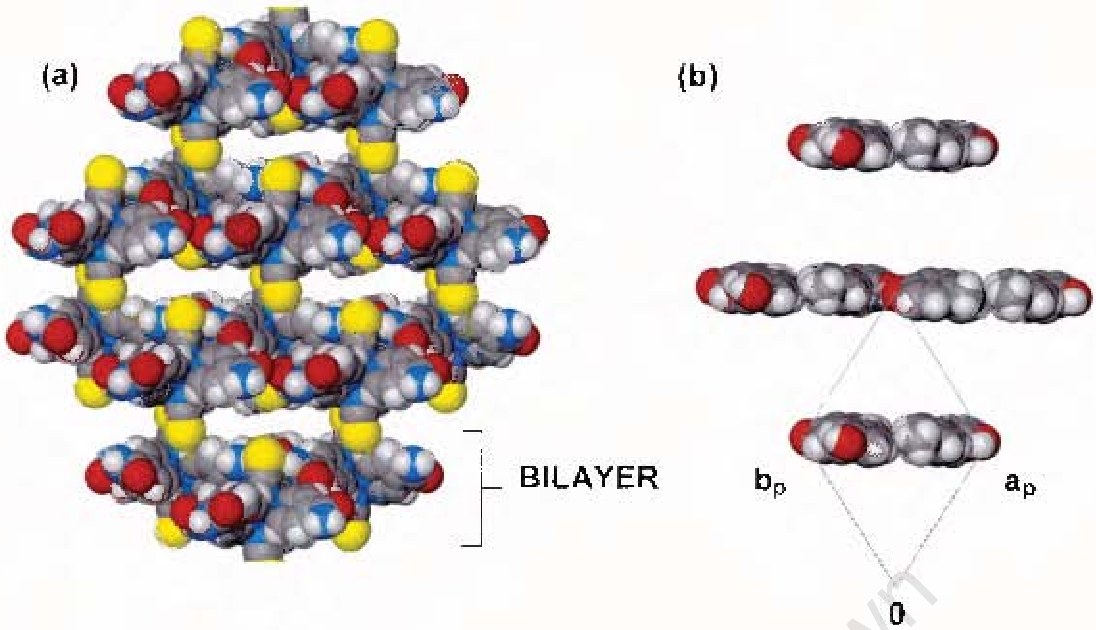

Fig3.3.7: (a) The stacking of host bilayers in Nipcres generates cavities running parallel to the [001] direction (guest *p*-cresol molecules omitted for clarity), (b) the positions of the layers of *p*-cresol guest molecules.

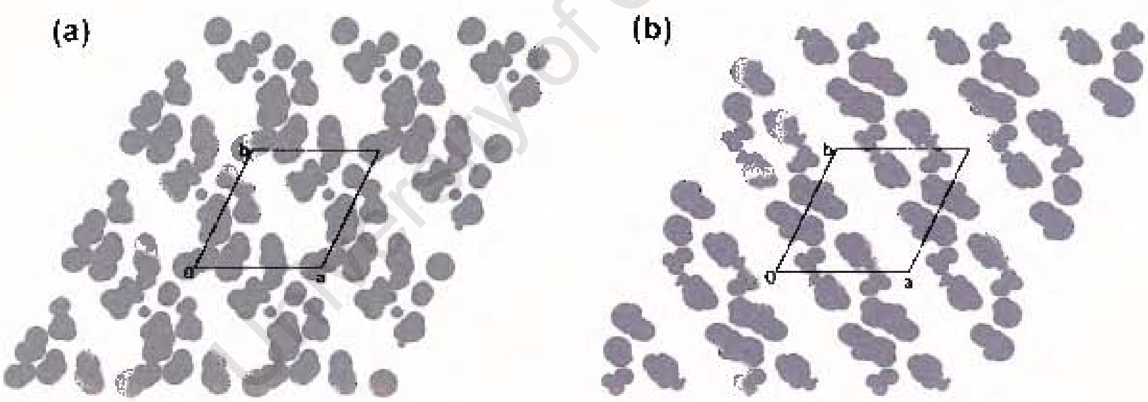

Fig 3.3.8: Space-filling representation of the host and ethanol molecules in Nipcres, viewed along the [001] direction, at (a) c = 0.39, showing channel arrangement and (b) c = 0, showing layer arrangement (*p*-cresol guest molecules omitted for clarity).

Nimcres: $Ni(NCS)_2(isonicotinamide)_4.4m$-cresol

PRELIMINARY X-RAY PHOTOGRAPHY:

Single crystals of **Nimcres** were unsuitable for photography as they decompose at room temperature and are unstable in air.

SINGLE CRYSTAL X-RAY DIFFRACTOMETRY:

STRUCTURE SOLUTION AND REFINEMENT:

The diffraction data revealed *2/m* Laue symmetry, indicating a monoclinic unit cell. Systematic absences were indicative of the chiral monoclinic space group $P2_1$. The structure was solved and fully refined in this space group, with the Ni atom occupying a general position in the unit cell.

All non-hydrogen atoms were located on the electron density map and refined anisotropically. The aromatic and amide hydrogens of the host were all located on the electron density map and refined isotropically. Three of the four guest hydroxyl hydrogens could be located, and were refined isotropically. The other hydroxyl hydrogen could not be located and was omitted from the final model. The guest aromatic and methyl hydrogens were placed in geometrically calculated positions (crystal structure and refinement details are given in Table 3.3.2).

STRUCTURE ANALYSIS:

As in **Nipcres**, the Ni centre is coordinated to two axial NCS^- counterions and four equatorial isonicotinamide ligands, resulting in an irregular octahedral coordination geometry for the Ni atom (Fig. 3.3.9). The isonicotinamide ligands adopt the propeller conformation.

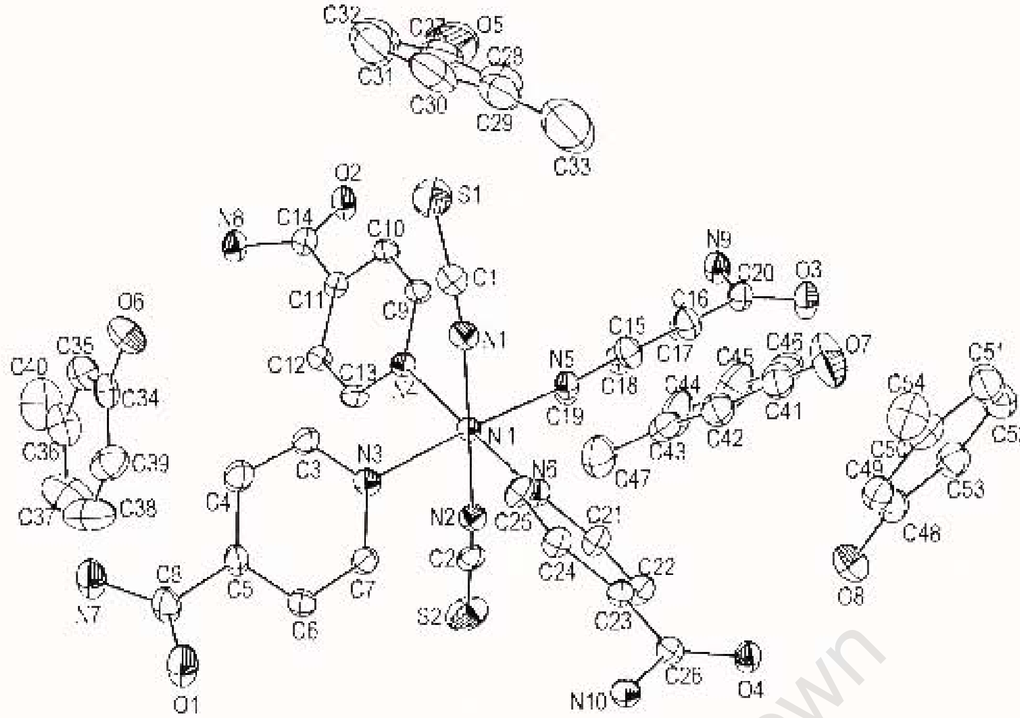

Fig 3.3.9: Ortep diagram of Nimcres, showing thermal ellipsoids (H atoms omitted for clarity).

The Ni–N_{CS} bonds are 2.044(2)Å and 2.045(2)Å in length, while the Ni–N_{pyr} bonds lie in the range 2.126(2) to 2.148(2)Å. These values correspond well with the literature values of 2.04(8)Å and 2.11(6)Å respectively[1]. Full bond lengths and angles are given in Appendix 3.

HYDROGEN BONDING INTERACTIONS AND CRYSTAL PACKING:

Each host complex is hydrogen bonded to four *m*-cresol guest molecules. Ten unique hydrogen bonding interactions, where the distance between the two heavy atoms was less than, or close to, the sum of the van der Waals radii for the two heavy atoms, could be identified (Table 3.3.6). These interactions can be divided into three main groups, those between two host molecules, those between a host and a guest molecule (Fig. 3.3.10), and those between two guest molecules.

Table 3.3.6: Hydrogen bonding Data for Nimcres

D–H···A	D – H (Å)	H ··· A (Å)	D ··· A (Å)	Angle (°)
		HOST ··· HOST INTERACTIONS		
N7–H5 ··· O2#1	0.790(36)	2.168(35)	2.919(3)	158.9(3.2)
N8–H11 ··· O3#2	0.833(29)	2.215(29)	3.024(3)	163.9(2.9)
N7–H6#3 ··· O4	0.912(32)	2.239(31)	3.102(3)	157.6(3.0)
N9–H17#4 ··· O1	0.815(36)	2.184(36)	2.945(3)	173.7(3.4)
N10–H24 ··· O2#5	0.890(30)	1.968(30)	2.836(2)	164.3(3.0)
N10–H23 ··· O3#6	0.794(34)	2.280(33)	2.963(3)	144.7(3.0)
		HOST ··· GUEST INTERACTIONS		
O8–H49 ··· O4	0.815(44)	1.859(43)	2.665(3)	169.9(4.2)
N8–H12 ··· O6	0.809(35)	2.173(35)	2.963(3)	165.7(3.3)
O7–H41 ··· S1#7	1.049(42)	2.126(41)	3.168(4)	171.9(3.2)
O5 ··· S2#8	-	-	3.214(4)	-
		GUEST ··· GUEST INTERACTIONS		
O6–H33#9 ··· O8	0.936(35)	1.822(34)	2.732(3)	163.3(3.4)

Symmetry codes: #1 = x, y, z-1, #2 = 1+x, y, z, #3 = x-1, y, z, #4 = x, y, z-1, #5 = x-1, y, z-1, #6 = x, y, z-1, #7 = −x, y-½, 1-z, #8 = 1-x, ½+y, 1-z, and #9 = x-1, y, z.

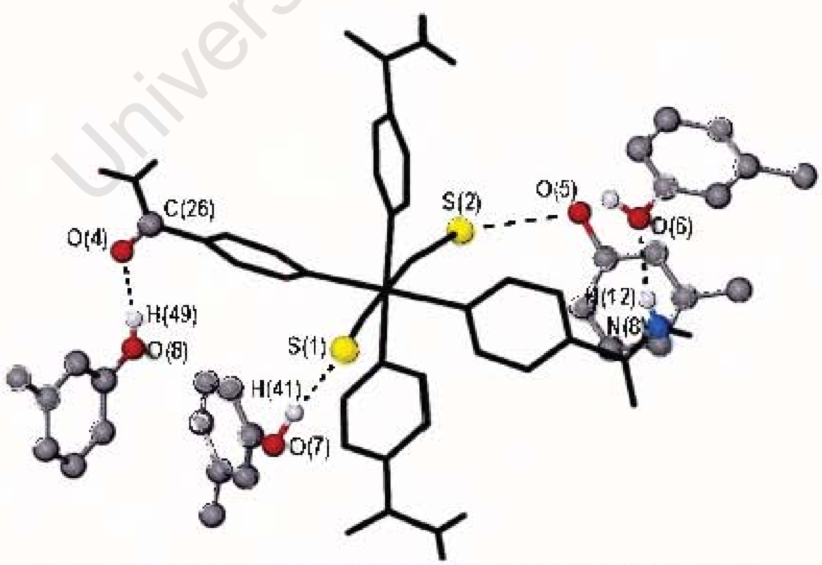

Fig 3.3.10: Host···guest hydrogen bonds in Nimcres

The host molecules pack to generate layers, running perpendicular to the [010] direction, and cutting the *b* axis at 0.25 and 0.75 (Fig. 3.3.11a). The layers are stabilised by intermolecular host···host hydrogen bonding interactions. Adjacent layers are related by rotation through 180°, followed by translation of half a unit cell length along *b*. The NCS^- counterions project into the spaces between layers, partitioning them into inclusion channels (Fig. 3.3.11b).

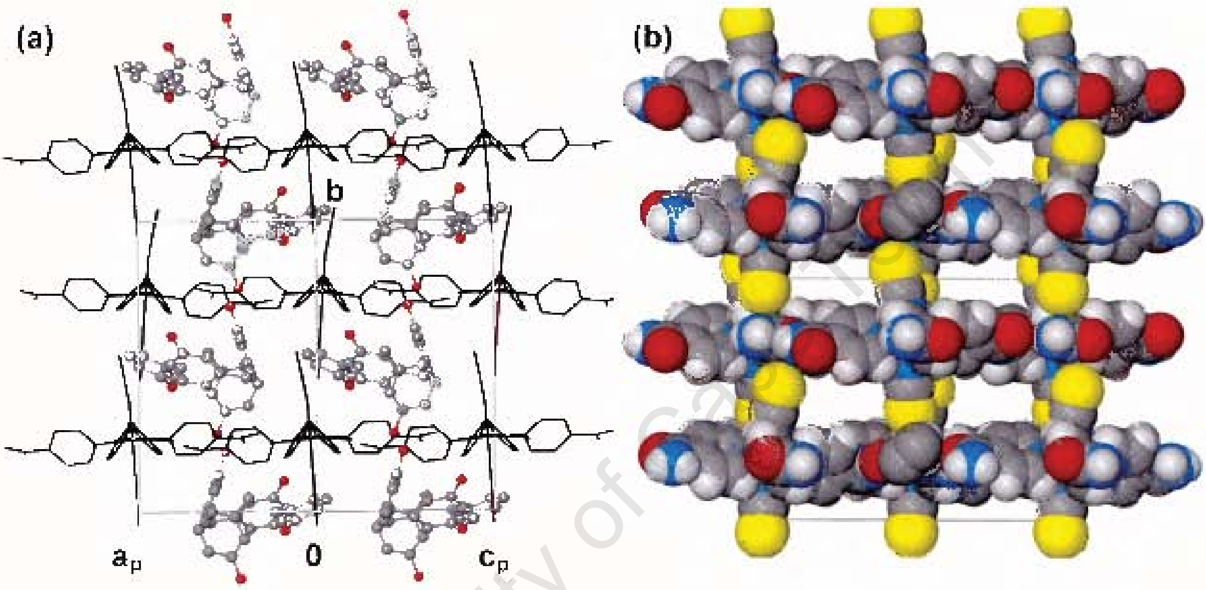

Fig. 3.3.11: (a) Stick representation of the layers of host molecules in Nimcres, viewed along [101] (guest molecules in ball-and-stick form; H atoms omitted for clarity). (b) Space-filling representation of the host complexes in Nimcres, showing the major channels (guest molecules omitted for clarity).

If sections of the unit cell are viewed perpendicular to the layers of host molecules, the geometry of the cavities in which the guest molecules are accommodated can be examined. The host layers are centered at b = 0.25 and 0.75 (Fig. 3.3.12a). The layers of guest molecules are therefore situated midway between these layers, at b = 0 and 0.5. Fig. 3.3.12b shows the positions of the isothiocyanate moieties at b = 0, while Fig. 3.3.12c shows the same view but with the *m*-cresol guests inserted. These diagrams reveal the *m*-cresol guest molecules to be situated in cross-channels in the [101] (major channels) and [$10\overline{1}$] (minor channels) direction. The major channels have a minimum cross-section of 5.4X2.5Å, while for the minor channels this cross-section measures 3.3X2.5Å.

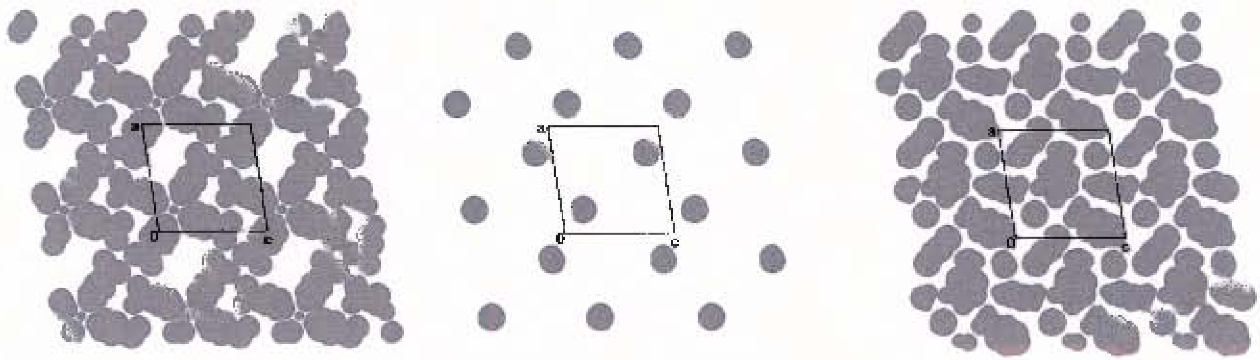

(a) (b) (c)

Fig 3.3.12: Space-filling representation, viewed along the [010] direction, of (a) host molecules, at b = 0.25, (b) host molecules at b = 0 and (c) host and guest molecules at b = 0.

THERMAL ANALYSIS

The thermal analyses of all three compounds are shown in Figs 3.3.13 and 3.3.15. In the TG of **Nitriaq**, three distinct weight loss processes are observed, labelled **a**-**c** in Fig. 3.3.13. Step **a** corresponds to the loss of the three water guests and one water ligand from the hydrate, while steps **b** and **c** correspond to the loss of one and two isonicotinamide ligands respectively. Steps **a** and **b** are accompanied by complex endotherms in the DSC. Between these two steps there is a small, broad exotherm, possibly due to a phase change in the host complex upon water loss. Step **b** is immediately followed by exothermic decomposition.

The decomposition of **Nitriaq** was followed by HSM (Fig. 3.3.14a). During step **a** the translucent blue crystals bubble and turn opaque blue. During step **b** the crystals turn from blue to green, while step **c** is accompanied by bubbling, and a gradual lightening of the crystals to an orange colour, which darkens until the crystals are completely black. The colour changes observed in step **c** are consistent with the exothermic decomposition observed in the DSC.

The TG of **Nipcres** reveals six distinct weight loss steps, labelled **a-f** in Fig. 3.3.15a. Steps **a** and **b** each correspond to the release of two ethanol guests, while step **c** corresponds to the loss of the two *p*-cresol guests. Steps **d** and **e** each correspond to the loss of one isonicotinamide ligand, and step **f** to the simultaneous loss of two isonicotinamide ligands. Due to a seeding problem, single crystals of **Nipcres** could not be remade, with the result that the DSC could not be measured.

The TG of **Nimcres** shows five distinct weight loss steps, labelled **a-e** in Fig. 3.3.15b. Steps **a** and **b** each correspond to the release of two *m*-cresol guests, per formula unit, from the clathrate. Thereafter, the decomposition process follows the same pattern described above, with steps **c**, **d** and **e** corresponding to the loss of one, one and two isonicotinamide ligands respectively. The DSC shows a single endotherm corresponding to steps **a** and **b** (T_{onset} = 97.4°C, ΔH = 90.7kJ.mol^{-1}). The remaining steps, however, are accompanied by exothermic decomposition.

The translucent purple crystals of **Nimcres** undergo several colour changes when observed by HSM. During steps **a** and **b** the crystals gradually turn opaque, going from purple to blue, and finally turquoise. At the onset of the ligand release steps, the crystals turn opaque green before melting to a dark green liquid, which bubbles until a black residue remains (Fig. 3.3.14b). These observations are consistent with the ligand decomposition observed in the DSC during steps **c-e**. Full TG data for all three compounds are given in Table 3.3.7.

Table 3.3.7: TG data for Niaq, Nipcres and Nimcres

Compound	Reaction	T_{onset} (°C)	Exp %	Calc%
Nitriaq	$Ni(NCS)_2(L)_3(H_2O).3H_2O \rightarrow Ni(NCS)_2(L)_3 + 4H_2O$	69.0	12.4	11.7
	$Ni(NCS)_2(L)_3 \rightarrow Ni(NCS)_2(L)_2 + L$	224.2	18.3	19.9
	$Ni(NCS)_2(L) \rightarrow Ni(NCS) + 2L$	289.8	38.2	39.8
Nipcres	$Ni(NCS)_2(L)_4.2p\text{-cresol}.4EtOH \rightarrow Ni(NCS)_2(L)_4.2p\text{-cresol}.2EtOH + 2EtOH$	34.7	7.3	8.6
	$Ni(NCS)_2(L)_4.2p\text{-cresol}.2EtOH \rightarrow Ni(NCS)_2(L)_4.2p\text{-cresol} + 2EtOH$	93.9	8.4	8.6
	$Ni(NCS)_2(L)_4.2p\text{-cresol} \rightarrow Ni(NCS)_2(L)_4 + 2p\text{-cresol}$	146.6	19.3	20.3
	$Ni(NCS)_2(L)_4 \rightarrow Ni(NCS)_2(L)_3 + L$	198.5	11.0	11.5
	$Ni(NCS)_2(L)_3 \rightarrow Ni(NCS)_2(L)_2 + L$	246.8	12.0	11.5
	$Ni(NCS)_2(L)_2 \rightarrow Ni(NCS)_2 + 2L$	280.5	23.8	23.0
Nimcres	$Ni(NCS)_2(L)_4.4m\text{-cresol} \rightarrow Ni(NCS)_2(L)_4.2m\text{-cresol} + 2m\text{-cresol}$	109.1	19.8	19.7
	$Ni(NCS)_2(L)_4.2m\text{-cresol} \rightarrow Ni(NCS)_2(L)_4 + 2m\text{-cresol}$	142.1	20.3	19.7
	$Ni(NCS)_2(L)_4 \rightarrow Ni(NCS)_2(L)_3 + L$	186.5	9.4	11.1
	$Ni(NCS)_2(L)_3 \rightarrow Ni(NCS)_2(L)_2 + L$	241.5	10.9	11.1
	$Ni(NCS)_2(L)_2 \rightarrow Ni(NCS)_2 + 2L$	274.2	21.8	22.3

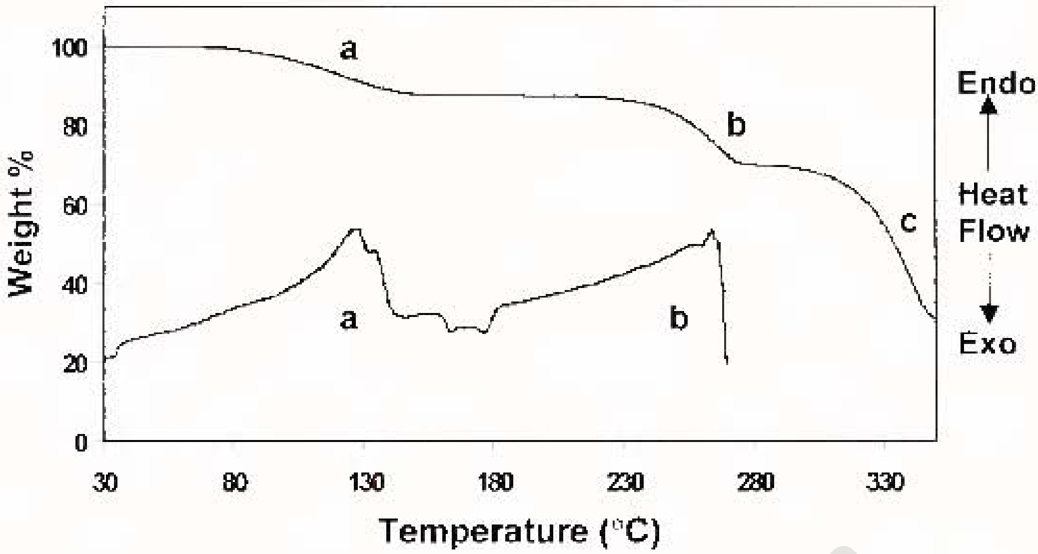

Fig 3.3.13: Thermal analysis of Nitriaq.

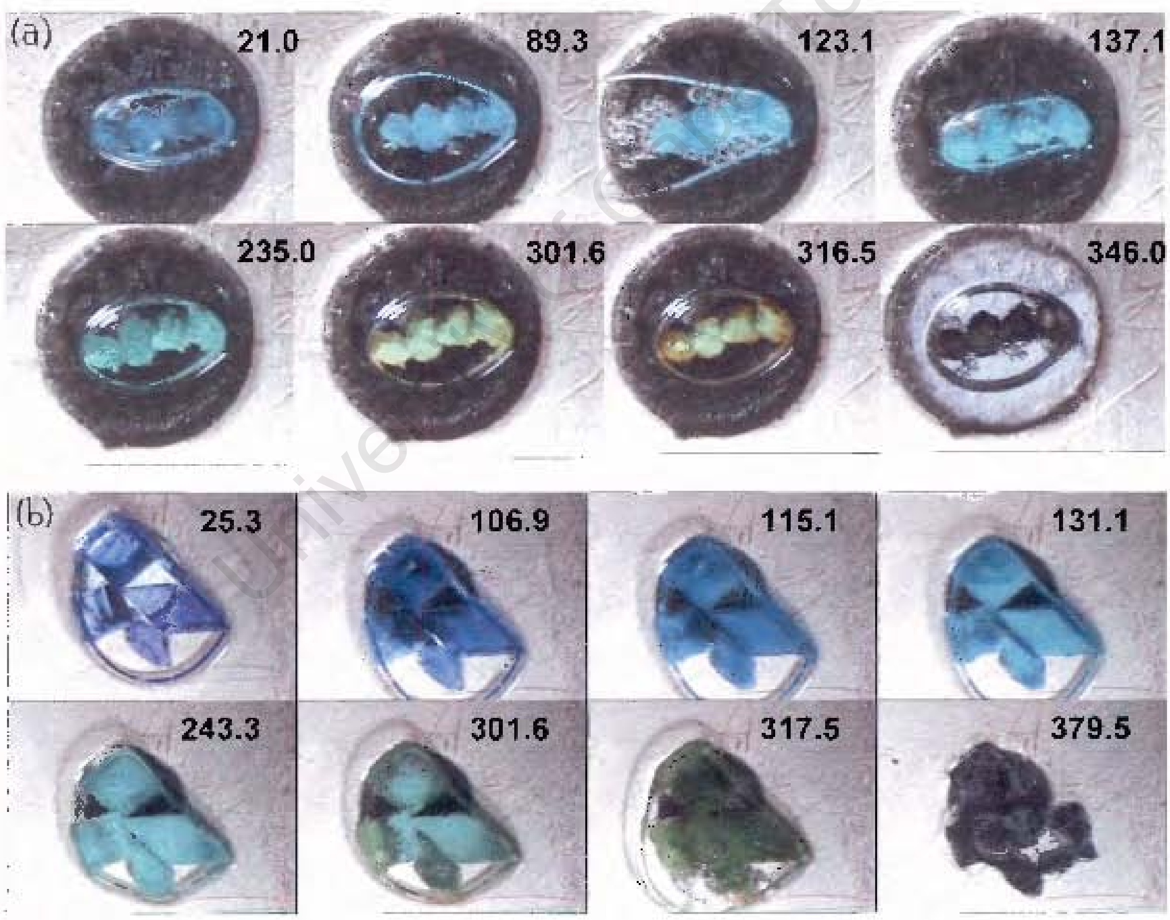

Fig 3.3.14: HSM of (a) Nitriaq and (b) Nimcres (Temperatures, in °C, are shown in top right hand corner)

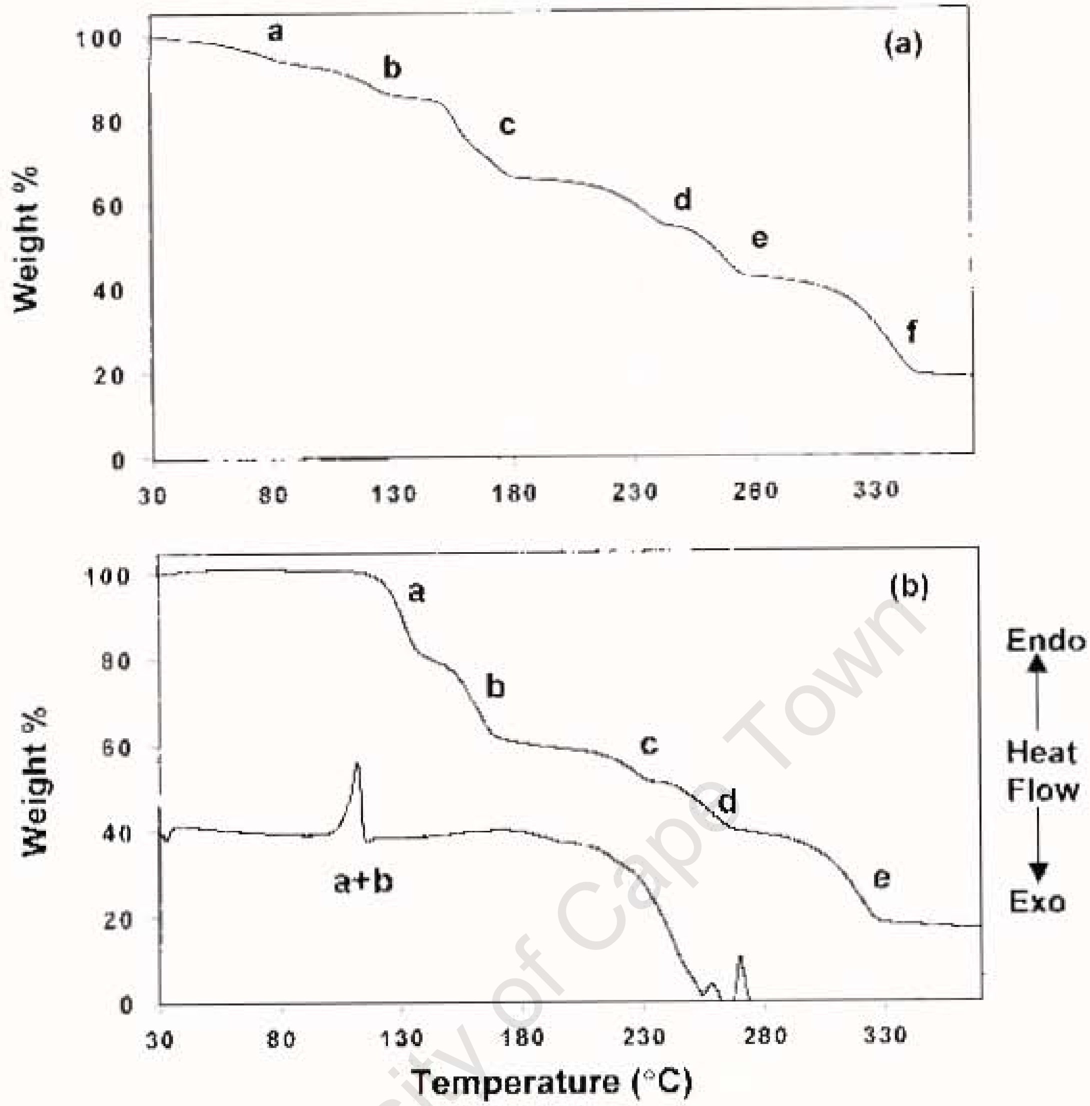

Fig 3.3.15: Thermal analyses of (a) Nipcres and (b) Nimcres.

DISCUSSION

Nipcres and **Nimcres** both adhere to the classical Werner clathrate formula, MX_2A_4. The **Nitriaq** host molecules, however, have the general formula, $MX_2A_3(H_2O)$. Despite being crystallised under virtually identical conditions, **Nipcres** includes ethanol and *p*-cresol, whereas **Nimcres** includes *m*-cresol only. This difference can only be attributed to the difference in shape between the cresol isomers. In all three structures, the amide substituents on the pyridine ligands form an intricate web of hydrogen bonding interactions.

All three compounds are examples of layer clathrates. In **Nipcres** the host complexes and ethanol guests form bilayers, stabilised by intermolecular hydrogen bonds. Layers of *p*-cresol guest molecules are located in the spaces between the bilayers. This clathrate is highly unstable, and decomposes within minutes when removed from the mother liquor.

Nimcres consists of layers of host molecules, with the *m*-cresol guest molecules located in cross-channels generated by projection of the isothiocyanate groups into the interlayer spaces. This structure, too, is kinetically unstable, with the guest molecules being released before the onset of host decomposition.

In **Nitriaq** the host molecules are arranged into bilayers. The spaces between the bilayers are partitioned into discrete V-shaped cavities, which enclose the water guests. This results in a kinetically stable clathrate, with the guest molecules only being released at the onset of host decomposition (i.e. as the water ligands are lost).

CHAPTER 3.4

POLYMERIC WERNER CLATHRATES

$H = Ni(NCS)_2(3\text{-aminopyridine})_x(H_2O)_{3-x}$

Table 3.4.1: Crystal Data and Refinement Parameters for NiEt and NiMe

	NiEt	**NiMe**
Molecular Formula	$C_{19}H_{24}N_8OS_2Ni$	$C_{18}H_{22}N_8OS_2Ni$
M_r (g/mol)	503.27	489.27
Crystal System	Monoclinic	Monoclinic
Space group	C2/c	C2/c
Z	8	8
a (Å)	24.7020(4)	23.981(1)
b (Å)	10.9545(2)	10.9301(3)
c (Å)	16.8574(3)	16.8867(3)
β (deg.)	90.595(1)	92.851(2)
V (Å^3)	4561.3(2)	4420.8(2)
D_{calc} (g/cm^3)	1.465	1.470
Crystal dimension (mm)	0.47 x 0.38 X 0.35	0.51 x 0.40 x 0.40
Temp of data collection (K)	173	173
Range scanned (θ)	2.36 – 27.63	1.70 – 27.50
Index Range	$21 \geq h \geq -30$, $14 \geq k \geq -12$, $21 \geq l \geq -15$	$31 \geq h \geq 0$, $14 \geq k \geq 0$, $21 \geq l \geq -21$
F (000)	2096	2032
μ (mm^{-1})	1.06	1.09
No. reflections collected	9202	23902
No. unique reflections	4585 (R_{int} = 0.0273)	5030 (R_{int} = 0.0)
Completeness	86.4%	99.2%
Refinement method	Full-matrix L.S. on F^2	Full-matrix L.S. on F^2
Data/restraints/parameters	4585/2/354	5030/0/359
Goodness of fit on F^2	1.095	1.009
Final R indices ($I>2\sigma(I)$)	R_1=0.0377, wR_2=0.0866	R_1=0.0252, wR_2=0.0605
R indices (all data)	R_1=0.0561, wR_2=0.0931	R_1=0.0319, wR_2=0.0644
Largest diff. peak and hole	0.554, -0.565 e.Å^{-3}	0.425, -0.447 e.Å^{-3}

Table 3.4.2: Crystal Data and Refinement Parameters for Niaq

	Niaq
Molecular Formula	$C_{12}H_{16}N_6O_2S_2Ni$
M_r (g/mol)	399.14
Crystal System	Monoclinic
Space group	$P2_1/n$
Z	4
a (Å)	12.000(1)
b (Å)	9.771(1)
c (Å)	14.465(1)
β (deg.)	94.478(2)
V (Å^3)	1690.9(3)
D_{calc} (g/cm^3)	1.568
Crystal dimension (mm)	0.20 x 0.15 X 0.10
Temp of data collection (K)	173
Range scanned (θ)	2.13 – 25.61
Index Range	$14 \geq h \geq -12$, $9 \geq k \geq -11$, $12 \geq l \geq -17$
F (000)	824
μ (mm^{-1})	1.41
No. reflections collected	7458
No. unique reflections	3138 (R_{int} = 0.0493)
Completeness	98.8%
Refinement method	Full-matrix L.S. on F^2
Data/restraints/parameters	3138/4/232
Goodness of fit on F^2	1.003
Final R indices ($I>2\sigma(I)$)	R_1=0.0383, wR_2=0.0755
R indices (all data)	R_1=0.0713, wR_2=0.0852
Largest diff. peak and hole	0.460, -0.429 e.Å^{-3}

NiEt : Ni(NCS)$_2$(3-aminopyridine)$_3$.EtOH

PRELIMINARY X-RAY PHOTOGRAPHY:

Oscillation photography gave a unit cell length of 10.6Å, while Weissenberg photography revealed the remaining two cell lengths to be 16.8.Å and 25.4Å, with an angle between them of close to 90°. Of the two photographs, only the oscillation photograph was mirrored. The resulting *2/m* Laue symmetry indicates a monoclinic unit cell.

SINGLE CRYSTAL X-RAY DIFFRACTOMETRY:

The unit cell obtained by diffractometry was identical to that obtained by photography.

STRUCTURE SOLUTION AND REFINEMENT:

The diffraction data revealed systematic absences indicative of the monoclinic space groups C2/c or Cc. Xprep calculated a mean $|E^2\text{-}1|$ value of 0.946, indicating that the centrosymmetric space group, C2/c, is correct. This choice was vindicated by the successful refinement of the structure in this space group.

The Ni atom was located in a general position in the unit cell. In the course of the structure solution it became apparent that two *cis* 3-aminopyridine ligands were present as incomplete fragments on the electron density map. In one case only the pyridine ring was found, and in the other only an amino group was found. However, by applying a simple symmetry operation, each ring fragment was found to complete the other. So, while the Ni centre is coordinated to four 3-aminopyridine ligands, only three complete ligands are present in the asymmetric unit.

The β-C of the ethanol guest molecule is disordered over two positions, which refined with site occupancy factors of 48.9% and 51.1%. The two C–C bond lengths did not refine well, and were fixed at the literature value of 1.51(2)Å.

All non-hydrogen atoms were located on the electron density map and refined anisotropically. The aromatic ring hydrogens as well as the amino hydrogens were all located and refined isotropically, with the exception of two amino hydrogens, H11 and H12, which were placed in geometrically calculated positions. The guest hydrogen atoms were omitted from the final model, due to the disorder (crystal structure and refinement details are given in Table 3.4.1).

STRUCTURE ANALYSIS:

Solving the structure in C2/c revealed a central Ni atom with an irregular octahedral coordination geometry (Table 3.4.3). Two NCS^- counterions occupy the axial positions, while the equatorial positions are occupied by four 3-aminopyridine ligands. Three of these ligands are coordinated through the ring N atom, while the fourth is coordinated through the amino group (Fig. 3.4.1a).

Table 3.4.3: Selected bond lengths and angles around the Ni centre

Bond	Length (Å)	Angle	Angle (°)
Ni1 – N1	2.051(2)	N2 – Ni1 – N1	178.31(8)
Ni1 – N2	2.059(2)	N1 – Ni1 – N3	90.32(8)
Ni1 – N3	2.194(2)	N2 – Ni1 – N6	85.79(8)
Ni1 – N4	2.093(2)	N3 – Ni1 – N5	177.00(8)
Ni1 – N5	2.183(2)	N6 – Ni1 – N3	90.62(8)
Ni1 – N6	2.162(2)	N4 – Ni1 – N5	89.88(8)

The Ni–N_{CS} and Ni–N_{pyr} bond lengths correspond well with the literature values of 2.04(8) and 2.11(6)Å respectively[1]. The Ni–N_{amino} bond is not significantly longer than the Ni–N_{pyr} bonds. The C–O bond of the ethanol guest measures 1.434(5)Å, which is close to the literature value of 1.43(1)Å[2]. Full bond lengths and angles are given in Appendix 4.

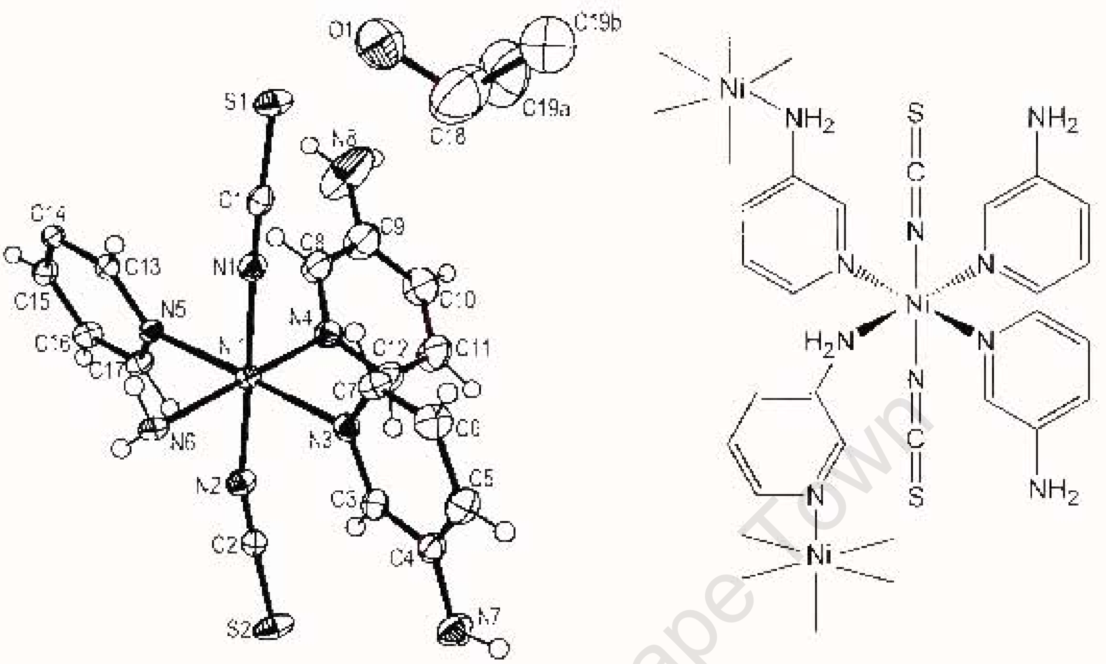

(a) (b)

Fig 3.4.1: (a) Ortep diagram of NiEt, showing thermal ellipsoids (a,b notation refers to atoms of a disordered system), (b) the polymeric structure of NiEt.

As shown in Fig. 3.4.1b, two of the 3-aminopyridine ligands acts as bridging ligands, linking two Ni centres via the ring N and amino N atoms. The other two 3-aminopyridine ligands are terminal. The presence of two bridging ligands in the asymmetric unit leads to the formation of 1-D polymeric chains of alternating Ni centres and 3-aminopyridine ligands. These chains form a spiral, or helical, polymer which runs parallel to the [010] direction (Fig. 3.4.2a). There are two asymmetric units per turn of the helix, resulting in a pitch of 10.95Å per helix turn.

HYDROGEN BONDING INTERACTIONS:

The oxygen atom of the ethanol guest forms hydrogen bonds to the amino groups of two terminal 3-aminopyridine ligands. Furthermore, the hydroxyl hydrogen may be hydrogen bonded to the S atom of a nearby isothiocyanato counterion (Fig. 3.4.2b). However, since this hydrogen atom could not be located on the electron density map, this interaction can only be inferred from the O···S distance.

While the two N–H···O hydrogen bonds are intrachain interactions (Fig. 3.4.2a), the postulated O–H···S hydrogen bond is directed towards an adjacent chain. All three hydrogen bonds are relatively weak, being close to the sum of the van der Waals radii for the heavy atoms (Table 3.4.4). In addition, there are several weak interchain and intrachain N–H···S and N–H···N interactions between host moieties.

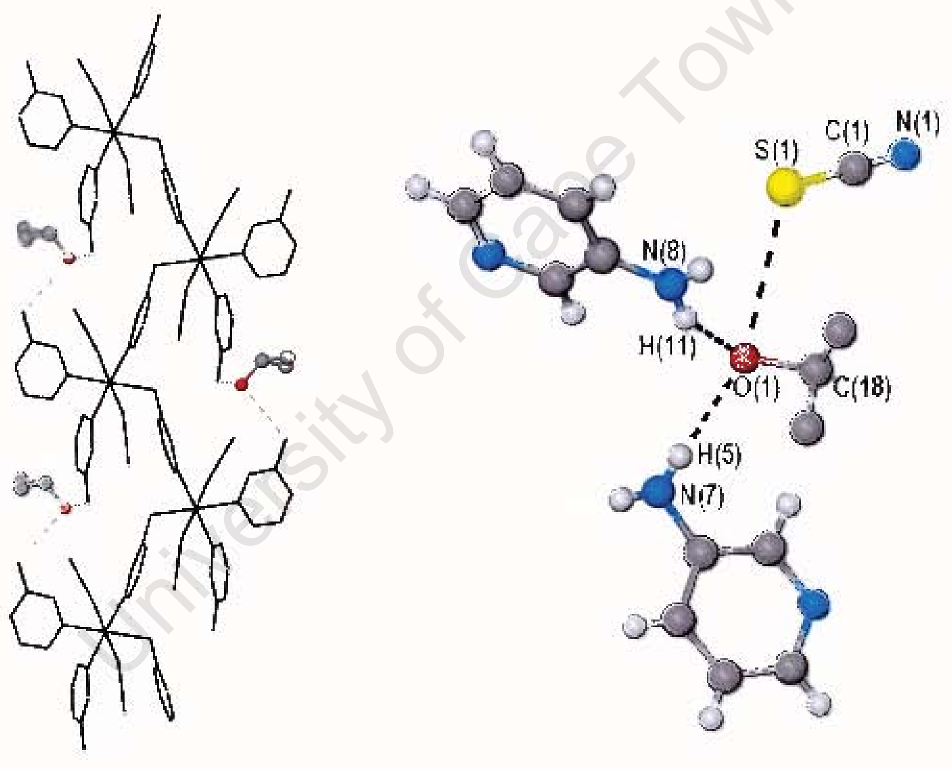

(a) (b)

Fig 3.4.2: (a) Intrachain N–H···O hydrogen bonds (H atoms omitted for clarity), (b) hydrogen bonding environment of the ethanol guest.

Table 3.4.4: Hydrogen Bonding Data for NiEt

D – H ··· A	D – H (Å)	H ··· A (Å)	D ··· A (Å)	Angle (°)
	HOST ··· GUEST INTERACTIONS			
N7 – H5[#1] ··· O1	0.833(34)	2.227(34)	3.059(4)	176.3(3.2)
N8 – H11[#2] ··· O1	0.880(3)	2.286(2)	3.105(4)	154.8(2)
O1 – (H) ··· S1	-	-	3.416(4)	-
	HOST ··· HOST INTERACTIONS			
N8 – H12 ··· S1[#3]	0.880(4)	2.631(1)	3.494(4)	167.2(2)
N6 – H18 ··· N7[#4]	0.857(28)	2.467(26)	3.232(4)	149.0(2.3)
N6 – H17 ··· S2[#4]	0.850(27)	2.625(27)	3.443(2)	161.7(2.4)
N7 – H6[#5] ··· S1	0.883(30)	2.625(30)	3.481(3)	163.43(2.6)

Symmetry codes: #1 = x,1-y,z-½, #2 = x,-y,z-½, #3 = 1-x, y, ½-z, #4 = ½-x, y-½, ½-z. #5 = x, y-1, z.

NiMe : $Ni(NCS)_2(3\text{-aminopyridine})_3.MeOH$

PRELIMINARY X-RAY PHOTOGRAPHY:

Oscillation photography gave a unit cell length of 10.8Å, while Weissenberg photography revealed the remaining two cell lengths to be 16.6Å and 24.6Å, with an angle between them of 92.3°. Of the two photographs only the oscillation photograph was mirrored. The resulting *2/m* Laue symmetry indicates a monoclinic unit cell.

SINGLE CRYSTAL X-RAY DIFFRACTOMETRY:

The unit cell obtained by diffractometry was identical to that obtained by photography.

STRUCTURE SOLUTION AND REFINEMENT:

The diffraction data revealed systematic absences indicative of the monoclinic space groups C2/c or Cc. Xprep calculated a mean $|E^2-1|$ value of 0.955, indicating that the centrosymmetric space group, C2/c, is correct. The structure was solved and fully refined in this space group.

The Ni atom occupies a general position in the unit cell. During the structure solution, two of the 3-aminopyridine ligands were found to be partially complete, in a manner identical to that of **NiEt**.

All non-hydrogen atoms were located on the electron density map and refined anisotropically. All host and guest hydrogen atoms were located on the electron density map and refined isotropically (crystal structure and refinement details are given in Table 3.4.1).

STRUCTURE ANALYSIS:

NiMe and **NiEt** are isostructural with respect to the host molecules, differing only in the positions of the guest atoms (Fig. 3.4.3a). The bond lengths around the Ni centre correspond well with the literature values[1]. The $Ni–N_{CS}$ bonds measure 2.045(1)Å and 2.056(1)Å. The $Ni–N_{amino}$ bond is 2.177(1)Å in length, while the $Ni–N_{pyr}$ bonds lie in the range 2.108(1)Å to 2.185(1)Å. The methanol guest molecule refined well, with a C-O bond length of 1.419(4)Å. This value corresponds well with the literature value of 1.43(1)Å[2].

The helical polymers in **NiMe** have a pitch of 10.93Å per turn of the helix, compared with 10.95Å for **NiEt**. Full bond lengths and angles are given in Appendix 4.

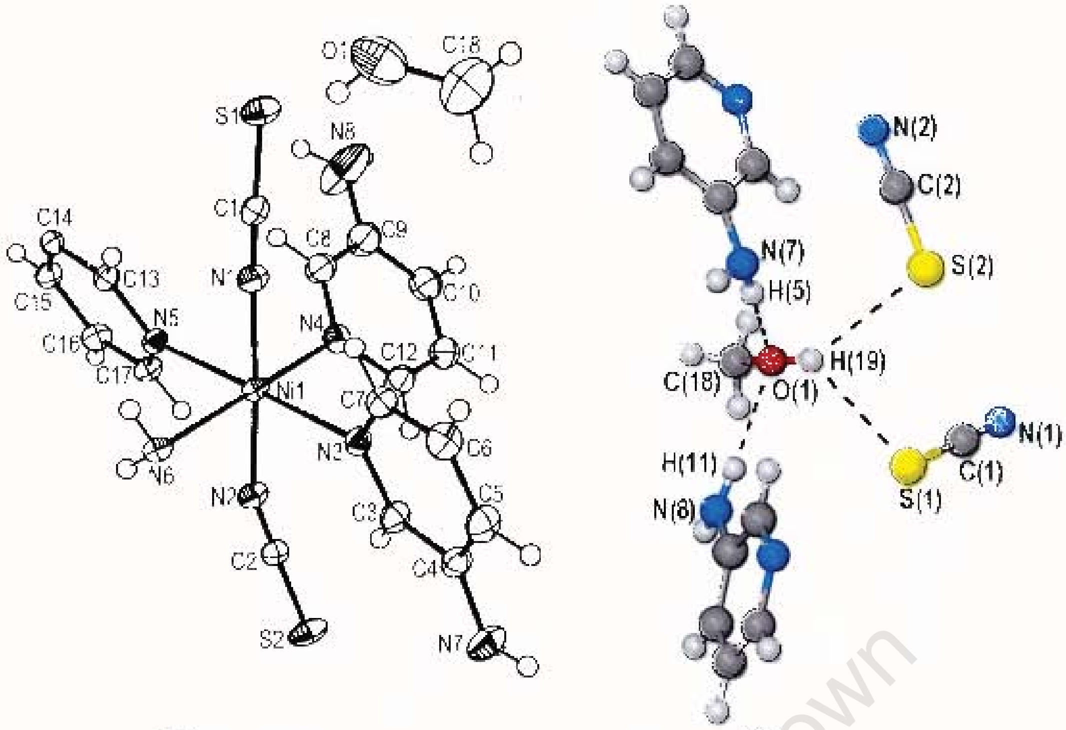

(a) **(b)**

Fig 3.4.3: (a) Ortep diagram of NiMe, showing thermal ellipsoids, (b) hydrogen bonding environment of methanol guest.

<u>HYDROGEN BONDING INTERACTIONS:</u>

As in **NiEt**, the oxygen atom of the methanol guest forms two intrachain N–HΛO hydrogen bonds to the amino groups of two terminal 3-aminopyridine ligands. The hydroxyl hydrogen of the methanol guest was found to be approximately halfway between two isothiocyanato sulphur atoms (in **NiEt**, S2 is more than 0.17Å further away than S1). All four interactions exceed the sum of the van der Waals radii for the two heavy atoms, and fall in the range generally associated with weak hydrogen bonds (Table 3.4.5, Fig. 3.4.3b).

In addition, the interchain and intrachain host···host interactions that were examined in **NiEt** were also found to be present in **NiMe**.

Table 3.4.5: Hydrogen Bonding Data for NiMe

D – H ··· A	D – H (Å)	H ··· A (Å)	D ··· A (Å)	Angle (°)
		HOST ··· GUEST INTERACTIONS		
N7 – H5$^{\#1}$ ··· O1	0.837	2.230	3.062	173.26
N8 - H11$^{\#2}$ ··· O1	0.849	2.249	3.080	166.39
O1 – H19 ··· S1	0.748	2.909	3.448	131.16
O1 – H19 ··· S2$^{\#}$	0.748	2.849	3.473	142.63
		HOST ··· HOST INTERACTIONS		
N8 – H12$^{\#3}$ ··· S1	0.839(31)	2.678(31)	3.487(3)	162.5(2.7)
N6 – H18 ··· N7$^{\#4}$	0.833(20)	2.531(19)	3.260(2)	146.8(1.8)
N6 – H17 ··· S2$^{\#5}$	0.876(19)	2.632(19)	3.480(1)	163.4(1.6)
N7 – H6 ··· S1$^{\#6}$	0.848(23)	2.665(24)	3.493(2)	165.7(2.1)

Symmetry codes: #1 = x, 1-y, z-½, #2 = x, 2-y, z-½, #3 = -x, y, ½-z, #4 = ½-x, ½+y, ½-z, #5 = ½-x, ½+y, ½-z , #6 = x, y-1, z

Niaq : $Ni(NCS)_2(3\text{-aminopyridine})_2(H_2O).H_2O$

PRELIMINARY X-RAY PHOTOGRAPHY:

The single crystals of **Niaq** were unsuitable for photography due to their small size.

SINGLE CRYSTAL X-RAY DIFFRACTOMETRY:

STRUCTURE SOLUTION AND REFINEMENT:

The diffraction data revealed *2/m* Laue symmetry, and systematic absences indicative of the monoclinic space group $P2_1/n$. From the unit cell parameters and space group, it was found that this structure had been published some years ago[3]. Nevertheless, data were recollected and the structure re-solved.

When the literature values for the atomic coordinates of the Ni atom and isothiocyanate groups were inserted the structure was solved and fully refined.

Two *cis* 3-aminopyridine ligands were located on the electron density map and refined as incomplete fragments, in a manner similar to **NiEt** and **NiMe**.

The Ni occupies a general position in the unit cell. All non-hydrogen atoms were located on the electron density map and refined anisotropically. The amino hydrogens, H5 and H6, as well as all aromatic ring hydrogens, were placed in geometrically calculated positions. Amino hydrogens, H11 and H12, and aqua hydrogens, H13–16, were located on the electron density map and refined isotropically. The O-H bonds of the water ligand and guest were fixed at 0.90±0.02Å (crystal structure and refinement parameters are given in Table 3.4.2).

STRUCTURE ANALYSIS:

Solving the structure in $P2_1/n$ revealed a central **Ni** atom in an irregular octahedral coordination environment. The Ni centre is coordinated to two axial NCS^- counterions, two bridging 3-aminopyridine ligands (one coordinated through the ring N atom and the other through the amino N atom), one terminal 3-aminopyridine ligand and one water molecule (Fig. 3.4.4a). The bond lengths around the Ni centre correspond well with the literature values (Table 3.4.6)[1]. Full bond lengths and angles are given in Appendix 4.

The coordination environment of the Ni centre is similar to that of **NiEt** and **NiMe**, the only difference being that a water ligand has replaced one of the terminal 3-aminopyridine ligands. In the literature, this structure is described as consisting of $Ni(NCS)_2(3\text{-}NH_2\text{-pyridine})_2(H_2O).H_2O$ dimers, in which two Ni centres are linked by two bridging 3-aminopyridine ligands. However, careful examination of the extended structure revealed a polymeric arrangement (Fig. 3.4.4b).

Infinite 1-D chains of alternating Ni centres and bridging 3-aminopyridine ligands extend along the [010] direction (Fig. 3.4.5a). As in **NiEt** and **NiMe**, the chains have a helical conformation. There are two asymmetric units per turn of the helix, resulting in a pitch of 9.77Å per helix turn.

Table 3.4.6: Selected bond lengths and angles around the Ni centre

Bond	Length (Å)	Angle	Angle (°)
Ni1 - N1	2.032(2)	N2 - Ni1 - N1	173.87(9)
Ni1 - N2	2.024(2)	N2 - Ni1 - N3	90.83(9)
Ni1 - N3	2.098(2)	N2 - Ni1 - O1	89.52(9)
Ni1 - N4	2.119(2)	N2 - Ni1 - N4	92.84(9)
Ni1 - N5	2.178(3)	N3 - Ni1 - O1	90.81(9)
Ni1 - O1	2.116(2)	O1 - Ni1 - N4	177.25(9)

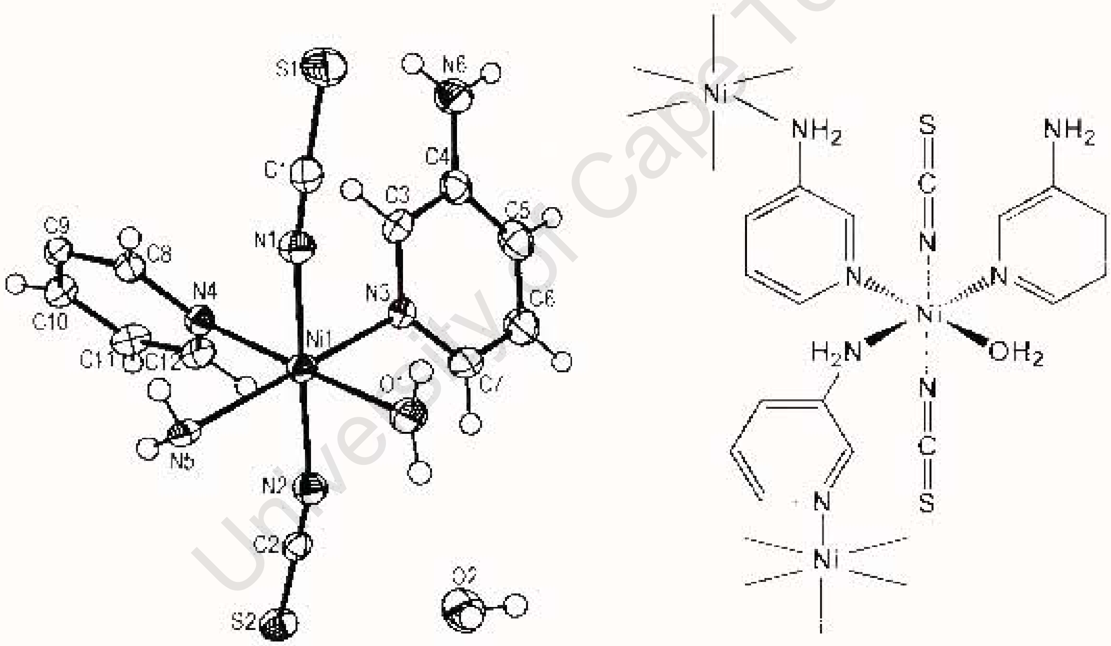

(a) (b)

Fig 3.4.4: (a) Ortep diagram of Niaq, showing thermal ellipsoids, (b) the polymeric structure of Niaq.

HYDROGEN BONDING INTERACTIONS:

An extensive hydrogen-bonded network is formed between the water, amino and isothiocyanato moieties. The water guest may be involved in up to four different hydrogen bonds (Table 3.4.7), all of which lie in the range generally associated with moderately strong hydrogen bonds. The oxygen atom of the water guest forms hydrogen bonds to the water ligand and bridging amino group of adjacent units within a chain (Fig. 3.4.5a).

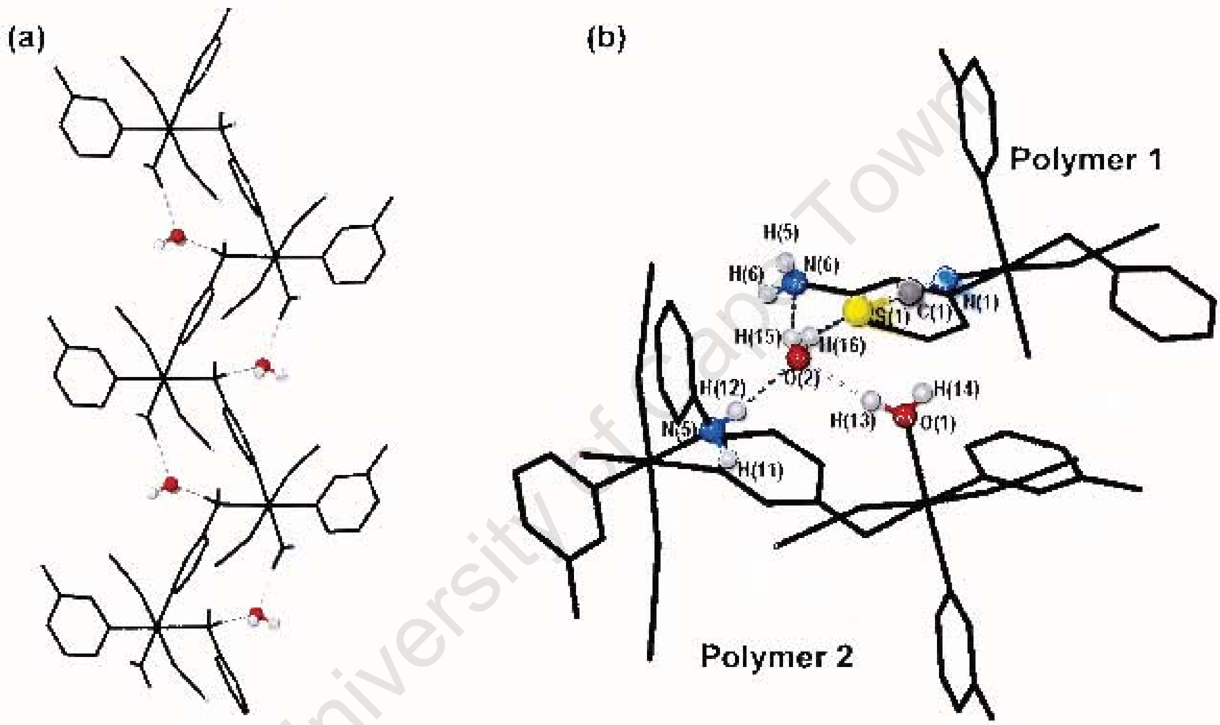

Fig 3.4.5: (a) Intrachain hydrogen bonding interactions between water guest (ball-and-stick form) and host polymer (stick form; ring H atoms omitted for clarity), (b) hydrogen bonding environment of water guest, showing its role in linking adjacent polymers.

The two hydrogen atoms of the water guest form hydrogen bonds to the isothiocyanato sulphur atom and terminal amino group of a single unit in a nearby chain (Fig. 3.4.5b). In this way the water guest is responsible for the linking of polymers via interchain hydrogen bonds, to generate a 3-D hydrogen bonded network. In addition, three weak N–H···S interactions were identified both within and between host polymers.

Table 3.4.7: Hydrogen Bonding Data for Niaq

D – H ··· A	D – H (Å)	H ··· A (Å)	D ··· A (Å)	Angle (°)
HOST ··· GUEST INTERACTIONS				
O1 – H13 ··· O2	0.869(24)	1.957(23)	2.822(3)	173.1(2.1)
N5 – H12$^{\#1}$ ··· O2	0.862(37)	2.130(37)	2.989(4)	174.1(3.5)
O2 – H15 ··· N6$^{\#2}$	0.861(31)	2.229(30)	3.076(4)	167.5(2.7)
O2 – H16 ··· S1$^{\#2}$	0.867(22)	2.476(22)	3.298(3)	158.6(1.9)
HOST ··· HOST INTERACTIONS				
N5 – H11 ··· S2$^{\#3}$	0.812(26)	2.744(26)	3.542(3)	168.1(2.4)
N6 – H5 ··· S1$^{\#4}$	0.880(3)	2.738(1)	3.539(3)	151.8(2)
N6 – H6 ··· S2$^{\#5}$	0.880(3)	2.745(1)	3.615(3)	169.7(2)

Symmetry codes: #1 = ½-x, y-½, ½-z, #2 = -x, 1-y ,-z, #3 = -x-½, y+½, ½-z, #4 = -x, 2-y, -z. #5 = -x-½, y+½, ½-z.

CRYSTAL PACKING FEATURES OF NiEt, NiMe AND Niaq

NiEt and **NiMe** may be regarded as isostructural with respect to the host molecules, differing only in the positions of the guest molecules. The direction of growth of the helical polymers is along the [010] direction, coincident with the twofold screw axis (Fig. 3.4.6a-b).

The ethanol and methanol guest molecules are located in sealed cavities, which run 3.4Å along *b*. Each cavity contains two guest molecules. Viewed along [010], the cavity cross-section is roughly elliptical, with a slight central constriction, resulting in a dumb-bell-like shape. The two guest molecules lie adjacent to each other in the cavity, at opposite ends of the centrally constricted region (Fig. 3.4.7a-b).

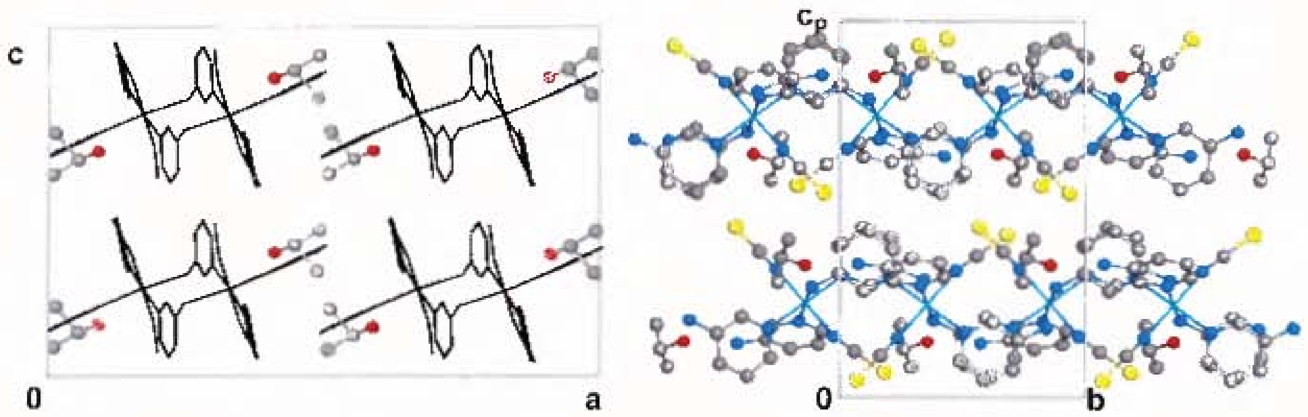

(a) (b)

Fig 3.4.6: (a) Stick representation of NiEt, viewed along [010], with ethanol guests in ball and stick form (H atoms omitted for clarity), (b) Ball and stick representation of NiEt, viewed along [100] (H atoms omitted for clarity).

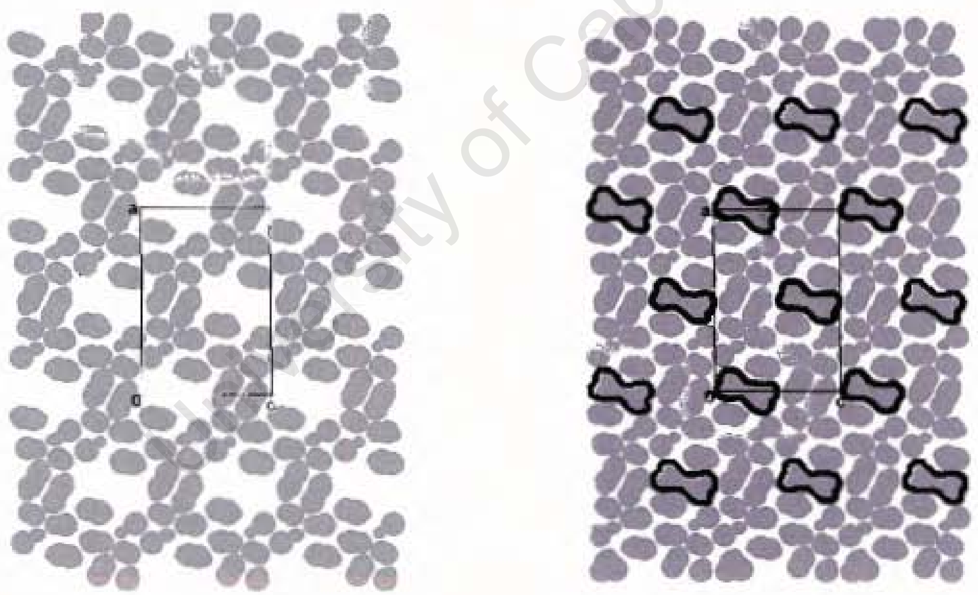

(a) (b)

Fig 3.4.7: Space-filling representation of (a) host molecules in NiEt, at b = 0.25, showing cavity cross-section and (b) host and guest molecules in NiEt, at b = 0.25, showing the position of the ethanol guests in the cavities. (each black outline encompasses the two entrapped ethanol guests per cavity).

The direction of polymer growth for **Niaq** is, similarly, along the [010] direction. Figs 3.4.8a and b describe end-on and side-on views of the polymers respectively. The water guests are located in cages, irregular in shape, which run 3.7Å along *b*, and have a cross-section of approximately 2.7X3.4Å. Each cavity encloses a single water guest.

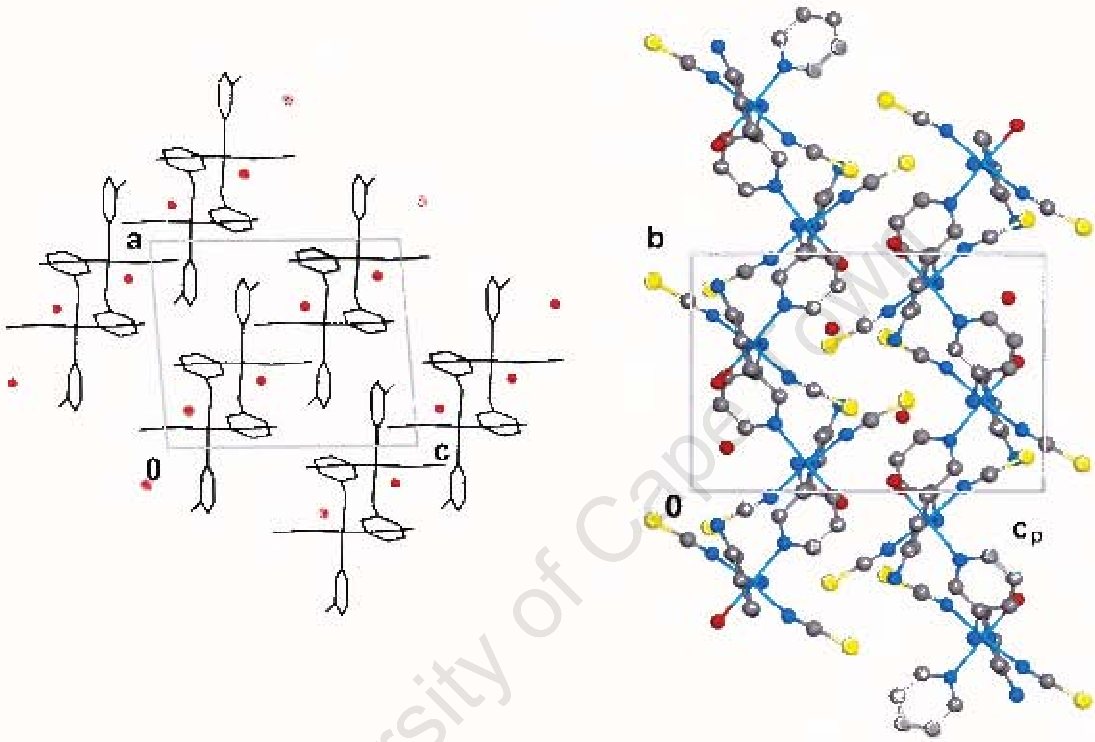

(a) (b)

Fig 3.4.8: (a) Stick representation of Niaq, showing guest water atoms as solid red spheres (H atoms omitted for clarity), (b) Ball-and-stick representation of Niaq (H atoms omitted for clarity).

THERMAL ANALYSIS

The thermal analyses of all three compounds are shown in Fig. 3.4.9. Both TG and DSC reveal that **NiEt** and **NiMe** decompose in four distinct steps, labelled **a–d** in Figs. 3.4.9a and b. Step **a** corresponds to the loss of the guest molecules, while steps **b–d** each correspond to the loss of one 3-aminopyridine ligand. Each weight loss step in the TG is accompanied by a single endotherm in the DSC.

The TG and DSC data for **Niaq** reveal that this compound, too, undergoes a four-step decomposition process, labelled **a-d** in Fig. 3.4.9c. Step **a** corresponds to the simultaneous release of the water ligands and guest molecules. Steps **b** and **c** each correspond to the loss of one half of a 3-aminopyridine ligand (In a polymeric chain, step **b** would correspond to the loss of alternate bridging ligands in the chain, resulting in the formation of dimers. Step **c** would correspond to the loss of the remaining, shared bridging ligands, to generate monomers). Finally, step **d** corresponds to the loss of the terminal 3-aminopyridine ligand. Each weight loss process in the TG is accompanied by a single endotherm in the DSC, with the exception of step **b**, for which the trace is complex. All four steps are accompanied by bubbling and colour changes, as observed by HSM. During step **a** the pale blue, translucent crystals turn opaque green. Steps **b** and **c** correspond to a gradual lightening of the crystals to a pale yellow-green, while in step **d** the crystals darken to a black residue. Full TG and DSC data are given for all three compounds in Tables 3.4.8-3.4.10.

Table 3.4.8: TG data for NiEt and NiMe

Reaction	**NiEt**			**NiMe**		
	Calc %	Exp %	T_{onset} (°C)	Calc %	Exp %	T_{onset} (°C)
$Ni(NCS)_2(L)_3.G \rightarrow Ni(NCS)_2(L)_3 + G$	9.2	9.2	100.0	6.5	6.1	102.0
$Ni(NCS)_2(L)_3 \rightarrow Ni(NCS)_2(L)_2 + L$	18.7	18.3	164.0	19.2	17.9	174.3
$Ni(NCS)_2(L)_2 \rightarrow Ni(NCS)_2(L)_1 + L$	18.7	20.0	222.0	19.2	18.6	245.6
$Ni(NCS)_2(L)_1 \rightarrow Ni(NCS)_2 + L$	18.7	21.0	290.0	19.2	21.5	300.6

Table 3.4.9: DSC data for NiEt and NiMe

Reaction	NiEt		NiMe	
	T_{onset} (°C)	ΔH ($kJ.mol^{-1}$)	T_{onset} (°C)	ΔH ($kJ.mol^{-1}$)
$Ni(NCS)_2(L)_3.G \rightarrow Ni(NCS)_2(L)_3 + G$	129.4	27.2 (2.5)*	138.1	22.1 (1.4)*
$Ni(NCS)_2(L)_3 \rightarrow Ni(NCS)_2(L)_2 + L$	197.1	66.8	197.0	17.3
$Ni(NCS)_2(L)_2 \rightarrow Ni(NCS)_2(L)_1 + L$	248.0	76.2	236.9	65.5
$Ni(NCS)_2(L)_1 \rightarrow Ni(NCS)_2 + L$	322.0	73.1	335.7	44.3

* values in brackets indicate enthalpies calculated in terms of kJ per mole of guest alone, for the release of one mole of guest per mole of host compound.

Table 3.4.10: TG and DSC data for Niaq

Reaction	TG			DSC	
	Calc %	Exp %	T_{onset} (°C)	T_{onset} (°C)	ΔH ($kJ.mol^{-1}$)
$Ni(NCS)_2(L)_2(H_2O).H_2O \rightarrow Ni(NCS)_2(L)_3 + 2H_2O$	9.0	9.0	92.5	91.3	94.4
$Ni(NCS)_2(L)_2 \rightarrow Ni(NCS)_2(L)_{1.5} + 0.5L$	11.8	11.5	209.8	-	-
$Ni(NCS)_2(L)_{1.5} \rightarrow Ni(NCS)_2(L)_1 + 0.5L$	11.8	12.5	245.0	225.3	55.7
$Ni(NCS)_2(L)_1 \rightarrow Ni(NCS)_2 + L$	23.6	22.6	291.0	325.3	75.6

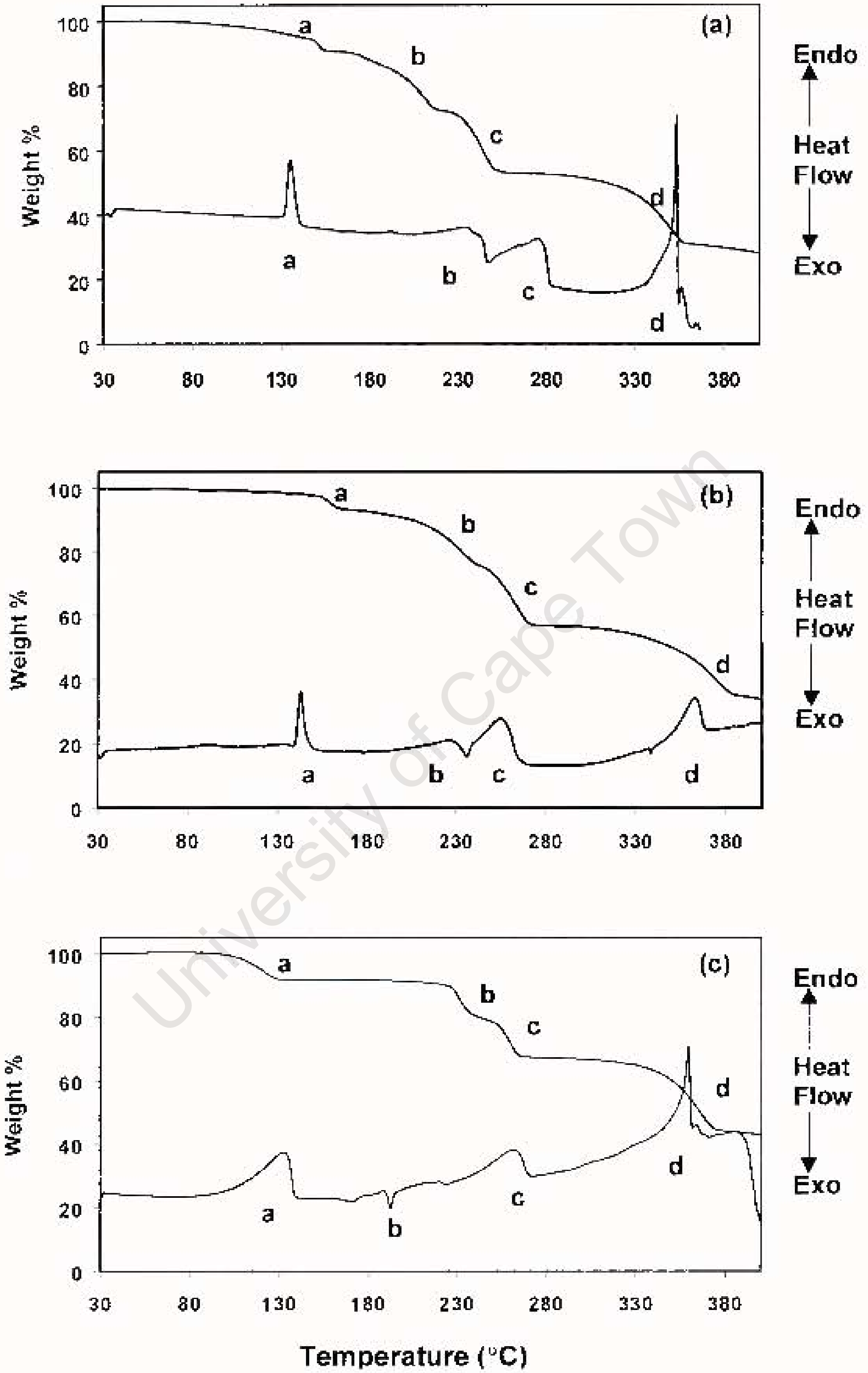

Fig 3.4.9: Thermal analysis of (a) NiEt, (b) NiMe and (c) Niaq.

XRD:

There is a good correlation between the calculated and experimental XRD traces for **NiEt** and **NiMe** (Fig. 3.4.10). The XRD of **Niaq** could not be measured as this compound could only be crystallised from solution as a mixture, from which the crystals of Niaq had to be separated by hand (see section 2.2.12).

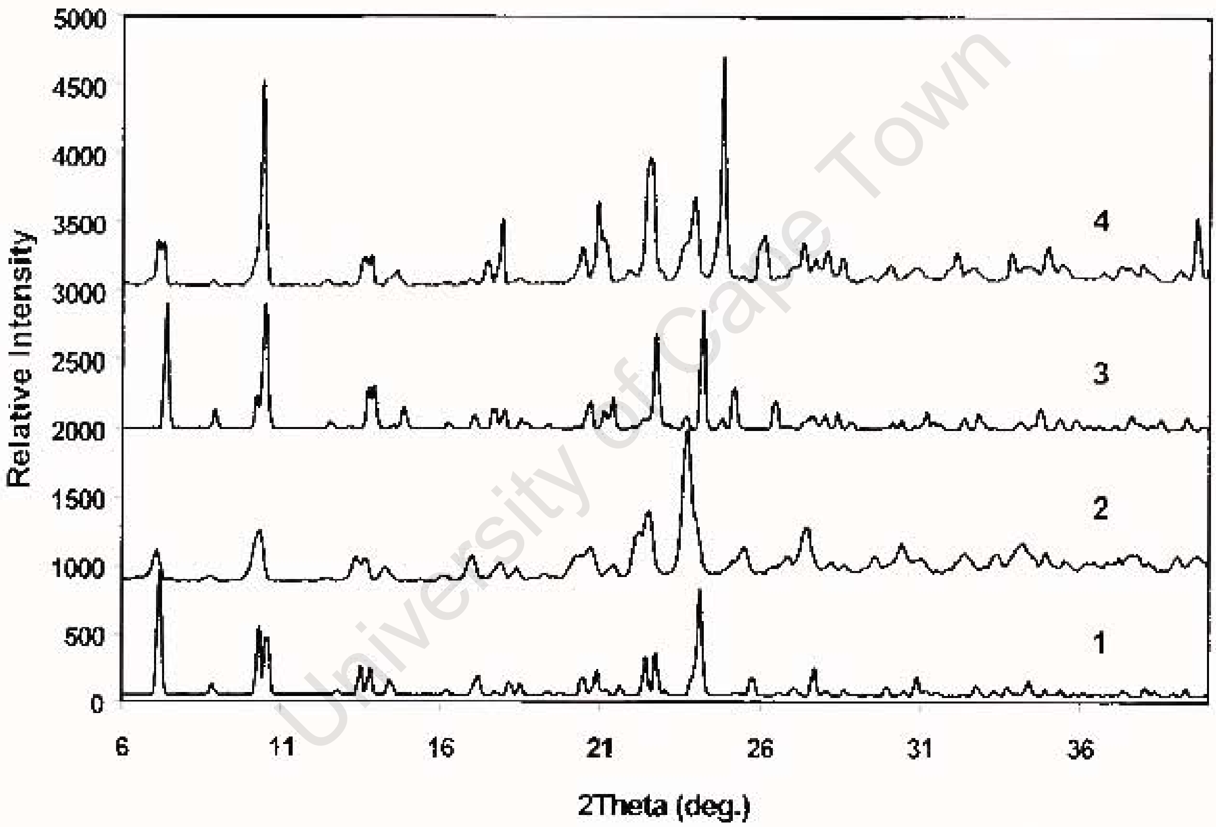

Fig 3.4.10: XRD traces of NiEt, calculated (**1**) and experimental (**2**) and NiMe, calculated (**3**) and experimental (**4**)

DISCUSSION

The three structures described in this chapter are examples of polymeric Werner clathrates. The presence of an amino substituent on the pyridine ring system allows two of the ligands in the coordination sphere of the **Ni** atom to act as bridging ligands. This generates 1-D helical polymers, comprising two asymmetric units per turn of the helix. Instead of the classical Werner formula, MX_2A_4, these complexes have the general formulae MX_2A_3 (**NiEt** and **NiMe**) and $MX_2A_2(H_2O)$ (**Niaq**).

Interchain and intrachain host···guest hydrogen bonding interactions generate a 3-D hydrogen bonded network. The guest molecules are trapped in cavities, and are therefore unable to diffuse through the crystal structure, resulting in a high kinetic stability for these clathrates. This is reflected in the thermal analysis of the compounds, where the guest release process coincides with the onset of host decomposition. In **NiEt** and **NiMe** the release of the guest is observed as a distinct process, which is immediately followed by host decomposition. This implies that, while the host molecules may need to shift their position in the crystal structure in order for the guest molecules to be released from the cages, the host complexes do not actually break up until the guest molecules have been released. In **Niaq**, however, the release of the water guests and water ligands occur as a single process. Thus the water guests cannot be released from the host cages until the host complexes themselves start to decompose.

CHAPTER 3.5

COORDINATION POLYMERS

COORDINATION POLYMERS

The compounds described in this chapter are all examples of coordination polymers rather than Werner clathrates. This class of compounds encompasses a diverse range of structure types, which cannot be fully explored in this project. Instead, this chapter highlights some of the more important aspects of coordination polymers, as well as those features that distinguish them from, for example, the polymeric Werner-type complexes.

Metal salts other than $Ni(NCS)_2$ were used, namely $ZnBr_2$, $ZnSO_4$ and $CuSO_4$. This adds a new dimension to the formation of inclusion complexes, both in terms of the preferred geometry of the metal centre and the behaviour of the counterion. Whereas Werner complexes display octahedral coordination geometry, coordination polymers in which the metal centre adopts a linear[4], trigonal[4,5], trigonal bipyramidal[6], T-shaped[7,8], tetrahedral[4,9,10], octahedral[11,12] and heptacoordinate[13-15] coordination geometry have all been reported.

In addition to the geometry of the metal centre, the choice of counterion is an important factor. In Werner clathrates the counterions remain coordinated to the metal centre. In coordination polymers, however, it is common for the counterion to be displaced, either by an incoming ligand[4,5,10] or by a water molecule[12,16,17]. These displaced counterions are accommodated in channels or pores formed by the host polymers. One must also consider the possibility of polymerisation occurring via bridging bidentate counterions, as observed in certain polymers containing the hexafluorosilicate ion (SiF_6^{2-})[18,19].

Table 3.5.1: Crystal data and refinement parameters for $ZnBr_2pyz_2$ and $ZnBr_2pyz$

	$ZnBr_2pyz_2$	**$ZnBr_2pyz$**
Molecular Formula	$ZnBr_2C_8H_8N_4$	$ZnBr_2C_4H_4N_2$
M_r (g/mol)	385.37	305.28
Crystal System	Orthorhombic	Monoclinic
Space group	Ccca	$P2_1/m$
Z	4	2
a (Å)	10.1904(4)	6.0068(4)
b (Å)	10.1981(6)	9.9518(8)
c (Å)	11.1516(7)	6.9936(6)
β (deg.)	90	110.472(5)
V ($Å^3$)	1158.9(1)	391.66(5)
D_{calc} (g/cm^3)	2.209	2.589
Crystal dimension (mm)	0.40 x 0.40 x 0.28	0.14 x 0.40 x 0.28
Temp of data collection (K)	173	298
Range scanned (θ)	3.37 – 27.48	3.72 – 28.28
Index Range	$10\geq h\geq-13$, $10\geq k\geq-13$, $13\geq l\geq-14$	$6\geq h\geq-8$, $13\geq k\geq-12$, $9\geq l\geq-6$
F (000)	736	284
μ (mm^{-1})	8.99	13.25
No. reflections collected	3623	2012
No. unique reflections	675 (R_{int} = 0.0619)	987 (R_{int} = 0.0736)
Completeness	100.0%	96.7%
Refinement method	Full-matrix L.S. on F^2	Full-matrix L.S. on F^2
Data/restraints/parameters	675/0/56	987/0/46
Goodness of fit on F^2	1.071	1.068
Final R indices ($I>2\sigma(I)$)	R_1=0.0301, wR_2=0.0737	R_1=0.0677, wR_2=0.1739
R indices (all data)	R_1=0.0451, wR_2=0.0841	R_1=0.0758, wR_2=0.1864
Largest diff. peak and hole	0.598, -1.095 eÅ^{-3}	2.126, -1.325 eÅ^{-3}

Table 3.5.2: Crystal data and refinement parameters for ZnpyzSulf and Cudiaq

	ZnpyzSulf	**Cudiaq**
Molecular Formula	$C_4H_4N_2O_{10}SZn$	$CuC_{12}H_{18}N_4O_9S$
M_r (g/mol)	337.52	457.90
Crystal System	Monoclinic	Monoclinic
Space group	$P2_1/n$	$P2_1/c$
Z	4	4
a (Å)	7.7052(8)	4.9125(7)
b (Å)	12.497(1)	24.108(4)
c (Å)	13.077(1)	15.115(1)
β (deg.)	98.533(6)	97.775(9)
V (Å^3)	1245.2(2)	1773.6(4)
D_{calc} (g/cm^3)	1.800	1.715
Crystal dimension (mm)	0.27 x 0.25 x 0.23	0.30 x 0.20 x 0.15
Temp of data collection (K)	173	298
Range scanned (θ)	3.30 – 28.52	1.69 – 24.97
Index Range	$7\geq h\geq -10$, $15\geq k\geq -16$, $17\geq l\geq -13$	$5\geq h\geq -5$, $19\geq k\geq 0$, $17\geq l\geq -2$
F (000)	672	940
μ (mm^{-1})	2.19	1.41
No. reflections collected	5612	2800
No. unique reflections	2639 (R_{int} = 0.0404)	2649 (R_{int} = 0.0456)
Completeness	83.3%	85.2%
Refinement method	Full-matrix L.S. on F^2	Full-matrix L.S. on F^2
Data/restraints/parameters	2639/8/193	2649/0/119
Goodness of fit on F^2	1.126	0.927
Final R indices ($I>2\sigma(I)$)	R_1=0.0724, wR_2=0.1876	R_1=0.0523, wR_2=0.1632
R indices (all data)	R_1=0.0833, wR_2=0.1939	R_1=0.1990, wR_2=0.2189
Largest diff. peak and hole	3.087$^{\#1}$, -0.682 eÅ^{-3}	0.949$^{\#2}$, -0.501 eÅ^{-3}

#1 = very close to Zn centre. #2 = in vicinity of sulphate counterion

The $ZnBr_2pyz_2$ AND $ZnBr_2pyz$ COORDINATION POLYMERS

MICROANALYSIS:

Table 3.5.3: Microanalysis results for $ZnBr_2pyz_2$ and $ZnBr_2pyz$

Compound	%C	%H	%N
Calc : $ZnBr_2pyz_2$	24.93	2.09	14.54
Exp : $ZnBr_2pyz_2$ crystals	25.21	1.73	13.83
Calc : $ZnBr_2pyz$	15.74	1.32	9.18
Exp : $ZnBr_2pyz$ crystals	16.39	1.13	9.18
Exp : $ZnBr_2pyz$ powder	15.84	1.21	9.02

$ZnBr_2pyz_2$: $ZnBr_2(pyrazine)_2$

X-RAY PHOTOGRAPHY:

Oscillation photography gave a unit cell length of 7.1Å, while Weissenberg photography revealed the remaining two unit cell lengths to be 7.0Å and 11.0Å, with an angle between them of 90°. Together, the photographs appeared to indicate *4/mmm* Laue symmetry.

SINGLE CRYSTAL X-RAY DIFFRACTOMETRY:

The unit cell obtained by diffractometry can be transformed into that obtained by photography by applying the matrix [½ –½ 0, ½ ½ 0, 0 0 1] to the unit cell.

STRUCTURE SOLUTION AND REFINEMENT:

The diffraction data revealed *mmm* Laue symmetry, and systematic absences indicative of the orthorhombic space group Ccca, with a≈b. The reflections of the *hk2* and *hk3* layers, which exhibit *mm* symmetry, confirm the orthorhombic rather than the tetragonal symmetry of this structure. These results are consistent with the literature, in which the isomorphous structures of $FeCl_2(pyrazine)_2$ and $CoCl_2(pyrazine)_2$ were similarly solved and fully refined in Ccca[20,21].

The Zn atom occupies a special position at (½, ¼, ¼), with *222* symmetry, in Wyckoff position *b*. The Br^- counterion occupies a special position at (½, ¼, z), with two-fold symmetry, in Wyckoff position *g*. The C and H atoms of the pyrazine ring are disordered over two positions, with site occupancy factors which refined to 52% and 48%. The mean planes of the two disordered rings are orthogonal.

The Patterson method was used to solve this structure, as direct methods proved unsuccessful. This was carried out by a subroutine in X-Seed, which solves the Patterson function, expands the structure, and immediately yields an electron density map. The latter showed the position of all the non-hydrogen atoms unambiguously. All non-hydrogen atoms were refined anisotropically. The aromatic ring hydrogen atoms were placed in geometrically calculated positions (crystal structure and refinement parameters are given in Table 3.5.1).

STRUCTURE ANALYSIS:

Solving the structure in Ccca revealed a central Zn atom coordinated to two axial Br^- anions and four equatorial pyrazine ligands (Fig. 3.5.1). The coordination geometry around the metal centre is that of an irregular octahedron (Table 3.5.4).

Table 3.5.4: Selected bond lengths and angles around the Zn centre

Bond	Length (Å)	Angle	Degrees (°)
Zn1 – N1	2.210 (2)	N1 – Zn1 – Br1	90.3 (2)
Zn1 – Br1	2.582 (1)	N1 – Zn1 – N1#	89.9 (1)
		N1# - Zn1 – Br1	89.7 (2)

Symmetry codes: # = 1-x, y, ½-z

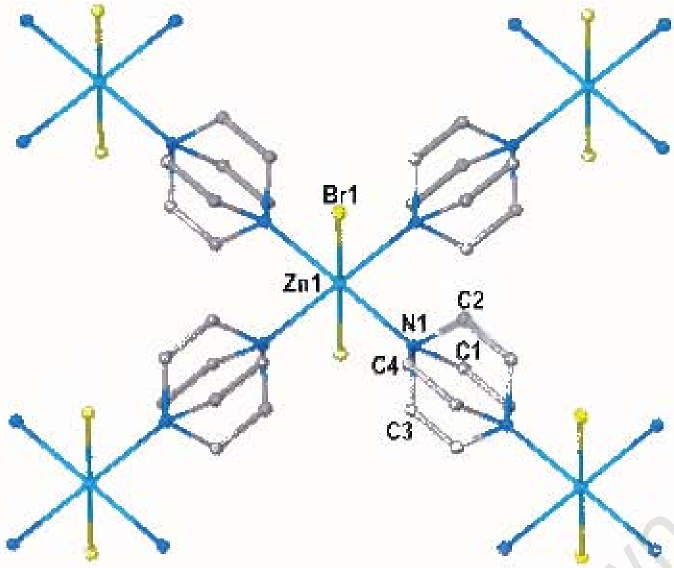

Fig 3.5.1: The coordination geometry of the metal atoms in $ZnBr_2pyz_2$ (only the asymmetric unit is labelled, H atoms omitted for clarity).

The Zn-N and Zn-Br bond lengths are slightly longer than the literature values of 2.10(6)Å and 2.39(3)Å respectively[1]. The pyrazine rings refined satisfactorily. The C-C bond lengths are 1.35(1)Å and 1.42(1)Å, while the aromatic C-N bonds lie in the range 1.33(1)Å to 1.36(1)Å. The literature values are 1.38(1)Å and 1.34(1)Å respectively[2]. Full bond lengths and angles are given in Appendix 5.

<u>CRYSTAL PACKING FEATURES:</u>

Each pyrazine ligand forms a bridge between two Zn centres through the ring N atoms. The linking of metal centres in this way leads to the formation of 2-D polymeric square grids (Fig. 3.5.2a). These square grids are neutral frameworks, as the Br anions remain coordinated to the metal centres. These grids are stacked along the [001] direction, with an interlayer spacing of *ca.* 5.6Å (Fig. 3.5.3a). The coordination networks have Zn–(pyz)–Zn distances of 7.2Å, resulting in inner cavities with effective dimensions *ca.* 2.4Å by 2.4Å (Fig. 3.5.3b). Adjacent layers are staggered such that the Br^- counterions of one layer project into the square cavities generated by the adjacent layers, thereby minimising unfavourable steric interactions (Fig. 3.5.2b). So, while the structure appears porous in 2-D, the 3-D packing arrangement of the layers along the *c* axis precludes guest inclusion.

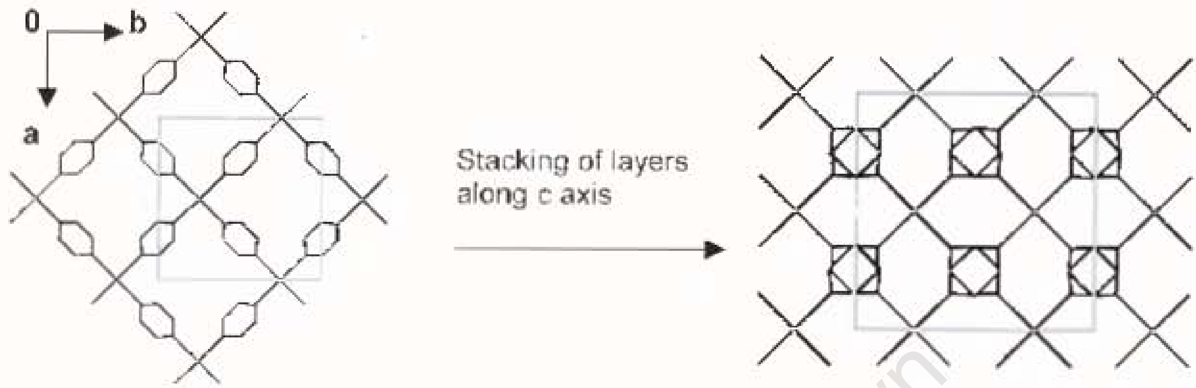

(a) (b)

Fig 3.5.2: Stick representation of $ZnBr_2pyz_2$, viewed along the [001] direction: (a) single layer, (b) double layer (H atoms omitted for clarity)

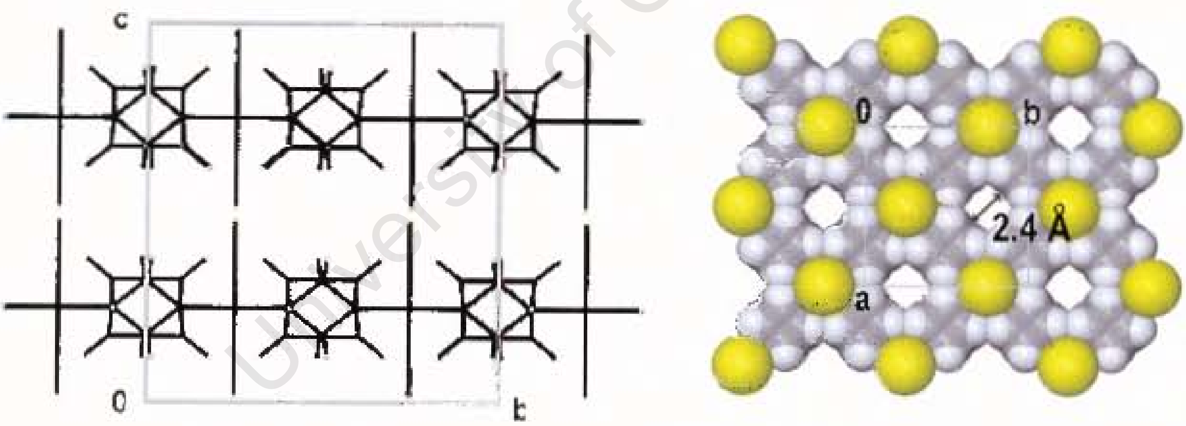

(a) (b)

Fig 3.5.3: (a) Stick representation of $ZnBr_2pyz_2$, viewed along the [100] direction, showing the stacking of the layers along the *c* axis, (b) Space-filling representation of a single polymeric layer, viewed along the [001] direction, showing the cavity dimensions.

$ZnBr_2pyz$: $ZnBr_2(pyrazine)_1$

X-RAY PHOTOGRAPHY:

Oscillation photography gave one unit cell length as 9.7Å, while Weissenberg photography revealed the remaining two cell lengths to be 5.7Å and 7.0Å, with an angle between them of 111.0°. Of the two photographs, only the oscillation photograph was mirrored. The resulting *2/m* Laue symmetry indicates a monoclinic unit cell.

SINGLE CRYSTAL X-RAY DIFFRACTOMETRY:

The unit cell obtained by diffractometry was identical to that obtained by photography.

STRUCTURE SOLUTION AND REFINEMENT:

The diffraction data revealed *2/m* Laue symmetry, and systematic absences indicative of the monoclinic space groups, $P2_1/m$ or $P2_1$. An $|E^2\text{-}1|$ value of 0.957 indicated that the centrosymmetric space group, $P2_1/m$, was correct, a choice that was vindicated by the eventual successful refinement of the structure in this space group. The Zn atom and both Br atoms were located on a mirror plane at (x, ¼, z), in Wyckoff position *e*.

The structure was solved using direct methods. All non-hydrogen atoms were located on the electron density map and refined anisotropically. The aromatic ring hydrogen atoms were placed in geometrically calculated positions (crystal structure and refinement details are given in Table 3.5.1).

STRUCTURE ANALYSIS:

Solving the structure in $P2_1/m$ revealed a central Zn atom coordinated to two Br anions and two pyrazine ligands (Fig. 3.5.4). The coordination geometry around the metal centre is that of an irregular tetrahedron (Table 3.5.5).

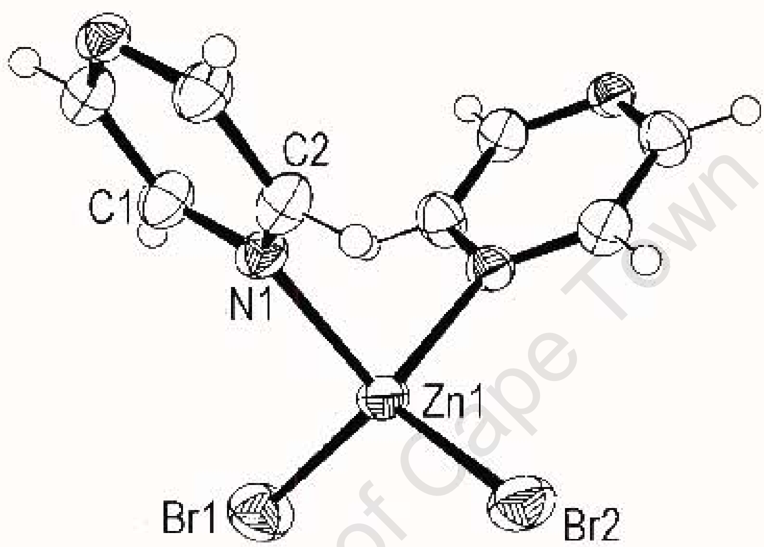

Fig 3.5.4: Ortep diagram of $ZnBr_2pyz$, showing thermal ellipsoids (only the asymmetric unit is labelled).

Table 3.5.5: Selected bond lengths and angles around the Zn centre

Bond	Length (Å)	Angle	Angle (°)
Zn1 – N1	2.084 (4)	N1 – Zn1 – Br1	108.2 (1)
Zn1 – Br1	2.330 (1)	N1 – Zn1 – Br2	109.7 (1)
Zn1 – Br2	2.323 (1)	Br2 – Zn1 – Br1	122.1 (1)

The Zn-N and Zn-Br bond lengths are consistent with the literature values of 2.10(6)Å and 2.39(3)Å respectively[1]. The Br–N–Br angle deviates significantly from that of a tetrahedron, due to the steric repulsion between these two large anions. Full bond lengths and angles are given in Appendix 5.

CRYSTAL PACKING FEATURES:

Each Zn centre is coordinated to two bridging pyrazine ligands which, due to the tetrahedral arrangement of ligands around the Zn centre, leads to the formation of infinite 1-D zig-zag chains of alternating Zn centres and pyrazine ligands (Fig. 3.5.5a). The direction of polymer growth is along the *b* axis (Fig. 3.5.5b).

(a)

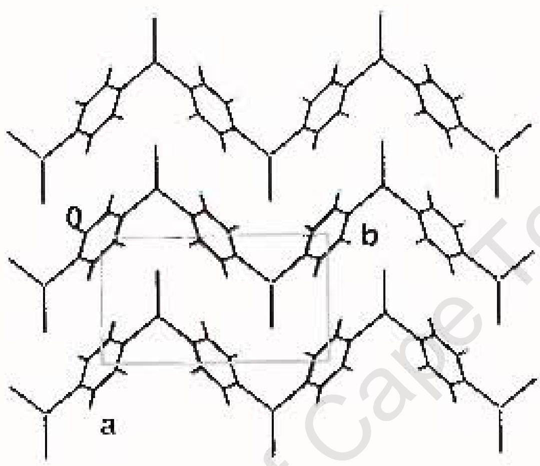

(b)

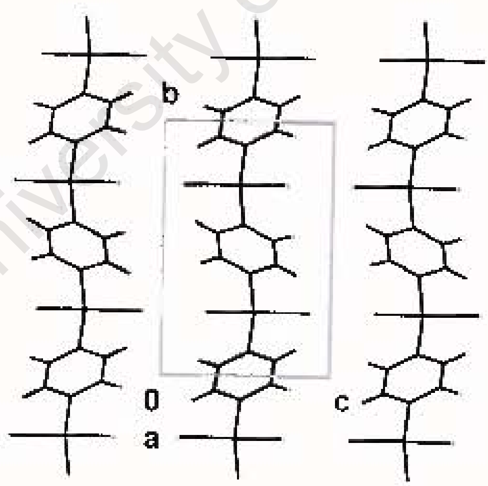

Fig 3.5.5: (a) Stick representation of $ZnBr_2pyz$, viewed along (a) [001], and (b) [100].

SOLID STATE SYNTHESIS OF $ZnBr_2pyz_2$ FROM $ZnBr_2pyz$

The product of the solid state reaction shown below, between **$ZnBr_2pyz$** powder and solid pyrazine, was characterised by XRD and thermal analysis.

$$\mathbf{ZnBr_2pyz_{\,(s)} + pyz_{\,(s)} \rightarrow ZnBr_2pyz_{2\,(s)}}$$

THERMAL ANALYSIS:

The TG of single crystals of **$ZnBr_2pyz$**, as well as the powdered starting material, show a continuous weight loss above 260°C, with 41% of the initial mass having been lost by 400°C. If the TG is run at an elevated heating rate of 45°C.min^{-1}, however, then an inflection in the curve is observed at 351.6°C. This inflection occurs after 25.5% of the mass has been lost (1 pyz = 26.2%) (Fig. 3.5.6a). The DSC shows a corresponding broad endotherm followed by exothermic decomposition. The TG of single crystals of **$ZnBr_2pyz_2$**, as well as the solid state reaction product, show an additional weight loss step between 100°C and 160°C, corresponding to the loss of one pyrazine ligand per formula unit (Fig. 3.5.6b). This step is accompanied by a broad endotherm in the DSC. Thereafter, both compounds decompose. Even at a heating rate of 45°C.min^{-1}, the loss of one pyrazine ligand per formula unit could not be distinguished. An inflection similar to the one described above does occur in **$ZnBr_2pyz_2$**, at 331.5°C for the crystals and 339.9°C for the solid state reaction product. The mass loss, however, is non-stoichiometric (14.7% for the crystals and 14.0% for the powder; 1 pyz = 20.8%). In addition, the corresponding broad endotherm in the DSC overlaps with exothermic decomposition, in both cases. Full TG and DSC data are given in Table 3.5.6.

The decomposition of a single crystal of **$ZnBr_2pyz_2$** was followed by HSM. Between 102°C and 200°C, the translucent yellow crystal bubbles and turns opaque white, corresponding to the release of the volatile pyrazine ligand. Above

300°C, discolouration of the crystal is observed, and it melts to a sticky mass with bubbling (Fig. 3.5.7).

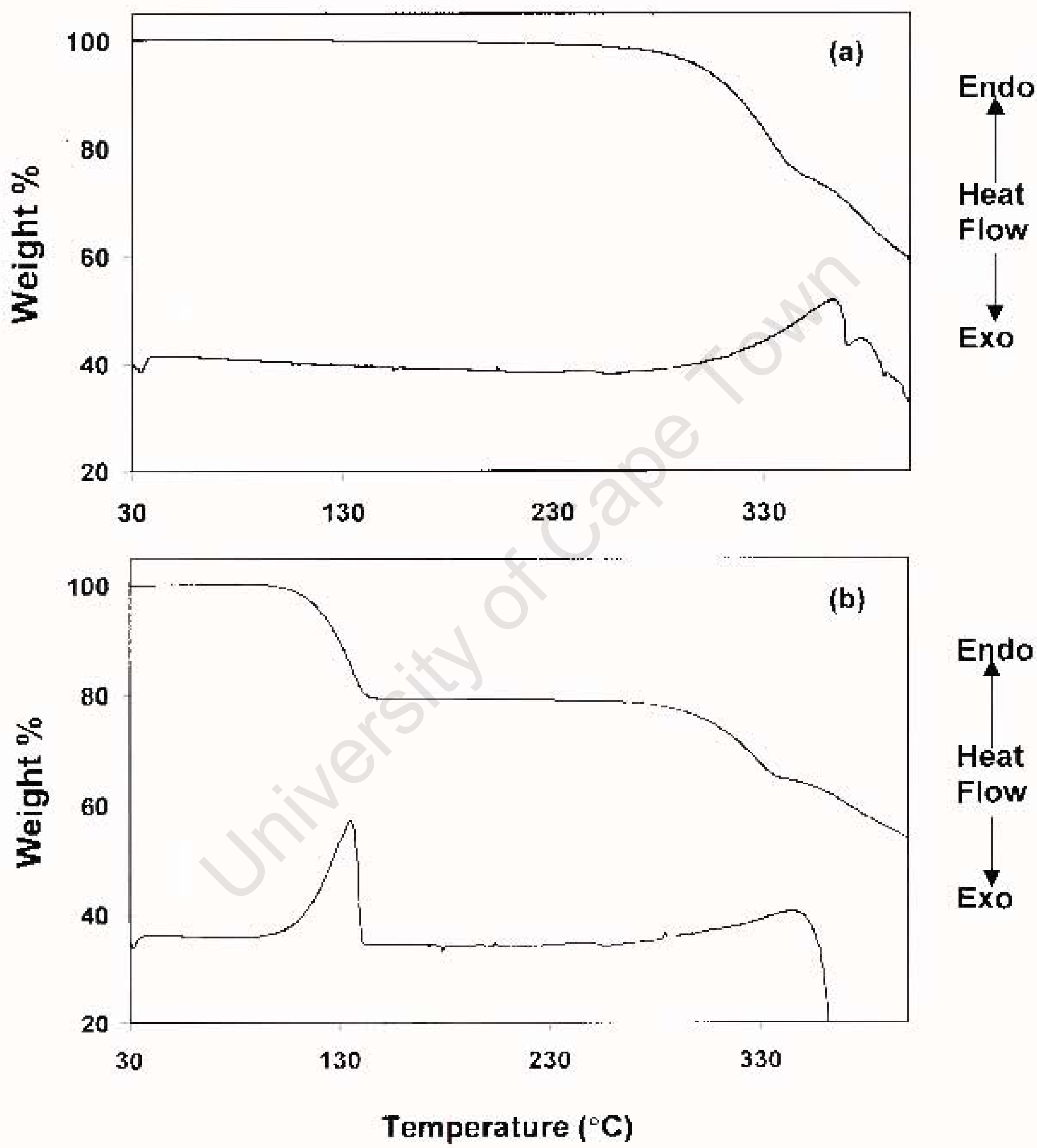

Fig 3.5.6: Thermal analysis of (a) $ZnBr_2pyz$ powder and (b) the $ZnBr_2pyz_2$ solid state reaction product.

Table 3.5.6: TG and DSC data for $ZnBr_2pyz_2$ and $ZnBr_2pyz$

Compound	Reaction	TG			DSC	
		T_{onset} (°C)	Exp %	Calc %	T_{onset} (°C)	ΔH (kJ.mol^{-1})
$ZnBr_2pyz$ crystals	$ZnBr_2pyz \rightarrow ZnBr_2 + pyz$ *	276.6	25.4	26.2	281.0	-
Powdered starting material	$ZnBr_2pyz \rightarrow ZnBr_2 + pyz$ *	257.6	25.5	26.2	271.5	-
$ZnBr_2pyz_2$ Crystals	$ZnBr_2pyz_2 \rightarrow ZnBr_2pyz + pyz$	100.8	19.7	20.8	96.5	66.5
	Decomposition	252.9	-	-	275.0	-
Solid state reaction product	$ZnBr_2pyz_2 \rightarrow ZnBr_2pyz + pyz$	100.2	19.6	20.8	96.5	60.8
	Decomposition	264.3	-	-	277.0	-

* immediately followed by further decomposition

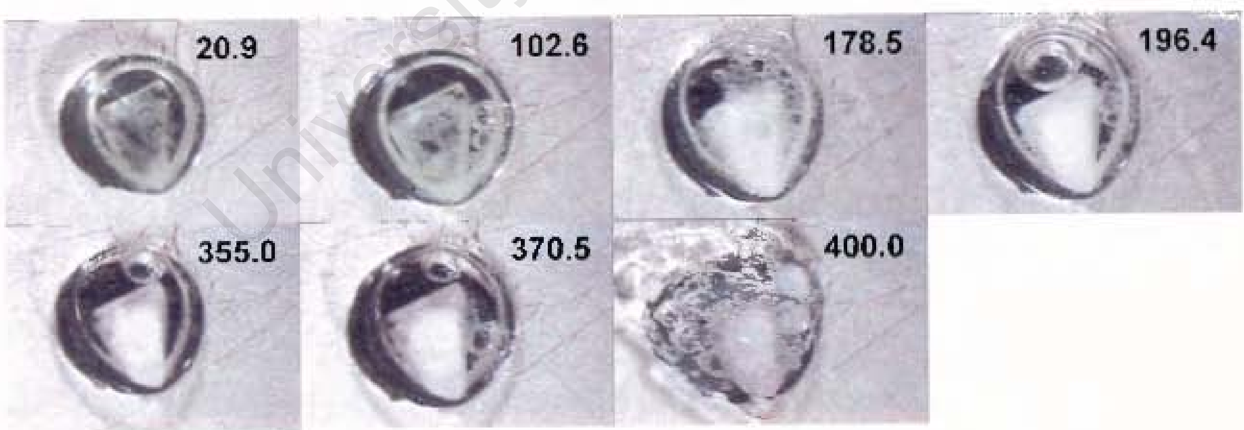

Fig 3.5.7: HSM of $ZnBr_2pyz_2$ (Temperatures, in °C, are given in top right hand corner).

XRD:

The product of the solid state reaction ($ZnBr_2pyz_{(s)}$ + $pyz_{(s)}$ → $ZnBr_2pyz_{2(s)}$) gives an XRD pattern (**3**) that is superimposable on the pattern calculated for **$ZnBr_2pyz_2$** (**4**), with the exception of two extra peaks in the experimental trace that are found to correspond to unreacted pyrazine (Fig. 3.5.8). This solid state reaction product was heated at 60°C for 120min. The resulting XRD trace (**5**) is superimposable on that of **$ZnBr_2pyz$** (**2**), confirming that the uptake of one pyrazine ligand per formula unit by **$ZnBr_2pyz$** is a fully reversible process.

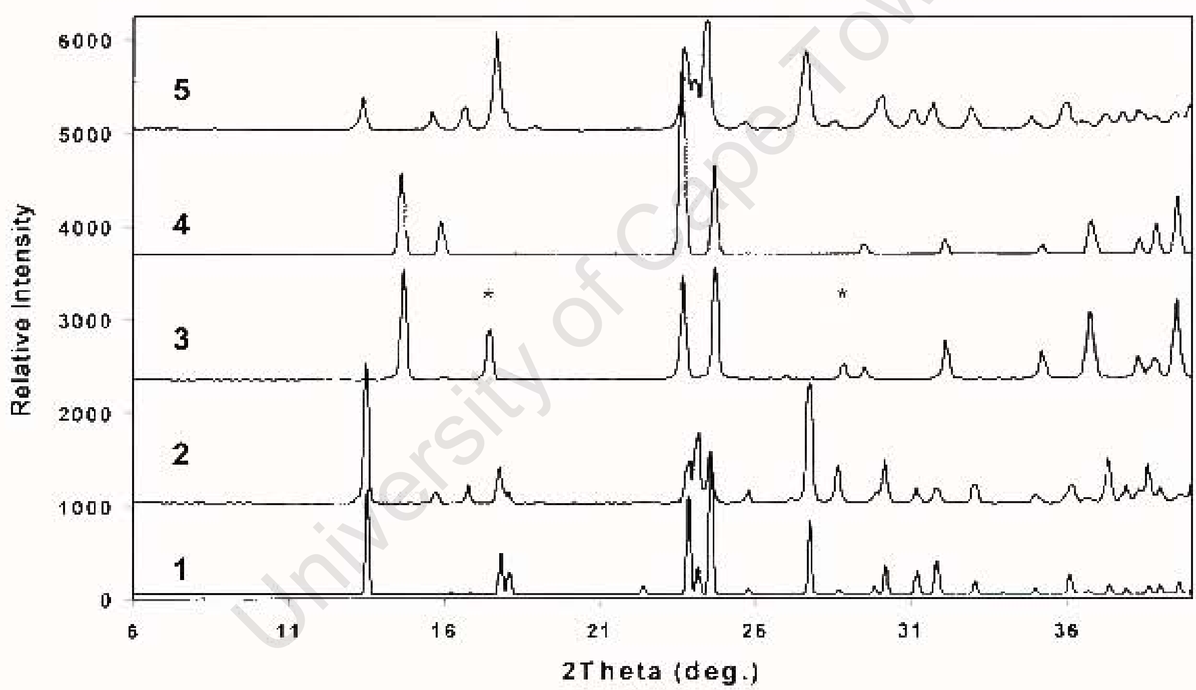

Fig 3.5.8: XRD traces of $ZnBr_2pyz$ (**1**, calculated and **2**, experimental); Solid state reaction product (**3**) (peaks marked * correspond to unreacted pyrazine); $ZnBr_2pyz_2$ (**4**, calculated), and product obtained on heating solid state reaction product (**5**).

These data indicate that the powder form of **$ZnBr_2pyz_2$** can be generated from the powdered starting material, **$ZnBr_2pyz$**, via a simple solid state reaction. The reverse reaction, a decomposition process, can be effected by heating the sample to release the volatile pyrazine ligand, thereby regenerating **$ZnBr_2pyz$**. The kinetics of decomposition of this reverse reaction was studied using Isothermal Thermogravimetry.

ISOTHERMAL DECOMPOSITION KINETICS OF $ZnBr_2pyz_2$

The isothermal decomposition kinetics of the reaction **$ZnBr_2pyz_{2\ (s)}$** $\rightarrow$ **$ZnBr_2pyz_{\ (s)}$** + **$pyz_{\ (g)}$** was investigated. Isothermal thermogravimetric analysis was used to determine the most probable decomposition mechanism of **$ZnBr_2pyz_2$**. The decomposition reactions were carried out under isothermal conditions, over a temperature range of 85°C to 110°C. The resulting % weight loss vs. time curves are shown in Fig. 3.5.9, below.

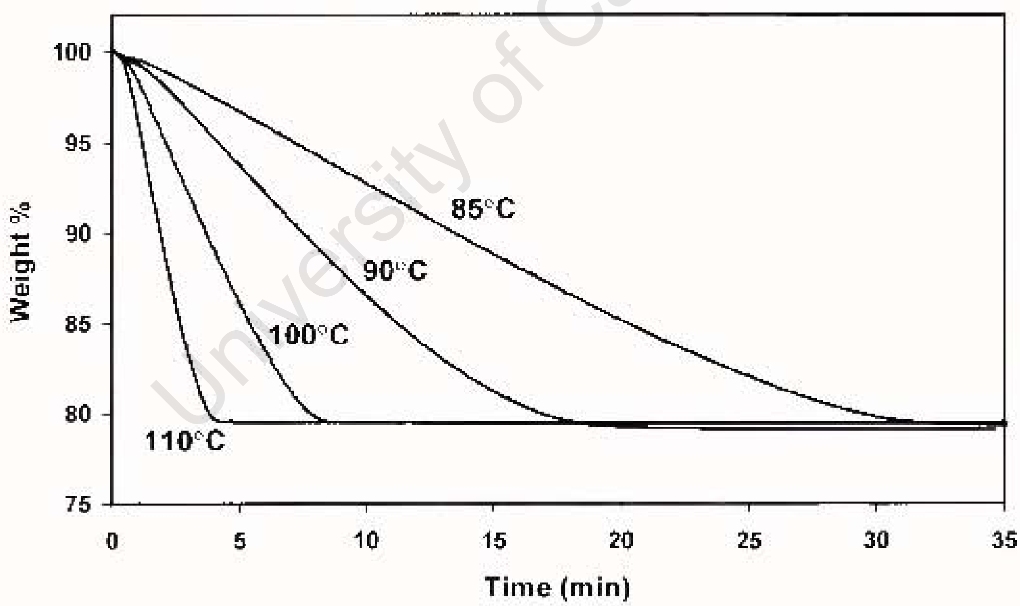

Fig 3.5.9: % Weight loss vs. time curves for the reaction $ZnBr_2pyz_{2\ (s)} \rightarrow ZnBr_2pyz_{\ (s)} + pyz_{\ (g)}$

Each % weight loss vs. time curve was converted into an extent of reaction, α, vs. time curve, using the program TGISODAT. The extent of reaction, α, is described by equation 1 below, where m_f is the final mass of the compound, m_i the initial mass and m_t the mass at any time, t, during the mass loss process.

$$\alpha = \frac{m_i - m_t}{m_i - m_f} \qquad (1)$$

Various kinetic models, of the form $f(\alpha) = kt$, were fitted to the α-time data using the program KINETIC. The kinetic model for which the function, $f(\alpha)$, was linear over the largest range of α was chosen as the best fit model, where the goodness of fit is reflected in the correlation coefficient, r (Table 3.5.7). The rate constant, k, is the slope of the resultant plot. For the release of one pyrazine ligand from **$ZnBr_2pyz_2$**, the best kinetic model was found to be the contracting area deceleratory α-time equation, $f(\alpha) = 1-(1-\alpha)^{1/2}$ (R2)[22]. The data were found to be isokinetic, in that the same rate law could be applied to all four isothermals.

Table 3.5.7: Kinetic data for the reaction: $ZnBr_2pyz_{2\,(s)} \rightarrow ZnBr_2pyz_{\,(s)} + pyz_{\,(g)}$

Temperature (K)	α Range	Correlation coefficient, r	Slope, k (min^{-1})	Y-Intercept
358	0.01-0.85	0.9934	0.0286	-0.0787
363	0.03-0.90	0.9973	0.0502	-0.0816
373	0.01-0.90	0.9932	0.1142	-0.1165
383	0.03-0.85	0.9943	0.2526	-0.1766

Given that the data were isokinetic, the Arrhenius equation (2) could be used to determine the activation energy, E_a, and pre-exponential factor, A, for this reaction. The activation energy and pre-exponential factor are measures of the energy barrier that must be overcome to enable the reaction to occur and the frequency of occurrence of the reaction respectively. Since the Arrhenius equation was derived for homogeneous systems, the validity of its application to heterogeneous systems has been questioned. It has been shown, however, that the activation energy and pre-exponential parameters do have practical value, and the Arrhenius equation is widely accepted and has been successfully applied to many reactions involving solids[23].

$$\ln k = \ln A - \frac{E_a}{RT} \qquad (2)$$

Plotting the semilogarithmic graph of ln k vs. T^{-1} gives a straight line of slope -1.20×10^{4}s and y-intercept 25.94, resulting in an activation energy for the reaction of 99.8kJ.mol^{-1} and a pre-exponential factor of 1.8×10^{11}s^{-1} (Fig. 3.5.10). This value compares well with activation energies calculated for the decomposition reactions of various metal-ligand complexes[24].

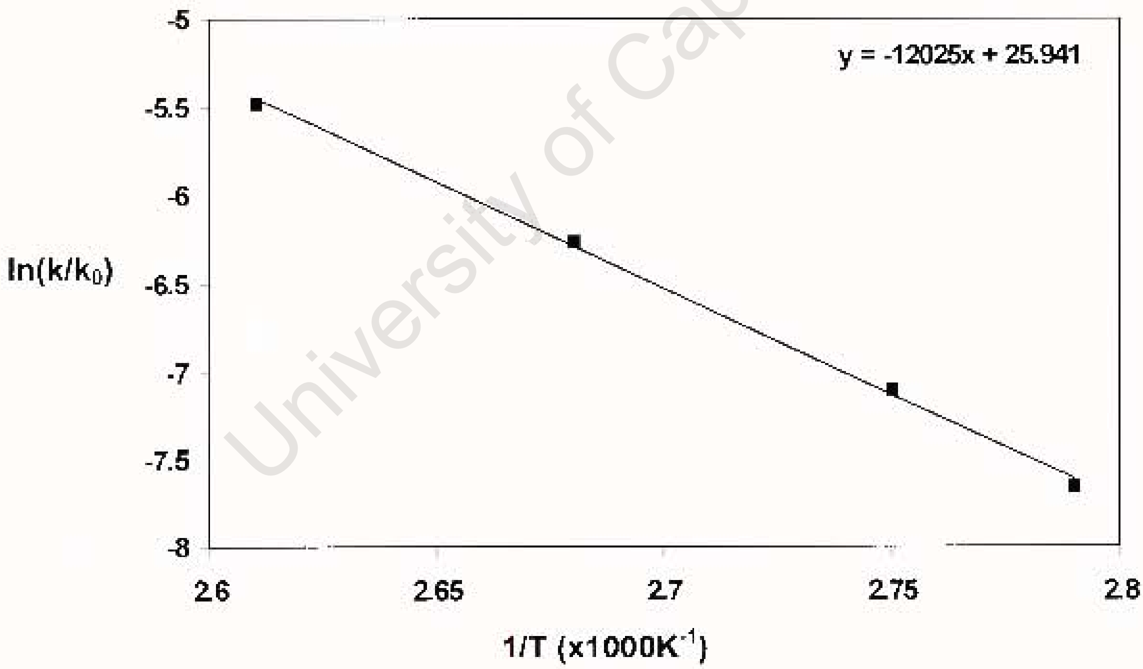

Fig 3.5.10: Arrhenius plot for the reaction $ZnBr_2pyz_{2\,(s)} \rightarrow ZnBr_2pyz_{\,(s)} + pyz_{\,(g)}$

ZnpyzSulf: $Zn(H_2O)_4(pyrazine).SO_4.2H_2O$

MICROANALYSIS:

	%C	%H	%N	%S
Calculated for $Zn(H_2O)_4(pyz).SO_4.2H_2O$	14.03	4.26	8.09	9.41
Experimental	13.75	4.61	8.02	9.18

X-RAY PHOTOGRAPHY:

These crystals proved to be unstable when exposed to air for any length of time, with the result that a single crystal was mounted in a sealed glass capillary containing a drop of mother liquor. The oscillation photograph gave the length of one unit cell as 13.9Å, while the Weissenberg photograph revealed the remaining two cell lengths to be 7.0Å and 12.8Å, with an angle between them of 90°. Of the two photographs only the Weissenberg photograph displayed mirror symmetry. The resulting *2/m* Laue symmetry indicates a monoclinic unit cell.

SINGLE CRYSTAL X-RAY DIFFRACTOMETRY:

The unit cell obtained by diffractometry was identical to that obtained by photography.

STRUCTURE SOLUTION AND REFINEMENT:

The diffraction data revealed *2/m* Laue symmetry, and systematic absences indicative of the monoclinic space group $P2_1/n$. The Zn atom was located in a general position in the unit cell. During the structure solution it became apparent that the two axial positions in the coordination environment of the Zn centre were each occupied by half a pyrazine ligand. The two halves were subsequently refined as two separate fragments, with each half completing the other through application of the symmetry operations (x-½, ½-y, z-½) and (x+½, ½-y, z+½).

All non-hydrogen atoms were located on the electron density map and refined anisotropically. The hydrogen atoms of the pyrazine ring were placed in geometrically calculated positions. Six of the eight hydrogen atoms belonging to the water ligands were located on the electron density map and refined isotropically. The remaining two hydrogens were placed in positions that were calculated by examining the most probable hydrogen bonding interactions. The hydrogen atoms of the two water guests could not be located and were omitted from the final model (crystal structure and refinement parameters are given in Table 3.5.2).

STRUCTURE ANALYSIS:

The coordination geometry around the Zn centre is that of an irregular octahedron. Each Zn atom is coordinated to two trans pyrazine ligands and four equatorial H_2O molecules (Fig. 3.5.11).

The Zn-O and Zn-N bond lengths are close to the literature values of 2.09(6)Å and 2.10(6)Å respectively[7] (Table 3.5.8). The Zn-O2 bond is significantly longer than the other three Zn-O bonds, possibly due to the hydrogen bonding interactions unique to the O2 atom. The pyrazine ring refined well, as illustrated by the bond and torsion angles given in Appendix 5. The C-C bonds lengths are 1.37(1)Å and 1.38(1)Å, while the C-N bonds lie in the range 1.34(1)Å to 1.35(1)Å. These correspond well with the literature values of 1.38(1)Å and 1.34(1)Å respectively[2].

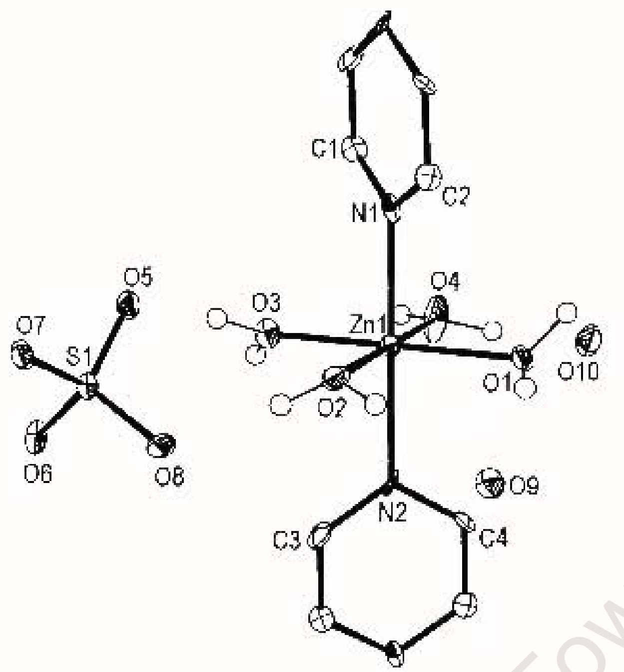

Fig 3.5.11: Ortep diagram of ZnpyzSulf, showing thermal ellipsoids (ring H atoms omitted: only the asymmetric unit is labelled).

Table 3.5.8: Selected bond lengths and angles around the Zn centre

Bond	Length (std.dev.)	Angle	Degrees (std.dev.)
Zn1 – O1	2.092 (4)	O1 – Zn1 – O2	90.6 (2)
Zn1 – O2	2.198 (5)	O3 – Zn1 – N1	90.4 (2)
Zn1 – O3	2.035 (5)	O1 – Zn1 – N1	90.2 (2)
Zn1 – O4	2.077 (5)	O1 – Zn1 – O4	90.7 (2)
Zn1 – N1	2.127 (6)	O1 – Zn1 – O3	178.9 (2)
Zn1 – N2	2.163 (6)	N1 – Zn1 – N2	175.2 (2)

This structure was found to be polymeric. Each pyrazine molecule acts as a bridging ligand, linking two Zn centres through the two ring N atoms. This leads to the formation of 1-D, linear, cationic chains of alternating Zn and pyrazine moieties (fig 3.5.12). The mean planes of adjacent pyrazine rings within a chain are orthogonal.

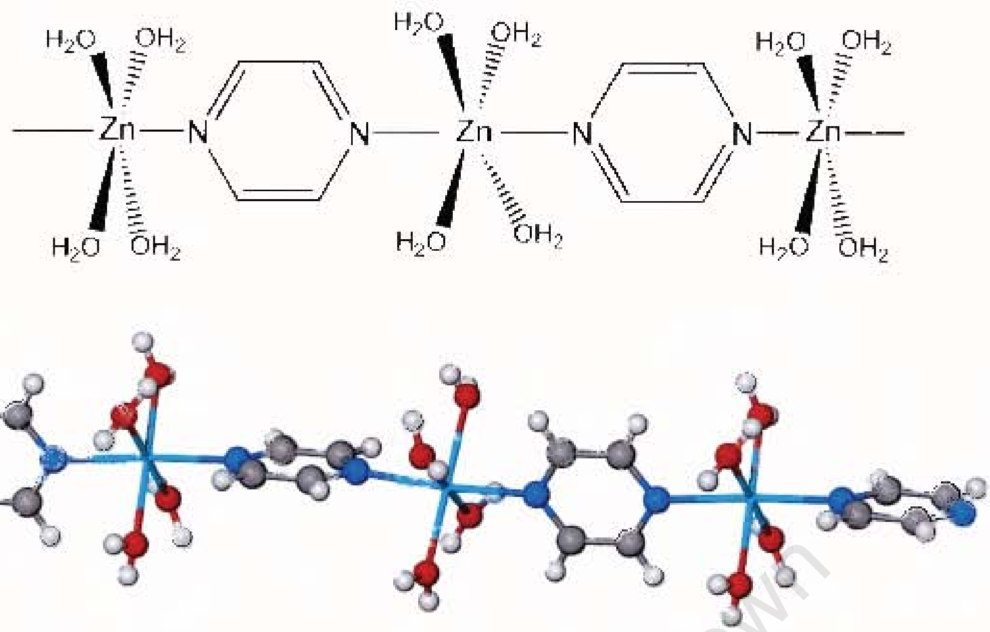

Fig 3.5.12: The linear, 1-D polymers in ZnpyzSulf.

HYDROGEN BONDING INTERACTIONS:

Extensive hydrogen bonding interactions exist between the water ligands, water guests and sulphate counterions. The four water ligands are hydrogen bonded to the oxygen atoms of the water guests and sulphate anions. The water guests in turn are hydrogen bonded to each other as well as the sulphate counterions (Fig. 3.5.13).

Since no hydrogen atoms could be located for the two water guests, the hydrogen bonding interactions were inferred from the O···O contacts. All twelve unique O···O contacts examined below are shorter than the sum of the van der Waals radii for two oxygen atoms (3.04Å), putting them in the range generally associated with moderately strong hydrogen bonds (Table 3.5.9).

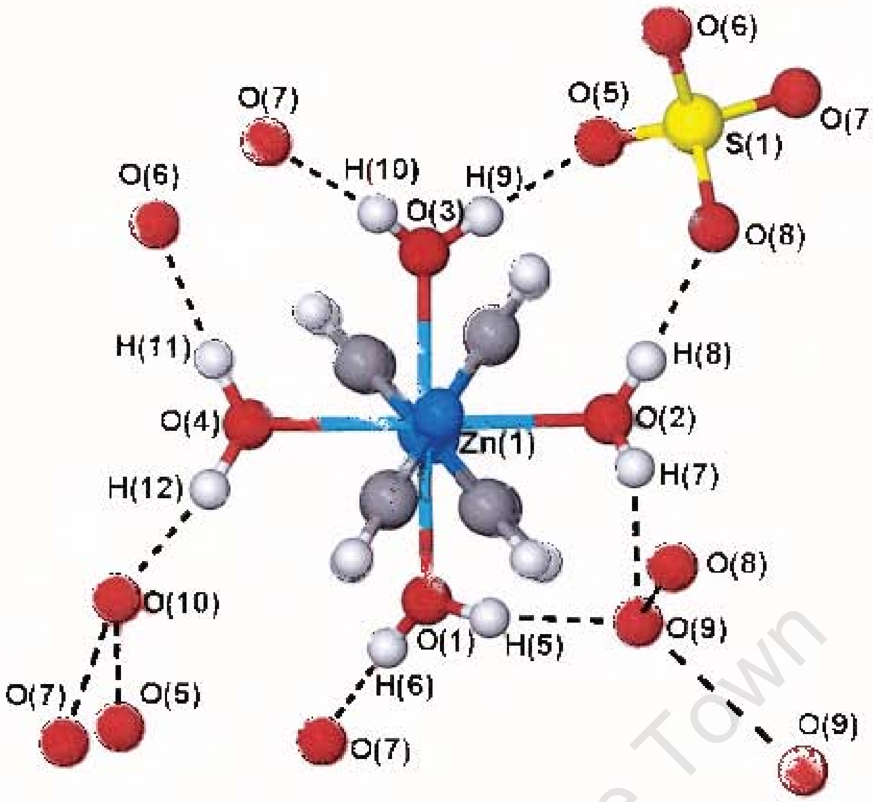

Fig 3.5.13: The 12 unique hydrogen bonding interactions in ZnpyzSulf (polymer viewed end-on).

Table 3.5.9: Hydrogen Bonding Data for ZnpyzSulf

O – H ··· O	O–H (Å)	H···O (Å)	O···O (Å)	Angle (°)
	HOST ··· GUEST (H_2O) INTERACTIONS			
O1– H5 ··· O9	0.844(79)	1.932(77)	2.765(7)	166.6(7.4)
O2– H7 ··· O9	0.732(89)	2.088(89)	2.774(7)	156.1(8.7)
O4 – H12 ··· O10	0.930(85)	1.740(84)	2.661(8)	170.0(7.6)
	HOST ··· GUEST (SO_4) INTERACTIONS			
O1– H6 ··· O7$^{\#1}$	0.934(83)	1.772(82)	2.705(6)	176.4(8.1)
O2– H8 ··· O8	0.850(80)	1.862(80)	2.708(7)	173.8(7.8)
O3– H9 ··· O5	0.909(74)	1.726(75)	2.633(7)	175.3(7.0)
O3– H10 ··· O7$^{\#2}$	0.848(76)	1.832(76)	2.676(6)	173.8(7.8)
O4– H11 ··· O6$^{\#2}$	0.869(79)	1.862(83)	2.685(8)	157.3(7.3)

O – H ··· O	O – H (Å)	H ··· O (Å)	O ··· O (Å)	Angle (°)
GUEST ··· GUEST INTERACTIONS				
O10 ··· O7#3	-	-	2.933(7)	-
O10 ··· O5#1	-	-	2.779(7)	-
O9 ··· O8#4	-	-	2.813(6)	-
O9 ··· O 9#5	-	-	2.741(7)	-

Symmetry codes: #1 = ½-x, ½+y, ½-z, #2 = –x-½, ½+y, ½-z, #3 = ½+x, $\frac{3}{2}$-y, z-½, #4 = –x, 1-y, -z, and #5 = 1-x, 1-y, -z.

CRYSTAL PACKING FEATURES:

The 1-D host polymers pack to form channels in the crystal (Fig. 3.5.14a,b). These channels, which run parallel to the [101] direction, contain the water guests and sulphate anions (Fig 3.5.14c). The channels are tubular in shape, with a minimum pore diameter of approximately 3.1Å.

The packing of the polymers is such that each chain has four nearest neighbours. The Zn–pyrazine chains are staggered, such that the Zn centre of any particular chain lies approximately halfway between the two Zn centres of an adjacent chain. This applies to all four of the nearest neighbouring chains.

While the backbones of the channels are formed by the 1-D chains of alternating Zn centres and pyrazine ligands, the walls of the channels are formed by the water ligands, which project from the Zn centres towards the four nearest neighbouring chains. Since there are no host∧host hydrogen bonds, the channel structure is stabilised by host(H_2O)···guest(H_2O/SO_4^{2-}) hydrogen bonding interactions.

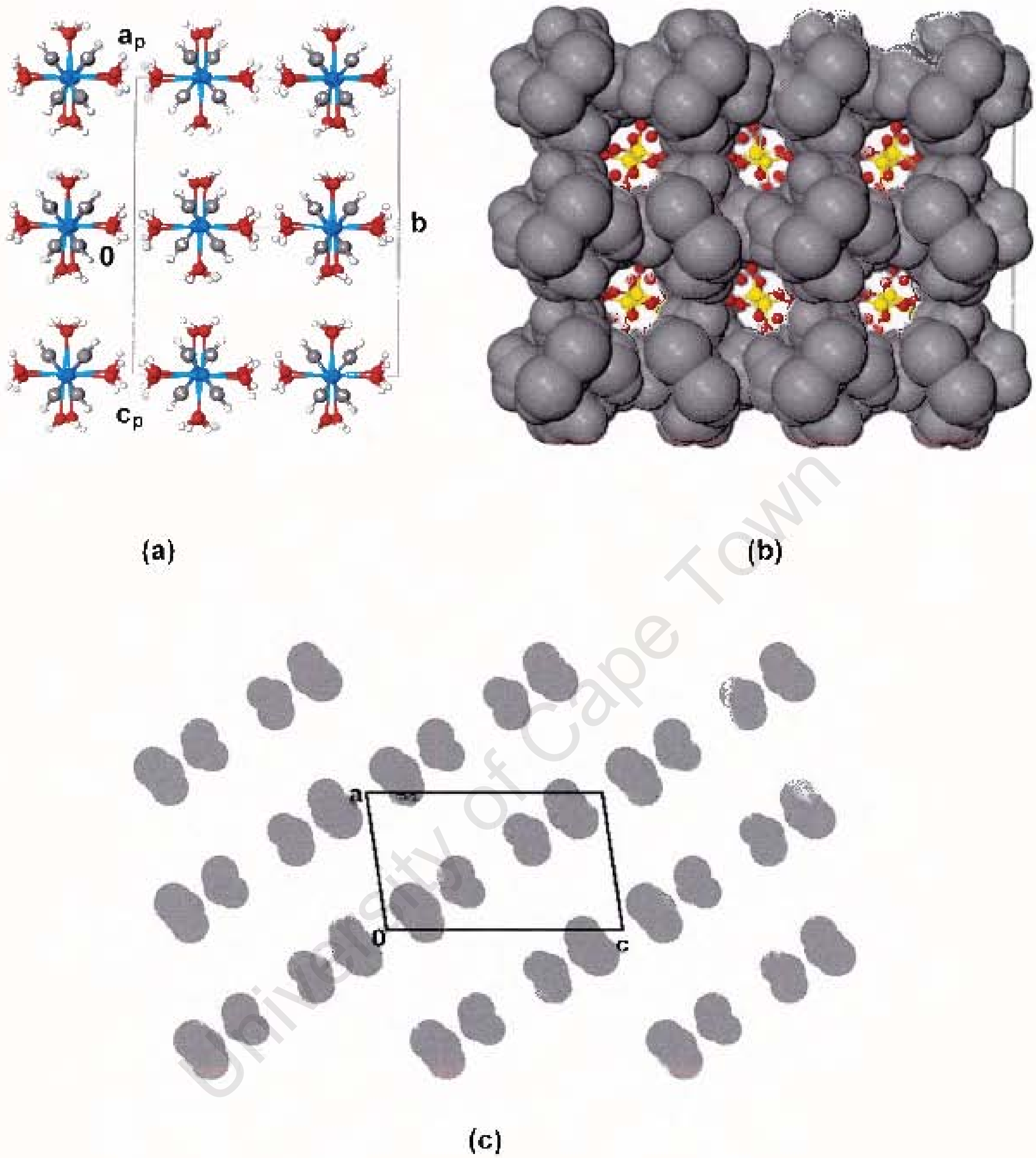

Fig 3.5.14: (a) Ball-and-stick representation of the channel structure in ZnpyzSulf, viewed along the [101] direction (guest molecules omitted for clarity), (b) Space-filling representation of channels, showing guest molecules in ball-and-stick form, (c) Space-filling representation of host polymers only, viewed along [010], at *b*=0.

THERMAL ANALYSIS

The thermal analysis of **ZnpyzSulf** is shown in Fig. 3.5.15. The crystals were finely crushed prior to analysis, due to their tendency to jump during the vigorous bubbling that occurs upon loss of the water ligands. The TG shows two distinct weight loss processes, corresponding to the loss of the two water guests (step **a**) and four water ligands (step **b**). Above 160°C, there is a gradual mass loss, corresponding to the loss of the pyrazine ligand (step **c**). Step **a** produces two small, broad endotherms in the DSC, while step **b** results in a large, broad endotherm. Step **c** produces a small, very broad endotherm. Full TG and DSC data are given in Table 3.5.10.

Single crystals were observed using HSM (Fig. 3.5.16). During step **a** the crystals turn slightly opaque. Vigorous bubbling is observed during step **b**, and the crystals turn completely white. Above 280°C the crystals resume bubbling, and a sticky, pale brown residue is formed.

Table 3.5.10: TG and DSC data for ZnpyzSulf

Reaction	TG			DSC	
	T_{onset} (°C)	Exp %	Calc %	T_{onset} (°C)	ΔH ($kJ.mol^{-1}$)
$Zn(H_2O)_4(pyz).SO_4.2H_2O \rightarrow Zn(H_2O)_4(pyz).SO_4 + 2H_2O$	33.6	11.7	10.3	39.5	45.6
$Zn(H_2O)_4(pyz).SO_4 \rightarrow Zn(pyz).SO_4 + 4H_2O$	81.7	19.4	20.6	98.0	165.5
$Zn(H_2O)_4(pyz) \rightarrow ZnSO_4 + pyz$	159.1	21.9	23.7	282.5	43.6

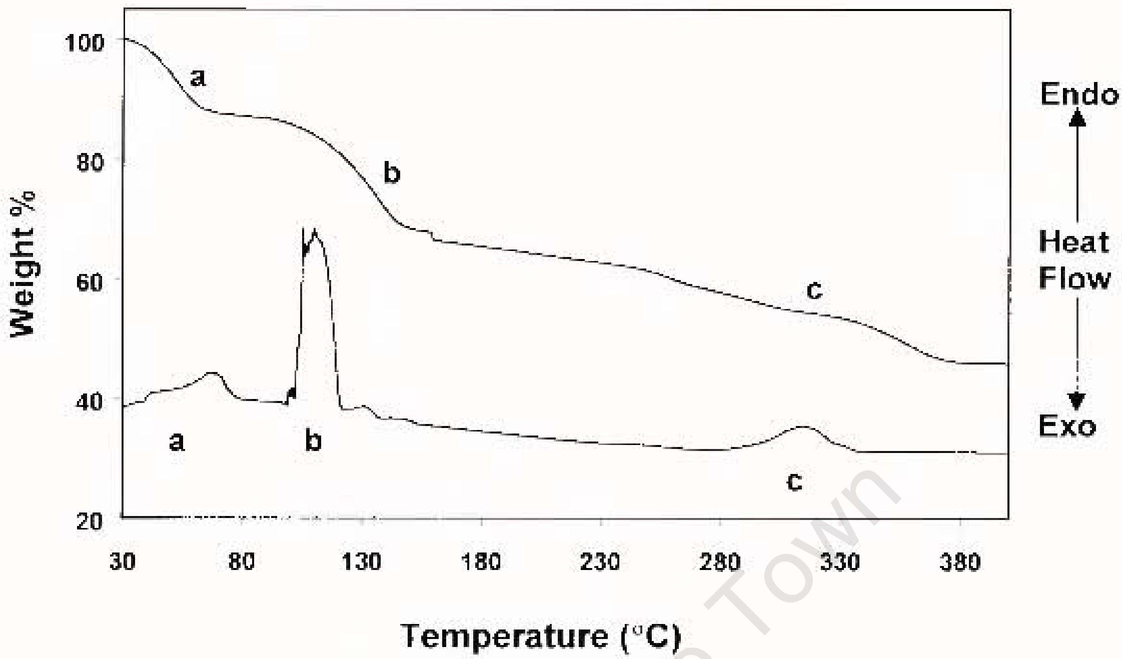

Fig 3.5.15: Thermal analysis for ZnpyzSulf

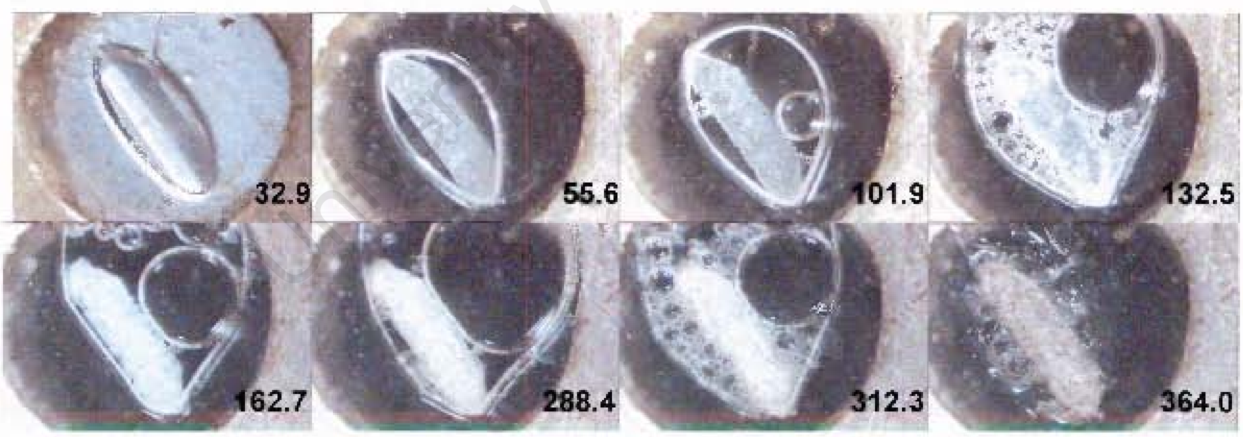

Fig 3.5.16: HSM of ZnpyzSulf (Temperatures, in °C, are given in bottom right hand corner)

XRD:

There are discrepancies between the calculated and experimental powder patterns for **ZnpyzSulf** (Fig. 3.5.17). This can be attributed to the loss of a small amount of H_2O guest from the powder on exposure to air, resulting in a deformation of the channel structure.

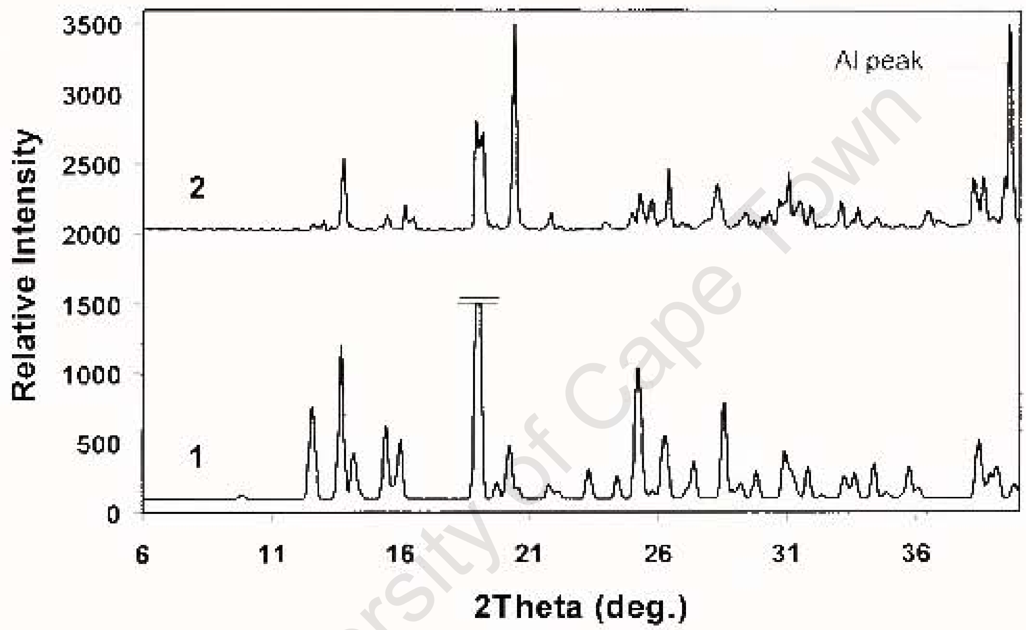

Fig 3.5.17: XRD traces for ZnpyzSulf (**1**, calculated and **2**, experimental).

Cudiaq: Cu(isonicotinamide)$_2$(H_2O)(SO_4).$2H_2O$

MICROANALYSIS:

	%C	%H	%N	%S
Calculated for $Cu(C_6H_6N_2O)_2(H_2O)(SO_4).2H_2O$	31.49	3.96	12.24	7.01
Experimental	31.60	3.96	11.91	6.77

PRELIMINARY X-RAY PHOTOGRAPHY:

Oscillation photography gave one unit cell length as 4.9Å, while Weissenberg photography revealed the remaining two cell lengths to be 24.1Å and 15.0Å, with an angle between them of 90°. Of the two photographs, only the Weissenberg photograph was mirrored. The resulting *2/m* Laue symmetry indicates a monoclinic unit cell.

SINGLE CRYSTAL X-RAY DIFFRACTOMETRY:

The unit cell obtained by diffractometry was identical to that obtained by photography.

STRUCTURE SOLUTION AND REFINEMENT:

The diffraction data revealed *2/m* Laue symmetry, and systematic absences indicative of the monoclinic space group $P2_1/c$. The Cu atom was located in a general position in the unit cell.

The Patterson method was used to solve this structure, as direct methods proved unsuccessful. This was carried out by a subroutine in X-Seed, which solves the Patterson function, expands the structure, and immediately yields an electron density map. The latter showed the position of all the non-hydrogen atoms unambiguously. The quality of the data did not allow for the anisotropic refinement of all non-hydrogen atoms, with the result that only the Cu, S and O atoms were refined in this way. The aromatic and amide hydrogens were placed in geometrically calculated positions, while the hydrogen atoms of the water ligand and guests were omitted from the final model (crystal structure and refinement details are given in Table 3.5.2).

STRUCTURE ANALYSIS:

Solving the structure in $P2_1/c$ revealed a Cu centre with an irregular square pyramidal coordination geometry (Fig. 3.5.18).

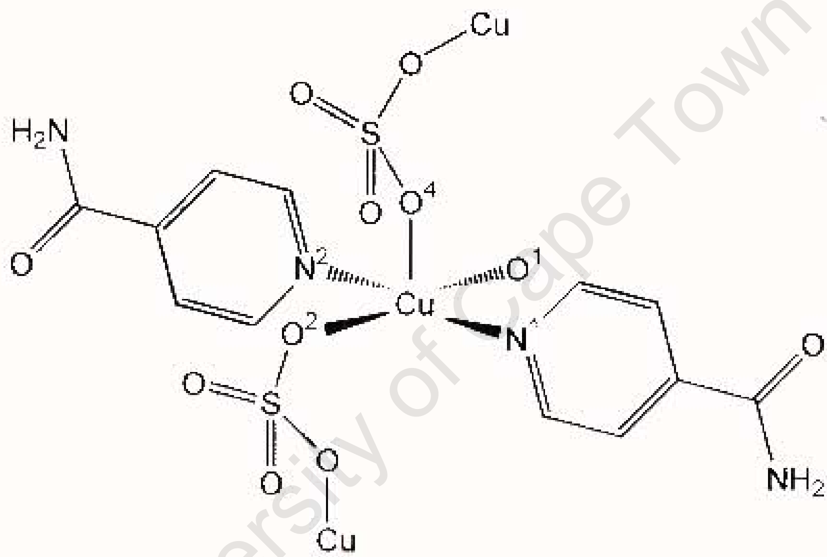

Fig 3.5.18: Coordination geometry around Cu(II) centre

In the square plane, the Cu centre is coordinated to one water molecule (O1), two *trans* isonicotinamide ligands (N1, N2) and one sulphate counterion (O2). The oxygen atom (O4) of another sulphate group occupies the axial position. The bond lengths and angles around the Cu centre are listed in Table 3.5.11, with full bond lengths and angles given in Appendix 5.

Table 3.5.11: Selected bond lengths and angles around the Cu centre

Bond	Length (Å)	Angle	Angle (°)
Cu1 – O2	1.975(5)	O2 - Cu1 – N1	90.1(8)
Cu1 – O1	1.977(6)	O1 - Cu1 – N1	89.8(9)
Cu1 – N1	2.015(18)	O1 - Cu1 – N2	86.5(8)
Cu1 – N2	1.997(16)	O1 - Cu1 – O4$^{\#1}$	90.2(2)
Cu1 – O4$^{\#1}$	2.169(6)	N1 - Cu1 – O4$^{\#1}$	97.5(8)

Symmetry codes: #1 = x-1, y, z.

The literature values for the bond lengths listed above are 2.05(3)Å (Cu–N_{pyr}) and 2.19(25)Å (Cu–OH_2)[1]. The Cu–OSO_3 bond lengths, for bridging sulphate ligands, found in the CSD range from 1.909Å to 2.374Å. The Cu–OSO_3 bond lengths obtained for this structure would, therefore, seem to be reasonable. The axial Cu–OSO_3 bond is significantly longer than the other four equatorial bonds, a feature that is often observed in square pyramidal coordination geometries.

This structure was found to be polymeric. The sulphate anions act as bridging ligands, each sulphate group coordinating to two Cu centres (Fig 3.5.19). This leads to the formation of 1-D polymeric chains of alternating Cu centres and sulphate counterions. The polymerisation of these units occurs along the *a* axis.

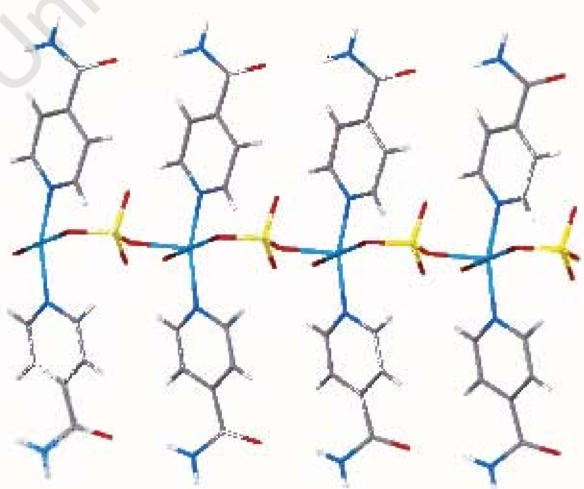

Fig 3.5.19: Stick representation of the polymers found in Cudiaq

HYDROGEN BONDING INTERACTIONS:

An extensive hydrogen-bonded network is formed between the water ligands, water guests, sulphate anions and amide moeities. The hydrogen bonding interactions can be divided into two main groups, those involving the amide moieties of the isonicotinamide ligands, and those involving the water molecules and sulphate ions (Table 3.5.12).

In the first case, the amide group of each isonicotinamide ligand forms intrachain N–H···O=C hydrogen bonds to the amide groups of the two adjacent isonicotinamide ligands in the polymer (N3–H3B···O8 and N4–H4B···O9). In addition, each amide group is hydrogen bonded to a water guest (N4–H4A···O6 and N3–H3A···O7). These interactions are shown in Fig. 3.5.20, below.

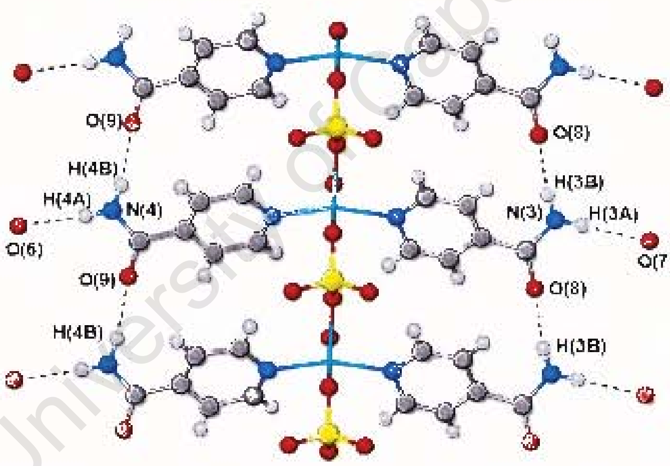

Fig 3.5.20: Hydrogen bonding interactions of the amide moieties

Each water guest is surrounded by two hydrogen bond donors and two hydrogen bond acceptors, with the result that four possible hydrogen bonding interactions are available to each water molecule (Fig. 3.5.21). As stated above, one of these is the amide N–H···O interaction. In addition each water guest is hydrogen bonded to a coordinated water ligand (O1···O6 and O1···O7), and to two oxygen atoms of adjacent sulphate anions within a chain (O7···O3 and O6···O5). In this way each water guest acts as a bridge between three different polymers through interchain hydrogen bonding interactions.

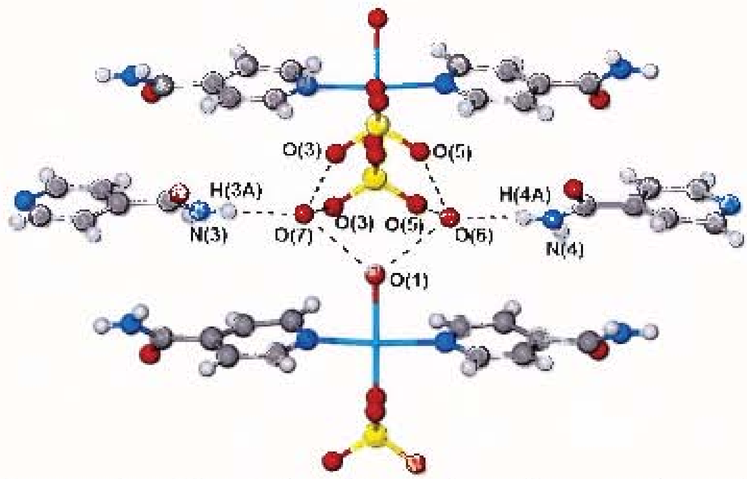

Fig 3.5.21: Hydrogen bonding interactions of water guests and sulphate counterions.

Table 3.5.12: Hydrogen Bonding data for Cudiaq

O ··· O	O ··· O (Å)			
	O ··· O CONTACTS			
O1 ··· O6	2.713(22)			
O1 ··· O7	2.710(22)			
O6 ··· O5$^{\#1}$	2.831(20)			
O6 ··· O5$^{\#2}$	2.947(18)			
O7 ··· O3$^{\#3}$	2.797(21)			
O7 ··· O3$^{\#4}$	2.810(22)			
N – H ··· O	N–H (Å)	H ··· O (Å)	N ··· O (Å)	Angle (°)
	N – H ··· O INTERACTIONS			
N3 – H3A$^{\#5}$ ··· O7	0.860(15)	2.211(17)	3.071(23)	178.9(1.1)
N4 – H4A$^{\#6}$ ··· O6	0.860(13)	2.149(16)	3.007(21)	175.4(1.0)
N3 – H3B ··· O8$^{\#7}$	0.860(12)	1.940(17)	2.764(20)	160.0(0.9)
N4 – H4B ··· O9$^{\#7}$	0.860(11)	2.054(16)	2.888(20)	163.1(0.9)

Symmetry codes: #1 = x-1, ½-y, ½+z, #2 = x, ½-y, ½+z, #3 = x-1, ½-y, ½+z, #4 = x, ½-y, ½+z, #5 = 1-x, ½+y, ½-z, #6 = 1-x, y-½, ½-z, #7 = x-1, y, z.

CRYSTAL PACKING FEATURES:

As mentioned above, the direction of polymer growth is along the [100] direction (Fig. 3.5.22a). Interchain host···guest hydrogen bonding interactions link the polymers into a 3-D hydrogen bonded network. The water molecules are located in undulating channels which run parallel to the [100] direction (Fig. 3.5.22b). The channels cut the *b* axis at *b* = 0.13, 0.37, 0.63 and 0.87. The undulations in the channel walls are caused by the projection of the sulphate groups, water ligands and isonicotinamide ligands into the main channel cavity.

(a)

(b)

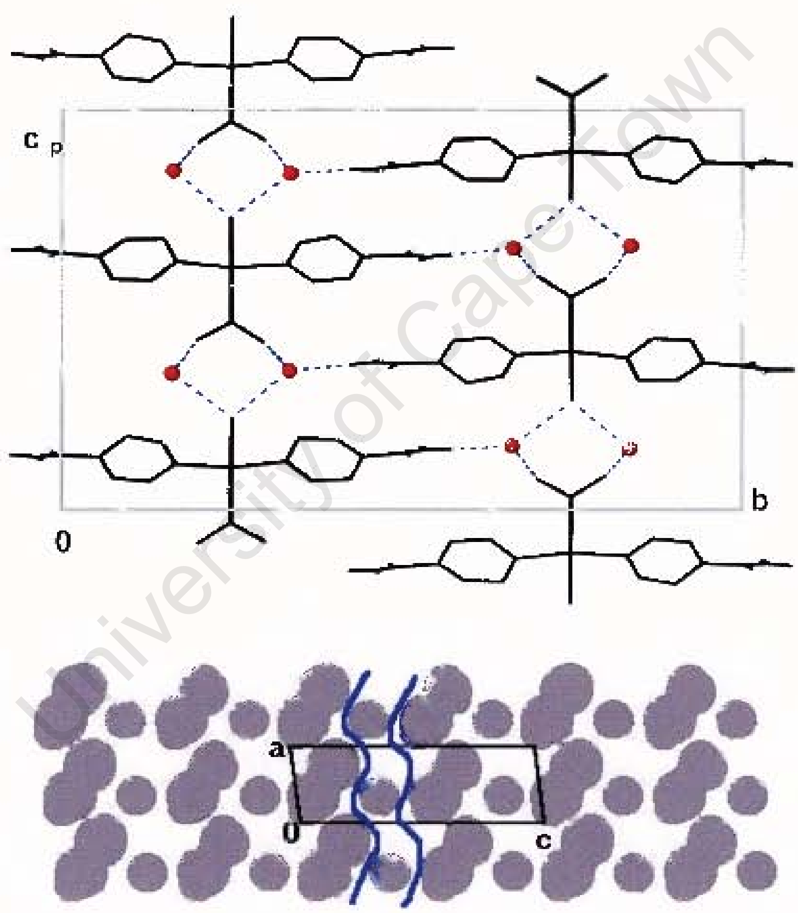

Fig 3.5.22: (a) End-on view of the polymeric chains in Cudiaq, viewed along [100]. (water guests are shown as red circles, hydrogen bonds as broken blue lines; ring H atoms omitted for clarity)), (b) The channels in Cudiaq, viewed along the [010] direction, at *b* = 0.13 (water guests are shown as spheres).

THERMAL ANALYSIS

Thermal analysis reveals Cudiaq to decompose in three steps, labelled **a**, **b** and **c** in Fig. 3.5.23a. The TG shows three distinct weight loss processes. Step **a** corresponds to the release of the two water guests and one water ligand from the asymmetric unit. Steps **b** and **c** each correspond to the loss of a single isonicotinamide ligand (Table 3.5.13). In the DSC, step **a** yields a single, large endotherm, while steps **b** and **c** result in overlapping endotherms. During step **a** the translucent blue crystals bubble and turn opaque. In step **b** the crystals bubble and turn green, before melting to a yellow-brown liquid at the onset of step **c** (Fig. 3.5.23b).

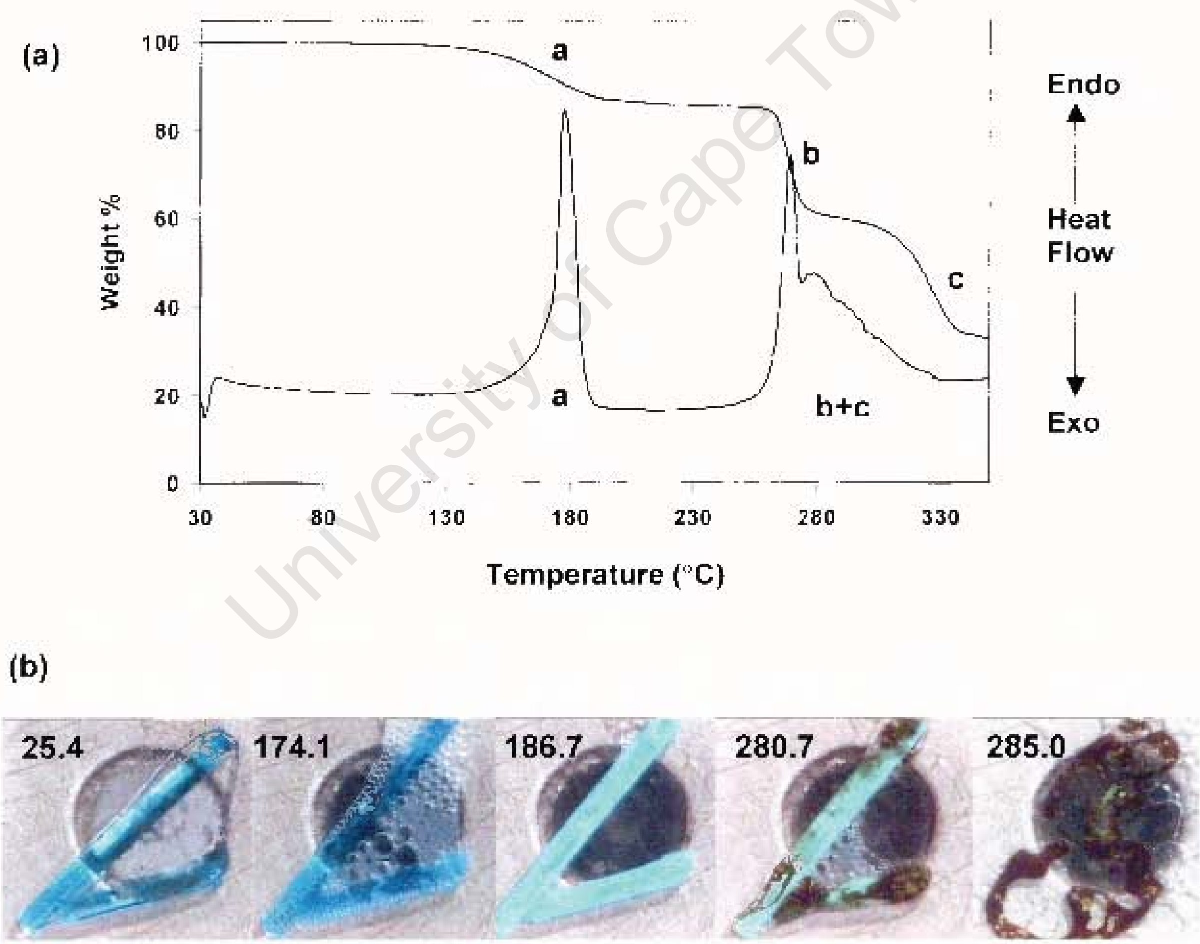

Fig 3.5.23: (a) Thermal analysis, and (b) HSM, of Cudiaq.

Table 3.5.13: TG and DSC data for Cudiaq

Reaction	TG			DSC	
	Calc %	Exp %	T_{onset} (°C)	T_{onset} (°C)	ΔH ($kJ.mol^{-1}$)
$Cu(L)_2(OH_2)(SO_4).2H_2O \rightarrow Cu(L)_2(SO_4) + 3H_2O$	11.79	12.55	129.6	139.5	167.4
$Cu(L)_2(SO_4) \rightarrow Cu(L)_1(SO_4) + L$	27.10	26.62	250.5	249.5	236.9
$Cu(L)_1(SO_4) \rightarrow Cu(SO_4) + L$	27.10	25.65	301.5		

XRD:

The experimental XRD trace corresponds well with the calculated pattern (Fig. 3.5.24)

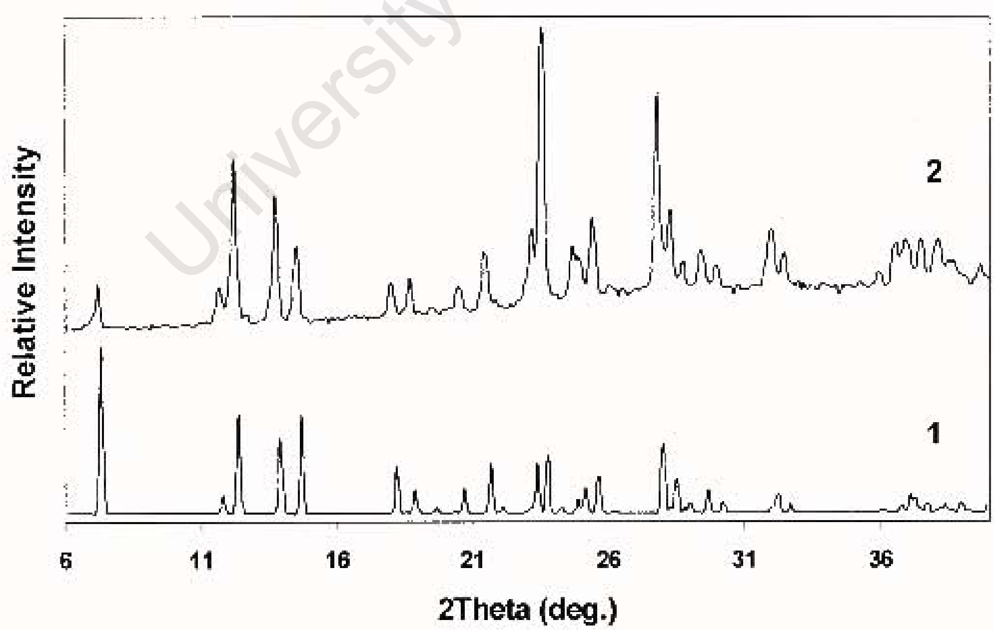

Fig 3.5.24: XRD patterns for Cudiaq: (**1**, calculated and **2** experimental).

DISCUSSION

The structures described in this chapter illustrate the diversity of coordination polymer structure types that can be generated, as well as the importance of the metal centre and counterion in the polymerisation process.

$ZnBr_2pyz_2$ consists of 2-D square grids of octahedrally-coordinated Zn centres and linear bridging pyrazine ligands. This structure, which crystallises in the space group Ccca, is isostructural to $CoCl_2(pyrazine)_2$[20] and $FeCl_2(pyrazine)_2$[21]. Similar packing arrangements are also observed in $Fe(NCS)_2(pyrazine)_2$[25], $Co(NCS)_2(pyrazine)_2$[26], $Cu(CH_3SO_3)_2(pyrazine)_2$[27], $Cu(ClO_4)_2(pyrazine)_2$[28] and $Cu(NCO)_2(methylpyrazine)_2$[29]. Due to the staggering of the layers, as well as the length of the pyrazine ligand, these complexes do not include solvent molecules. When the slightly longer bridging ligand, 4,4'-bipyridine, is used, the square nets that are generated are able to entrap solvent molecules and generate inclusion compounds. This is exemplified by the inclusion compounds formed by the coordination polymers $Cd(NO_3)_2(4,4'\text{-bpy})_2$[30] and $Co(NCS)_2(4,4'\text{-bpy})_2$[26].

$ZnBr_2pyz$ consists of 1-D zig-zag chains of alternating tetrahedrally-coordinated Zn centres and linear bridging pyrazine ligands. Similar chains are found in $[Ag(pyrazine)_3][BF_4]$[4], where the Ag centre is coordinated to two bridging and two terminal pyrazine ligands. $Ag(NO_3)(pyrazine)$[6] also forms 1-D polymers, in which the conformation of the chains fall between zig-zag and linear. XRD and thermal analysis show **$ZnBr_2pyz_2$** and **$ZnBr_2pyz$** to be readily interconvertible, according to:

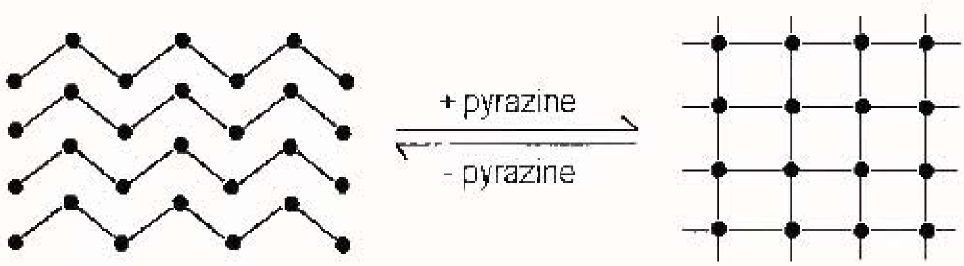

ZnpyzSulf consists of 1-D linear polymers of alternating octahedrally-coordinated Zn centres and linear bridging pyrazine ligands. The SO_4^{2-} counterions are not coordinated to the metal centre, which instead coordinates to four water ligands. The chains pack to form channels in the crystal, which contain the displaced sulphate counterions and the water guests. Similar linear chains are found in the polymers $Cu(NO_3)_2$(pyrazine)[31] and $Cu(hfac)_2$(pyrazine)[32], where the Cu centres adopt an octahedral coordination geometry due to the bidenticity of the counterions.

The final structure differs from the three previous structures by virtue of the fact that it is the counterions, rather than the organic ligands, which link the metal centres. **Cudiaq** consists of 1-D polymers of alternating square pyramidal Cu centres and bridging sulphate counterions. The CSD contains only two examples of sulphate-bridged coordination polymers with Cu as the metal centre[33], neither of which displays the square pyramidal coordination geometry observed for **Cudiaq**.

The most important features of the four coordination polymers presented in this chapter can be summarised as follows:

	$ZnBr_2pyz_2$	**$ZnBr_2pyz$**	**ZnpyzSulf**	**Cudiaq**
Metal Coordination Geometry	≈Oh	≈Td	≈Oh	≈Square pyramidal
Role of Counterion	Remains coordinated to metal centre	Remains coordinated to metal centre	Displaced by H_2O	Remains coordinated to metal centre
Polymerisation Agent	pyrazine ligand	pyrazine ligand	pyrazine ligand	sulphate counterion
Type of Network generated	2-D square grids	1-D zig-zag chains	1-D linear chains	1-D chains

REFERENCES

1) A. G. Orpen, L. Brammer, F. H. Allen, O. Kennard, D. G. Watson, R. Taylor, *J. Chem. Soc., Dalton Trans.*, (1989) S1-83.
2) F. H. Allen, O. Kennard, D. G. Watson, L. Brammer, A. G. Orpen, R. Taylor, *J. Chem. Soc., Perkin Trans.*, (1987) S1-19.
3) M. H. Moore, L. R. Nassimbeni, M. L. Niven, Inorg. Chim. Acta, 132 (1987) 61.
4) L. Carlucci, G. Ciani, D. M. Proserpio, A. Sironi, *J. Am. Chem. Soc.*, 117 (1995) 4562.
5) L. R. MacGillivray, S. Subramanian, M. J. Zaworotko, *J. Chem. Soc., Chem. Comm.*, (1994) 1325.
6) R. G. Vranka, E. L. Amma, *Inorg. Chem.*, 5 (1966) 1020.
7) F. Robinson, M. J. Zaworotko, *J. Chem. Soc., Chem. Comm.*, (1995) 2413.
8) O. M. Yaghi, H. Li, *J. Am. Chem. Soc.*, 118 (1996) 295.
9) L. Carlucci, G. Ciani, D. M. Proserpio, A. Sironi, *J. Chem. Soc., Chem. Comm.*, (1994) 2755.
10) L. Carlucci, G. Ciani, D. M. Proserpio, A. Sironi, *Inorg. Chem.*, 34 (1995) 5698.
11) K. Biradha, K. V. Domasevitch, C. Hogg, B. Moulton, K. N. Power, M. J. Zaworotko, *Cryst. Engineering*, 2, 1 (1999) 37.
12) R. W. Gable, B. F. Hoskins, R. Robson, *J. Chem. Soc., Chem. Comm.*, (1990) 1677.
13) M. Kondo, T. Yoshitomi, K. Seki, H. Matsuzaka, S. Kitagawa, *Angew. Chem. Int. Ed. Engl.*, 36 (1997) 1725.
14) M. Fujita, Y. J. Kwon, O. Sasaki, K. Yamaguchi, K. Ogura, *J. Am. Chem. Soc.*, 117 (1995) 7287.
15) P. Losier, M. J. Zaworotko, *Angew. Chem. Int. Ed. Engl.*, 35 (1996) 2779.
16) L. R. MacGillivray, R. H. Groeneman, J. Atwood, *J. Am. Chem. Soc.*, 120 (1998) 2676.
17) C. B. Aakeröy, A. M. Beatty, D. S. Leinen, *Angew. Chem. Int. Ed. Engl.*, 38 (1999) 1815.
18) S. Subramanian, M. J. Zaworotko, *Angew. Chem. Int. Ed. Engl.*, 34 (1995) 2127.

19) S. Noro, S. Kitagawa, M. Kondo, K. Seki, *Angew. Chem. Int. Ed.*, 39 (2000) 2081.

20) C. Gairing, A. Lentz, E. Große, M. Haseidl, L. Walz, *Zeitschrift für Kristallographie*, 211 (1996) 804.

21) R. Jooss, A. Kult, A. Lentz, L. Walz, *Zeitschrift für Kristallographie*, 210 (1995) 766.

22) Handbook of Thermal Analysis and Calorimetry, Vol. 1: Principles and Practice, ed. M. E. Brown, Elsevier, Amsterdam, 1998, ch.3, pp169-170.

23) A. K. Galway, M. E. Brown, *Proc. R. Soc. London A*, 450 (1995) 501.

24) A. Coetzee, PhD Thesis, University of Cape Town, 1996.

25) J. A. Real, G. de Munno, M. C. Muñoz, M. Julve, *Inorg. Chem.*, 30, (1991) 2701.

26) J. Lu, T. Paliwala, S. C. Lim, C. Yu, T. Niu, A. J. Jacobson, *Inorg. Chem.*, 36 (1997) 923.

27) J. S. Haynes, S. J. Rettig, J. R. Sams, R. C. Thompson, J. Trotter, *Can. J. Chem.*, 65 (1987) 420.

28) J. Darriet, M. S. Haddad, E. N. Duesler, D. N. Hendrickson, *Inorg. Chem.*, 18 (1979) 2679.

29) T. Otieno, S. J. Rettig, R. C. Thompson, J. Trotter, *Inorg. Chem.*, 32 (1993) 4384.

30) M. Fujita, Y. J. Kwon, S. Washizu, K. Ogurak, *J. Am. Chem. Soc.*, 116 (1994) 1151.

31) A. Santoro, A. D. Mighell, C. W. Reimann, *Acta Cryst. B*, 26 (1970) 979.

32) R. C. E. Belford, D. E. Fenton, M. R. Truter, *J. Chem. Soc., Dalton Trans.*, (1974) 17.

33) CSD reference numbers: HANROD and FAKQIR.

CHAPTER 4

CONCLUSIONS

CONCLUSION

The crystal structures of several Werner-type clathrates and coordination polymers have been elucidated, and their decomposition reactions analysed by thermal techniques, including TG, DSC and HSM. The most important structural features of the compounds studied are summarised in Table 4.1.

Of the Werner clathrates studied to date, the vast majority incorporate pyridine ligands with hydrophobic substituents, thereby minimising the interactions between the host and guest components of the crystal. As a result, these inclusion compounds display a marked preference for hydrophobic, rather than hydrophilic, guest molecules.

The clathrates **NiEtAc**, **NiDMSO**, **NidiEt**, **NidiDCM**, **Nipcres** and **Nimcres**, while retaining the classical MX_2A_4 Werner-type formula, comprise hydrogen bonded networks more akin to the 3-D hydrogen bonded porous networks studied by Aakeröy et. al[†]. This is due to the presence of potential hydrogen bond donor or acceptor groups on the ligand substituent, resulting in clathrates that are stabilised by intermolecular host∧host and host∧guest interactions. These clathrates readily include polar guest molecules, such as ethanol, acetone, dichloromethane, cresol and DMSO, which contain potential hydrogen bonding groups.

The polymeric Werner clathrates studied in Chapter 3.4 (**NiEt**, **NiMe** and **Niaq**) also exhibit hydrogen bonding interactions between the components of the crystal. In addition, individual metal complexes are bridged by amino-substituted pyridine ligands, leading to the formation of 1-D helical polymers. These polymeric Werner clathrates provide the link to the class of compounds known as coordination polymers, to which **ZnpyzSulf**, **$ZnBr_2pyz_2$** and **$ZnBr_2pyz$** belong. In coordination polymers the metal centres are directly linked by bridging organic ligands to generate a diverse range of 1-, 2- and 3-D covalently-bonded networks.

If we now revisit the scheme described in Section 1.9, we see that the compounds synthesised in this project define a continuous group, extending from the hydrogen bonded Werner-type clathrates through to the coordination polymers.

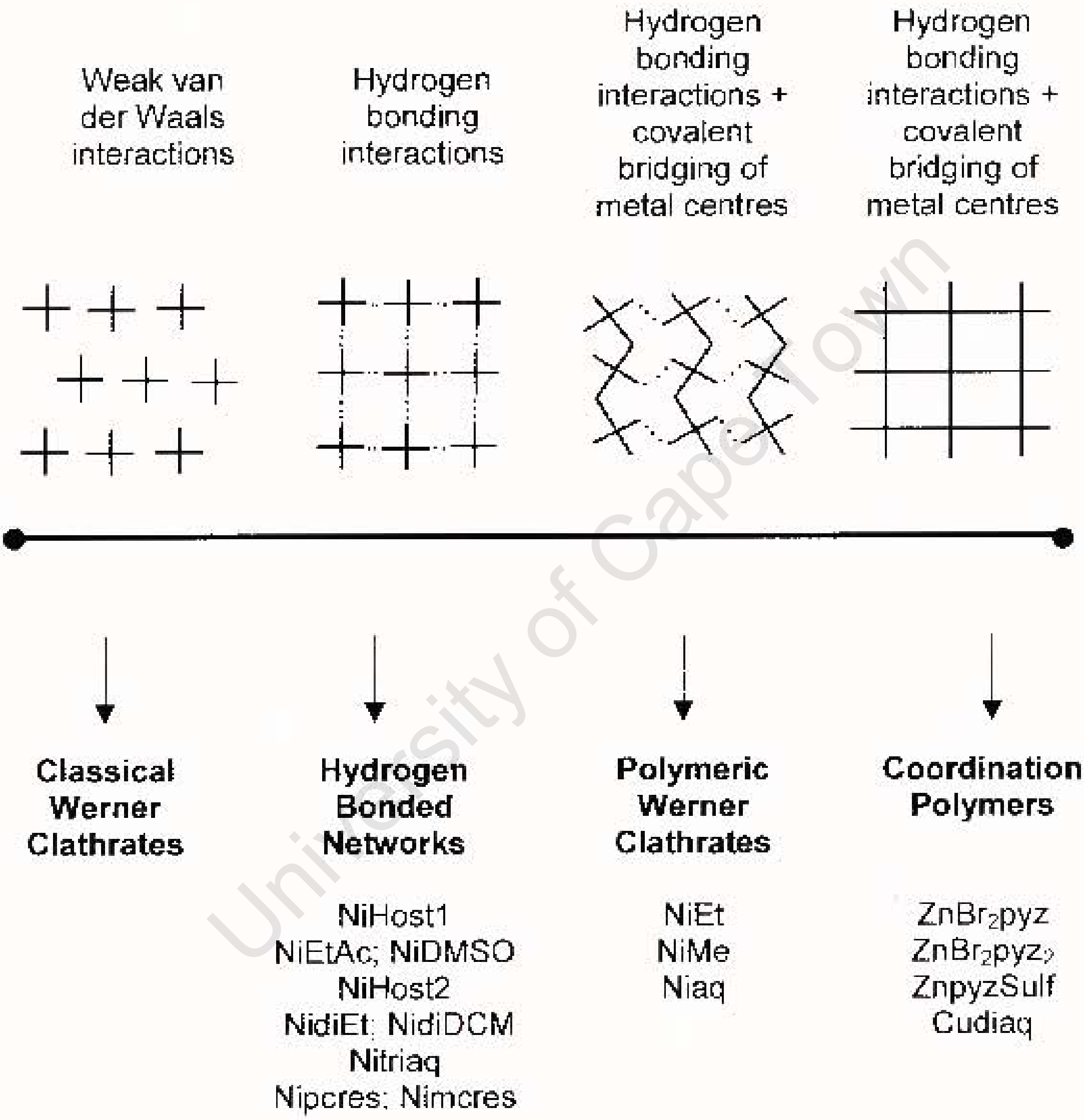

Table 4.1: Important Structural Features

Host Complex	Compound Name	Guest Species	H:G Ratio	Clathrate Type
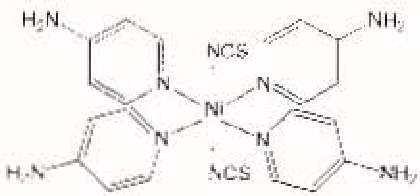	**NiHost1**	-	-	Non-porous α-phase
	NiEtAc	ethanol + acetone	1:1:1	Channel
	NiDMSO	DMSO	1:2	Channel
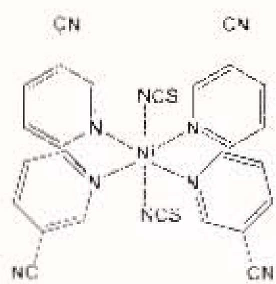	**NiHost2**	-	-	Non-porous α-phase
	NidiEt	ethanol	1:2	Channel
	NidiDCM	dichloro-methane	1:2	Channel
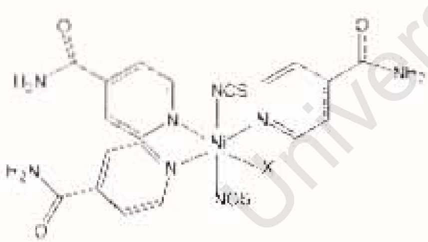	**Nitriaq**	H_2O	1:3	Cage
	Nipcres	*p*-cresol + ethanol	1:2:4	Layer
X = H_2O or isonicotinamide	**Nimcres**	*m*-cresol	1:4	Layer
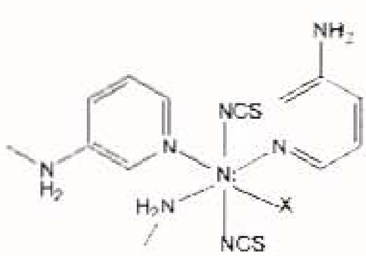	**NiEt**	Ethanol	1:1	Cage
	NiMe	Methanol	1:1	Cage
X = H_2O or 3-aminopyridine	**Niaq**	H_2O	1:1	Cage

Coordination Polymer	Compound Name	Guest Species	H:G Ratio	Polymer Type
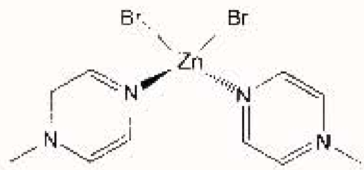	**$ZnBr_2pyz$**	-	-	1-D zig-zag chains
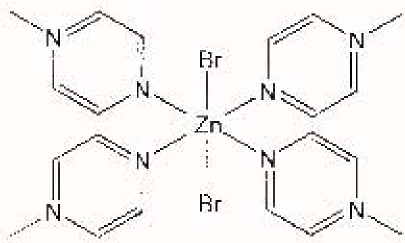	**$ZnBr_2pyz_2$**	-	-	2-D square nets
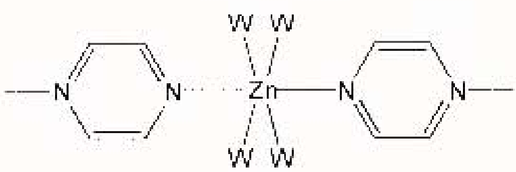 W = water	**ZnpyzSulf**	SO_4^{2-} + H_2O	1:1:2	1-D linear chains with channels
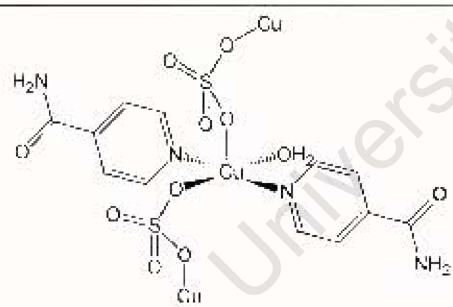	**Cudiaq**	H_2O	1:2	1-D chains with undulating channels

Although the Werner-type inclusion compounds studied in this project differ somewhat from the classical Werner clathrates due to the presence of polar substituents on the pyridine ligands, they can still be classified according to the cage/zeolite/channel/layer scheme described in Section 1.3. A review of the literature reveals that the host:guest (H:G) ratio is dependent on the clathrate type[2], with the general trend being:

Cage clathrate
(H:G = 1:0.67)

↓

Zig-zag channels of β-phase clathrate
(H:G = 1:1)

↓

Layer and some channel clathrates
(H:G = 1:2)

We find that for the cage clathrates (**NiEt** and **NiMe**), the H:G ratio is 1:1, for the channel clathrates (**NiEtAc**, **NiDMSO**, **NidiEt** and **NidiDCM**) the H:G ratio is 1:2 and for the layer clathrates (**Nipcres** and **Nimcres**) the H:G ratios are 1:2:4 and 1:4. The H:G ratios quoted for the classical Werner clathrates, however, all pertain to aromatic guest molecules. If we assume that one aromatic guest is roughly equivalent, in terms of volume, to two smaller organic guests (e.g. ethanol, acetone, DMSO), then this trend holds true for the clathrates presented in Chapter 3 (Lipkowski et. al. have shown that this assumption is a valid one, by investigating the stoichiometries of clathrates containing methanol as the guest[3,4]). We then find that, in terms of the volume of an aromatic guest, the H:G ratios are in accordance with the general trend described above for the classical Werner clathrates (Table 4.2).

Table 4.2: Clathrate host:guest ratios

Clathrate Type	**Compound Name**	**H:G**[#1]
Cage	NiEt; NiMe	1:0.5
Channel	NiEtAc; NiDMSO; NidiEt ;NidiDCM	1:1
Layer	Nipcres[#2]; Nimcres	1:2 and 1:4

#1 = H:G ratios quoted in terms of the volume of an aromatic guest; #2 = ethanol guests not included in calculation, as they form part of the host bilayers

As well as influencing the host:guest ratio, the clathrate type also determines the kinetic stability of the clathrate. Inclusion compounds in which the guest molecules are trapped in cages are found to have a high kinetic stability, with the guest molecules only being released at the onset of host decomposition. This is indeed the case for the cage structures of **NiEt**, **NiMe**, **Niaq** and **Nitriaq**. The more open channel and layer structures, on the other hand, are usually less stable, as it is easier for the guest molecules to diffuse through the crystal structure. In these structures, the guest molecules are released before the onset of host decomposition. This trend is found to hold true for the channel and layer clathrates studied here.

Where possible, the enthalpy of the guest release reaction was calculated from the area under the DSC peak, in kJ per mole of the guest component alone. The results, given in Table 4.3, show that the enthalpy of evaporation of the liquid guest is roughly 5 to 30 times greater than the enthalpy of the guest release reaction, in all cases. This underscores the fact that the guest molecules in the clathrate do not interact like they do in the liquid phase. This is confirmed by examining the closest intermolecular contacts between guest molecules, as shown for **NiEtAc** and **NiEt** in Fig. 4.1 below. In both cases, the closest contacts between the guest molecules exceed the sum of the van der Waals radii for the two heavy atoms considerably (the same is also found to apply to the other clathrates listed in Table 4.3).

In fact, a careful examination of the different clathrate structures reveals that the only interactions available to the guest molecules are intermolecular host···guest interactions. These interactions must be much weaker than those found between the guest molecules in the liquid phase, as the energy required to overcome these forces and release the guest molecules from the host structure is significantly lower than the energy required for evaporation. As a result, the guest molecules can be considered to be in the gaseous rather than the liquid phase.

Table 4.3: Enthalpies of guest release for several clathrates compared with the enthalpies of evaporation of the respective liquid guests

Compound	**Guest**	**ΔH_{vap} of liquid guest (kJ per mole G)**	**ΔH of guest release (kJ per mole G)**	**Ratio of ΔH_{vap} to $\Delta H_{guestrelease}$**
NidiEt	C_2H_5OH	40.5	3.4	11.9
NiEt	C_2H_5OH	40.5	2.5	16.2
NiEtAc*	C_2H_5OH	40.5	3.4	11.9
	C_3H_6O	32.0	5.4	5.9
NiMe	CH_3OH	39.2	1.4	28.0
NidiDCM	CH_2Cl_2	31.7	2.4	13.2

* calculated enthalpies were weighted according to the ratio of the molar mass of ethanol to acetone

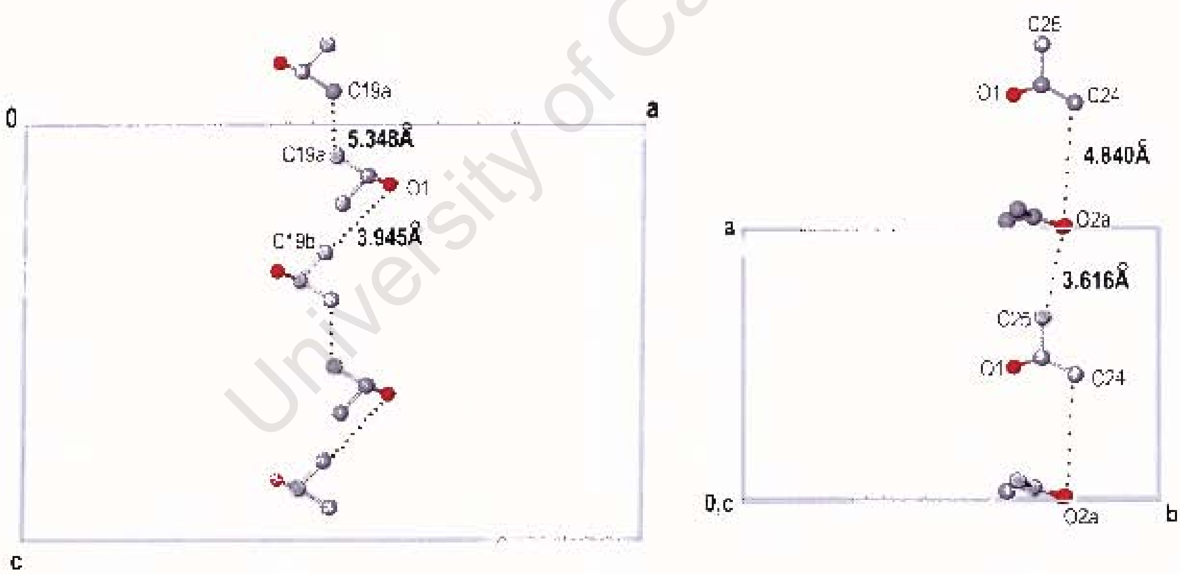

Fig 4.1: Closest guest···guest interactions in NiEt, left, and NiEtAc, right.

REFERENCES

1) C. B. Aakeröy, A. M. Beatty, D. S. Leinen, *Angew. Chem. Int. Ed.*, 38 (1999) 1815.
2) J. Lipkowski, in Inclusion Compounds, Vol. 1, ed. J. L. Atwood, J. E. D. Davies, D. D. MacNicol, (1984), ch. 3, pp59-103.
3) J. Lipkowski, A Zielenkiewicz, J. Hatt, W. Zielenkiewicz, *J. Incl. Phenom. Mol. Recog. Chem.*, 7 (1989) 519.
4) J. Lipkowski, K. Suwinska, G. D. Andreetti, K. Stadnicka, *J. Mol. Struct.*, 75 (1981) 101.

APPENDICES

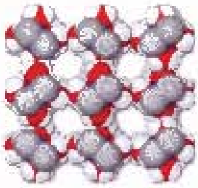  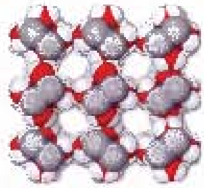 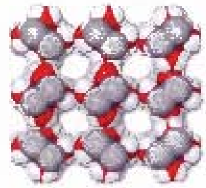 

APPENDICES

Supplementary material can be found on CD-ROM (attached). Three files are included for each structure, namely:

1) **CompoundName.res**: A .RES file, which allows the user to view the molecule and its packing features. This file can be viewed through the X-SEED interface.
2) **CompoundName1.doc**: An MSWord97 document containing tables of calculated and observed structure factors.
3) **CompoundName2.doc**: An MSWord97 document containing tables of atomic coordinates, isotropic and anisotropic displacement parameters, bond lengths, bond angles and torsion angles.

The files have been grouped into five appendices. The data files in appendices 1 to 5 correspond to the structures described in chapters 3.1 to 3.5 respectively. The names and contents of the appendices are listed below.

Folder name	Structural data contained therein
Appendix 1	NiHost1, NiEtAc, NiDMSO
Appendix 2	NiHost2, NidiEt, NidiDCM
Appendix 3	Nitriaq, Nipcres, Nimcres
Appendix 4	NiEt, NiMe, Niaq
Appendix 5	$ZnBr_2pyz^*$, $ZnBr_2pyz_2^*$, ZnpyzSulf, Cudiaq

* for convenience the data files for $ZnBr_2pyz$ and $ZnBr_2pyz_2$ have been renamed Znpyz1 and Znpyz2 respectively